The University Of Sheffield.

Determining the functions of telomerase involved in modulating zebrafish immune cell biology and their potential implications for tissue ageing

Luke Samuel Mansfield

A thesis submitted in partial fulfilment of the requirements for the degree of

Doctor of Philosophy

The University of Sheffield

Faculty of Medicine, Dentistry and Health

Department of Oncology and Metabolism

July 2023

Acknowledgements

This journey would not have been possible without the support and guidance of key people throughout the last 4 years and 8 months. Thus, I would like to acknowledge them here.

To my supervisor, Dr Catarina Henriques. Thank you for patience and advice, for guiding my development, and encouraging me to be the best scientist I can be. It has been a pleasure to work with you and in your lab, and your dedication to science and this field continues to inspire me.

To my second supervisor, Professor Ilaria Bellantuono. Thank you for your advice, both scientific and on life in general. Your feedback and encouragement has helped me to understand what I want to accomplish in life, and how to go about it.

To current and former members of the lab. To Pam Ellis, your teaching, demonstration, knowledge, and kindness were invaluable to me and helped me keep pushing forward. To Dr Raquel Martins, thank you for encouraging and guiding me when I first joined, and for your continued advice throughout.

To Dr Betsy Pownall and the Pownall lab at the University of York for your help in housing and caring for the zebrafish during the single-cell RNA sequencing experiment.

To my parents, Karen and Mark, and my dog, Bluey. Your support and love has kept me moving. You have always encouraged me to achieve my goals, but also to be kind to myself. Without you both I would be but a lone ship in a stormy sea.

To my friends. To Oliver Hargreaves, Alex Howard, and Eleftherios Stefanakos. Thank you for the late-night chats and keeping me laughing, you're the best buds a guy could ask for. To Mary Stewart and Augusta Moore, our kitchen therapy sessions and long walks were a bandage to my weary mind. To Christopher Griffiths, your support, wisdom and encouragement steeled my resolve and helped me to cope with the rigors of PhD life. To Hayley Hardstaff, your advice and support helped me to reach the finish line.

Declaration

I, the author, confirm that this thesis is my own work. I am aware of the University of Sheffield's guidance on the use of unfair means and confirm that this work has not previously been presented for an award at this, or any other, university.

Contributions to the work

People who have contributed to the work presented in this thesis are:

- Pam Ellis, who produced the *mpeg1.1:tert-gfp* construct and F_0 generation, and performed gut dissociations alongside myself for FACS and alongside Dr Henriques for single-cell RNA sequencing sample preparation.
- Dr Catarina Henriques, who aided in the design of the *mpeg1.1:tert-gfp* construct and performed gut dissociations for the single-cell RNA sequencing sample preparation.

Abstract

Ageing is the main risk factor for chronic diseases including dementia, CHD, and cancer. This leads to high levels of multimorbidity associated with an ageing population that is observed in some western countries. One of the hallmarks of ageing is telomere erosion. Telomeres erode in somatic cells with each round of cell division, and due to secondary factors, such as Reactive Oxygen Species (ROS) induced stress. Telomeres are elongated by the ribonucleoprotein complex telomerase that is expressed in some cell subsets, such as stem cells. The enzymatic subunit of telomerase, TERT, has also been shown to have functions outside of its role in telomerase termed non-canonical functions that include protecting mitochondria from ROS and influencing the activation state of some immune cells. Zebrafish have been shown to age in a telomere dependent manner as humans do, and therefore provide a useful model organism with which we can study telomere related ageing.

This project aimed to establish two novel transgenic lines to be used to study the non-canonical functions of TERT. One of these lines would rescue the expression of TERT under the control of the *mpeg1.1* promoter in a telomerase mutant background *(tert$^{-/-}$)*. The other line would rescue the expression of a mutant version of TERT (ΔTERT) that lacked the RNA-binding section of TERT in a telomerase mutant background. Together, these two transgenic lines would be used to explore the non-canonical functions of TERT in zebrafish *mpeg1.1^{+}* immune cells. In this study, I investigate how rescuing the expression of TERT *mpeg1.1^{+}* immune cells affects gene expression using single-cell RNA sequencing.

I find evidence that indicates both transgenic lines have been successfully produced. In the *tert$^{-/-}$;mpeg1.1:mCherry.caax;mpeg1.1:tert-gfp* line I see evidence that expression of the transgenic TERT in *mpeg1.1^{+}* cells is rescuing telomere length. To explore how rescuing TERT expression affects zebrafish ageing I use single-cell RNA-sequencing to compare the gene expression in the intestines of three zebrafish lines: *tert$^{-/-}$;mpeg1.1:mCherry.caax, tert$^{+/+}$;mpeg1.1:mCherry.caax,* and *tert$^{-/-}$;mpeg1.1:mCherry.caax;mpeg1.1:tert-gfp*. I isolate distinct immune cell populations using markers reported in the literature, and explore how the insertion of the *mpeg1.1:tert-gfp* transgene affects the prematurely aged zebrafish immune system, and how this may influence gene expression in cells that have been reported to interact with the immune system. Single-cell RNA-sequencing analysis indicated that insertion of the *mpeg1.1:tert-gfp* transgene rescued the expression of genes associated

with mitochondrial health, ATP production, and both B-cell and macrophage activation and polarization state. This indicates that insertion of the *mpeg1.1:tert-gfp* transgene may be affecting zebrafish immune cell populations to rescue the aged immune cell state. However, further work should be performed to characterize if the gene expression changes are resulting in a rescue of immune cell function, if mitochondrial health is improved, or if the insertion of the transgene is resulting in a pro-inflammatory shift in gene expression.

Table of Contents

List of Figures

List of Tables

Abbreviations

Acronym	Definition
AAV9	Adenovirus Associated Vector 9
ACR	Anterior Cruciate Ligament
ADP	Adenosine Diphosphate
AKT	Protein Kinase B
ALD	Alcoholic Liver Disease
AML	Acute Myeloid Leukaemia
ANOVA	Analysis of Variance
APE	A Plasmid Editor
ASXL1	Putative Polycomb group protein ASXL1
AT2	Angiotensine 2
ATM	Ataxia-telangiectasia mutated
ATP	Adenosine Triphosphate
BCA	Bicinchoninic acid
BCL	B-cell lymphoma
BLAST	Basic Local Alignment Search Tool
BSA	Bovine Serum Albumin
CA	Cornu Amonis
CALCR	Calcitonin Receptor
CCL	Chemokine Motif Ligand
CCR2	C-C Chemokine Receptor type 2
CD	Cluster Differentiation
CDK	Cyclin Dependent Kinase
CDKI	Cyclin Dependent Kinase Inhibitor
CHD	Chronic Heart Disease
CHIP	Clonal Hematopoesis of Indeterminate Potential
CMV	Cytomegalovirus
COPD	Chronic Obstructive Pulmonary Disease
COX3	Cytochrome c oxidase subunit III
CRISPR	Clustered regularly interspaced short palindromic repeats
CSF	Colony Stimulating Factor
CSV	Comma Seperated Values
CXCR4	C-X-C chemokine receptor type 4
DAF	Forkhead Box Protein
DAPI	4',6-diamidino-2-phenylindole
DCR2	Decoy death receptor 2
DDR	DNA Damage Response
DFLE	Disability-Free Life Expectancy
DNA	Deoxyribonucleic acid

DNMT3A	DNA methyl transferase 3 A
DPF	Days Post-fertilisation
DTT	Dithiothreitol
EAT	Dynamin-like 120 kDa protein
EBP	Enhancer binding protein
EDTA	Ethylenediaminetetraacetic acid
ELISA	Enzyme-linked immunosorbent assay
ENU	N-Ethyl-N-nitrosourea
EP2	Prostaglandin E2 Receptor 2
EPO	Erythropoietin
ERK	Extracellular Signal-regulated Kinase
ERR	Oestrogen receptor related
FACS	Fluorescence Associated Cell Sorting
FBS	Foetal Bovine Serum
FISH	Fluorescence in situ Hybridisation
G3	Generation 3
GA	Gibson assembly
GDF	Growth/Differentiation Factor
GFP	Green fluorescent protein
GO	Gene Ontology
GOBP	Gene Ontology Biological Processes
GOCC	Gene Ontology Cellular Components
GOMF	Gene Ontology Molecular Functions
GTP	Guanosine triphosphate
H2AX	H2A histone family member X
HF	Heart Failure
HFD	High Fat Diet
HIV	Human Immunodeficiency Virus
HK	Head Kidney
HMGN2	High Mobility Group Nucleosome-binding 2
hpf	Hours post fertilisation
HSC	Hematopoietic Stem Cells
IAP	Inhibitor of Apoptosis
ICE2	Interactor Of Little Elongation Complex ELL Subunit 2
IEL	Inter-epithelial lysate
IF	Immunofluorescence
IFABP	Intestinal Fatty Acid Binding Protein
IGF	Insulin-like Growth Factor
IGV	Integrative Genome Viewer
IL	Interleukin
ILFS1	Infantile Liver Failure Syndrome type 1
IPEX	Intraperitoneal exudate
IPF	Idiopathic pulmonary fibrosis

IPTG	Isopropyl β-d-1-thiogalactopyranoside
IRES	Internal Ribosomal Entry Site
IRI	ischemia-reperfusion injuries
ISC	Intestinal Stem Cells
ISP	Individual Study Plan
JAK	Janus Kinase
KB	Kilobases
KEGG	Kyoto Encyclopaedia of Genes and Genomes
L15	Leibovitz's media
LB	Lysogeny Broth
LC3B	Light-chain 3-B
LEPR	Leptin Receptor
LPS	Lipopolysaccharide
MAPK	Mitogen Activated Protein Kinase
MCP1	Monocyte Chemoattractant Protein 1
MDM	Monocyte-derived macrophages
MDR2	Multi-drug resistant 2
MHC	Major Histocompatibility Chain
MMD	Monocyte to Macrophage Differentiation 1
MMP	Matrix Metallopeptidase
MS	Tricaine Mesylate
MSC	Mesenchymal Stem Cell
MST1	Macrophage Stimulating 1
NACWO	Named Animal Care and Welfare Officer
NAD	Nicotinamide Adenine Dinucleotide
NADH	Nicotinamide Adenine Dinucleotide Hydrogen
NADPH	Nicotinamide Adenine Dinucleotide Phosphate
NAMPT	Nicotinamide Phosphoribosyltransferase
NEB	New England Biosciences
NF-κβ	Nuclear factor kappa-light-chain-enhancer of activated B cells
NGFR	Nerve Factor Growth Receptor
NK	Natural Killer
NOP10	Nuclear Protein 10
NRF1	Nuclear Respiratory Factor 1
NRG1	Neuregulin 1
NTP	Nucleoside Triphosphates
ON	Overnight
ONS	Office for National Statistics
PACS	Population Ageing and Care
PAMP	Pathogen Associated Molecular Patterns
PBS	Phosphate Buffered Saline
PCR	Polymerase Chain Reaction

PD	Parkinsons Disease
PDAC	Pancreatic Ductal Adenocarcinoma
PFA	Paraformaldehyde
PGC	Putative Germ Cell
PGC-1α	Proliferator-activated Gamma Coactivator 1α
PGE2	Prostaglandin E2
PK	Pseudoknot
PKC	Protein Kinase C
PNA	Peptide Nucleic Acid
PPAR	Peroxisome Proliferator-Activated Receptor
PPL	Project Licence
PRKDC	DNA-dependent protein kinase
QC	Quality Control
RANKL	Receptor Activator of NF-κβ Ligand
RAPTOR	Regulatory-associated protein of mTOR
RB	Retinoblastoma
REG	Regenerating Protein
RNA	Ribonucleic acid
ROS	Reactive Oxygen Species
RPM	Rotation Per Minute
RT	Room Temperature
RTA	Relative Telomerase Activity
SAHF	Senescence Associated Heterochromatin Foci
SASP	Senescence-associated Secretory Phenotype
SDS	Sodium Dodecyl Sulfate
SFCM	Senescent Foam Cell Macrophages
SIPS	Stress-Induced Premature Senescence
SIRT	Silent Information Regulator
SOC	Super Optimal Broth
SRC	Proto-oncogene tyrosine-kinase Src
SSC	Sodium Citrate Solution
STAT	Signal-Transducer and Activator of Transcription
TERC	Telomerase RNA Component
TERT	Telomerase Reverse Transcriptase
TET2	Ten-Eleven-Translocation 2
TGF	Transforming Growth Factor
TLR	Toll-Like Receptor
TNF	Tumour Necrosis Factor
TOR	Target Of Rapamycin
TORC1	Target Of Rapamycin Complex 1
TRAP	Telomerase Repeat Amplification Protocol
T_{VM}	Virtual T-memory cells
UK	United Kingdom

UMI	Unique Molecular Identifier
USA	United States of America
UTR	Untranslated Region
VA	Veteran Affairs
VEGF	Vascular Endothelial Growth Factor
WHO	World Health Organisation
WRAP53	WD40-encoding RNA antisense to p53
WT	Wild-type
ZFIN	Zebrafish Information Network
ZIRC	Zebrafish International Resource Centre

Chapter 1: Introduction

1.1 The impact of Ageing in the 21st century

Initially it is important to establish that humans age in both a chronological and a biological manner. Your chronological age is a measure of the amount of time that has passed from your birth to the present. On the other hand, biological age is a measure of biological markers that indicate your age on a cellular level and evidence is emerging that biological age is a better measure of your health with age than chronological(1). Ageing is broadly defined as the process by which our body begins to fail with the passing of time. More specifically, ageing is the breakdown of the homeostatic systems that maintain our body in a healthy state(2). The question of why we age has intrigued humans for millennia, with the ideal of immortality being a pertinent goal of scholars through antiquity up to modern day. It is only in the previous few decades that our reductionist scientific methods have allowed us to begin to understand the physical mechanisms that contribute to the ageing process.

Human populations around the world are rapidly ageing with a widespread increase in the number of individuals over the age of 60(3). As of 2019 25% of the population of Europe is over 60(3). It is estimated that by 2050 a quarter of the population of every region in the world (bar sub-Saharan Africa) will be aged over 60(3). Further to this, the number of people aged 80 years and older is increasing. The estimated population of 80 years and over in 1950 was 14 million; by 2050 it is predicted to reach 402 million, an almost 29-fold increase(4). *Kingston et al.* used their Population Ageing and Care Simulation (PACSim) model to estimate the prevalence of multimorbidity in England up to the year 2035(5). The researchers found that by 2035 the number of individuals aged 65-74 with multimorbidity will have increased to 52.8% from 45.7% in 2015. Further, the number of individuals 65 and older suffering from four or more chronic diseases simultaneously will increase to 17% from 9% in 2015(5).

Chronic disease, and by extension multimorbidity, is not immediately lethal. Therefore, the longer an individual lives, the greater the likelihood of developing one or more chronic diseases (6, 7). *Bähler et al.* showed that, in a study of 229,493 Swiss individuals of 65 or over, the prevalence of multimorbidity was 76.6.%, and the average costs of healthcare were 5.5 times higher for those with multimorbidity(8). Moreover, there was an increased cost of 33% per additional chronic condition. These results demonstrate the strain that an

increasingly elderly population can place on a country(8). Meanwhile, a separate study was performed by *Stokes et al.* on a sample size of 8,440,133 patients in England in 2017 to 2018. These researchers found that 55.3% of the total costs of the cohort were accounted for by patients with multimorbidity, despite these patients only accounting for 31.8% of the total group. These results indicated the disproportionate cost of caring for those 65 and over compared to other age groups(9). This is further supported by *Yoon et al.* who analysed the costs associated with multimorbidity among the American Veteran's Affairs (VA) patients(10). Of a cohort of 5,233,994, one third had three or more chronic diseases. This third of the group accounted for 66% of total VA healthcare costs(10).

Overall, we can see that countries with an increasing population of people aged 65 and over will see an increased strain on their economies. Further, the actual cost will be much greater than the increase in numbers due to the disproportionate cost of caring for those with multimorbidity. Hence, research into improving health with ageing is an integral part of cushioning the impact of ageing populations.

1.1.1 Lifespan vs Healthspan

The study of the biological basis of ageing and age-related diseases is termed biogerontology(11). Biogerontologists study the biological aspects of ageing to better understand the mechanisms that cause ageing and how they may contribute to diseases associated with ageing(11). By better understanding these mechanisms we may alleviate the detrimental effects associated with ageing with the hopes of improving the quality of life of an individual(12). However, an under-discussed aspect of biogerontology is the end point of an individual who may hypothetically receive a treatment aimed at alleviating an aspect of ageing. Are we extending their life with treatment but also prolonging the suffering of an individual incapable of independent function? Are we improving an individual's health at an age where they would previously begin to see a serious decline? At what point are we extending an individual's life in an unnatural manner and what are the ethical implications of this? To consider these questions we must make the important distinction between the Lifespan and Healthspan of an individual.

The lifespan of a human is the length of their life measured from the moment of their birth to the moment of their death(13). While lifespan is an inherited factor it is also influenced

by socioeconomic and environmental factors that influence an individual's health. Such factors include access to clean water, food, and modern healthcare and medicine, and any potential cause of mortality such as accidents or occupational hazards. Inherited factors that that affect lifespan are genetic and epigenetic and can include how well the body reacts to Deoxyribonucleic acid (DNA) damage and repair, the length of one's telomeres, and the ability of the individual's body to maintain homeostasis(14, 15)

Healthspan on the other hand is the section of an individual's lifespan that is spent free of chronic disease or the disabilities we commonly associate with ageing(16). Like lifespan, the healthspan of an individual is subject to environmental and genetic factors(17). For example, once a person reaches fifty years of age, we witness a steady decline in muscle mass known as sarcopenia, with a reduction of 1-2% a year and a reduction in strength of 1.5-3% per year(18). Therefore, this individual's body is beginning to fail as the homeostatic mechanism's breakdown. If this breakdown leads to disease, then the healthspan of the individual is being affected. Healthspan is affected by environmental and genetic variables in much the same way as lifespan. However, it is much more appealing to extend the healthspan of an individual than to extend the lifespan, as by doing so we may be able to maintain quality of life into old age before seeing a rapid failure to thrive. Alternatively, we may see an increased quality of life for longer, but also an increased lifespan.

Importantly, lifespan and healthspan are separate measures and so do not necessarily follow the same trajectory. This is illustrated by data obtained from the United Kingdom (UK) Office for National Statistics (ONS). The ONS had reported that life expectancy at birth is estimated to be 79.3 years for males and 83.1 years for females(19). Additionally, those who reached the age of 65 are expected to live a further 18.5 years for males and 21 years for females(19). However, the ONS also reported that the Disability-Free Life Expectancy (DFLE) at birth for males was 62 years and 60.7 years for females(20). Therefore, this indicates that males may expect to live for 17.3-21.5 years, and females 18.1-21 years, with one or more chronic diseases. This comparison clearly illustrates how healthspan and lifespan are not interchangeable. Furthermore, considering the disproportionate cost of caring for those with multimorbidity (see section 1.1), there is a clear case for increasing the healthspan of an ageing population.

1.2 Ageing associated diseases are caused by the breakdown of homeostasis.

As discussed in section 1.1.1 an increase in the aged population will be accompanied by a rise in the incidence of chronic disease. Ageing is broadly considered to be the "time-dependent functional decline" of an organism and its cells (12). This functional decline results from a breakdown of homeostatic mechanisms, where homeostasis is the steady maintenance of physical and chemical conditions that produce a functional state optimal for the continued health of the organism(21). This breakdown of homeostatic mechanisms is due to factors termed "The Hallmarks of Ageing" which have been outlined by *López-Ótin et al.*(12). According to *López-Ótin et al.* a hallmark of ageing is defined by the application of three criteria as follows:

1. The hallmark causes time-dependent manifestations of alterations accompanying the ageing process.
2. It is possible to accelerate ageing by experimentally accentuating the hallmark.
3. Therapeutic interventions targeting the hallmark present the opportunity to decelerate, halt, or reverse ageing(12).

These hallmarks include stem cell exhaustion, telomere attrition, cellular senescence, genomic instability, epigenetic alterations, loss of proteostasis, deregulated nutrient sensing, mitochondrial dysfunction, and altered intercellular communication. All of these hallmarks lead to a disruption of the homeostatic state(12, 22). By disrupting homeostasis, each hallmark contributes to diseases associated with ageing(12). One method of understanding how the hallmarks of ageing interact with each other is to compartmentalise them into "primary", "antagonistic", or "integrative" hallmarks. Primary hallmarks include genomic instability, telomere attrition, epigenetic alterations, and loss of proteostasis(12). Primary hallmarks are determined by the fact they have solely detrimental effects on organismal health(12). Antagonistic hallmarks are classed in this category as they are beneficial in some respects and detrimental in others, and this category includes the cellular senescence, deregulated nutrient sensing, and mitochondrial dysfunction(12). Integrative hallmarks result when the organism can no longer compensate for the damage caused by primary and antagonistic hallmarks. Integrative hallmarks include stem cell exhaustion and

loss of proteostasis(12) By studying and understanding these mechanisms and their interactions with each other, we may be able to alleviate multiple diseases of ageing simultaneously. However, a significant challenge in biogerontology is developing therapies that can not only ameliorate, but also prevent, multimorbidity in ageing. To do this, we need to develop a more complete understanding of the fundamental mechanisms that underlie ageing and its associated diseases.

1.2.1 Genetic Instability

Genetic instability is implicated as one of the main causal factors of ageing via the constant exposure of the genome to sources of DNA damage such as ionising radiation and ROS(23) Despite the sophistication of DNA damage detection and repair mechanisms, errors are inevitable. Additionally, errors may also occur during the process of DNA replication. Therefore, there are many ways that mutations may occur to cause genetic instability over the course of a lifetime. This acquired genetic instability contributes to diseases related to ageing. A major example of this can be seen with cancer, which is a disease that is commonly linked with ageing whereby acquired mutations in the genome lead to cell exhibiting the hallmarks of cancer and becoming malignant(24). A notable example of this can be seen via the Sirtuin 6 (*sirt6*) gene, which encodes a regulator of histone deacetylation. *Simon et al*. sequenced the *sirt6* locus of 450 centenarians and 550 individuals without a family history of longevity(25). The team identified two linked substitutions in the centenarian allele of *sirt6* (N308K/A313S) that were not present in the *sirt6* found in non-centenarians(25). Characterising the centenarian SIRT6 indicated that it conferred a high resistance to cancer development associated with stronger mono-Adenosine Diphosphate (ADP) ribosyl activity but weaker deacetylase activity(25). Therefore, a clear link is indicated between a genetic mutation in a population predicating a resistance to cancer leading to a longer average lifespan.

Genetic instability can also influence the ageing phenotype by working in tandem with other hallmarks of ageing such as stell exhaustion. For example, Hematopoietic Stem Cells (HSCs) in the bone marrow ensure haematopoietic homeostasis by regulating the proliferation of new progenitor cells(26). As people age, stem cells accumulate mutations that go

undetected by proofreading mechanisms during cell division. This can give rise to a condition termed Clonal Hematopoesis of Indeterminate Potential (CHIP)(27). CHIP occurs when the majority of an individual's circulating blood cells are derived from a single mutated HSC that has gained an advantageous mutation allowing it outcompete other HSCs(27). CHIP is commonly associated with mutations in the transcriptional regulators DNA methyl transferase 3 A (*DNMT3A*), Ten-Eleven-Translocation 2 (*TET2*), and Putative Polycomb group protein ASXL1 (*ASXL1*)(28). In the aged population CHIP is hypothesised to be a pre-malignant state of acute myeloid leukaemia (AML) as well as having been shown to lead to an increased prevalence of coronary heart disease (CHD) and heart failure (HF), all of which are chronic conditions associated with ageing(28). Therefore, a combination of genetic changes acquired over time and stem cell exhaustion leads to a state of chronic disease that increases the risk of multimorbidity associated with ageing.

1.2.2 Epigenetic Alterations

Epigenetic alterations are changes to an organism's phenotype that concern the expression of genes but that do not alter the genetic code itself(29). Examples of epigenetic changes include changes to histone protein and chromatin structure via the addition of subunits such as acetyl or methyl groups(29). During the ageing process a global reduction in heterochromatin is observed alongside an increase in areas termed Senescence Associated Heterochromatin Foci (SAHF). This is accompanied by a decrease in repressive histone markers such as methylation (global DNA hypomethylation) except at CpG islands where DNA hypermethylation is reported(29). Epigenetic alterations with ageing have been closely studied to the point that two epigenetic clocks have been produced, the Hannum epigenetic clock(30) and the Horvarth epigenetic clock(31, 32).

Epigenetic clocks are used to measure an individual's age on a molecular level based on the methylation of specific epigenetic regions. *Higham et al.* studied human DNA methylation in a cohort of 600 individuals from the ages of 67 to 80. The researchers found that 80% of the CpGs in the Hannum epigenetic clock and 88% in the Horvarth epigenetic clock had a statistically significant increase in methylation with age(33). Further to this *Hillje et al.* studied mice liver to determine how histone modification altered with ageing(34). *Hillje et al.* determined an increase in methylation on H3 histones and a decrease in acetylation when comparing 12-month-old liver to that of 6-month-old(34). While further work needs

to be carried out to determine the effects of the increased methylation, we can logically hypothesise that the increased methylation will lead to decreased gene expression at the methylation sites as methylation supresses gene expression. Furthermore, by comparing *Hillje et al.* and *Higham et al.* we can see that the increased methylation is conserved between species(33, 34). *Hillje et al.* also observed a slower rate of increased methylation in dietary restricted mice(34). Therefore, an interesting avenue of future research may involve examining the effects of dietary restriction on methylation in humans.

A further example of epigenetic alterations influencing chronic disease outcomes was reported by *Kugel et al.* The researchers determined that mice with a SIRT6 knockout displayed *kras*-driven PDAC tumours with a greater propensity to metastasize compared to those in *sirt6* wild-type (WT) mice(35). *Kugel et al.* found that deacetylation of H3K56Ac by SIRT6 led to a downregulation of the Ribonucleic Acid (RNA)-binding protein Lin28b, which had previously been correlated with advanced cancer and poor prognosis(35). Thus, the researchers demonstrated that loss of SIRT6 is correlated to poor prognosis in PDAC. Comparing the work of *Kugel et al.* and *Simon et al.* from section 1.2.1 we can see that a single gene (*sirt6*) is linked to longer life and decreased risk of cancer, and that dysregulation of that same gene leads to an increased risk of severe Pancreatic Ductal Adenocarcinoma (PDAC). This is a striking illustration of how genetic instability impacts ageing associated diseases, and other hallmarks of ageing such as epigenetic alterations(12, 25, 35).

1.2.3 Altered intercellular communication.

With ageing, we observe changes in intercellular communication systems, such as in endocrine and neuronal signalling, leading to deregulation of such signalling(12). The impact of this loss of intercellular communication is observed with ageing in diseases such as CHD and dementia. A large proportion of the alterations to intercellular communication observed with ageing is accounted for by increased inflammation mediated by Nuclear Factor Kappa B (NF-κB) and SIRT1(12). However, beyond inflammation and the inflammageing gerotype there are tissue specific examples of altered intercellular communication. For example, *Huang et al.* observed dopaminergic neurons in a Parkinson's Disease (PD) model displaying interactions with non-neuronal cells but a decrease in the number of different non-neuronal cell clusters interacted with(36). *Huang et al.* further demonstrated that the Chemokine Motif Ligand (CCL), Vascular Endothelial Growth Factor

(VEGF), Growth/Differentiation Factor (GDF), and Nicotinamide Phosphoribosyltransferase (NAMPT) pathways were upregulated in PD(36). Additionally, between dopaminergic neurons and non-neuronal cells Wnt, Galectin, Interleukin (IL)-4, Calcitonin Receptor (CALCR), and Erythropoietin (EPO) were all upregulated(36). The upregulation of Wnt in this context is particularly interesting considering that it is a well reported regulator of cell fate determination in the neural crest. This potentially implyies that PD results in the remodelling of non-neuronal cell clusters. However, this hypothesis would require further investigation(36, 37).

1.2.4 Stem cell exhaustion

As people a decline in the regenerative potential of tissues is observed that results from a slow exhaustion of stem cell(12). Further, exhaustion occurs in every tissue in the body where cellular turnover occurs, including the brain, bone, and muscle fibres(12). In the gut we see a rapid turnover of somatic cells at the ends of the gut villi that leads to an increased turnover of Intestinal Stem Cells (ISCs)(38). This rapid turnover occurs due to the extreme environment found within the gut due to the mixing of various digestive enzymes with corrosive stomach acid or bile. Due to this rapid turnover, the average epithelial cell of a gut villi has a turnover of five days and in turn, ISCs have a renewal rate of 3-5 days(38). ISCs and their progenitor cells reside in inter-villi crypts, and it is the balance between the loss of intestinal epithelial cells and the renewal rate of ISCs that determines how rapidly the gut ages(39). One of the hallmarks of ageing described by *López-Ótin et al.* is stem cell exhaustion(12). Due to the high turnover of cells in the gut, ISCs accumulate DNA damage faster, which leads to a reduction in the capacity of the ISCs to replicate(38). Over time, gut tissue homeostasis is, diminished reducing nutrient sensing ability(38).

Bone strength is preserved throughout life due to the homeostatic activity of osteoclasts and osteoblasts constantly remodelling the skeleton. One of the chronic diseases commonly observed with ageing is osteoporosis, which occurs due to disruption of the homeostatic mechanisms that maintain bone strength. One cell subset responsible for this maintenance is the osteoblasts. Osteoblasts are derived from mesenchymal stem cells (MSCs) and synthesize new bone(40). Exhaustion of MSCs leads to a decrease in the number of progenitor cells that descend from MSCs, including chondrocytes, myocytes, fibroblasts, and osteoblasts, so contributing to osteoarthritis(40). For example, *Čamernik et al.* isolated and

cultured MSCs from primary osteoarthritis patients(41). The cultured MSCs derived from primary osteoarthritis had reduced osteogenic and chondrogenic potential compared with MSCs derived from patients with osteoarthritis occurring due to hip dysplasia(41). *Čamernik et al.* further observed lower expression of Leptin Receptor (LEPR) in the MSCs derived from primary osteoarthritis than in those from the hip dysplasia-derived sample(41). Considering that *Zhou et al.* previously indicated that LEPR-expressing MSCs are responsible for the majority of bone and adipocyte formation in adult bone marrow(42), the results from *Čamernik et al.* indicate that the lack of expression of LEPR in the primary osteoarthritis derived MSCs is a contributor to the onset of osteoarthritis in aged individuals.

1.2.5 Mitochondrial dysfunction

Tissue homeostasis is further disrupted by changes in mitochondrial function with age(12). Damage to mitochondrial DNA occurs due to the reactivity of the oxidative environment inside mitochondria and the lack of protection mitochondrial DNA has from this damage in the form of histones or repair mechanisms(12). Evidence suggests that the fission and fusion of mitochondria may be indicative of the ageing phenotype(43). For example, mitochondrial fusion in *Caenorhabditis elegans* has been shown to promote longevity via the conserved insulin/Insulin-like Growth Factor (IGF)-1 pathway(44). *Chaudhari et al.* demonstrated that disruption of mitochondrial fusion using interfering Ribonucleic Acid (RNAi) of Dynamin-like 120 kDa protein (EAT-3) led to a decreased lifespan in *C. elegans*(44). Another regulator of mitochondrial fusion is proliferator-activated gamma coactivator (PGC-1α) via its regulation of Mfn2 and Drp1(43). PGC-1α also regulates nuclear respiratory factor 1 (NRF1) which acts through a signalling cascade to stimulate mitochondrial DNA transcription, maintenance, and replication(45). PGC-1α further regulates the oestrogen receptor related (ERR) family of proteins, which play a role in regulating mitochondrial biogenesis, cell differentiation, and progression through the cell cycle(45). Finally, PGC-1α expression has been shown to decrease with age in lung cell mitochondria(46). However, the PGC-1α/mammalian target of rapamycin (mTOR) pathway, which activates mitochondrial biogenesis, is upregulated in senescent lung cells(46). Therefore, we can see a distinct link between the disruption of mitochondrial homeostasis and the advancement of the ageing phenotype, with PGC-1α acting as a sensitive regulator of this process.

1.3 Cellular senescence.

Senescent cells are cells that have permanently entered a state of cell-cycle arrest and that excrete the Senescence-associated Secretory Phenotype (SASP)(47). These cells have been shown to accumulate in tissues as we age, and this accumulation has been linked to the diseases we have come to associate with ageing such as cataracts, CHD, and cancer(47-49). Cells may enter senescence for several reasons, including replicative senescence, the presence of DNA lesions, high levels of ROS, and chronic exposure to mitogenic signals(49-51). Replicative senescence occurs in the absence of telomerase activity when telomere degradation in conjunction with cell division triggers a mitotic cell to enter senescence due to the activation of the DNA Damage Response (DDR)(52). Damage to the DNA via other avenues, such as oxidative stress, also leads to an activation of the DDR. This may then also cause the cell to begin apoptosis or enter senescence(53). Evidence that the DDR causes cellular senescence has led to the hypothesis that senescent cells have evolved to protect young organisms from cancer early in their life(54, 55). Alongside this, the hypothesis of antagonistic pleiotropy for senescent cells suggests that while they are advantageous in a young organism, they become detrimental as the organism ages(54, 56). It is important to note that only mitotic cells can enter replicative senescence due to their proliferative capacity. Thus conversely, it is due to their lack of proliferation that post-mitotic cells will not enter replicative senescence(50).

1.3.1 Senescence markers and formation of senescent cells

Senescence was first described by Hayflick and Moorhead in their report on the irreversible growth arrest of human fibroblasts in serial culture(51). There are four well established markers of senescence. The first is the Cyclin Dependent Kinase Inhibitor (CDKI) $p16^{INK4a}$. The activation of $p16^{INK4a}$ prevents the phosphorylation of the retinoblastoma protein (RB), which in turn, prevents the progression of the cell cycle into S-phase(57). Increased expression of $p16^{INK4a}$ has been documented in aged tissues(58). The elimination of $p16^{INK4a}$-expressing cells in aged mice has been shown to reduce the phenotypes of ageing and rescue age-related disorders in mice(58).

A second established marker of senescence is the Cyclin Dependent Kinase (CDK) p21, which regulates the progression of a cell through the cell cycle, albeit in a manner independent of

p16(59, 60). When a cell becomes stressed to the point that p53 expression is upregulated, p53 activates p21 which arrests the cell cycle(60). However, *Marhenke et al* demonstrated that p21 must be tightly regulated(61). The researchers indicated that Multi-Drug Resistant 2 (MDR2)-p21 knockout mice had delayed hepatocellular carcinoma tumour development but also had reduced liver regeneration rate when exposed to injury(61). Additionally, *Marhenke et al* found that expression of p21 in patient derived hepatocellular carcinoma was associated with a shorter patient survival rate(61). Therefore, while p21 plays an important role in liver regeneration from injury, its expression negatively impacts the survival of hepatocellular carcinoma patients. Thus, with the link between p53, p21, cancer and wound healing, we can see an indication of the antagonistic pleiotropy exhibited by senescent cells; while they protect us from cancer, they also begin to negatively affect organismal health with their accumulation in ageing(62).

A third marker of senescent cell manifests as the activity of the enzyme β-galactosidase. The expression of β-galactosidase is significantly higher in senescent cells than in non-senescent cells(60). The activity of senescence-associated β-galactosidase (SA-β-gal) can be determined using a colorimetric assay whereby the substrate X-gal is added to the tissue at pH6. In this assay, a colour change is seen in proportion to the number of senescent cells(63). There are two significant drawbacks of using this SA-β-gal assay to assess senescence. The first is that the assay can only be performed on fresh or frozen samples as the active site of SA-β-gal will be inactivated by crosslinking if the sample is embedded in paraffin. The second drawback is that β-gal is expressed in cells as part of their normal function. Therefore, the SA-β-gal assay may detect non-senescent cells expressing a high level of β-gal due to their function. However, in non-senescent cells, it has been reported that the β-gal is activated at pH4 allowing senescent cells to be detected using the pH6 assay without detecting non-senescent cells(64).

The final established marker of senescence is lipofuscin. Lipofuscin is a protein and lipid aggregate that accumulates around the nucleus with age(57). There is currently little evidence that lipofuscin can be degraded *in vivo*. However, *Terman et al.* determined that lipofuscin degraded with the serial passage of cells *in vitro*(65). Lipofuscin can be detected in fresh, frozen, and fixed tissue samples using GL-13, a biotinylated Sudan Black-B

derivative(66). Thus, lipofuscin is a particularly useful marker for determining senescence in paraffin-fixed samples.

Further to these markers, cells may enter senescence via three different routes: Replicative senescence, Stress-induced senescence, and Cancer-induced senescence. Each type of senescence is defined by specific biomarkers and the route the cell has taken to arrive at senescence.

1.3.1.1 Replicative senescence

Replicative senescence was the first form of senescence to be described in 1961 by Hayflick and Moorhead(51). With each round of division in a human cell, telomeres shorten by 50-100bp(51). Replicative senescence occurs when the telomeres of somatic cells shorten to the point that the cell cannot undergo further divisions without its chromosomes entering crisis. This is termed 'The Hayflick Limit'(67). At this point further divisions will lead to chromosomal instability and potentially, apoptosis(51). Once a cell reaches the point where it can no longer divide, there are three potential outcomes: 1. the cell enters senescence, 2. the cell undergoes apoptosis, or 3. the cell becomes cancerous. Replicative senescence described the cell moving down the first pathway. Cells will continue to grow and divide due to mitogenic signalling. Mitogens induce a cell to begin to begin division and can increase rate of cell division. One example of a mitogen is Neuregulin 1 (NRG1) which enables zebrafish to regenerate wounds to their heart(68). Chronic mitogenic signalling can instigate chronic ROS activity within the cell via the $p16^{INK4A}$/RB pathway. Instead of allowing the cell to grow and divide, this chronic ROS activity leads to DNA damage and the cell entering senescence(69).

1.3.1.2 Stress-Induced Premature Senescence (SIPS)

SIPS occurs when a cell undergoes stresses that lead to it entering a senescent state before it reaches the Hayflick limit. There are several stresses that may cause a cell to enter premature senescence including free radical build-up, accumulation of mutations, and prolonged exposure to mitogenic signalling(70). SIPS occurs not due to a specific inducer of stress but rather as a response to the cell being in a chronic state of stress. For example, oxidative stress causes damage to DNA, which leads to a DDR. Should the DDR fail to recognise the damage, then mutations or double-strand breaks may build up over time causing the cell to enter senescence(71). SIPS is characterised by the persistent

accumulation of DDR factor phospho- Ataxia-telangiectasia mutated (ATM)/γ-H2A histone family member X (H2AX), morphological changes such as increased cell size, and premature β-gal staining(72).

1.3.1.3 Cancer-induced senescence

Cancer-induced senescence is hypothesised to occur as a mechanism for protecting young organisms from cancer. When a cell begins to move down the pathway of carcinogenesis, it accumulates mutations that give it the hallmarks of cancer(23). However, before the cell becomes carcinogenic it may enter senescence instead. This forms part of the antagonistic pleiotropy theory of senescent cells, whereby one advantageous trait has evolved that has a secondary effect that is disadvantageous(62). Here, the advantageous effect is that the body is protected from cancer, and the disadvantageous effect is that over time, senescent cells accumulate to the point that they contribute to the ageing phenotype. The body is protected from cancer via this mechanism because the cell enters senescence, division ceases, and so the chance of the cell accumulating further DNA mutations is reduced. This allows the protection of the organism from cancer that would be more immediately detrimental than the slow accumulation of senescent cells. Cancer-induced senescence is hypothesised to be regulated via the $p16^{INK4}$ pathway. $p16^{INK4}$ inhibits CDK 4/6 and cyclin 2 to block the advancement through the cell cycle via the RB pathways(73).

1.3.2 Senescent cells aggravate ageing associated diseases.

Despite senescent cells residing at a point of permanent cell cycle arrest, they remain metabolically active and adopt a senescence phenotype. One component of the senescence phenotype is the SASP(49, 50, 54). The SASP includes the secretion of multiple pro-inflammatory cytokines including IL-1α, IL-1β, IL-6 and IL-8, chemokines, and matrix metalloproteinases (74-76). As senescent cells accumulate with age, the burden of the coinciding increase in SASP output contributes to a multifaceted process known as “inflammaging”(77, 78). Inflammaging describes the chronic, systemic inflammation that has been characterised to occur with ageing(79). Initially it was hypothesised in the biogerontology field that the elimination of senescent cells would alleviate the ageing phenotype. This hypothesis was tested notably by *Baker et al.* whereby a mice strain was developed that contained a $p16^{Ink4}$ green fluorescent protein (GFP) reporter and a mutated inactive version of the mitotic checkpoint regulator *BubR1*(58, 59). The $p16^{Ink4a}$ reporter

enabled easy visualisation of the senescent cell burden in tissue sections, while the *BubR1* mutation led to the mice displaying a prematurely aged (progeroid) phenotype that included infertility, sarcopenia, dermal thinning, fat loss, lordokyphosis (spinal curvature), and the accumulation of senescent cells(58). *Baker et al.* found that clearing senescent cells in the progeroid mice delayed the onset of lordokyphosis, and attenuated muscle atrophy and the loss of subdermal adipose tissue in older mice(58). Therefore, *Baker et al.* demonstrate a clear link between the burden of senescent cells and the onset of ageing and age-related multimorbidity(48, 58).

There are several further studies that also support the notion that as senescent cells accumulate with age they contribute to the development of multimorbidity associated with ageing(80). For example, *Yao et al.* generated a novel p53-Angiotensin 2-dependent senescence phenotype in mice via the silencing of *Sin3a*(81). *Yao et al.* demonstrated that in mice with induced senescence in their lung, the accumulation of senescent cells was a predictor of the onset of idiopathic pulmonary fibrosis (IPF)(81). This indicates that the accumulation of senescent cells may contribute to IPF progression, where IPF is a chronic disease associated with an ageing phenotype. Further, *Aghali et al.* examined biopsies of lung tissue from elderly patients and found that those with asthma displayed greater fibrosis than those without asthma(82). Additionally, *Aghali et al.* found that tissue isolated from elderly patients with asthma displayed increased markers of senescence including elevated phosphor-p53, p21, and p16(82). Taken together, this evidence indicates how the accumulation of senescent cells may contribute to tissue remodelling in the lungs of elderly patients. This tissue remodelling may then lead to the onset of chronic diseases including IPF and asthma, and hence, multimorbidity.

Bone is another important tissue type that the accumulation of senescent cells may impact. The maintenance of bone is a dynamic process that relies on the constant balanced action of osteoblasts and osteoclasts (section 1.2.4). It can be hypothesised that the action of senescent cells in preventing efficient wound healing in bone and cartilage may also affect bone homeostasis. For example, *Jeon et al.* found that senescent cells develop at the site of anterior cruciate ligament (ACR) injury in mice but that removing senescent cells that formed at the site of the ACR injury attenuated chondrogenesis and alleviated pain and post-injury osteoarthritis development(83). Therefore, *Jeon et al.* showed that the removal

of senescent cells during ACR injury improved wound healing(83). This is supported by the work of *Peilin et al.* who demonstrated that the clearance of senescent cells in rats with post-traumatic osteoarthritis, attenuated subchondral bone reconstruction(84). This result indicated that the presence of senescent cells at the site of injury inhibited efficient wound healing. Therefore, there is some evidence to support the hypothesis that senescence contributes to osteoporosis and that the presence of senescent cells leads to alterations in tissue physiology that are detrimental to dynamic processes such as wound healing.

1.3.3 Immuno-senescence

Immunosenescence is the remodelling of the immune system that occurs with aging. Unlike replicative or induced senescence, immunosenescence is a phenotypic shift in the immune system that affects its ability to function(85, 86). These changes include impaired phagocytosis, natural killing functions, and antigen-presenting capabilities, as well as alterations in cytokine and chemokine expression(87, 88). These changes lead to an altered inflammatory state(87, 88). Therefore, immunosenescence affects several immune cell subtypes including T-cells, B-cells, macrophages, and Natural Killer (NK) cells(87). Immunosenescence is a significant risk factor in an ageing population, with indications that it contributes to limited efficacy of vaccines and to diseases such as osteoporosis(86, 89, 90). Thus, immunosenescence presents an appealing area of study to investigate methods for its functional rescue.

1.3.3.1 Immunosenescence of the innate immune system

Macrophages are cells of the innate immune system that enter immunosenescence with ageing. Their principal function is to phagocytose foreign particles and, following activation, bridge the gap between cytokine signalling and antigen presentation of the innate and adaptive immune systems(91). Additionally, macrophages have been shown to have a wide variety of regulatory roles both in wound healing and throughout developmental stages(92-96). However, there is evidence to suggest that macrophages may undergo immunosenescence, with aged macrophages characterised by less effective phagocytosis, autophagy, and immune regulation(97). With the advance of ageing, we begin to witness diseases linked to the dysregulation of macrophage biology, including Alzheimer's, cancer, and osteoporosis(98, 99). Therefore, it has been hypothesised that macrophages may contribute to the decline in function and increase of multimorbidity we see with ageing(98,

99). This has been demonstrated by *Childs et al.* who indicated a link between immunosenescent macrophages and the progression of CHD(100). *Childs et al.* demonstrated that in low-density lipoprotein receptor deficient (*Ldlr-/-)* mice fed with a high fat diet (HFD) atherosclerotic lesions developed that contained a high number of Senescent Foam Cell Macrophages (SFCMs)(100). Additionally, *Childs et al.* showed that eliminating the SFCMs led to a regression of the atherosclerotic lesions (100). This indicated that the SFCMs played a role in the progression of the atherosclerotic lesions(100). Furthermore, it has been indicated that macrophages associated with unstable atherosclerotic lesions are pro-inflammatory M1 macrophages that secrete cytokines such as Tumour Necrosis Factor-α (TNF-α), IL-1β and ROS (101). Therefore, it can be hypothesised that these senescent macrophages may be contributing to the accumulation of senescent cells via their excretion of these senescence inducing cytokines(102, 103). Thus, ageing macrophages present an appealing target for therapies aimed at alleviating age related chronic disease(104). For example, *Minhas et al* identified a significant increase in Prostaglandin E_2 (PGE2) synthesis in Monocyte-derived macrophages (MDMs) from elderly individuals as well as an increase in the expression of Prostaglandin E_2 Receptor 2 (EP2)(105). The researchers found that inhibition of EP2 in human MDMs increased their phagocytic capacity and polarized them to an anti-inflammatory activation state(105). Further, they found that pharmacological inhibition of EP2 in aged mice rescued hippocampal mitochondria to a youthful state and reversed age-associated spatial memory deficits(105). Therefore, it has been indicated that aged macrophages and their mitochondria are promising targets for alleviating age-associated cognitive decline.

1.3.3.2 Immunosenescence of the adaptive immune system

Immunosenescence is indicated to exacerbate the ageing phenotype by exhibiting an inflammatory phenotype that prevents an effective response being mounted to infection or vaccines(106). T-cells are an integral part of the adaptive immune systems response to infection and vaccines. T-cell can be split into two groups, Cluster Differentiation (CD)8+ and CD4+, both of which undergo initial maturation in the thymus. CD8+ T-cells are also termed cytotoxic T-cells as their primary role is to identify and destroy self-cells. These target cells may be infected with viruses or may be tumour cells(107). CD8+ T-cells recognise the cells to be destroyed by interacting with polypeptides presented as part of Major Histocompatibility

Chain 1 (MHC1), which interacts with the CD8 receptor(108). CD4+ T-cells can become regulatory T-cells or helper T-cells. Regulatory T-cells control the immune response by preventing autoreactivity and maintaining immunological tolerance(109). Helper T-cells initiate a wider response to an infection by stimulating the maturation of B-cells into plasma cells and memory B-cells, and activating CD8+ T-cells(110). In the elderly a significant decrease in the response of the adaptive immune system to both infection and vaccinations is observed due to a process termed thymic involution. Thymic involution described the process by which the number of circulating naïve T-cells exponentially declines with age(111). For example, *Palmer et al.* developed an *in-silico* model examining the number of T-cells in an aged population with respect to the incidence of disease(111). From their model, *Palmer et al.* found that increases in both pathogenic diseases and cancer followed the decline of circulating naïve T-cells that occurs due to thymic involution(111). However, *Palmer et al.* also noted that incidences of breast and thyroid cancer did not correlate with naïve T-cell decline and instead plateaued around middle age. Further, most of the cancers they surveyed plateaued after 80 years(111). These results potentially indicate that factors alternative to thymic involution had a greater influence on cancer incidence after the 80-year mark. However, this hypothesis would require further validation.

The decline in production of true naïve T-cells that occurs as part of immunosenescence is accompanied by an increase in T-cells termed "virtual T memory cells" (T_{VM}-cells), which are antigen specific despite no previous antigen encounters(106). This lack of new 'true' naïve T-cells combined with the increase in terminally differentiated memory T-cells accumulated throughout life, inhibits the ability of the adaptive immune system to respond to novel pathogens and vaccines with age(106). A potential 'model' of immunosenescence may be chronic infections such as Human Immunodeficiency Virus (HIV) and cytomegalovirus (CMV) as they are associated with an increase in the number of memory T-cells(112). In patients with chronic HIV or CMV infections, memory T-cells have been observed to upregulate CD57, a marker of senescence in immune cells, and to downregulate CD28, which is required for T-cell activation in conjunction with CD8. These markers indicate that the T-cells have entered a state similar to immunosenescence(112).

Interestingly, *Morris et al.* demonstrated that these immunosenescent memory T-cells are still capable of proliferation when they are stimulated by IL-15(113). This indicates that

immunosenescence, in the case of memory T-cells at least, may be able to be reversed to some extent. Further, *Morris et al.* determined that IL-15 was preventing apoptosis via regulation of the anti-apoptotic protein Bcl-2 and promoting proliferation via the Signal-Transducer and Activator of Transcription 5 (STAT5) and mammalian target of rapamycin complex 1 (mTORC1) pathways(113). As such, *Morris et al.* indicated that stimulation of the immunosenescent T-cells is inhibited by the administration of rapamycin, which inhibits the activity of mTORC1(113). Rapamycin is indicated to increase the lifespan of treated individuals. Therefore, it can be hypothesised that the expansion of this immunosenescent T-cells subset is detrimental to organismal health and may contribute to the increase in incidence of diseases associated with inflammageing(114).

In addition to the lack of response to novel infections and vaccines, there is evidence that the pro-inflammatory phenotype associated with immunosenescence contributes to increased tissue ageing. For example, *Yousefzadeh et al.* selectively deleted *Ercc1* in mouse lymphoid tissues to stimulate premature senescence of the murine immune system(115). *Ercc1* protects cells from DNA damage caused by ROS. Therefore, deleting *Ercc1* induces senescence due to a lack of DNA protection(115). *Yousefzadeh et al.* found in their *Ercc1*$^{-/fl}$ model that both T-cell and B-cell populations declined with age, whereas in WT mice they remained stable(115). Further, *Yousefzadeh et al.* found increased levels of senescence markers in T-cells, B cells, NK, and CD11b^{+} myeloid cells (macrophages, microglia, and dendritic cells(116)) of the *Ercc1*$^{-/fl}$ mice, which indicates that large sections of the immune system were entering premature senescence(115). *Yousefzadeh et al.* also found that expression of senescent cell markers *p16* and *p21* was increased in non-lymphoid organs of *Ercc1*$^{-/fl}$ mice, including in the lung, intestines, kidney, heart, and brain(115). Therefore, evidence suggests that immunosenescence is a driver of tissue ageing independent of the non-immune cells within that tissue entering senescence.

1.4 Telomeres and telomerase

1.4.1 The structure and function of telomeres

Telomeres are repeating 5'-TTAGGG-3' units of non-coding DNA around 15 kilobases (KB) in length found at the end of linear chromosomes (Fig.1.4.1). Together with the protein shelterin, telomeres prevent the ends of chromosomes from being recognised as DNA

double strand breaks by forming a T-loop structure (Fig.1.4.1)(117, 118). Due to the end-replication problem, the ends of our chromosomes shorten with each cell division. The end-replication problem occurs because DNA polymerase requires a template to replicate DNA. When DNA polymerase reaches the end of chromosomes there is no Okazaki fragment providing a basis for replication of that section, leading to a 20-40 bp loss per cell division(119). Capping chromosomes with non-coding telomeric structures prevents genes located at the end of the chromosome from being lost during subsequent rounds of cell division. However, the shortening of telomeres will eventually lead to telomere uncapping and the consequent activation of a DDR(120). This DDR leads to either cell death by apoptosis or the cell entering replicative senescence(121). Therefore, telomere shortening effectively limits the number of times a cell may divide, and this limit is known as the Hayflick limit(51). The interaction of telomeres with shelterin has two major functions(118). The first function is to coordinate the formation of T-loop structures at the end of telomeres, which prevents the recognition of telomere ends by DNA repair mechanisms(118). The second function of the interaction is the regulation of telomerase accessibility and activity(118). The T-loop structure forms due to the overhang found at the end of telomeres (Fig.1.4.1). The formation of the T-loop structure is facilitated by shelterin but also by the guanine rich sequence of telomere DNA forming G-quadruplexes(Fig.1.4.1)(122).

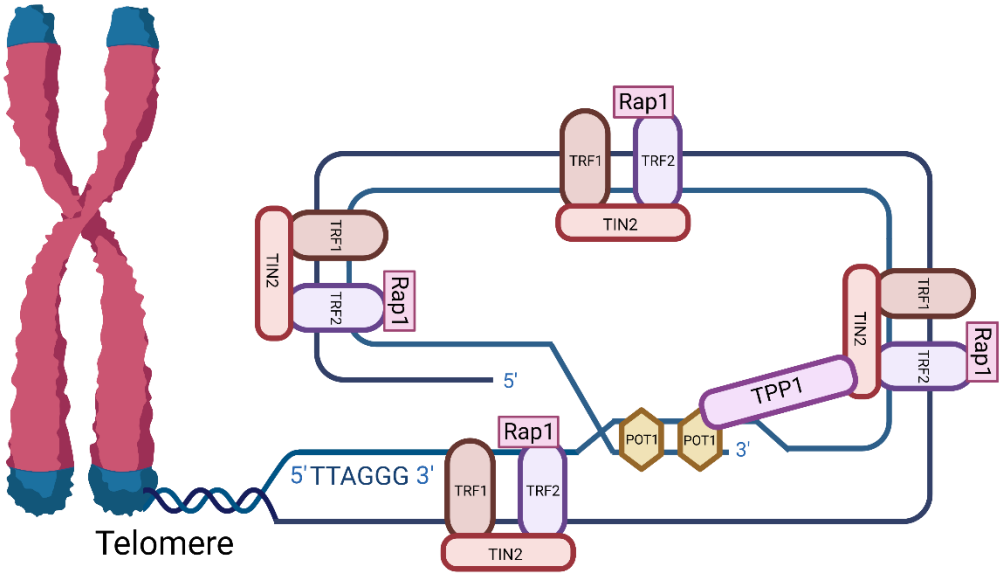

Figure 1.4.1: A representative figure of the end structure of a telomere forming a T-loop structure in conjunction with the shelterin complex. Shelterin is complex made up of the protein subunits: Telomere Repeat binding Factor 1 (TRF1), Telomere Repeat binding Factor 2 (TRF2), Repressor/Activator Protein 1 (RAP1), Protector of Telomere 1 (POT1), TRF1 and TRF2 Interacting Nuclear Protein 2 (TIN2), and TPP1 which is associated with the ACD gene.

1.4.2 The structure and function of telomerase

Telomerase is a ribonucleoprotein complex, the canonical function of which is to elongate telomeres. The telomerase complex in humans is made up of two of each of Telomerase Reverse Transcriptase (TERT), telomerase RNA component (TERC) and Dyskerin(123). Dyskerin recruits and stabilises the structure in conjunction with shelterin (Fig.1.4.2)(123). There are several peripheral components: Nuclear Protein 10 (NOP10), NHP2, GAR1, WD40-encoding RNA antisense to p53 β (WRAP53β), Reptin, and Pontin (Fig.1.4.2)(124, 125). The TERC component of telomerase is considered a long noncoding RNA that has two regions integral to the canonical function of telomerase; the Pseudoknot template region (t/PK) and the H/ACA domain(126). Data from *Ghanim et al.* indicate that it is the double hairpin H/ACA domain of TERC that enables the recruitment and binding of copies of dyskerin, NHP2, NOP10, and GAR1, with one copy of each component going to each hairpin loop(123).

In humans, telomerase is only expressed in certain cell subsets such as progenitor stem cells, cancer cells, germ cells, and in some circumstances, immune cells(127-129). In most human cells tested so far, TERC appears to be ubiquitously expressed(130). As such, the rate limiting component for telomerase is the TERT subunit of the complex. The expression of TERT is tightly regulated in humans(131). Further to its telomere-lengthening function, known as the "canonical function" of telomerase, telomerase and its subunits have functions that are not associated with the lengthening of telomeres, termed "non-canonical functions," that are still being elucidated(132).

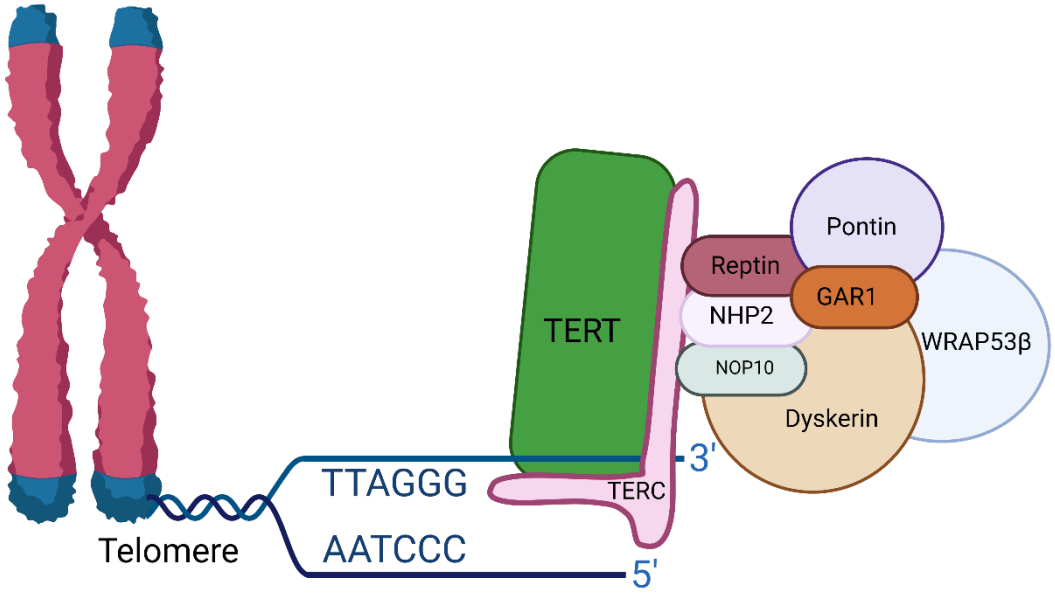

Figure 1.4.2: A representative image of the structure and function of human telomerase. Human telomerase elongates telomeres in a repeating TTAGGG manner using the TERC subunit as a template. Telomerase complex assembly requires the recruitment of two of each of TERT, TERC, and Dyskerin as well as recruitment of the proteins Nuclear Protein 10 (NOP10), NHP2, GAR1, WD40-encoding RNA antisense to p53 β (WRAP53β), Reptin, and Pontin

1.4.2.1 The structure and function of the Telomerase Reverse Transcriptase subunit

The telomerase subunit TERT is an enzymatic subunit that contains the telomerase active site, giving telomerase its enzymatic function of elongating telomeres. The TERT subunit of telomerase has four tertiary structural domains: an N-terminal domain, an RNA-binding domain, a reverse transcriptase domain, and a C-terminal extension(123, 126). TERT binds to the telomere at the same time as accommodating the alignment of TERC to the telomere whereby the 3' of TERC aligns with the 3' of the overhang allowing bases to be added by TERT until they reach the 5' end of TERC(124). In this manner, TERC acts as a pseudo-Okazaki fragment providing both the template for the addition of new nucleotides, and the foundation for the extension of the telomere.

The first TERT structure to be visualised was of the unicellular eukaryote, *Tetrahymena*. *Jiang et al.* used cryo-electron microscopy to report a 4.8Å resolution structure of *Tetrahymena* TERT bound to telomeric DNA(133). Recently *Ghanim et al.* reported the structure of human telomerase bound to telomeric DNA determined using cryo-electron microscopy at a 3.8Å resolution (123). This elucidation indicated that human telomerase has a double-lobed structure unlike that of *Tetrahymena*, which has only a single-lobed structure(123, 133). In the active site of TERT the t/PK region of TERC encircles TERT allowing the formation of the DNA/RNA duplex used to elongate telomeres(123). However, instead of the full TTAGGG interaction, only the AGGG has been observed binding to the 3' end of the DNA substrate(123). *Ghanim et al.* hypothesised that the remaining TT is added via the addition of free Nucleoside Triphosphates (dNTPs), and that the TERT motif Y717 acts a steric gate that only allows dNTPs to enter the vacant TT site and not rNTPs(123).

1.4.2.2 The non-canonical functions of TERT

The canonical function of the TERT subunit of telomerase is synthesising telomeric 5'-TTAGGG-3' repeats as part of telomerase to maintain telomere length. However TERT is also indicated to have non-canonical functions independent of its enzymatic role in telomere maintenance and extension(134).

The activity of TERT is regulated post-transcriptionally via phosphorylation by the kinases Protein Kinase C (PKC), Extracellular Signal-regulated Kinase (ERK), and Protein Kinase B

(Akt)(135, 136). Specifically, phosphorylation by Akt on serine 227 marks TERT for transport into the nucleus, whereas phosphorylation at tyrosine 707 by Src marks TERT for transport to the mitochondria (Fig.1.4.2.2)(137, 138). The localisation of TERT to the mitochondria has been indicated to increase positive prognosis for various disease and injuries due to its protective effects against the activity of ROS(139). For example, *Haendeler et al.* found that TERT localizes and binds to mitochondrial DNA, which in turn increases respiratory chain activity and protects mitochondrial DNA from oxidative stress-induced damage (Fig.1.4.2.2)(Table 1.4.2.2)(139). *Haendeler et al.* hypothesised that the protective effects of TERT *in vivo* are most pronounced in tissues that have a high respiratory rate and low regenerative capability, such as the myocardium, as these tissues would rely more on healthy mitochondria over time due their low cellular turnover(139). *Haendeler et al.* demonstrated that mitochondria isolated from myocardial samples taken from TERT mutant mice displayed a significant reduction in respiratory chain complex-1 functionality that was not observed in their wild-type TERT counterparts(139). Further to this, *Haendeler et al.* isolated liver mitochondria from mutant TERT and wild-type TERT mice and found no significant difference in their function. This result provided evidence to support their hypothesis as liver cells have a much higher turnover than those of the myocardium(139).

If it is true that the protective effects of TERT are most pronounced in cells with high respiratory rates and low turnover, then it can be hypothesised that TERT will have a non-canonical protective effect in low-proliferation, low-turnover cell types such as nerve cells, and subsets of immune cells that do not undergo clonal expansion, such as macrophages. Supporting this hypothesis, *Spilsbury et al.* demonstrated the expression of TERT in human hippocampal neurons and microglia and found that TERT was localised to the soma and dendrites rather than the nucleus. This indicated that TERT was not performing its canonical function of elongating telomeres(140). *Spilsbury et al.* found that wild-type TERT cultured neurons were less susceptible to hydrogen peroxide induced ROS build-up than TERT mutant neurons. This suggested that wild-type TERT was protecting the neuronal mitochondria from the detrimental activities of ROS(Table 1.4.2.2)(140). Together these experiments indicate that TERT has a protective effect on hippocampal neurons independent of telomere elongation.

Further evidence of the protective effects of TERT have been provided by *Hu et al.*(141). *Hu et al.* demonstrated that administering the α_2-adrenergic receptor agonist, dexmedetomidine, to rats with intestinal ischemia-reperfusion injuries (IRI) led to increased shuttling of TERT to the mitochondria (Fig.1.4.2.2)(Table 1.4.2.2)(141). Dexmedetomidine treatment in the high-dose group had a protective effect on mitochondrial DNA and morphology, leading to less deletions resulting from oxidative stress and less mitochondrial membrane destruction(141). Therefore, *Hu et al.* demonstrated that dexmedetomidine treatment can alleviate cellular stress resulting from IRI. It can be hypothesised that this is due to the protective effects of TERT in the mitochondria. Examining the results from *Haendeler et al., Spilsbury et al., and Hu et al.* together it can be seen that there is evidence that TERT can protect cells, and more specifically their mitochondria, from the effects of ROS-induced damage. Therefore, that TERT may play an important role in continued mitochondrial health.

A further non-canonical function of TERT that has been reported in the literature is its role in brain development(142). *Zhou et al.* generated a mutant version of TERT (here referred to as ΔTERT) that lacked amino-acid residues 702-712. These residues are integral to the function of the active site. Therefore, ΔTERT was unable to elongate telomeres when incorporated into telomerase(142). *Zhou et al.* observed that *tert*$^{-/-}$ mice had poor spatial learning ability compared to their *tert*$^{+/+}$ counterparts, demonstrating that TERT is involved in the formation of spatial memory(142). *Zhou et al.* then examined a primary culture of *tert*$^{-/-}$ mouse hippocampal neurons and found that both the dendritic length and spine density were significantly lower than for wild-type TERT cultured neurons(142). However, when *Zhou et al.* introduced ΔTERT into the primary cultured *tert*$^{-/-}$ neurons via a lentiviral vector, the reduced dendritic length and spine density that had previously been observed was rescued(142). This indicates that TERT has a role in maintaining neuronal health independent of its canonical functions of elongating telomeres as part of the telomerase enzyme (Table 1.4.2.2)(142).

In further experiments by *Zhou et al.*it was found that levels of Synapsin 1 expression in the cornu amonis 3 (CA3) region of the hippocampus was lower in *tert*$^{-/-}$ mice than in *tert*$^{+/+}$(142). Synapsin 1 has been indicated to be involved in modulating the release of neurotransmitters and the CA3 region is integral to the formation of spatial memory in

mice(143, 144). Therefore, *Zhou et al.* hypothesised that TERT is integral to the formation of spatial memory in mice (Table 1.4.2.2)(142). However, further investigation into the mechanism by which TERT is involved in this non-canonical function is needed. *Zhou et al.* made no indications on the localisation of TERT within the cultured neurons so we cannot assume that this non-canonical function is linked to TERT's previously discussed role in mitochondrial protection from ROS. Further experiments may be performed to determine the mechanism that links Synapsin1 and TERT.

Miwa et al. investigated the interactions of TERT in the brain with mitochondria, mTOR, and the regulation of ROS damage (145). The researchers found that mice on a calorie restricted diet accumulated TERT in brain mitochondria which led to an improvement in spatial memory in aged mice(145). Rapamycin inhibits the activity of mTOR so acting as a dietary restriction mimic. *Miwa et al.* found that in mice fed with rapamycin for 4 months TERT transcription was increased in the brain when compared to control mice that had not been fed rapamycin. Further, TERT protein levels were elevated in brain cell mitochondria but not in brain tissue homogenate. These results indicated that TERT was localising to the mitochondria(Fig.1.4.2.2)(Table 1.4.2.2)(145) *Miwa et al.* found that the localisation of TERT to the mitochondria correlated with a decrease in intracellular ROS levels, but this decrease was not found in *tert*$^{-/-}$ mice. This result suggested that the observed protection of mitochondria from ROS was TERT dependent(145). In further experiments, *Miwa et al.* found that in mice treated with the Proto-oncogene tyrosine-kinase Src (SRC) inhibitor, bosutinib, TERT was not localised to the mitochondria and ROS damage increased (Fig.1.4.2.2)(145). This supports previous findings by *Haendeler et al.* that TERT shuttling to the mitochondria is SRC dependent(139, 145). Considering that *Zhou et al.* reported a non-canonical function of TERT in the health of neurons and *Miwa et al.* have indicated TERT shuttling to the mitochondria in the brain has a protective effect, we can see that TERT is integral to brain health in a manner independent of its role in elongating telomeres.

Additional to its potential roles in neural cell development and protection discussed above, the telomerase subunit TERT has been indicated to have non-canonical functions in other tissues,systems, and cells. For example, *Gizard et al.* showed that macrophages stimulated with pro-inflammatory mediators displayed increased TERT mRNA expression and telomerase activity, indicating that the TERT expressed was localised to the nucleus(146).

Further, the same researchers showed that TERT expression was modulated by NF-κB, as sequencing detected an NF-κB binding site in the TERT promoter region (Fig.1.4.2.2)(Table 1.4.2.2)(146). NF-κB was mediating the upregulation of TERT and pro-inflammatory cytokines(146). Further evidence published by *Wu et al.* indicates that the regulation of TERT by NF-κB is part of a negative feedback loop that influences macrophage physiology(147). In a murine model of Alcoholic liver disease (ALD), *Wu et al.* demonstrated that TERT expression and telomerase activity were upregulated in liver-associated macrophages(147). *Wu et al.* also demonstrated that using small-interfering RNA (siRNA) to knockdown TERT expression in cultured RAW264.7 macrophages led to a decrease in the secretion of inflammatory cytokines including TNF-α, IL-1β, IL-6, and IL-12(147). As these cytokines are associated with the pro-inflammatory M1 macrophage phenotype, this led to the hypothesis that TERT may be regulating macrophage polarisation. To examine this hypothesis, *Wu et al.* demonstrated that NF-κB stimulated the expression of p65 in liver tissue and Kupfer cells (KCs) (specialised liver macrophages). Further, the overexpression of TERT led to increased expression of p65, indicating again that NF-κB and TERT are part of the same feedback loop (Fig.1.4.2.2)(Table 1.4.2.2)(147). This supports the idea that TERT may be involved in regulating macrophage polarization and influencing the M1 phenotype due to its regulation of the expression of p65 and association with other inflammatory cytokines.

Further evidence of a regulatory relationship between TERT and NF-κB has been indicated by *Yang et al.* These researchers showed that micro-RNA 216a (mir216a). Mir216a is a mediator of Akt activation by Transforming Growth Factor-β (TGF-β) (Fig.1.4.2.2)(148). Overexpression led to increased TERT expression and telomerase activity, which potentially indicated that the additional TERT expressed remained localised to the nucleus(149). Further, *Yang et al.* showed via immunofluorescence (IF) analysis that mir-216a increased the translocation of NF-κB p65 subunit to the nucleus in macrophages and that this upregulation was further mediated by SMAD3(Fig.1.4.2.2)(149). Interestingly, mir216a also upregulated the expression of p53, p16, and SA-β-gal in M1-polarised macrophages indicating that mir216a may play a role in M1 macrophages entering senescence and further indicating that mir216a may play a role in modulating immunosenescence(149). Finally, *Yang et al.* showed that TERT overexpression in M2-polarised (anti-inflammatory)

macrophages *in vitro* caused them to switch to a phenotype more characteristic of M1, as measured by the markers Monocyte Chemoattractant Protein 1 (MCP1) and TNF-α(149). Together, data from *Gizard et al.*, *Yang et al.*, and *Wu et al.* suggest that TERT expression can modulate phenotypic characteristics of macrophages specifically contributing to the polarization of macrophages into the M1 subset, via NF-kB modulation(Table 1.4.2.2)(147, 150). However, further work needs to be performed to determine if the switching of macrophage subsets is mediated by the telomere elongating activity of telomerase, or by a non-canonical function of TERT that is independent of telomerase canonical activity.

Nuclear factor kappa-light-chain-enhancer of activated B cells (NF-κβ) is an important regulator of several processes in macrophage biology that can affect ageing tissues. For example, osteoclasts are cells responsible for the breakdown of bone tissue for the purpose of bone remodelling over time(92). Osteoclasts are formed from the fusion of macrophages due to the activity of Receptor Activator of NF-κβ Ligand (RANKL) and Macrophage Colony-Stimulating Factor (M-CSF)(40). The action of NF-κβ can be inhibited by Silent Information Regulator T1 (SIRT1), and it has been reported by *Edwards et al.* that this inhibition in osteoclasts and osteoblasts is integral to healthy bone remodelling in a murine model(Fig.1.4.2.2)(151). Additionally, *Edwards et al.* have shown that osteoclastogenesis is regulated by the interaction between NF-κβ and SIRT1 where osteoclastogenesis was promoted in *SirT1* knockout mice(151). Notably, further findings bring us back to the previously discussed non-canonical role of TERT in protecting mitochondria from ROS damage. SIRT1 was found to be a regulator of mitochondrial biogenesis via the PGC-1α pathway(152, 153). Additionally, SIRT1 is well reported to be involved in the macrophage inflammatory response pathway(154). As well as being an anti-inflammatory, the stimulation or increased expression of SIRT1 is indicated to increase positive outcomes in inflammatory disease and cancer(153, 155, 156). Thus, overall, I have discussed here how TERT, NF-κβ, SIRT1, and PGC-1α are potentially linked in a regulatory web. Further, there is evidence that TERT plays a role in protecting mitochondria from the activities of ROS and is linked via NF-κβ to SIRT1. Thus, it can be hypothesised that TERT is linked to the continued health and function of cells and tissues in a non-canonical manner that is extra to its function in elongating telomeres. Further, considering that TERT is evidenced to also play a

role in macrophage physiology, the role of TERT in macrophage immunosenescence may be an unexplored area of significant research interest.

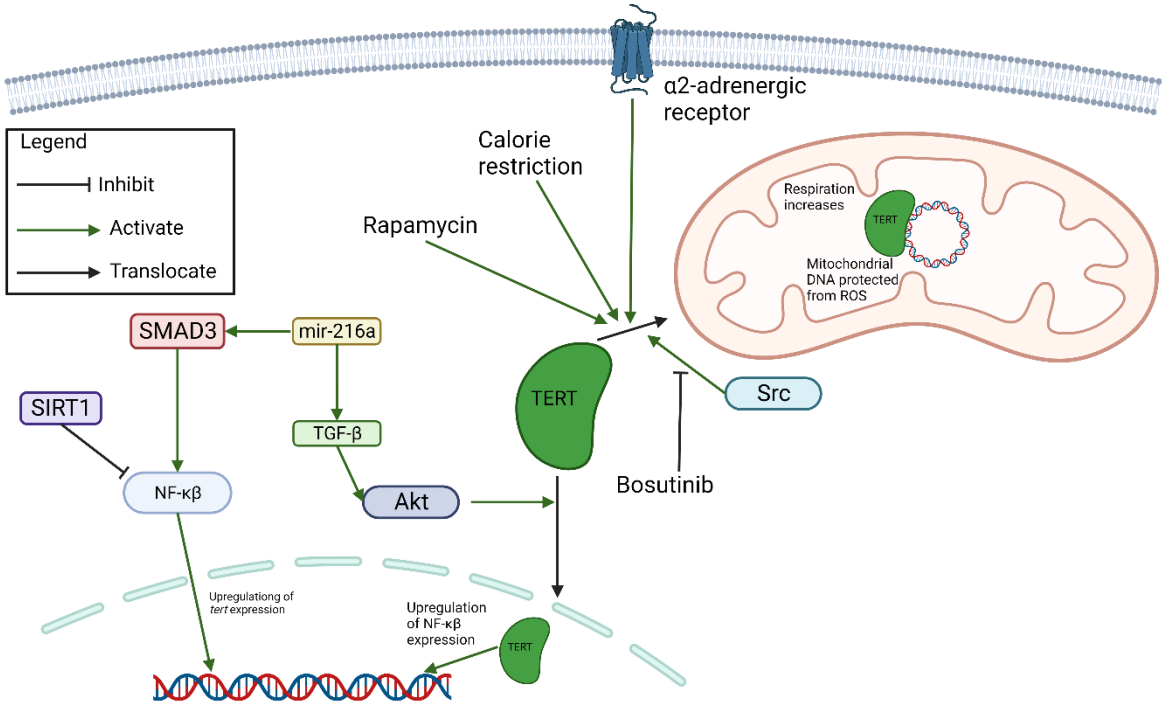

Figure 1.4.2.2: A representative diagram indicating non-canonical functions of the telomerase subunit TERT that have been reported. Separate publications indicate that TERT upregulates NF-κβ expression and this in turn is regulated by Sirtuin 1 (SIRT1), and micro-RNA 216a (mir-216a). TERT is also indicated to localise to the mitochondria, but this localisation may be influenced by molecular Target of Rapamycin (mTOR) and proto-oncogene tyrosine-protein kinase Src (Src). Overall this image indicates that TERT has several non-canonical functions that are tightly regulated by both intracellular and extracellular mechanisms.

Tissue or cell non-canonical function is observed in	**Location in Cell**	**Specific non-canonical function**	**Paper reported in**
Liver	Mitochondria	Protection from effects of ROS	Haendeler et al.
Brain	Mitochondria	Protection from ROS	Spilsbury et al.
Intestine	Mitochondria	Protection damage due to reperfusion injury	Hu et al.
Brain	-	Neuronal health/development	Zhou et al.
Brain	-	Neurotransmitter production	Zhou et al.
Brain	Mitochondria	Protection from effects of ROS	Miwa et al.
Macrophages/Liver	Nucleus	Feedback loop with NF-kβ via p65 regulating inflammatory cytokine expression	Gizard et al. Wu et al. Yang et al.

Table 1.4.2.2: Summary table of the non-canonical functions discussed in section 1.4.2.2 with the tissue or cell studied, the localization of TERT in the cells studied, the non-canonical function reported, and the paper reporting it.

1.5 Alleviating ageing and ageing-associated multimorbidity

As discussed in section 1.1, as humans age, the occurrence of multimorbidity increases(157). The increasingly ageing population coupled with the increase in multimorbidity occurrences has a disproportionate economic impact on healthcare infrastructure(10). Additionally, with ageing we observe an increase in frailty that occurs due to the hallmarks and diseases associated with ageing(12). Therefore, it is of great economic and social importance that we investigate potential treatments for ageing-associated diseases with the hope of alleviating their burden on both individuals and healthcare.

1.5.1 Lifestyle changes

One hypothesis proposes that as people age their activity levels decline and they become more sedentary. This causes a "chronic positive energy state" leading to weight gain and obesity(158, 159). Obesity leads to inflammation, and an increased risk of cancer, diabetes, and dementia; all of which are chronic diseases that increase in incidence with ageing. Therefore, obesity can, to a certain extent, act as a model of the effects of ageing(160, 161). Additionally, it has been observed that fat accumulates with age and that this accumulation is associated with a chronic low-grade inflammation caused by adipokines(162). However, regular physical exercise has been associated with a reduction in visceral fat that, in turn, leads to a decrease in the associated inflammation(162). This reduced inflammation has been suggested to be due to a decrease in the levels of pro-inflammatory cytokines including IL-6 and TNF-α, and an increase in the anti-inflammatory cytokine IL-10(162). Further, *Lowder et al.* demonstrated increased survival of mice that undertook moderate exercise when infected with influenza with respect to infected mice that did not undertake exercise(163). However, in the same study it was reported that mice that undertook vigorous exercise displayed a reduced survival rate(163). These results indicate that the benefits of exercise may be dependent on the type and duration of said exercise(163). However, these studies indicate the beneficial effects of exercise in an ageing-model context.

A second lifestyle change suitable for reducing the negative effects of ageing is calorie restriction. Calorie restriction is a well-documented method for extending lifespan in model organisms such as rats, mice, and apes(162). Further to this, calorie restriction has been

indicated to improve maintenance of the thymic microenvironment, reducing the effects of immunosenescence such as thymic involution, and increasing the number of circulating naïve T-cells (162). However, there are contraindicatory effects of calorie restriction. For example, *Effros et al.* have reported that calorie-restricted mice were able to mount an effective immune response to influenza(164). In contrast, *Ritz et al.* found that calorie-restricted mice displayed increased susceptibility to infection(162, 165). *Ritz et al.* hypothesised that increased susceptibility to infection had been masked by influenza vaccines being used as a proxy for infection(165). Logically they concluded that while the immune response may be upregulated in mice with calorie restriction, if the mice lack the calories necessary to mount an effective immune response then calorie restriction may be detrimental(165). Therefore, there is both evidence for and against calorie restriction as a method for alleviating age-related multimorbidity in mammals.

1.5.2 Anti-ageing therapeutics

Evidence indicates that the build-up of senescent cells with ageing is detrimental to health(12, 57). Therefore, senescent cells present an appropriate target for novel therapeutics aimed at their elimination, or the alleviation of their effects. By modulating senescence and removing senescent cells, we may be able to improve the healthspan of an individual. Senolytic therapies are aimed at the removal of senescent cells to extend healthspan and delay the onset of age-related diseases(166). Meanwhile, senostatic therapies target the SASP with the aim of alleviating its pro-inflammatory effects(167-169).

1.5.2.1 Senolytics

Two of the first senolytic drugs tested were Dasatinib and Quercetin(166, 170). Dasatinib is a chemotherapy drug primarily used to treat cancers that involve the Philadelphia chromosome translocation, whereby translocation of genetical material from chromosome 9 and chromosome 22 leads to the creation of the fusion gene *BCR-ABL1*, such as chronic myelogenous leukaemia and acute lymphoblastic leukaemia(171). Quercetin is a flavonol found in plants where it acts as polar auxin transport inhibitor. *Xu et al.* indicated that the administration of Dasatinib and Quercetin as a dual therapy to aged mice extended their median lifespan by 36%, independent of affecting physical fitness or the burden of multimorbidity(172). Subsequently the efficacy of a dual therapy of Dasatanib and Quercetin is being explored in humans. For example, *Justice et al.* conducted a pilot study on

fourteen patients with IPF(173). The researchers found that physical function in the patients was significantly improved after three weeks of the dual treatment(173). However, the reported health of the patients was unchanged and the effects on circulating SASP factors were undetermined, but changes were observed(173). In a separate pilot study, *Hickson et al.* used Dasatinib and Quercetin as a dual therapy to treat nine individuals with diabetic kidney disease(174). *Hickson et al.* found that administering the dual therapy for 3 days significantly decreased $p16^{Ink4a}$-positive cells in adipose tissue and significantly reduced circulating SASP factors IL-1α, IL-6, Matrix Metallopeptidase (MMP)-9 and MMP-12(174, 175). Therefore, these studies provide promising preliminary evidence that Dasatinib and Quercetin can prove an effective dual therapy for the improvement of healthspan and the alleviation of age-related multimorbidity. However, the small sample size of these studies prevents significant conclusions being drawn other than that further investigation is warranted.

Besides Dasatinib and Quercetin, there is evidence that the flavonoid, Fisetin, may also be a useful senolytic. *Yousefzadeh et al.* demonstrated in a progeroid *Ercc*$^{-/\Delta}$*;p16*^{Ink4a}*-luciferase* mouse line fed with a Fisetin diet (60mg/kg/day), that the expression of $p16^{INK4a}$-luciferase were significantly reduced with respect to untreated progeroid mice(176). Therefore, both flavonoids, Fisetin and Quercetin, have been reported to be functional senolytics. These findings warrant that other members of the flavonoid family be investigated for their senolytic potential(177).

Even considering these promising avenues for exploring senolytic, the removal of senescent cells may not be wholly desirable despite their evidenced contribution to increased frailty with ageing. *Grosse et al.* indicated that the majority of cells expressing high concentrations of p16 (marking that they had entered senescence) in mice livers were endothelial cells, macrophages, or adipocytes(178). *Grosse et al.* found that removal of senescent cells in the livers of young mice did not lead to the replacement of the senescent cells by younger cells, but instead by fibrosis(178). Further, investigating the removal of senescent cells in the liver of aged mice, *Grosse et al.* found that the blood vessels became more permeable(178). Therefore, we can hypothesise that the removal of senescent cells is not strictly better for the aged animal, and that further investigation into the effects of removing senescent cells in the aged is required before this becomes common practice.

1.5.2.2 Senostatics

The SASP burden that comes with a build-up of senescent cells is an appealing target for interventions intended to alleviate ageing and the symptoms experienced by long term cancer survivors(179). To alleviate this burden, research is being conducted into therapies termed senostatics that reduce the pro-inflammatory effects of the SASP. Currently the most widely researched senostatic is Metformin, which was originally developed to treat diabetes and polycystic ovary syndrome(180). *Hu et al.* found that in mice grafted with head and neck squamous cell carcinoma administration of Metformin plus a CDK4/6 inhibitor led to no significant change in the number of senescent cells, but did lead to the downregulation of SASP components IL-6 and IL-8(167). Further, *Fielder et al.* found that in a low-dose irradiation model of senescence in mice, administering Metformin led to a reduction in the levels of SASP components IL-17, CCL2, and TNF-α for over 6 months after the end of treatment(168). Together, these studies indicate that Metformin may provide a novel senostatic therapy for use in conjunction with senolytics to alleviate the effects of the SASP in the elderly, and in patients experiencing an increased senescence burden after chemotherapies aimed at inducing senescence in cancer.

1.5.3 Improved immunosurveillance with ageing

Immunosurveillance is the process by which the immune system detects immunogenic threats. Most commonly the immune system is searching for pathogens however evidence suggests that the immune system can also recognise and eliminate senescent cells(181-183). Therefore, a potentially fruitful avenue of research is enhancing the immune system's ability to remove senescent cells with ageing. Macrophages are essential to the clearance of senescent cells during tissue development. However, with ageing, macrophages enter immunosenescence and become less efficient at phagocytosis and so the clearance of senescent cells contributing to their accumulation(184, 185). *Tasat et al.* demonstrated that immunosenescent alveolar macrophages in rats have a decreased response to Toll-like Receptor (TLR) stimulation by Lipopolysaccharide (LPS) as well as reduced phagocytosis(186). Therefore, we can hypothesise that the elimination of senescent cells by macrophages is inhibited with ageing. Additionally, NK cells have been demonstrated by *Sagiv et al.* to remove senescent cells via granule exocytosis in mice liver tissue utilising upregulation of Decoy death receptor 2 (DCR2)(182). Therefore, both macrophages and NK

cells may be promising targets for improving the function of the immune system in removing senescent cells(183).

1.6 Model organisms of ageing

The field of gerontology has expanded since its inception and with it our understanding of how the mechanisms of ageing interact to cause disease. Significant progress has been made thanks, in no small part, to the use of different model organisms in the lab. Model organisms have conserved traits that allow the study of human traits without performing human trials. Model organisms are used widely in medical science as a basis to study the causes and treatments of human diseases. In ageing we look at organisms that share the mechanisms of ageing identified in humans, such as the erosion of telomeres and the accumulation of senescent cells.

1.6.1 *Saccharomyces cerevisiae*

Saccharomyces cerevisiae or yeast is a single-cell fungus that is estimated to share 30% of its genome with humans(194). Yeast has been widely used to study ageing(195). Yeast ageing is monitored using both replicative and chronological lifespan(195). The replicative lifespan refers to the number of cell divisions a mother cell can undergo before it dies and is used as a reference for undifferentiated stem cells(195). The chronological lifespan refers to using yeast to model differentiated cells that have ceased rapidly dividing(195). A drawback of yeast is that being a single-celled organism it cannot be used to accurately model the effects that ageing, or treating ageing, will have on the systems of a multicellular organism. Further, the separation of mother and daughter cells *in vivo* can provide a technically frustrating hinderance to ageing studies. However, yeast exhibit several phenotypes of ageing that are reflected in humans, such as the accumulation of ROS, and damaged organelles and DNA(195). The advantage of using yeast as a model is that it can be easily and quickly cultured, the maintenance of the culture is economically viable, it can be easily genetically manipulated, and it offers an *in vivo* model of ageing that is comparable to other eukaryotic organisms(195). Yeast has been used widely for the study of ageing at the genetic and molecular level(196). For example, the overexpression of *sir2* in yeast was one of the first identified interventions demonstrated to extend replicative lifespan(196). Further, yeast has been used to study the molecular basis for several hallmarks of ageing(12). These include

changes to the epigenome, mitochondrial dysfunction, and a decay of proteostasis(196). This has led to yeast being integral in the discovery of potential anti-aging compounds such as resveratrol and rapamycin(195).

1.6.2 *Caenorhabditis elegans*

Caenorhabditis elegans is a nematode worm that is one of the primary models used to study ageing. This worm presents advantages to studying ageing due to its affordability and having high fecundity. Additionally, as *C. elegans* is a multicellular organism, it contains some of the homeostatic organs we find in other multicellular model organisms, including a digestive tract, a reproductive system, and an early nervous system(197). *C. elegans* has been used extensively as model of ageing for lifespan studies due to it having genes homologous to those found in humans, testing experiments on caloric restriction and genetic manipulations proposed to extend lifespan(44, 197). For example, *Tullet et al.* found the short lifespan exhibited by *skn-1* mutants was mediated by the Forkhead Box Protein (DAF-16) transcription factor(198). The researchers found that overexpression of DAF-16 rescued the reduced lifespan of *skn-1* mutants up to 34%(198). As DAF-16 is conserved in humans, this study is an example of the use of *C. elegans* as a model of mammalian ageing(199). Drawbacks of using *C. elegans* as a model organism include the lack of organ systems that present in mammals, such as a circulatory system and respiratory system. Further, *C. elegans* lacks a complex immune system comparable to those found in vertebrates, and so the effects of ageing on the immune system cannot be studied. Further, the role of senescence and the SASP in *C. elegans* is not as well understood as in higher organisms(197). Additionally, while *C. elegans* is a useful model in the study of ageing, a study by *Bayat et al.* indicated that overexpression of telomerase did not lead to the elongation of telomeres in *C. elegans* (200).

1.6.3 *Drosophila melanogaster*

Drosophila melanogaster is a widely used model organism, the genome sequence of which was first published in its entirety in 2000(201). Using *D. melanogaster* as a model organism has many advantages including that it has high fecundity (a generation time of 10 days dependent on temperature), is cheap to maintain populations, and is easily genetically manipulable. However, there is a significant disadvantage in using *D. melanogaster* to study

telomere biology as *D. melanogaster* does not elongate telomeres in a manner comparable to humans (202, 203). Further, *D. melanogaster* does not age in a telomere-dependent manner as humans do. Instead of using the telomerase enzyme and instead uses the retrotransposon HeT-A (204) to elongate telomeres via the integration of telomere lengths post-reverse transcription. This is not to say that *D. melanogaster* is not a useful model organism in ageing research, as it has been used extensively to study neurodegenerative disorders that occur with ageing such as Alzheimer's disease(205), and how oxidative stress influences ageing(206).

1.6.4 Zebrafish - *Danio rerio*

Zebrafish are freshwater fish native to India and southern Asia that were pioneered as a model organism in the 1970's and 1980's by George Streisinger(207). Initially zebrafish rose to prominence as one of the first vertebrates to be successfully cloned(207)**.** However, in the following decades zebrafish has been cemented into the model organism pantheon in part due to its ease of use in toxicology screens, and its ability to regenerate injured tissues leading to its use in the fields of oncology, developmental biology, and regenerative biology(208-211)**.** Keeping zebrafish as a vertebrate model is considered more affordable when compared to keeping rodents or apes due to their small size allowing several thousand fish to kept in an aquarium, whereas a mouse colony of a similar number would require much more space, and apes even more. Zebrafish are a shoaling fish so are kept in groups of 4-12 fish per litre of water(212). Additionally, zebrafish have high fecundity and quickly develop to sexual maturity (3 months) enabling better statistical powering of experiments as the N can be increased(213). Further, the zebrafish genome has been fully sequenced, and it has been found that approximately 70% of human genes have at least one orthologue indicating good translatability into other model organisms and humans(214). A further advantage of using zebrafish to study ageing is that their genome can be readily altered to facilitate transgenic studies, using techniques such as small interfering RNA (siRNA), transposon-mediated mutagenesis using the tol2 system, and CRISPR/Cas9(216, 217). With regards to biogerontology, zebrafish have been shown to age in a telomerase-dependent manner comparable to that found in humans, demonstrating that zebrafish provide a useful model for studying the ageing phenotype in a whole organism context(218-220) (Fig. 1.6.4). Zebrafish ageing has been well-characterised in the literature, with several

of the hallmarks of ageing observed in humans also being observed in zebrafish, including telomere attrition and cellular senescence(12, 219, 221). Further to this, it has been demonstrated that zebrafish age in a telomerase-dependent manner analogous to that of humans, whereby with each round of cell division their telomeres shorten eventually leading to the cell becoming senescent or undergoing apoptosis(218, 220). Additionally, telomere length in zebrafish can be rescued via the activity of telomerase the same as it can be in humans, further demonstrating the similarities between zebrafish and human ageing(218, 219). Accordingly, the telomerase mutant zebrafish *tert*$^{-/-}$ model has been described as a premature ageing model, displaying several phenotypes associated with natural aging but in an accelerated manner; specifically, the *tert*$^{-/-}$ model exhibited gastrointestinal wasting, infertility, sarcopenia, and retina degeneration(218, 222). This indicates that zebrafish provides us with a useful model for gastrointestinal ageing(185, 219, 223).

Further to gastrointestinal ageing, there is evidence that indicates zebrafish are also a suitable model organism for use in studying immune cells. The presence gut resident immune cells such as macrophages and dendritic cells has been demonstrated, and zebrafish have both an innate and adaptive immune system comparable to that of other vertebrates(210, 224). Transgenic models have also been produced for the specific study of immune cell subsets, such as the *mpeg1.1:mCherry.caax* line(225, 226). Additionally, demonstrating the translatability of immune system studies, *D. rerio* macrophages have been shown to have active and immune-regulatory phenotypes as has been seen with mammalian macrophages(227). For example, *Nguyen-Chi et al.* has found that zebrafish macrophages, as with human macrophages, have the subsets M1 and M2(227). M1 macrophages are reported to have a pro-inflammatory phenotype whereas M2 macrophages have a regulatory phenotype(227). *Nguyen-chi et al.* found that macrophages of the M1 subset would switch to the M2 subset once local inflammation resolved, with M2 being identified by looking for mammalian M2 markers also found in humans, including transforming growth factor beta-1 (TGFβ-1), C-C chemokine receptor type 2 (CCR2), and C-X-C chemokine receptor type 4 (CXCR4), demonstrating the translatability of studies on zebrafish macrophages(227).

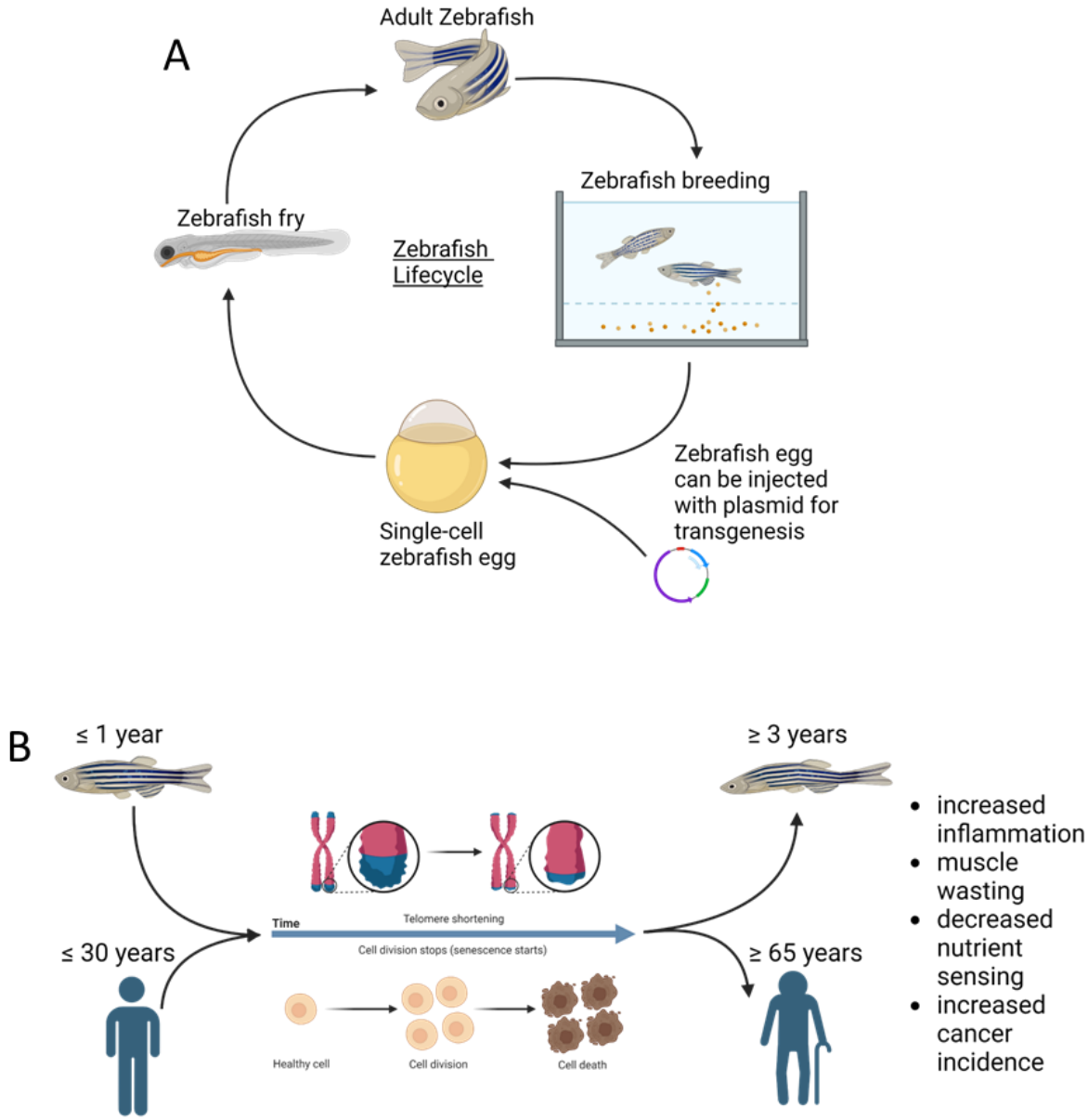

Figure 1.6.4: Zebrafish lifecycle and ageing. **A.** Illustrative figure of the zebrafish lifecycle indicating the ability to genetically engineer transgenic lines at the single-cell stage of development after breeding, and the ease of which internal organs can be observed in fry enabling easy study and selection using microscopy techniques. **B.** Illustrative comparison of zebrafish and human ageing indicating how both age in a telomere dependent manner which the accumulation of senescent cells leading to comparable ageing phenotypes.

1.6.5 Mice

Mice are one of the most widely utilised model organisms in research due the high homology they share with humans in terms of genes, proteins, and tissue structure and function(228). *Muñoz-Lorente et al.* demonstrated that generating mice with hyper-long telomeres in all tissues led to increased longevity and improved glucose and cholesterol regulation without increased cancer incidence(188). Further, work by *Amano et al.* demonstrated that telomere shortening in telomerase-knockout mice led to the repression of all seven characterised sirtuins(229). The sirtuin family of proteins are involved in DNA damage repair and knockout models have been shown to exhibit a prematurely-aged phenotype(230). Additionally, work from the Blasco lab performed on either aged WT mice or progeroid mice has been seminal in characterising the role of telomeres and telomerase in diseases of ageing such as CHD(231). However, the use of mice in telomere biology research was previously hindered due to the telomeres of inbred lab strains not shortening for several generations despite knocking out the action of telomerase(232). Furthermore, relative to the other model organisms discussed above mice are more expensive to maintain and require a greater level of care to ensure that the animal does not undergo unnecessary stress or disease. Therefore, as with all experiments utilising protected organisms, it is necessary to consider if the experiment truly requires the use of an entire model organism or if alternative methods such as cell culture would prove equally useful.

1.7 Previous work that led to the hypothesis and chosen model organism.

In this introduction we have discussed the hallmarks of ageing, with a focus on immunosenescence and the role of telomeres and telomerase. Further, we have briefly covered model organisms that are currently used to study ageing. From these discussions it can be concluded that telomeres, and by extension the telomerase enzyme, are an integral part of cell function and zebrafish present an appropriate model organism with which we can study telomere and ageing biology(213, 233). For example, prior work by *Henriques et al.* has shown that *tert*$^{-/-}$ zebrafish age and die prematurely(218). The researchers demonstrated that *tert*$^{-/-}$ zebrafish develop premature infertility, sarcopenia, accumulation of DNA damage, p53 activation, and accumulation of senescent cells in(218). Moreover,

premature necrotising enteritis was observed in the *tert*$^{-/-}$ zebrafish and correlated with the accumulation of senescent cells in their guts(218). These ageing markers are also observed in naturally aged zebrafish, confirming that the telomerase mutant zebrafish represents a premature model of ageing and that ageing phenotypes in zebrafish are therefore likely to be telomerase and telomere dependent(220).

Additional advantages of using zebrafish to study ageing include the ease with which they are genetically manipulated, and that as vertebrates their physiology is largely conserved to humans including an adaptive and innate immune system. For example, *Nguyen-Chi et al.* has found that zebrafish macrophages have pro-inflammatory M1 and regulatory M2 subtypes comparable to humans(227). These subsets were identified by looking for mammalian M2 markers also found in humans, including TGFβ-1, C-C chemokine receptor type 2 (CCR2), and C-X-C chemokine receptor type 4 (CXCR4)(227). This indicates the translatability of studies on zebrafish macrophages to humans(227). Additionally, transgenic zebrafish lines exist that increase the ease with which we can study immune cell subsets, such as the *mpeg1.1:mCherry.caax* line(225, 226). This line utilises the *mpeg1.1* promoter to express the mCherry fluorophore in macrophages and B-cells(226, 234). Therefore, we can see that zebrafish are both an appropriate model of ageing, and a useful experimental animal in studying the immune system. Hence, they provide us with a system for studying the aged immune system.

The *mpeg1.1* promoter was initially identified as a macrophage specific promoter in murine macrophages under the name *mpg-1*, with evidence also being observed in human macrophages (235). Subsequently, *mpeg1.1* expression was identified in embryonic macrophages in zebrafish larvae (236). Consequently, work by *Ellett et al.* details the production of a novel line of transgenic zebrafish that contains the *mpeg1.1* promoter conjugated to *mCherry*, which codes for the mCherry fluorophore (226). The generation of the *mpeg1.1:mCherry.caax* reporter line allowed *Ellett et al.* to study macrophages more easily, as previously the identification of macrophages in zebrafish was based on physical characteristics (i.e. motility, location, morphology) and by utilising the *mpx:eGFP* reporter line which indicated both macrophages and neutrophils (226). However, work published by *Ferrero et al.* indicated that the *mpeg1.1* promoter was not exclusive to macrophages, but instead may also be expressed in B-cell populations derived from zebrafish gut, peritoneum,

and head kidney (234). Additionally, work published by *Moyse et al.* demonstrated that -*mpeg1.1*$^{+}$ B-cells and NK-like cells can be detected in the skin, spleen, heart, and blood of adult zebrafish (237).

Demonstrating the use of zebrafish as a useful model of the ageing immune system, *Ellis et al.* identified populations of *mpeg1.1*$^{+}$ cells in the zebrafish gut with telomerase dependent hyper long telomeres(185). The researchers found that that a high number of these cells were macrophages with telomeres longer than macrophages found in their haematopoietic tissue of origin, indicating a regulation of the expression of *tert* and therefore telomerase activity(185). Further, *Ellis et al.* found a subset of *mpeg1.1*$^{+}$ immune cells expressed *tert* in young zebrafish (<6 months) but that the number of these *tert* expressing *mpeg1.1*$^{+}$ cells decreased with age(185). Additionally, the decrease in *tert* expression occurs in tandem with increased DDR, telomere shortening, decreased expression of immune response and autophagy markers, reduced phagocytic function *in vivo*, and increased gut permeability(185). Therefore, we can hypothesise that rescuing *tert* expression in these *mpeg1.1*$^{+}$ cells may rescue their aged phenotype. Further, that rescuing *tert* expression in *mpeg1.1*$^{+}$ cells may impact tissue ageing in the gut.

1.7.1 PhD hypothesis and aims.

The primary hypothesis of this project is that telomerase has non-canonical functions that affect the health of gut-associated macrophages via the TERT subunit. To test this hypothesis, we have generated two transgenic zebrafish lines with differing telomerase activities. To generate these lines, we have used an existing telomerase mutant (*tert*$^{-/-}$) zebrafish line that possess an *mpeg1.1:mCherry.caax* transgene. This allows for the convenient visualization of cells that utilise the *mpeg1.1* promoter. Both transgenic lines were generated in zebrafish that were bred to be homozygous *tert*$^{-/-}$ which has been characterised to have no detectable telomerase activity(218).

The first transgenic line will express canonically active TERT under the control of the *mpeg1.1* promoter. The second transgenic line will express an alternative version of TERT that lacks the TERC binding site, and so will be canonically inactive such that it will not elongate telomeres as part of the telomerase complex. This expression of this second transgene will also be under the control of the *mpeg1.1* promoter. I will refer to the

mutated version of TERT as ΔTERT and correspondingly the mutated *tert* gene will be referred to as *Δtert*. Zebrafish were chosen as the model organism for this study as they age in a telomerase-dependent manner that is comparable to humans(218, 232). The objective of this PhD thus became to generate two novel zebrafish lines, one containing *mpeg1.1:tert* and one containing *mpeg1.1:Δtert*, for the further study of the role of telomerase in zebrafish *mpeg1.1*$^{+}$ cells. An additional aim was to determine the effects that zebrafish ageing has on immune cell populations present in the zebrafish gut using single-cell RNA sequencing. Therefore, in summary, the objectives were as follows:

1. Establish a transgenic zebrafish line that is *tert*$^{+/-}$*;mpeg1.1:mCherry.caax;mpeg1.1:tert-gfp.*
2. Establish a second transgenic zebrafish line that is *tert*$^{+/-}$*;mpeg1.1:mCherry.caax;mpeg1.1:Δtert-gfp.*
3. Perform single-cell RNA sequencing on whole zebrafish gut using the generated transgenics.
4. Determine how ageing alters the gene expression in the zebrafish gut and how rescuing the expression of TERT or ΔTERT affects gene expression in the prematurely aged zebrafish gut.

The establishment of the *tert*$^{+/-}$*;mpeg1.1:mCherry.caax;mpeg1.1:tert-gfp* line had been initiated before I entered the research programme, with Pam Ellis using the *tol2* transposon system to establish G_0 founders. I continued with the selection and breeding of the line, as well as the characterisation of the insertion. To establish the *tert*$^{+/-}$*;mpeg1.1:mCherry.caax;mpeg1.1:Δtert-gfp* line I planned to use the Gibson assembly (GA) method to produce a construct containing the *mpeg1.1:tert-gfp* gene. I then aimed to use the *tol2* transposon system to insert the gene into fertilised zebrafish eggs. Breeding and selection will then be performed to establish a stable line, which can then be characterised in the same manner as the *tert*$^{+/-}$*;mpeg1.1:mCherry.caax;mpeg1.1:tert-gfp* line. To characterise the two lines, the first step would be to determine if the transgene was being expressed in mCherry^{+} cells using fluorescence immunohistochemistry. Whole genome sequencing would then be used to establish the insertion site of the transgenes to ensure that their insertion did not affect zebrafish biology by disrupting other genes. At the same time, I aimed to optimise a process for the isolation of a zebrafish live whole gut suspension

that is suitable for single-cell RNA sequencing. Single-cell RNA sequencing of *tert*$^{+/+}$*;mpeg1.1:mCherry.caax* and *tert*$^{-/-}$*;mpeg1.1:mCherry.caax* would be used to characterise the ageing zebrafish gut, focusing on the resident immune cell populations. Single-cell RNA sequencing would also be used to determine if *mpeg1.1:tert-gfp* rescues the gene expression in *tert*$^{-/-}$*;mpeg1.1:mCherry;mpeg1.1:tert-gfp* fish.

Chapter 2: Materials and Methods

2.1 Zebrafish

2.1.1 Zebrafish husbandry

All zebrafish were housed in the aquarium at the Bateson Centre, University of Sheffield, and maintained with a 14 hour-light and 10 hour-dark cycle, at 27-28°C. Zebrafish were supervised by the NACWO (Named Animal Care and Welfare Officer) from the Biomedical Sciences Department, University of Sheffield. All experimental procedures involving zebrafish were performed in accordance with UK legislation – Animals (Scientific Procedures) Act 1986 - under the Project Licence (PPL) 70/8681, PPL holder Dr. Catarina M. Henriques and the personal license I1FEC8906 held by Luke Mansfield. All tests involving zebrafish manipulation were approved beforehand through the submission and respective approval by the aquarium manager of an Individual Study Plan (ISP).

2.1.2 Zebrafish lines

The telomerase mutant line (*tert*$^{AB/hu3430}$), available at the Zebrafish Information Network (ZFIN) repository (ZFIN ID: ZDB-GENO-100412-50) from the Zebrafish International Resource Centre (ZIRC), was previously described by *Henriques et al*(218). In brief, the *tert*$^{AB/hu3430}$ contains a point mutation in the *tert* gene, generated by N-Ethyl-N-nitrosourea (ENU) mutagenesis, that prevents RNA translation and consequent protein formation. For simplicity, the *tert*$^{AB/hu3430}$ homozygous mutants will be referred to as *tert*$^{-/-}$. Due to it having been indicated that *tert* mutants are generally infertile, the *tert*$^{AB/hu3430}$ used in this project are derived from in-crossing *tert*$^{AB/hu3430}$ heterozygotes, which for the sake of simplicity will be referred to as *tert*$^{+/-}$(218, 238). Zebrafish that do not contain the *tert*$^{AB/hu3430}$ mutation and so have fully functional telomerase are referred to as *tert*$^{+/+}$.

The *mpeg1.1:mcherry.caax* line is an immune reporter line where phagocytes express the fluorescent protein mcherry and therefore can be easily identified(226, 234). This line was used in some experiments of this project to identify phagocytes. For that, *tert*$^{+/-}$; *mpeg1.1:mcherry.caax* progeny were incrossed to generate both *tert*$^{+/+}$; *mpeg1.1:mcherry.caax* and *tert*$^{-/-}$;*mpeg1.1:mcherry.caax*.

When possible, when comparing *tert*$^{+/+}$;*mpeg1.1:mcherry.caax* and *tert*$^{-/-}$; *mpeg1.1:mcherry.caax* age-matched siblings were used. In some tests due to the limitation

in numbers of fish at specific ages age-matched non-siblings were used instead, including *tert*$^{+/+}$;*mpeg1.1:mcherry.caax* and *tert*$^{-/-}$;*mpeg1.1:mcherry.caax* reporter lines. Additionally, age-matched WT(AB) fish were used on occasion when appropriate due to a lack of available age-matched *tert*$^{+/+}$;*mpeg1.1:mcherry.caax* siblings at the time the experiment was carried out. Unless otherwise stated, WT(AB) refers to *tert*$^{+/+}$ fish.

2.2 Plasmids used for cloning.

Two pre-existing lab plasmids and one novel plasmid were used for the cloning process used to produce the sections for the *mpeg1.1:Δtert-gfp* plasmid.

2.2.1 *mpeg1.1:tert-gfp*

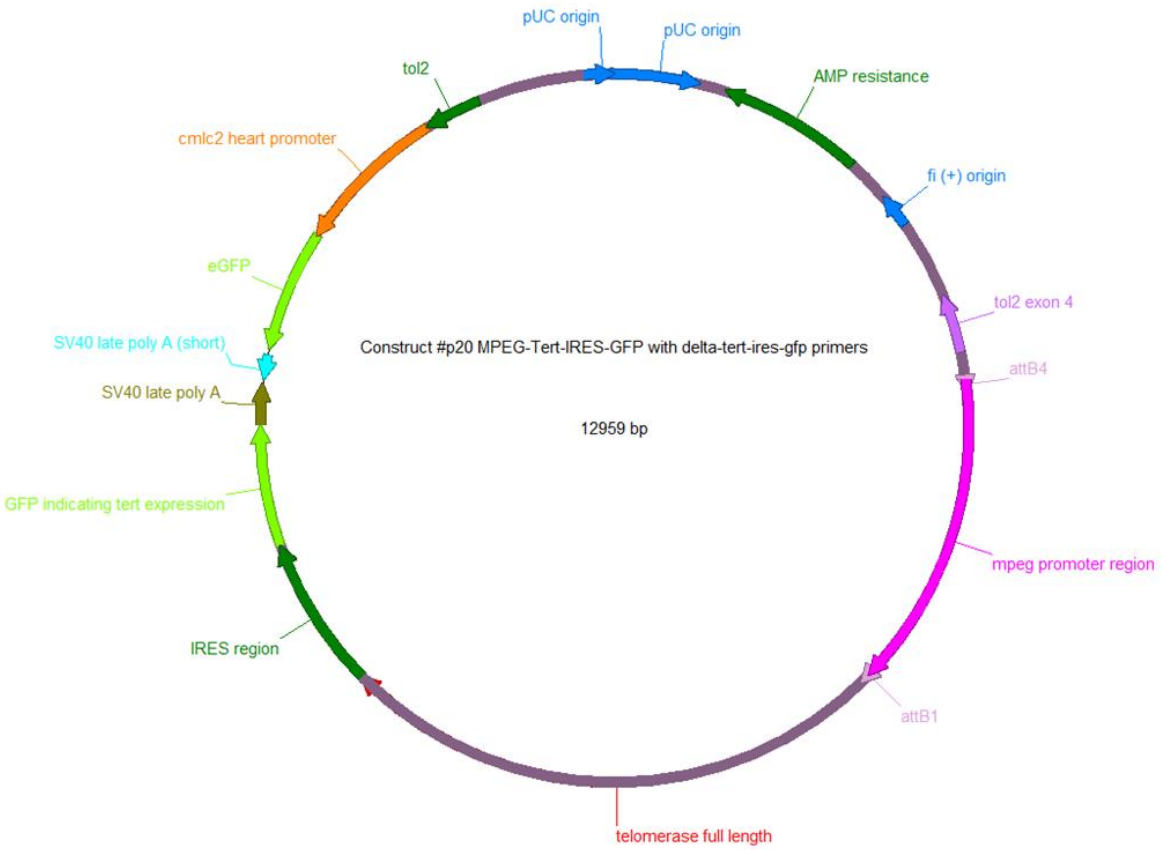

Figure 2.2.1: Map of the *mpeg1.1:tert-gfp* construct used to produce ligation components for the generation of the *mpeg1.1:Δtert-gfp*.

2.2.2 *IFABP:tert-gfp*

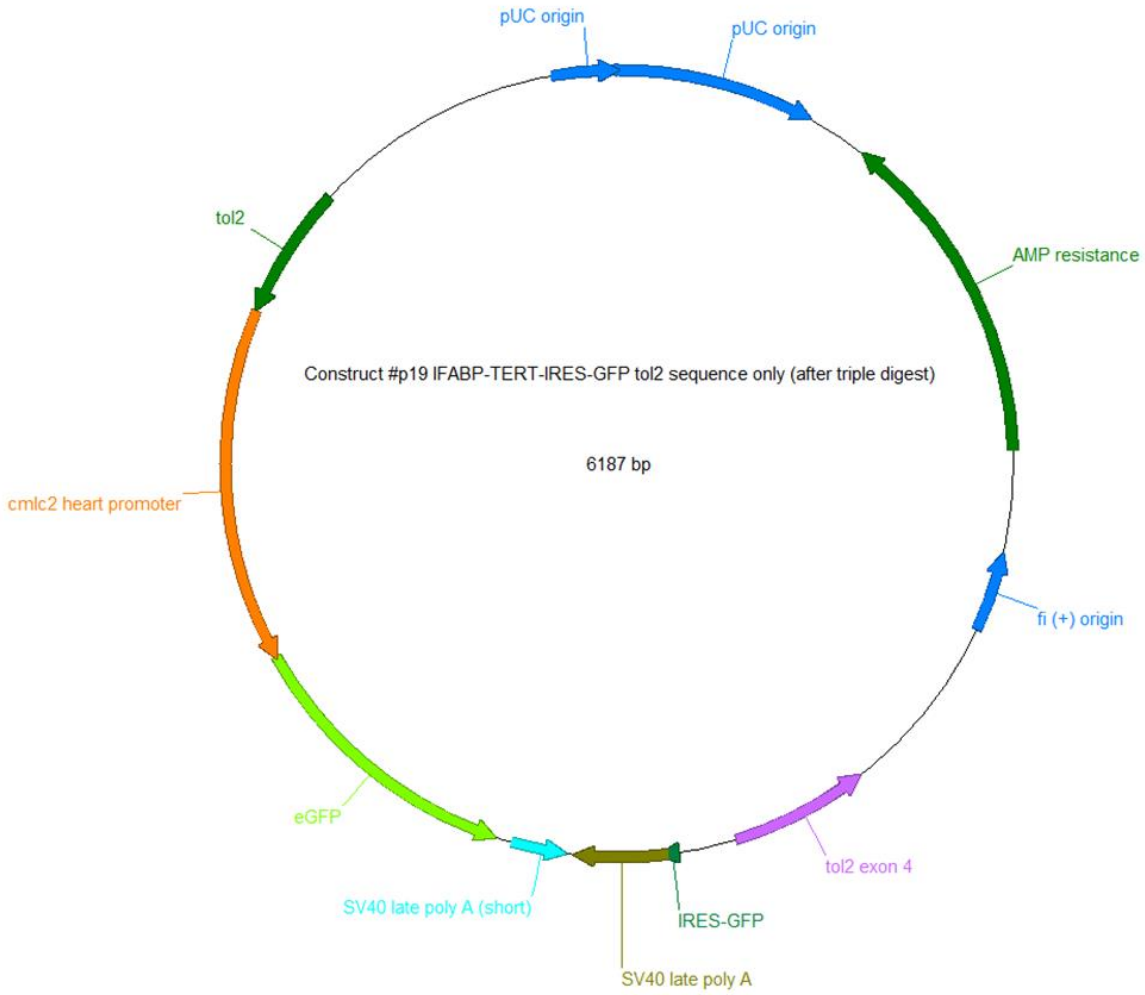

Figure 2.2.2: Map of the *IFABP:tert-gfp* construct used to produce ligation components for the generation of the *mpeg1.1:Δtert-gfp*.

2.2.3 *Δtert* inserted into the pGEM-T easy vector

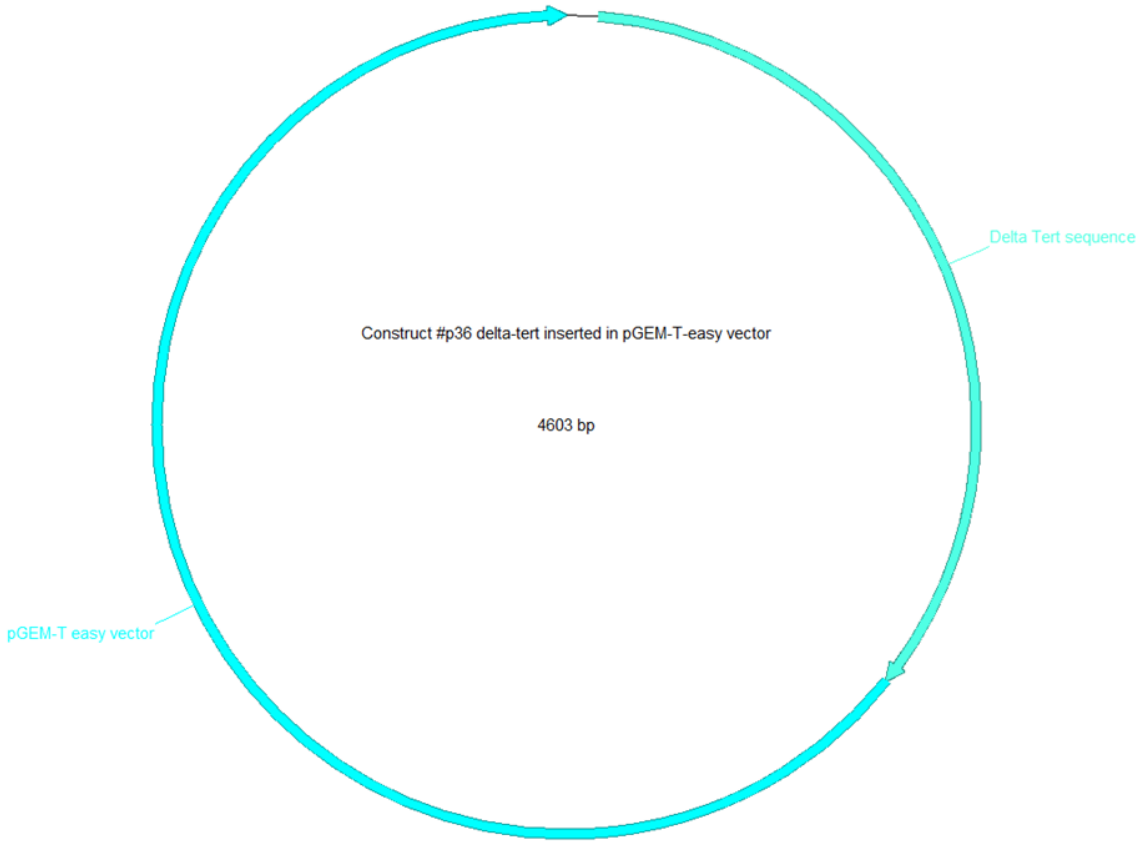

Figure 2.2.3: Map of the *Δtert* component inserted into the pGEM-T easy construct later used to produce ligation components for the generation of the *mpeg1.1:Δtert-gfp*.

2.3 Enzymatic digestions

2.3.1 Plasmid linearisation

An 80µl mixture was made that contained 2µl of Sal1-HF (New England Biolabs, #R3138), 8µl of 10x NEB buffer (New England Biolabs, Ipswich, MA, #B7200S), plasmid to a final concentration of 50ng/µl and dH_2O up to 80µl. The mixture was incubated at 37°C for 5 hours.

2.3.2 Diagnostic digests

Diagnostic digests were performed on constructs before sequencing to filter out clones that did not contain the desired sequence. Diagnostic digests give a specific banding pattern according to the enzyme used. This banding pattern can be predicted in silico and compared to that observed when the digested DNA is analysed using gel electrophoresis. Digests were performed using 0.3µl of each desired enzyme, 5µl of the purified miniprep, 2.5µl 10X Cutsmart buffer, and dH_2O up to a final volume of 25µl. The digestion was performed in a Bio-rad T100 thermal cycler at 37°C for 5 hours. Using the NEB software NEB cloner® we checked the activity of the enzymes in Cutsmart buffer, the recommended digestion temperature and time, before digestion, to avoid star activity.

2.3.3 Tol2 backbone production

To isolate the tol2 backbone section for use in GA of the lab stock *IFABP:tert-gfp* plasmid was triple digested in a 90µl mixture. The mixture contained 28.8µl plasmid with a final concentration of 100ng/µl, 1.5µl each of SalI-HF, ClaI and BamH1, 9µl 10x cutsmart buffer, and dH_2O up to 90µl.

2.4 PCR amplification

Polymerase Chain Reaction (PCR) was performed using a Bio-rad T100 Thermal cycler. Amplification was achieved in a 50µl reaction volume consisting of 10µl 5x Q5 reaction buffer (New England Biolabs, Ipswich, MA, #MO491S), 1µl dNTPs (final concentration 200µM) (Thermo Fischer scientific, Waltham, MA, #R0181) 2.5µl forward primer (final concentration 0.5µM) (Integrated DNA technologies, Coralville, IA) 2.5µl reverse primer (final concentration 0.5µM) (Integrated DNA technologies), 1µl plasmid template (1ng/µl stock), 0.5µl Q5 High-Fidelity DNA polymerase (New England Biolabs, Ipswich, MA, #MO491S), and nuclease free water up to 50µl. The thermal cycler was programmed for 2 minutes at 98°C for initial denaturation, followed by 35 cycles of 30 seconds at 98°C for denaturation, 30 seconds at variable temperatures for annealing, 72°C for extension with variable times, and a final extension for 2 minutes at 72°C.

2.4.1 Primers used.

Primers used for PCR reactions reported in this thesis can be found listed below.

Primer Number	Primer name	5'-3' sequence
1	mpeg1.1-promoter-forward	aaacagactacAAAGTTGTTGGAGCACATCTG
2	mpeg1.1-promoter-reverse	tggcccttcatAAACTTGTTTTGCTGTCTCC
3	Δtert forward primer	TCATCTGTGTAAGGGCCAGT
4	Δtert reverse primer	CAGGTTTTTTTTACACCCGC
5	Δtert-IRES-GFP Reverse	ttatcatgtctggatcatcatcgatCATCGATTGTATAA TAAAGTTGGAAAAAACCTCCC
6	Δtert-IRES-GFP Forward	caaaacaagtttgATGAAGGGCCAGTGGAGGCC
7	tol2-vector-ires+heart_fwd_corrected	aaaacctgaaCTTTCTTGTACAAAGTGGCC
8	tol2-vector-ires+heart_rev	acaactttGTAGTCTGTTTTTTATGCAAAATC

Table 2.4.1: A table of all primers used for the experiments described in this thesis.

2.5 Gel electrophoresis

DNA products were examined by electrophoresis at 130V for 3 hours in a 0.7% (w/v) agarose (Lonza, Basel, Switzerland, #50004) gel with 0.5% gel red (Biotium, Fremont, CA, #41003) stain in 1x TAE buffer (made in house). The electrophoresis gel was examined under a U.V. light and the marker used was a 1kb DNA ladder (Bioline reagents, London, U.K., #BIO-33026).

2.5.1 1x TAE stock

The 1x TAE stock was produced using 4.488g/l of Tris Base, 1.21ml/l of Acetic acid, and 0.372g/l of Ethylenediaminetetraacetic acid (EDTA).

2.6 NEBuilder® HiFi DNA Assembly Cloning Kit cloning protocol

To produce a *mpeg-tert-IRES-GFP* clone for injection the NEBuilder® HiFi DNA Assembly Cloning Kit (New England Biolabs, # E2621) was used according to the manufacturer's guidelines. The guidelines recommend using a 1:2 molar ratio of vector to insert. The

concentrations of the assembly reaction components were worked out using the equation pmols = (weight in ng) x 1,000 / (base pairs x 650 daltons) as recommended by the manufacturers protocol. A mixture was made that 0.03–0.2pmols of each section of the assembly, 10µl of NEBuilder® HiFi DNA Assembly Master Mix (New England Biolabs, # E2621), and dH_2O up to 20µl.

2.7 NEBuilder® HiFi DNA Assembly Cloning Kit transformation protocol

Transformation of the clone produced using the NEBuilder® HiFi DNA Assembly Cloning Kit (New England Biolabs, # E2621) was performed using NEB 5-alpha competent cells provided with the kit, recommended for use with assemblies of less than 15kb, according to the manufacturers protocol. Chemically competent cells were thawed on ice before 2 µl of the chilled assembly product was added. This was then mixed gently by pipetting up and down 4–5 times. Due to the fragility of the competent cells, it is not recommended to use a vortex to mix. The mixture was then placed on ice for 30 minutes. The mixture was then heat shocked in a water-bath at 42°C for 30 seconds. The tubes were then transferred to ice for 2 minutes before 950µl of room-temperature Super Optimal Broth (SOC) media was added. The tubes were then incubated at 37°C for 60 minutes while being shaken at 250 rpm. While the tubes were incubating 100µg/ml Ampicillin selection plates were warmed to 37°C. After 1 hour of incubation 100µl of the incubated cells were spread onto the warmed selection plates, which were then incubated overnight at 37°C.

2.8 *Δtert* PCR product A-tailing

For the *Δtert* PCR product to be cloned into the pGEM-T easy vector it first had to undergo A-tailing. A-tailing was performed in a 10µl reaction volume consisting of 7µl of *Δtert* PCR product, 1µl of 10x standard taq buffer (New England Biolabs, #B90145), 1µl of standard taq polymerase (New England Biolabs, #M02735), and nuclease free water up to 10µl. The reaction was incubated at 70°C for 30 minutes then placed on ice.

2.9 pGEM-T easy cloning

DNA products such as PCR amplifications can be inserted into the pGEM-T easy vector as it contains multiple restriction enzyme sites that allow the easy digestion and purification of

any insert from minipreps of transformed competent cells. This was performed using the pGEM-T easy vector systems cloning kit (Promega, Madison, WI, #A1380). Insertion was performed according to the manufacturer's guidelines. Insertion was performed in a reaction mixture consisting of 5µl 2X Rapid Ligation Buffer, 1µl pGEM-T easy vector (stock concentration 50ng/µl), 1µl T4 DNA ligase (stock at 3 Weiss units/µl), varying concentrations of DNA insert, nuclease free water up to 10µl. The concentrations of DNA insert added were calculated using the equation: (ng of vector x kb size of insert/kb size of vector) x insert:vector molar ratio = ng of insert.

2.10 LB/ampicillin/Isopropyl β-d-1-thiogalactopyranoside (IPTG)/X-Gal plates

Sterile warm LB (lysogeny broth) agar with 100µg/ml Ampicillin was poured into a petri dish (35ml). The LB agar was left to set in the petri dish at room temperature on a sterilised workbench (sterilised using 70% ethanol) for 1 hour. After this, 40µl of X-Gal Solution (20 mg/ml) (Thermo Scientific, Cat #R0941) was added and spread around the plate use a sterile glass spreader, before 40µl of 100mM IPTG Solution (Thermo Scientific, Cat #R1171) was also spread around the plate using a sterile glass spreader. If plates are to be used on the day, they should be incubated at 37°C until needed, if plates are not to be used on the day, they may be stored for up to one month at 4°C.

2.11 Liquid culture protocol

To 50ml of LB broth Ampicillin was added to a final concentration of 50µg/ml. To this broth the either the colony or glycerol stock that a culture was to be made of was added using a sterile wire loop to remove either the colony or some of the glycerol stock. The wire loop was sterilised using a blue Bunsen flame and 70% ethanol once cool.

2.12 pGEM-T easy transformation protocol

Before transformation prepare two LB/ampicillin/IPTG/X-Gal plates for each ligation reaction and warm the plates to room temperature. First 2µl of each ligation reaction was added to separate 1.5ml microcentrifuge tubes on ice. The frozen JM109 High Efficiency Competent Cells (Promega, #A1380) from storage and place on ice until just thawed (this will take around 5 minutes). The defrosted competent cells were mixed by gently flicking the

tube. The manual recommends avoiding excessive pipetting due to the competent cells being extremely fragile. 50µl of competent cells were transferred into each tube containing a ligation reaction. These mixtures were then mixed by gently flicking the tubes before they were then placed on ice for 20 minutes. Next the mixtures were heat-shocked for 45 seconds in a water bath at exactly 42°C. The tubes were then immediately returned to ice for 2 minutes. 950µl of room-temperature SOC medium was then added to the mixtures, which were then incubated for 1 hour 30 minutes at 37°C with shaking at around 150rpm. After this incubation period 100µl of each transformation culture was plated onto LB/ampicillin/IPTG/X-Gal plates. Additionally, the remaining mixture was centrifuged at 1,000*g* for 10 minutes, resuspended in 100µl of SOC medium, and plated onto LB/ampicillin/IPTG/X-Gal plates. The plates were then incubated overnight at 37°C. White colonies contain inserts whereas blue colonies do not. Storing the plates at 4°C for several hours can aid in the development of the blue colouration.

2.13 Agar plates

3g of bacto-agar was added to 200ml LB broth, the mixture autoclaved and 200ul of Ampicillin (stock 50mg/ml) added when the agar was cool enough to handle. Pour plates aseptically and allow to set and dry in aseptic conditions.

2.14 Quick mini-prep protocol

The quick mini prep is a faster, cheaper, miniprep than a miniprep kit that is performed using reagents made in-house. Colonies were chosen to be cultured over-night in a liquid culture of 10ml LB broth with 50µg/µl Ampicillin. 1.5ml of the culture was centrifuged for 3 minutes at 3000 RPM and the pellet then re-suspended in 100µl of TE+ (Tris-EDTA) and 1/100 RNAse A dilution from RNAse A stock (#R4642-50MG Sigma). 300µl of Tris-EDTA-Sodium hydroxide (NaOH)-Sodium Dodecyl Sulfate (SDS) (TENS) was added and mixture vortexed until sticky/viscous. 150µl of 3M Potassium Acetate pH 5.2 was then added and the mixture vortexed for 2-5 seconds before being centrifuged for 5 minutes at 13,000 Rotations Per Minute (RPM) and the supernatant transferred to a fresh tube and mixed with 900ul of chilled (in -20^{O}C freezer) 100% ethanol. The mixture was then centrifuged for 2 minutes at 13,000 RPM at 4°C, the supernatant discarded, and the pellet washed by adding 500ul (chilled in -20°C) 70% ethanol and centrifuging for a further 2 minutes at 13,000 RPM.

The pellet was then dried for 15 minutes at 37°C in an Eppendorf thermomixer F1.5 to remove excess ethanol, before being re-suspended in 50µl dH_2O

2.14.1 TENS solution

The EDTA present in the TENS solution chelates Mg^{2+} and Ca^{2+} which are required for the function of DNAses, therefore preventing the degradation of the DNA by these enzymes. TENS solution is made in-house to the following protocol (for 50ml):

-10mM Tris pH 7.5 (0.5ml of 1M stock)

-1mM EDTA pH 8.0 (0.1ml of 0.5M stock)

-0.1M NaOH (1ml of 5M stock)

-0.5% SDS (2.5ml of 10% stock)

2.15 Glycerol stocks protocol

Glycerol stocks are made of any successfully transformed bacteria by adding 500µL of the overnight culture to 500µL of 50% glycerol in a 2ml eppendorf tube and freeze immediately in dry ice. Glycerol stocks are stored at -80°C.

2.16 Clean Miniprep protocol

For a higher quality purification of DNA for sequencing the Sigma-Aldrich GenElute HP Plasmid Miniprep Kit (#NAO150) was used according to the manufacturer's instructions. 1.5ml of transformed cells were centrifuged at 12,000g for 1 minute. The supernatant was discarded, and the cells resuspended in 200µl of resuspension solution with the RNase A added. The pellet was pipetted up and down to thoroughly resuspend the cells until they were homogeneous 200 µl of the lysis buffer was added. The solution was then mixed gently inverting the tube until the mixture became clear and viscous. It is not recommended to use vortex due to the fragility of the DNA, additionally the lysis reaction should not be left for longer than 5 minutes as this may also affect the quality of the final eluted DNA. 350µl of the neutralization buffer was added and the tube gently inverted 6 times to mix. The cellular debris were then pelleted by centrifuging at 12,000g for 10 minutes. While the mixture was centrifuging, the columns were prepared by inserting them into the provided microcentrifuge tubes, adding 500µl of the column preparation solution to each column and

centrifuging at 12,000g for 1 minute. After centrifuging the cleared lysate was loaded into the prepared columns, and these were then centrifuged at 12,000g for 1 minute. The flow through was discarded, and the columns washed with by adding 500µl of wash solution 1 and centrifuging 12,000g 1 minute. The flow through was then discarded and the column washed again by adding 750µl of the diluted wash solution 2 to the column and centrifuging at 12,000g for 1 minute. The flow through was discarded, and excess ethanol removed by centrifuging the column at 12,000g for 1 minute. Finally, the DNA was eluted by transferring the column to a fresh tube and adding 50µl of dH_2O before centrifuging at 12,000g for 1 minute.

2.18 Sequencing

2.18.1 Plasmid sequencing

Sequencing was performed by the Core Genomics Facility at University of Sheffield Medical school.

2.18.2 Whole genome sequencing

Whole genome sequencing was performed on DNA extracts from zebrafish tail fin clips using the DNA extraction kit (Fermentas). DNA quality and concentration was initially assessed using a Nanodrop spectrophotometer by loading 1µl of DNA extract and observing the 260nm and 280nm readings to determine protein contamination levels. Sequencing was performed by Source Bioscience using Illumina 150bp paired-end sequencing.

2.18.2.1 DNA extraction using kit

Zebrafish are put under anaesthetic before fin clips are taken from end of the zebrafish tail. Zerbafish recovery is observed throughout the procedure to ensure that the fish does not suffer with the stress levels assessed and recorded after each procedure. Fin clipped fish are kept separate from their shoal until the tail clip has healed sufficiently that the shoal will not act aggressively towards the clipped fish.

Cut fins are placed into a 2 ml eppendorf tube containing the lysis buffer and incubated at 50°C overnight with shacking at 700 RPM. The next day add 630µl cold chloroform and emulsify by gently inverting 4-5 times then centrifuge 13,300 RPM for 7 mins. The upper aqueous phase is transferred to a new 1.5 ml eppendorf tube. Next 720µl dH_2O and 80 µl of

Precipitation solution are added and the Eppendorf is inverted constantly for 2 mins at Room Temperature (RT). Centrifuge at 13,300 RPM for 10 mins and then remove the supernatant completely. Dissolve the DNA pellet in 100µl NaCl and add 300µl 100% ethanol that is cooled to -20°C and let DNA precipitate overnight at -20°C. The next day centrifuge at 13,300 RPM for 10 mins then remove the ethanol with a micropipette. Wash the pellet (flick gently with your finger) with 200µl 70% ethanol cooled to -20°C. Centrifuge at 13,300 RPM for 10 mins then remove the supernatant with a micropipette. Place the tubes opened on a hotplate at 37°C and let it dry for 15-30 min. Add 30µl DNA-free sterile dH_2O and store at 4°C for at least 1hr before Nanodrop quantification.

2.19 Whole genome sequencing data analysis

Raw data was received in the form of paired fastq files. After generating Quality Control (QC) reports using FastQC, the Trimmomatic tool was used to remove any poor-quality bases (base quality < 20) and bases that match sequencing adapters(239). The trimmed reads for each sample were then aligned to a reference genome comprising the GRCz10 reference genome from Ensembl version 91, which was supplemented by additional reference sequences corresponding to the sequences of the transgenes. The bwa mem tool was used for the alignment with the default parameters(240). Prior to analysis and visualization, potential PCR duplicates (reads with identical sequence and alignment) were identified using the sambamba tool(241). Aligned reads were visualised using the Integrative Genome Viewer (IGV). Potential structural variants were identified using lumpy and delly(242, 243). These methods take advantage of read pairs whose alignment is discordant (the distance between the alignments is greater or smaller than expected or aligning to different reference sequences) and aligned reads that contain soft-clipped bases (bases that are masked during alignment as they do not align to the reference sequence).

2.20 Wizard® SV Gel and PCR Clean-Up System protocol

The Wizard® SV Gel and PCR Clean-Up System protocol was used to purify DNA from agarose gel. This system was used according to the manufacturers guidelines. Following gel electrophoresis, the DNA band from was removed from the gel using a scalpel and stored in a 1.5ml microcentrifuge tube. 10µl of membrane binding solution was then added per 10mg of gel slice (to calculate this it is best to weigh the microcentrifuge tubes before they are

used for storing the bands, weighing them again after, and comparing for the difference in weight). The mixture was vortexed intermittently, while incubating 56°C until the gel slice was completely dissolved. Next the SV minicolumn is placed into a collection tube and the dissolved gel mixture transferred to the minicolumn assembly. The assembly was then incubated at room temperature for 1 minute before being centrifuged at 16,000g for 1 minute. The flowthrough was discarded, and the minicolumn reinserted into the collection tube. 700µl of membrane wash solution was added and the assembly centrifuged at 16,000g for 1 minute. The flowthrough was discarded, and the minicolumn reinserted into the collection tube. 500µl of membrane wash solution was added and the assembly centrifuged at 16,000g for 5 minutes. The collection tube was emptied, and the assembly centrifuged for 1 minute to allow for evaporation of any residual ethanol. The minicolumn was then carefully transferred to a clean 1.5ml microcentrifuge tube and 30µl of nuclease free water added to the minicolumn. This was then incubated at room temperature for 1 minute before being centrifuged at 16,000g for 1 minute. The minicolumn was then discarded and the eluted DNA stored at –20°C.

2.21 Cryopreservation of zebrafish tissue for cryosectioning

Transgenic Zebrafish larvae were culled at 3 days post-fertilization by immersion in concentrated MS-222 and fixed in 4% Paraformaldehyde (PFA) (SIGMA-ALDRICH, St. Louis, MO, USA) overnight at 4°C, washed in 3 ml cold Phosphate Buffered Saline (PBS, 1x), and embedded in 3 ml of 30% sucrose overnight at 4°C for cryoprotection. Before embedding in mounting media (O.C.T. compound, VWR International, #00411243), the larvae were immersed in 50%:50% solution of 30% sucrose: O.C.T. for 30 mins at 4°C. Finally, the larvae were mounted in a base mold (Electron Microscopy Sciences, Hatfield, PA, USA), with O.C.T., snap frozen using dry ice, and stored at -20°C. Prior to use, the tissues were sliced onto positively charged slides in coronal sections using a cryostat, air dried overnight and kept at -20°C until required.

2.22 Imaging of zebrafish

Imaging was performed using either a widefield fluorescent DeltaVision microscope or Nikon widefield fluorescent microscope both using a 40x oil objective lens at the Wolfson Light Microscopy Facility at the University of Sheffield Biomedical sciences department. To

quantify changes in fluorescence and staining images were quantified via a Z-projection generated using imageJ (Rasband, W.S., ImageJ, U. S. National Institutes of Health, Bethesda, Maryland, USA, https://imagej.nih.gov/ij/, 1997-2018.).

2.23 Statistical analysis

Statistical analysis was performed using GraphPad Prism v7.00. For normally distributed data the unpaired students T-test was used to determine significance. For non-normally distributed data the Mann-Whitney test was used instead. The value of $p<0.05$ was used to denote significance throughout this thesis.

2.24 Protocol for fish embryo injections

Day 1: Agarose plates for injection were made using 50ml of 2% agarose, using E3 media with methylene blue. Dishes were set up with western blotting glass 'short' plates, with the glass pate resting on 2 petri dishes to create a ridge for the eggs to lie on. Once the agarose had set the glass plates were removed and cleaned with ethanol before being returned to storage. The agarose plates were wrapped with parafilm and can be stored at 4°C for up to 1 month. After using a plate for injection, it is rinsed with distilled water, re-wrapped in parafilm, and stored in the fridge. Glass needles are made using a P-100 Falming/Brown micropipette puller. Fish are paired at 4pm to minimise their time in the breeding tanks.

Day 2: An injection mix was made up that contained 1µl of RNA-free plasmid miniprep (stock concentration at 200ng/µl), 0.8µl tol2 mRNA (stock concentration 250ng/µl), 0.8µl phenol red (Sigma-Aldrich, St Louis, MI, #P0290). Injections were performed on fertilised eggs at the blastodisc stage of development. 0.5nl was injected into the yolk of each egg, with the volume being measured by assessing the size of the drop produced which should be the width of one of the smallest divisions on the graticule (Psyer optics, Edenbridge, Kent, #S1 stage micrometer 10mm/0.1mm).

2.24.1 E3 Media Recipe

To prepare a 60X stock, dissolve the ingredients in dH_2O, to a final volume of 2 L. Adjust the pH to 7.2 with NaOH. Autoclave. To prepare 1X medium, dilute 16.5 mL of the 60X stock to 1 L. Add 100 µL of 1% methylene blue (Sigma-Aldrich).

For a 60X stock solution:

- 34.8 g NaCl
- 1.6 g KCl
- 5.8 g CaCl2
- 9.78 g MgCl2

2.25 Paraffin embedding of zebrafish and sectioning

Adult fish were culled by immersion in concentrated tricaine mesylate (MS-222, SIGMA-ALDRICH, St. Louis, MO, USA) with confirmation of death via cessation of breathing. After confirmation of death fish were fixed by immersion in 50ml of 4% paraformaldehyde buffered at pH 7.0 (PFA, SIGMA-ALDRICH) at 4°C for 48-72h with rolling. Fish were then decalcified in 50ml of 0.5M EDTA, pH 8.0 for additional 48-72h with rolling. Subsequently the whole fish was paraffin-embedded via the following process: formalin (SIGMA-ALDRICH) for 10min, formalin (SIGMA-ALDRICH) for 50min, ethanol 50% for 1h, ethanol 70% for 1h, ethanol 95% for 1h 30min, ethanol 100% for 2h, ethanol 100% for 2h 30min, 50:50 ethanol 100%:xilol for 1h 30min, xylene (SIGMA-ALDRICH) for 3h, xylene (SIGMA-ALDRICH) for 3h, paraffin for 4h 30min. For the solutions absolute ethanol (Thermo Fisher Scientific, Waltham, MA, USA) diluted in distilled water (dH_2O, VWR International) and paraffin histosec pastilles (Merck & Co, Kenilworth, NJ, USA) were used. Paraffin-embedded fish were sectioned by the histology staff at the SkeletAL lab, at the Medical School of the University of Sheffield (UoS), using a Leica TP 1020 cryostat, and stored at room temperature (RT). Unless otherwise stated paraffin embedded tissue sections were longitudinal (sagittal) 3µm-thick slices.

2.26 Immunofluorescent staining (IF)

For the purpose of IF paraffin-embedded sections were deparaffinised and hydrated via the following protocol and incubations: histoclear (Scientific Laboratory Supplies, Wilford, Nottingham, UK) 2x 5min, ethanol 100% 2x 5min, ethanol 90% 5min, ethanol 70% 5min, and dH_2O 2x 5min. To produce the diluted ethanol, absolute ethanol (Thermo Fisher Scientific) was diluted in dH_2O. Antigen retrieval is performed by incubating the sections in 0.01M citrate buffer at pH 6.0, made with Trisodium citrate dihydrate (SIGMA-ALDRICH) heated to just below boiling at 800W in a microwave for 10min. After antigen retrieval the tissue

sections are permeabilised in PBS (PBS, SIGMA-ALDRICH) 0.5% Triton X-100 (SIGMA-ALDRICH, for 10min) and blocked in blocking solution for 1h. Blocking solution is made from 3% bovine serum albumin (BSA, SIGMA-ALDRICH), 5% Goat Serum (or Donkey Serum, both from SIGMA-ALDRICH), and 0.3% Tween-20 in PBS (SIGMA-ALDRICH). Blocking slides are incubated overnight (ON) at 4°C, with the primary antibody, in a humidified box. Following ON incubation slides are washed in PBS 0.1% Tween-20 (SIGMA-ALDRICH, 3x 10min) before secondary antibody incubation (1h at RT or ON at 4°C). All primary and secondary antibodies were diluted in blocking solution before incubation on the slides. Note that two primary antibodies can be added at the same time if they come from different species (e.g., a mouse monoclonal antibody with a chicken polyclonal antibody) and if the secondary antibody is conjugated with different fluorophores (e.g., anti-mouse Alexa Fluor® 488 with anti-chicken Alexa Fluor® 568). Finally, the tissues were incubated in 1µg/ml of 4',6-diamidino-2-phenylindole (DAPI, Thermo Fisher Scientific), a DNA stain that binds strongly to DNA, diluted in PBS (SIGMA-ALDRICH), for 10min at RT. After 3x 10min washes in PBS 1x (SIGMA-ALDRICH), the slides were mounted with vectashield (Vector Laboratories, Burlingame, CA, USA), covered with a glass coverslip (Scientific Laboratory Supplies), and sealed with clear nail varnish.

2.26.1 Antibodies used for IF.

Antibodies used for experiment reported in this thesis can be found listed below.

Antibody Name	**Source of acquisition**
Living Colors® mCherry Monoclonal Antibody	Clontech Laboratories
Goat Anti-Mouse IgG Alexa Fluor 647	Thermo-Fischer
Goat Anti-Mouse IgG Alexa Fluor 568	Thermo-Fischer
Sheep Anti-GFP	Bio-Rad
Goat Anti-Chicken IgY Alexa Fluor 488	Thermo-Fischer
Chicken Anti-GFP	Abcam

Table 2.26.1: Table of the antibodies used for immunofluorescent staining experiments detailed in this thesis.

2.27 Telomere-Fluorescence *in situ* Hybridization (Telo-FISH)

Telo-FISH is used to detect telomeres using a peptide nucleic acid (PNA) telomere oligonucleotide. Relative telomere length can be quantitatively measured using the intensity of the signal of probe in the assayed tissues compared to a control. We use Telo-FISH in conjunction with IF, therefore this protocol should be considered as a continuation of the IF protocol in section 2.24 after the secondary antibody staining step. All work for the following protocol should be performed in a dark/dim room.

Following appropriate incubation wash excess secondary antibody off, 3x10min RT with 0.1% Tween20 in PBS, with slow shaking. Crosslink the sample with 4% paraformaldehyde in PBS for 20 min with shaking. Wash for 3x5 min with PBS. Dehydrate by in 70%, 90%, and 100% icy cold ethanol for 3 min each then allow the sections to air dry for at least 20min. Apply 10µl hybridization mix per slide and place glass cover slip over the section. Denature the DNA at 80°C for 10 min in a pre-heated oven. Remove slides from the oven and allow the probe to hybridize to the sections in a humidified chamber in the dark for 2 hr at RT. Gently remove the cover slips and wash 1x10 min with 70% formamide/30% 2x Saline Sodium Citrate Solution (SSC) diluted from a 20x SSC stock solution. Wash 2x10 min with 100% 2x SSC. Wash 3x 5min in 1x PBS. Counterstain the nucleus DAPI (1:2000) for at least 20min. Wash with PBS 10min mounted with vectashield and clear nail varnish.

2.27.1 Solutions for Telo-FISH

SSC 20x stock solution

- 88.3g Tri-sodium citrate dihydrate (Sigma-Aldrich)
- 175.3g NaCl (Sigma-Aldrich)
- Diluted to a volume of 1L in dH_20 and adjusted to pH7.0
- Autoclaved

4% PFA:

- 4g PFA in 1× PBS at 65°C

Magnesium chloride buffer ($MgCl_2$)

- 25mM magnesium chloride (Sigma-Aldrich)

- 9mM citric acid (Sigma-Aldrich)
- 82mM sodium hydrogen phosphate (Sigma-Aldrich)

Blocking buffer

- 10x blocking reagent (Merck and Co.) diluted to 1x in maleic acid (Sigma-Aldrich)

Hybridisation mix for 20 slides (10ul per fish):

- 2.5µl 1M Tris pH 7.2 (1mM)
- 21.4µl Magnesium chloride buffer
- 175µl Formamide deionized
- 5µl PNA probe (25µg/ml, Applied biosystems)
- 12.5µl of 1x Blocking reagent (Roche)
- 1ml of 10x stock blocking buffer in 9ml autoclaved maleic acid, pH7.5
- 33.6µl des. Water

2.28 Fluorescence Associated Cell Sorting (FACS) dissociation

First sacrifice and confirm the death of the zebrafish as previously described, making sure that the fish was not fed for 24hr beforehand. Dissect out the gut, discard the colon, and open the gut longitudinally with scissors or a small blade and trim into smaller pieces. Wash these pieces twice in cold, filtered 1x PBS. Transfer the washed pieces to a 1.5ml eppendorf tube containing 0.3ml filtered PBS (calcium and magnesium free)/2mM EDTA/1mM Dithiothreitol (DTT). Further chop the tissue inside the tube to encourage dissociation. Agitate at 700rpm for 15 min at RT. Collect supernatant and transfer to a clean 1.5ml Eppendorf tube on ice. Add 0.3ml fresh 1x PBS/2mM /1mM DTT to tissue pieces and repeat the process twice more, each time collecting Inter-epithelial lysate (IEL) into same tube as before. After the last media change, remove as much liquid as possible, add to the IEL and store on ice. Dissociate the remaining fragments of gut by incubating with 0.3ml Leibovitz's media (L15) + liberase for 30mins at 37°C at 700 RPM shaking. After 15 mins of incubation gently pipette up and down with 5-8 times to help dissociate tissue then continue incubation. After 30 mins repeat pipetting to encourage final dissociation. Use a 1ml syringe tip to filter the liberase-treated tissue through a 70µm cell strainer into a new 1.5ml eppendorf tube. After filtering, rinse strainer with 150µl of L15+liberase and incubate for another 10 minutes at 37°C with 700 RPM shaking. After this incubation filter through a 40µm strainer into a fresh 2ml tube. Gently resuspend IEL cells from before with blue tip and pass through same 40um strainer into the same tube and rinse the strainer with 150µl L15+liberase. Spin at 600g for 5 mins at 4°C then again immediately for 3 mins at 4°C. Check pellet is visible and attached to tube wall. Remove all liquid and discard supernatant. Disperse pellet by dragging across tube rack 3-5 times and flick the tube to ensure pellet dispersion (don't overdo this as will result in increased cell lysis and death). Resuspend in

800ul fresh filtered cold 1x PBS and transfer cells to a 1.5ml Eppendorf tube. Repeat double centrifugation as previously described and disperse pellet as above.

2.28.1 Solutions for FACS dissociation

10ml of 1x PBS/2mM EDTA/1mM DTT:

- 9.95ml 1x PBS
- 40µl 0.5M EDTA (Sigma)
- 10µl 1M DTT (Thermo-Fischer)

0.3ml L15 + liberase

- 1.2µl Liberase (Roche)
- 0.3ml L15 (Roche)

20ml 1x PBS/0.2% BSA

- 20ml 1x PBS
- 0.04g BSA (Sigma)

2.28.2 FACS data analysis

FACS data analysis, visualisation and processing was performed using FlowJo V.10.8.1.

2.29 Telomerase Repeat Amplification Protocol (TRAP) assay

The TRAP assay is a laboratory kit supplied by Roche called *TeloTAGGG* Telomerase PCR ELISA^{PLUS} (Roche). This kit is used to qualitatively detect the activity of telomerase in cell or tissue lysate. Telomerase in the lysate elongates an artificial telomere that is then amplified using PCR. The telomere is then immobilised within the Enzyme-linked immunosorbent assay (ELISA) plate and a colorimetric reaction occurs the intensity of which can be quantified.

2.29.1 Telomerase Repeat Amplification Protocol assay

This protocol is a continuation of the FACS dissociation protocol from section 2.26. Based on pellet size, resuspend cells in 50-100ul TRAP lysis buffer in RNAse free conditions. Pipette up and down repeatedly to homogenise cells until the homogenate is uniform. Incubate lysates on ice for 30 mins. Centrifuge lysate at 16,000g for 20 mins at 4°C. Carefully remove supernatant and transfer to a precooled fresh tube. Determine the protein concentration using the Bicinchoninic acid (BCA) kit. If using the lysate on the same day store at 4°C until

use, otherwise flash-freeze lysate in liquid nitrogen. The TRAP assay is carried out according to the manufacturer's instructions for the *TeloTAGGG* Telomerase PCR ELISA^{PLUS} (Roche) following the steps for preparation of extracts from cells. Absorbance readings were taken using a Varioskan plate reader. Telomerase activity is measured by the colorimetric change of the sample and is determined via the equation: Relative Telomerase Activity (RTA) = ((absorbance of sample – absorbance of negative control)/Absorbance of the internal standard)/((Absorbance of control template – absorbance of the lysis buffer)/Absorbance of the internal standard of the control template).

2.29.2 BCA kit protocol

This protocol is performed using the BCA Protein Assay kit (Thermo-Fischer). In 1.5ml tubes prepare the protein standard curve as shown in table 4. Pepare fresh 1.5ml tubes for each of your protein samples, including the BCA standards. For each sample you want to quantify prepare one fresh tube and add 5µl of your protein homogenate taken from the previous cell lysis steps to 45µl of dH_2O (RNAse free). Add 1ml of bicinchoninic acid (reagent A) to all samples and the standard curve tubes. Vortex all tubes. Incubate all tubes for 10 mins in a water bath at 37°C. Add 20µl of copper sulphate solution (reagent B) to each tube after incubation. Vortex all tubes. Incubate at for 20 mins in a water bath heated to 37°C. Transfer 200µl of each sample and BSA curve to a 96-well plate, all in duplicates. Read the absorbance at 562nm in the Varioskan microplate reader.

BSA protein standard/µl	**dH_2O/µl**
0	50
5	45
10	40
20	30
30	20
40	10
50	0

Table 2.29.2: BSA protein standard

2.30 IPEX dissociation

Zebrafish were culled using 100% tricaine before blood Intraperitoneal exudate (IPEX). A ventral, midline incision was made, and 5ul ice-cold 1× PBS 2% Foetal Bovine Serum (FBS) was injected to lavage the intraperitoneal space. IPEX cells were collected via lavage with phosphate-buffered saline using four sequential 5 µL washes using a 10-µL syringe (Hamilton) for a total volume of 20 µL.

2.31 Wright-giemsa staining

Wright-Giemsa staining was performed on methanol fixed FACS sorted cell populations so that we might visualise and quantify the cell populations that were being sorted from the mCherry positive populations. Sorted cells were first incubated on poly-D lysine coated glass slips to prevent cell loss from cytospinning. Cells were incubated with the poly-D-lysine coated slips for 2hrs to allow adherence in L15 + 2% BSA serum. Slips were removed from the culture media and dehydrated in 70% ethanol for 1 minute, 90% ethanol for 1 minute, 100% for 1 minute. 2-3 drops of Wright-giemsa stain were added by dropper to the air-dried slips and incubated at RT for 3 minutes. Wright-giemsa stain was rinsed off the slip by dipping the slip in dH_2O 7-8 times until the stain turned a pinker hue. Coverslips were mounted onto microscope slides using glycergel mounting media (Agilent).

2.31.1 Poly-D-Lysine coating

A stock solution of 50µg poly-D-lysine was prepared in 1x PBS to a concentration of 50ug/ml. Coverslips were sterilised by incubating them in 95% ethanol and drying before coating. To coat coverslips are placed in a single layer in a petri dish containing enough 50µg/ml stock solution to fully cover the layer of coverslips. Coverslips are incubated for 1hr at 37°C. Remove coverslips using sterile forceps and allow surface to dry on blue roll. Do not wipe dry as this will disturb the Poly-D-lysine coating. Coated coverslips can be stored for up to 3 months at 4°C.

2.32 Single-cell RNA-sequencing

Sample preparation was performed by Catarina Henriques and Pam Ellis from the University of Sheffield. Samples were prepared in the lab of Betsy Pownall of the University of York Frog Group. Dissociated samples were prepared such that there were three males and three females for each genotype to control for differences in gene expression due to sex. Samples were prepared and submitted as three fish per day with alternating sex to control for batch effect. Dissociated cells were run on a 10X Chromium platform using 10x v.2 chemistry targeting 10,000 cells. The resulting cDNA libraries were amplified with 75 cycles of PCR and sequenced on an Illumina MiSeq at the University of Nottingham.

2.32.1 Computational analysis of Single cell RNA-sequencing data

2.32.1.1 Cellranger pipeline

The resulting sequencing data was analysed using the 10X Cellranger pipeline, version 2.2.0 using standard quality control, normalization, and analysis steps to remove empty droplets and potential doublets(244). Cellranger mkfastq was used initially to demultiplex the raw base call files generated by illumina sequencing into FASTQ files. The FASTQ files generated were then run through cellranger count for alignment, filtering, barcode counting and Unique Molecular Identifier (UMI) counting to produced feature-barcode matrices. Cellranger aggr then aggregated and normalised the runs from each fish and aggregated them into groups based on their genotype. Reads were aligned to the zebrafish genome GRCz11. Additional quality control was applied during reclustering whereby cells with <200 or >4000 uniquely expressed genes were excluded from further analysis.

2.32.1.2 Loupe browser analysis

Cell clustering and annotations were performed using Loupe Browser version 4.0. Cell types were assigned according to specific marker genes for the cell types based on reported markers in the literature. Differential gene expression is determined by comparing the mean expression of a gene in the cluster to the mean expression in all other clusters being analysed at that point.

2.32.1.3 Gene set enrichemnet

Gene set enrichment analysis was carried out using ShinyGO version 7.7 with a minimum P value of 0.05(245). Pathways are indicated as green circles with the number of genes

involved in a pathway corresponding to the intensity of the green shading. Pathway connections are indicated in grey with the significance of the connection corresponding to the thickness of the connector. Further analysis of protein-protein interaction networks was performed using STRING using a minimum network score of 0.4. Interactions are identified by STRING using text-mining (yellow), experiments previously performed (pink), databases (light blue), co-expression (black), neighbourhood in the genome (green), gene fusion (red) and co-occurrence in publications (dark blue)(246). Gene expression lists were compared using Venny v2.1. Cell types were determined using FishSCT and EnrichR(247, 248).

2.33 Statistical analysis

Statistics were performed using GraphPad Prism v9.5.1. Normality was assessed by the Shapiro–Wilk test. For normally distributed data either an unpaired t-test or a one-way ANOVA was used depending on the number of variables. For non-normally distributed data the Mann–Whitney test or the Kruskal–Wallis tests were used instead. A critical value for significance of $p < 0.05$ was used throughout all analysis.

Chapter 3: Generating novel transgenic zebrafish telomerase rescue lines.

3.1 Introduction

Previous work by *Ellis et al.* has shown that a subset of zebrafish-gut immune cells has telomerase-dependent, proliferation-independent "hyper-long" telomeres, relative to surrounding epithelial cells and that these are also present in human gut tissue (185). These "hyper-long telomeres" cells are mostly macrophages and dendritic cells (*mpeg1.1*$^{+}$ or *cd45*$^{+}$ *mhcII*$^{+}$)(185). Further, *Ellis et al.* describe *mpeg1.1*$^{+}$ cells as having much longer telomeres in the gut than in their haematopoietic tissue of origin, the Head Kidney (HK), suggesting that there is further modulation of telomerase in these immune cells(185). In addition, telomerase activity is higher in the gut than in the HK, and there is a higher percentage of *mpeg1.1*$^{+}$ *tert*$^{+}$ cells in the gut in the HK(185) indicating that the "hyper-long telomeres" did not result from the cell's originating in the HK. Further, *Ellis et al.* indicate that in the absence of telomerase activity there is an observed impairment of phagocytosis as well as a decrease in the expression of Light-Chain 3-B (LC3B)(a marker of autophagy), a decrease in the expression of TNF-α, and a decrease in expression of IL-6(185). Additionally, these observations were also made independent of telomere shortening, indicating that they may depend on non-canonical functions of telomerase(185). In section 1.4.2.2 I explored the published non-canonical roles of TERT, the enzyme component of telomerase, whereby there is plenty of evidence that TERT has functions beyond its canonical role in the elongation of telomeres. Therefore, the hypothesis that TERT may have further non-canonical roles in the regulation of immune cell physiology presented itself as an interesting avenue of research that would add to the existing knowledge of the non-canonical roles of telomerase.

Building on the work of *Ellis et al.* (185) I aimed to further explore the role of telomerase in the zebrafish immune system and to further explore the non-canonical roles of telomerase in this context. To do this I would need to determine which roles of telomerase could be rescued by a canonically active TERT that enabled telomerase activity. Further, I would also need to establish which roles of telomerase could be rescued using a version of TERT that was incapable of performing the canonical function of elongating telomeres. This form of TERT had already been described in a paper by *Imamura et al. (238)* and termed ΔTERT

which I have described in section 1.7.1. To study these effects of TERT and ΔTERT I would need to generate two new transgenic zebrafish lines that expressed the proteins of interest. Therefore, in this chapter I had two aims:

1. Establish and characterise the *mpeg1.1:tert-gfp* transgenic zebrafish line whereby TERT is being expressed in an *mpeg1.1* specific manner and retains its canonical ability to elongate telomeres as part of telomerase.
2. Establish and characterise the *mpeg1.1:Δtert-gfp* transgenic zebrafish line whereby ΔTERT is being expressed in an *mpeg1.1* specific manner and determine that this does not retain its canonical ability to elongate telomeres as part of telomerase.

3.2 Results

3.2.1 Plasmid structure and assembly method

Both the *mpeg1.1:tert-gfp* and the *mpeg1.1:Δtert-gfp* transgene were produced using the GA method (Fig. 3.2.1.A). GA utilises a 5' exonuclease, DNA polymerase, and DNA ligase to anneal complementary strands together (Fig. 3.2.1.A). Furthermore, GA requires a 1:1 ratio of components that will be ligated together. The range of concentration of components it is possible to use is 0.2-1pmols. I calculated the concentration of each component to be added in pmols using the following equation: pmols = (weight in ng) x 1000/ (base pairs x 650 daltons). The *mpeg1.1:tert-gfp* transgene (Fig. 3.2.1.B) had already been established by the Henriques lab and G_0 founders produced. The *mpeg1.1:Δtert-gfp* transgene (Fig. 3.2.1.B) would be produced by annealing together the *mpeg1.1* promoter, the *Δtert-gfp* gene, and the *tol2* region that contained the transposon sites.

The design of the transgenes was based on the *mpeg1.1* promoter being a published immune cell marker in zebrafish (226, 227, 234). To detect the expression of telomerase a GFP region was added downstream of the *tert* or *Δtert* gene, with an Internal Ribosomal Entry Site (IRES) separating the *gfp* from the *tert* or *Δtert*. The IRES region acts as a ribosomal binding point leading to the translation of the *tert* or *Δtert* and the *gfp* as two separate proteins (249)(Fig. 3.2.1.B). In addition to the *mpeg1.1:tert-gfp* or *mpeg1.1:Δtert-gfp* section, a *cmcl2-eGFP* was introduced in a 3' to 5' orientation so as not to be expressed in conjunction with the *mpeg1.1:tert-gfp* or *mpeg1.1:Δtert-gfp* (Fig. 3.2.1.B). The *cmcl2* promoter is utilised in early heart development of zebrafish fry(250). Therefore, having eGFP expressed under the control of the *cmcl2* promoter leads to expression of GFP at an early developmental stage (2dpf). This allows the early detections and selection of zebrafish fry with successful transgenic insertion and expression and prevents the unnecessary raising of excess non-transgenic zebrafish (250). The transposase system was the method chosen to introduce the *mpeg1.1:Δtert-gfp* and *mpeg1.1:tert-gfp* transgenes into the zebrafish as it is a well-documented method for zebrafish genetic manipulation that utilises an adapted version of the naturally occurring *tol2* transposon to insert the desired gene(251, 252).

To study the effects of rescuing TERT or ΔTERT expression in a prematurely aged model both the *mpeg1.1:tert-gfp* and the *mpeg1.1:Δtert-gfp* transgene would be inserted into zebrafish lines that contained the hu3430 telomerase mutation. The hu3430 mutation is a T to A point mutation in the second exon of the telomerase gene which does not affect telomerase transcription but prevents the full translation of telomerase by introducing a premature stop codon. The introduction of a premature stop codon causes the translation of a truncated, inactive, form of TERT. Zebrafish with both alleles of their *tert* gene containing the hu3430 mutant have been reported to be accurate models of premature ageing, exhibiting an ageing phenotype at a relatively young age (12mo) (218, 222). Furthermore, a line of the hu3430 telomerase mutant was available that also contained the *mpeg1.1:mCherry.caax* reporter gene which has been characterised as a fluorescent reporter for cells that utilise the *mpeg1.1* promoter and so would provide a method for verifying that the expression of the rescued *tert* or *Δtert* is present in *mpeg1.1*$^{+}$ positive cell via the mCherry fluorophore(226, 234).

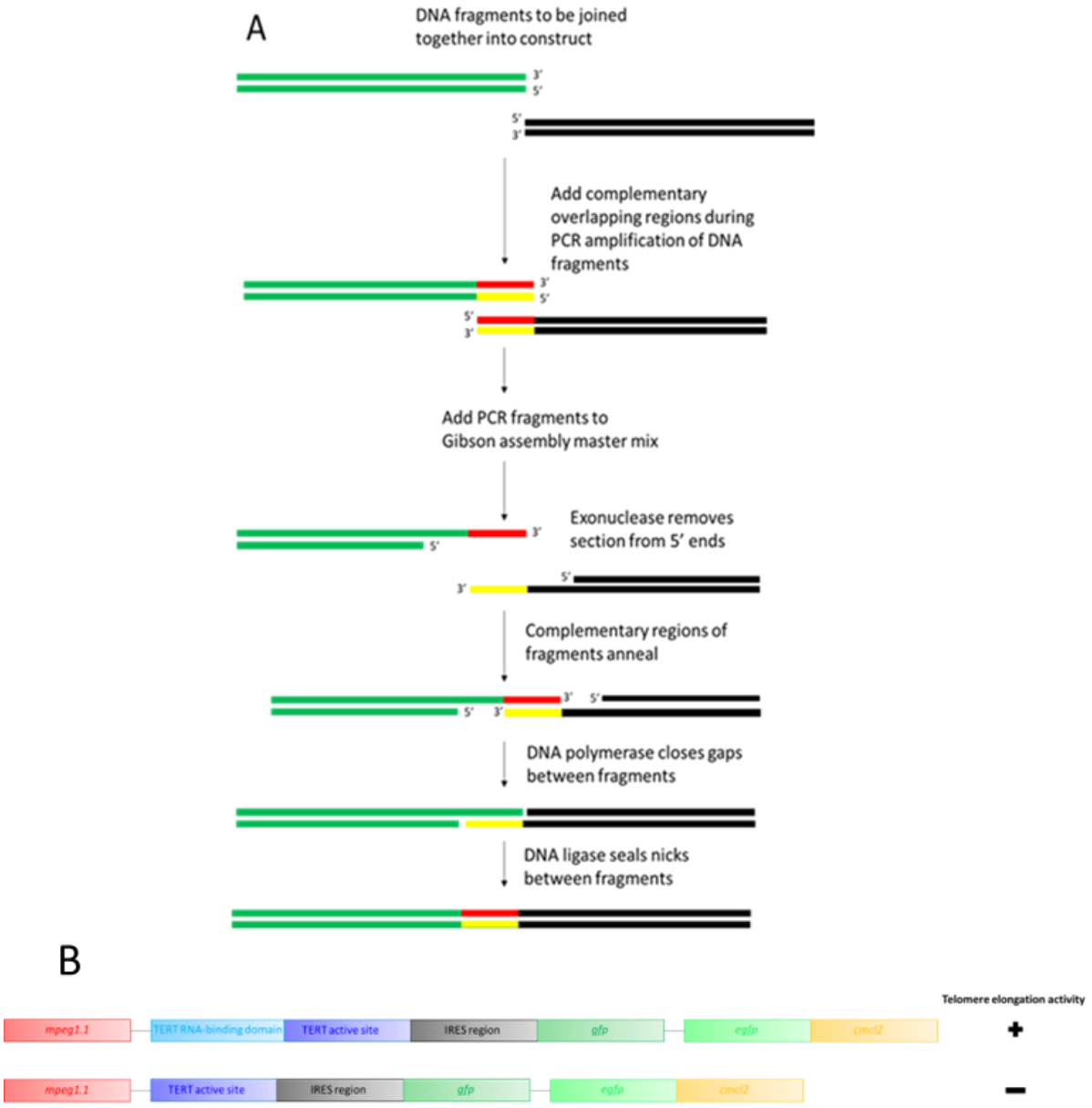

Figure 3.2.1: Method used for the producing transgenic constructs. **A.** Representative diagram of the process of GA. **B.** Representative diagram of the *mpeg1.1:tert-gfp* transgene and *mpeg1.1:Δtert-gfp* transgenes indicating their canonical telomerase activity.

3.2.2 Optimising PCR amplification of the *mpeg1.1* promoter region and production of the *mpeg1.1* promoter region for producing the *mpeg1.1:Δtert-gfp* transgene.

The *mpeg1.1* promoter is an established marker in zebrafish immune cell development(226, 234, 237). Therefore, the *mpeg1.1* promoter would be used to specify that rescue of *Δtert* expression only occurred in zebrafish *mpeg*$^{+}$ immune cells. To generate the novel *mpeg-Δtert-gfp* transgene using GA I needed to produce the *mpeg1.1* promoter fragment in a high concentration that also had a high purity to avoid adding unwanted sections to the GA reaction. To produce a sample of the *mpeg1.1* promoter suitable for use in the GA reaction I optimised the PCR amplification of *mpeg1.1* from an available plasmid (Fig. 2.2.1). I used primers one and two (Table 2.4.1) (Figure 3.2.2.B) and the software NEBtm calculator to estimate an annealing temperature at which both primers would anneal to the construct in a sequence specific manner. This annealing temperature considers the length of the primers, the GC content of the primers, and the solvents used for the reaction. Based on this temperature I decided upon a range of annealing temperatures to test from 55.6^{o}C to 65.1^{o}C (Fig. 3.2.2.D). I ran the PCR products on gel electrophoresis and found a strong band for each of the five temperatures tested at the predicted size of the *mpeg1.1* fragment of 1866bp (Fig. 3.2.2.C). As each band was at the correct predicted size of the fragment all bands were excised from the gel, pooled, and purified together for a final concentration of 115.6ng/µl of the *mpeg1.1* fragment used during GA.

Figure 3.2.2: Optimising of the PCR reaction to produce the *mpeg1.1* promoter region for the *mpeg1.1:Δtert-gfp* transgenic construct. **A.** Linear map of the construct used as a basis for the PCR optimisation of the *mpeg1.1* region including forward primer* and reverse primer** sites. **B.** Forward and reverse primer sequences. **C.** Predicted position of PCR band at 1866bp with DNA ladder representation. **D.** Optimisation of *mpeg1.1* promoters using varied annealing temperatures with amplified products outlined in green: lane 1, 65.1°C, lane 2, 63.6°C, lane 3, 61.3°C, lane 4, 58.6°C, lane 5, 56.3°C, lane 6, 55.6°C, lane 7 negative control.

3.2.3 Optimisation of the PCR amplification of the *Δtert* region

To produce the *mpeg1.1:Δtert-gfp* transgene I needed to produce *Δtert* of a sufficient concentration for the GA process. To do this I used PCR amplification of a plasmid containing *tert* using primers designed to amplify *Δtert* from *tert.* To do this I used the software NEBtm to provide an estimate of the ideal annealing temperature for primer three and four (Table 2.4.1) then tested a range of temperatures around the estimated ideal annealing temperature (Fig. 3.2.3.B, D).

To determine if the bands amplified by the primers were *Δtert* I ran the amplified samples using gel electrophoresis. I determined that *Δtert* would be 1586bp long so I should see a band at 1586bp relative to the DNA ladder (Fig. 3.2.3.C). The bands produced were at the predicted size however also that the circular control (Fig. 3.2.3.D lane 7) was at a similar position to the PCR products which meant I could not be certain the PCR products were not circular plasmid. To remove the possibility of circular plasmid contaminating the product I optimised the PCR amplification using varying concentrations of a linearised version of the template plasmid with an annealing temperature of 71.2^{o}C (Fig. 3.2.3.E). The bands produced using linear plasmid as a template matched the predicted weight of the *Δtert* section (Fig, 3.2.3.E). The bands were removed from the gel and purified, and the concentrations measured: lane one 31.4ng/µl, lane two 29.5ng/µl, lane three 18.6ng/µl, lane four 53.2ng/µl.

As the bands were found to be at the predicted size for the *Δtert* fragment and they had been produced using a linearised template they were deemed suitable for use in GA. Specifically, the sample from lane 4 (Fig. 3.2.3.E) was taken forward for GA as it was the most concentrated sample produced. Were the experiment to be repeated I would have included a circular template control into the same gel I ran the linearised bands on to aid in the identification of any circular template contamination in the linearised samples.

A

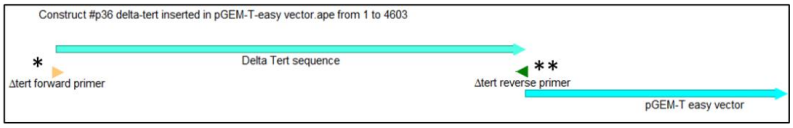

B

Primer Name	5' – 3' sequence
Δtert forward primer	TCATCTGTGTAAGGGCCAGT
Δtert reverse primer	CAGGTTTTTTTTACACCCGC

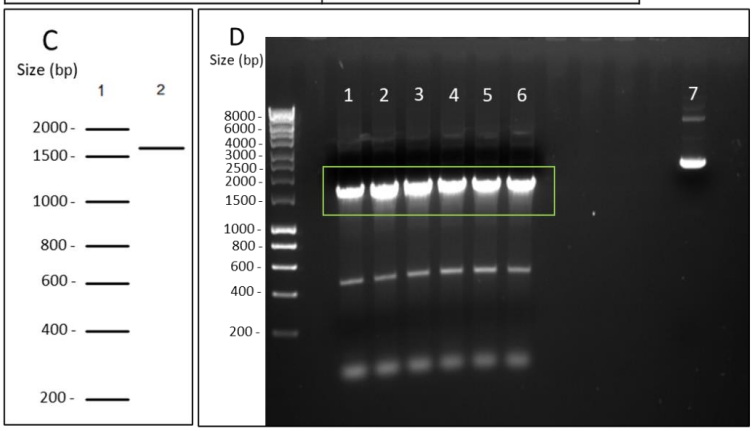

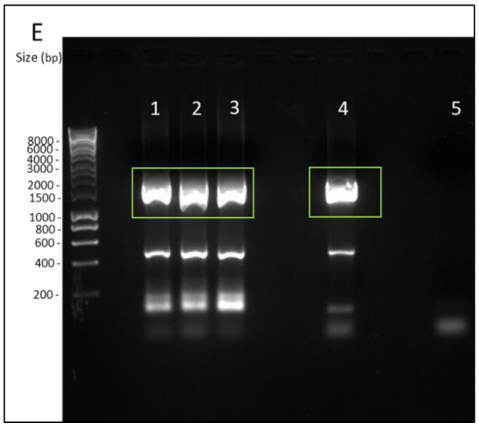

Figure 3.2.3: Optimisation of the PCR protocol to produce the *Δtert* gene for the *mpeg1.1:Δtert-gfp* transgenic construct. **A.** Linear map of the 5'-3' hypothesised insertion of the *Δtert* inserted into the pGEM-t easy vector with forward primer* and reverse primer** sites indicated. **B.** Forward and reverse primer sequences. **C.** Estimated position of band of *Δtert* if amplified using the primers from table 2.4.1 at 1586bp. **D.** Annealing temperature optimisation using a range of temperatures: lane 1, 71.2°C, lane 2, 70.4°C, lane 3, 69.5°C, lane 4, 68.8°C, lane 5, 68.3°C, lane 6, 68°C, lane 7 is a positive control of the circular p36 construct (Fig. 2.2.1). **E.** Further optimisation of the amplification of the *Δtert* section using varied concentrations of linear p36 construct as a template: lane 1, 1ng linear template, lane 2, 3ng linear template, lane 3, 5ng linear template, lane 4, 1ng circular template, lane 5, negative control.

3.2.4 Generating the *tol2* region using PCR amplification.

The *tol2* region of the construct is the DNA component of the transposon system that will allow the insertion of the transgene. To produce the *tol2* section of the construct to be used in GA I optimised the PCR amplification of the *tol2* section of an available lab construct using primers seven and eight (Table 2.4.1) (Fig. 3.2.4.B). I used NEBtm software to estimate the ideal annealing temperature for primers seven and eight (Table 2.4.1) and then used a range of temperatures based on this estimated annealing temperature to determine which temperature led to the highest concentration of *tol2* to be produced (Fig. 3.2.4.D). Initially I did not see a successful PCR amplification of the *tol2* region as no bands were indicated when the PCR sample was run using gel electrophoresis (Fig. 3.2.4.D). I hypothesised that this was due to the length of the primers making it difficult for them to anneal to the template and begin the PCR reaction, so I decided to use a range of higher temperatures to improve increase the chance of the primer annealing to the template. Three of the higher temperatures led to bands being produced which can be seen in lanes two, four, and five of Figure 3.2.4.E. Additionally, these bands were at the predicted length of 7763bp when compared to the DNA ladder (Fig. 3.2.4.E). These bands were isolated from the gel and purified with the following concentrations: lane two at 3.1ng/µl, lane four at 5ng/µl, lane five at 8ng/µl.

The maximum volume of the reaction was 20µl, 10µl of which was the GA master mix, therefore I could add up to 10µl of my component samples which would need to be divided between the three components. Therefore, the concentrations were too low to be appropriate for use in GA. To increase the concentration of the sample for GA I used PCR to amplify the *tol2* section using 65.5^{o}C as the annealing temperature as this had given the highest concentration of product previously (Fig. 3.2.4.F). Two bands were produced from four reactions, and these bands were excised from the gel, pooled, and purified together to produce a sample with the concentration 24.8ng/µl. I calculated this to have a concentration of 0.005 pmol/µl. While this was still very low I could feasibly use this sample due to the high concentrations I had isolated from the other components allowing me to add smaller volumes of them to the mixture. However, due to how low this concentration was I deemed that a higher concentration should also be tried that was produced using an alternative method.

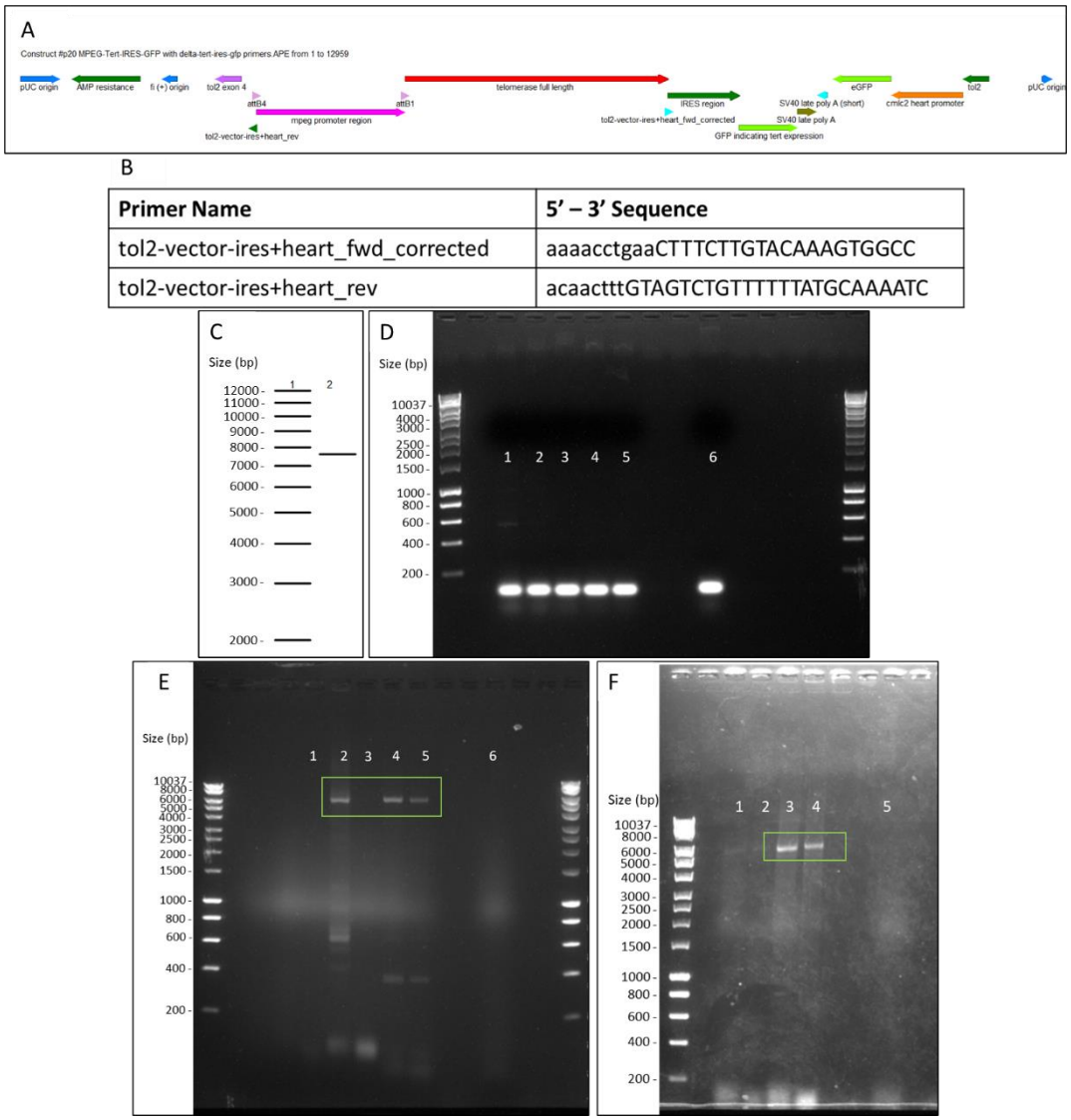

Figure 3.2.4: Optimisation of the PCR protocol to produce the *tol2* transposon section of the *mpeg1.1:Δtert-gfp* transgenic construct. **A.** Linear map of the construct used as the template for the PCR reaction with forward* and reverse** primers indicated. **B.** Forward and reverse primer sequences. **C.** Predicted weight of the amplified band at 7763bp. **D.** Annealing temperature optimisation: lane 1, 65.1°C, lane 2, 63.6°C, lane 3, 61.3°C, lane 4, 58.6°C, lane 5, 56.3°C, lane 6, negative control. **E.** Further optimisation of primer annealing temperature using higher annealing temperatures: lane 1, 70.7°C, lane 2, 69.2°C, lane 3, 67.7°C, lane 4, 66.4°C, lane 5, 65.5°C, lane 6, negative control. **G.** PCR amplification of *tol2* using linear template and annealing temperature of 65.5°C (lane 3 and lane 4), *tol2* indicated by green box, with lane 5 being a

3.2.5 Generating an alternative *tol2* region using enzymatic digestion.

Due to the *tol2* section produced using PCR being of a low concentration, we decided to also use an alternative method for its production. We chose restriction digestion of a plasmid that had been transformed into bacteria for culture and purification. We hypothesised that we would be able to produce a higher concentration of the *tol2* section as we would be able to grow the transformed bacteria to confluence before purification. I determined to use the existing lab plasmid named #p19 (Fig. 3.2.5. A) as a transformed sample stored in glycerol was readily available to be cultured. I determined that I could use a triple digestion of the available lab plasmid #p19 to digest the plasmid into separate regions. By using a triple digest, I would be able to digest the remaining plasmid I did not require into smaller pieces which would improve their separation from *tol2* when the digest was run on agarose gel before purification. I used A Plasmid Editor (APE) software to determine that the enzymes Sal1, BamH1 and Cla1 had binding sites within the plasmid (Fig. 3.2.5. A) and that these enzymes would digest the *tol2* section. I then used the APE software to predict the size of the bands if using single digests for each of the enzymes I would use (Fig.3.2.5. B, C, D) and the band positions with the triple digest (Fig. 3.2.5. E). However, due to the points of incision by the restriction enzymes I would not be able to produce a *tol2* section that contained the IRES-GFP region as the previous method had attempted to do.

E. coli containing the #p19 plasmid were first cultured on an agar plate before being brought to confluence in liquid culture. The culture was lysed, and the DNA purified before being digested and loaded into an agarose gel. I saw clean separation of four bands, with the bands of interest indicated (Fig. 3.2.5.F). These bands were removed from the gel and purified together to give a concentration of 62ng/µl, much higher than I was getting from the PCR amplification process. Using the 62ng/µl sample would allow me to add the *tol2* section at a concentration of 0.015pmol/µl, threefold more concentrated than the PCR sample giving a higher chance of it being incorporated during GA and so a higher probability of the *mpeg1.1:Δtert-gfp* construct being produced.

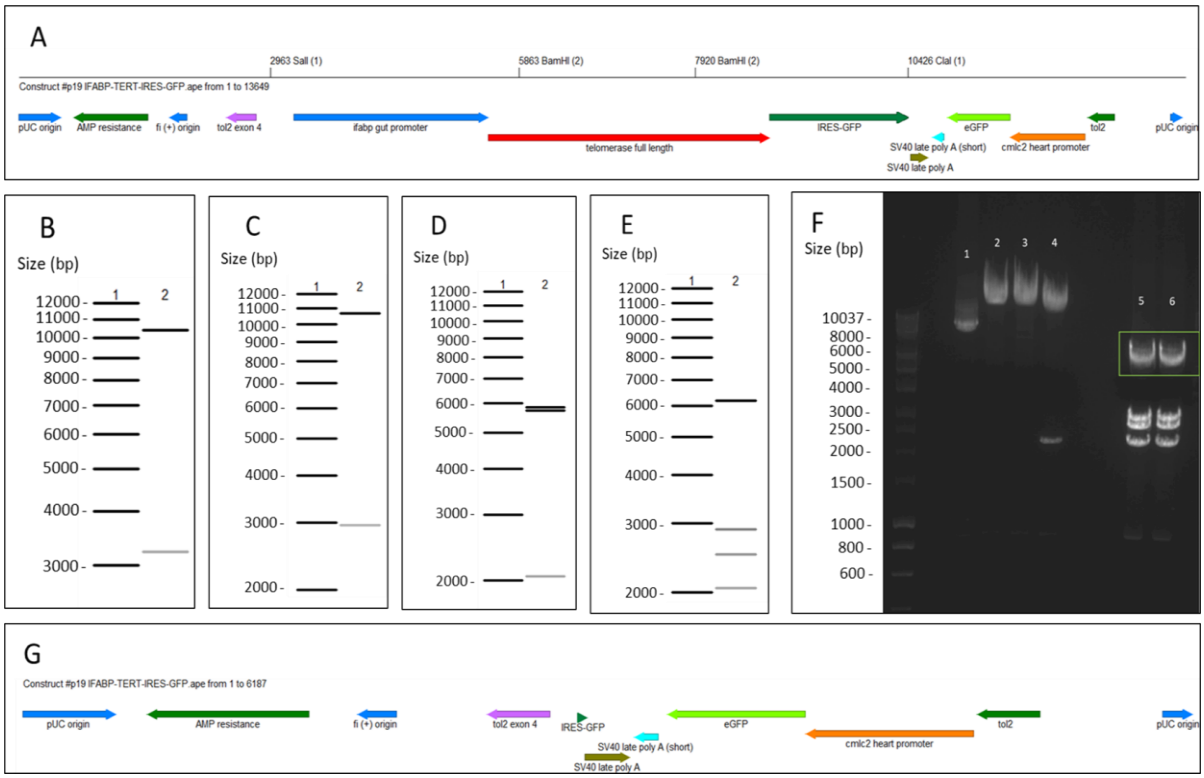

Figure 3.2.5: Optimisation of the production protocol for the *tol2* region of the *mpeg1.1:Δtert-gfp* transgenic construct. **A.** Map of the construct digested to produce the desired section for GA using the indicated enzymes. **B.** Predicted banding pattern of digestion using Cla1. **C.** Predicted banding pattern of digestion using Sal1. **D.** Predicted banding pattern of digestion using BamH1. **E.** Predicted banding pattern of digestion using triple digest of Cla1, Sal1, and BamH1 with desired band at 6187bp **F.** Enzymatic digest of the p19 construct: lane 1, circular template positive control, lane 2, Sal1-HF only digest control, lane 3, Cla1 only digest control, lane 4, BamH1 only digest control, lane 5 and lane 6 are triple digests with the desired bands at 6187bp indicated by the green box. **G.** Linear map of the desired region that would be obtained from the triple digest.

3.2.6 Generation of the *Δtert-ires-gfp* region using PCR amplification

The new *tol2* section I had produced in section 3.2.5 lacked the *ires-gfp* region unlike the *tol2* region produced in section 3.2.4. Therefore, I needed to introduce the *ires-gfp* region into the construct in a different way. I hypothesised that I could do this either by using PCR to amplify the *ires-gfp* section on its own to be added to the GA mix, or by producing a *Δtert-ires-gfp* section. We decided to produce the *Δtert-ires-gfp* as one section instead of just *ires-gfp* as it would ensure that the *ires-gfp* section was oriented in-line with the *Δtert* section during the GA as well as keeping the number of different sections that needed to be added during GA to three rather than increasing it to as this which would increase the chance of an undesirable construct being produced during GA.

I decided to use PCR amplification of the existing *mpeg1.1:tert-gfp* construct (Fig. 3.2.6.A) to produce the *Δtert-ires-gfp* section. For the amplification I designed two new primers designated primers five and six (Table 1) (Fig. 3.2.6.B) and used the NEBtm software to calculate an estimated ideal annealing temperature. I then decided to optimise the amplification using a range of annealing temperatures based upon the estimated ideal annealing temperature calculated by the NEBtm software. I tested the range of temperatures using both circular and linear template (Fig. 3.2.6.C). Linear template is the preferred template as there is very little chance of linear template being carried over and transformed into the *E. coli* after the GA step, whereas any circular template carried over could be transformed into the bacteria and be produced instead of the construct made during GA. However, in previous PCR amplification using a circular template had produced higher concentrations of the purified PCR product than linear template making the circular template still worth testing. Despite this, if I could obtain a high concentration of product from the linear template it would be preferable.

On an agarose gel the PCR amplification using a circular template showed several additional bands which may be non-specific amplification of regions within the template that have some complementarity to the primers, or it may be that primer dimers are being amplified during the reaction into long products (Fig. 3.2.6.D). However, I can see that there are bands

from both circular and linear template PCR amplifications that at the predicted size for the *Δtert-ires-gfp* product 3180bp (Fig. 3.2.6.B, D). The bands from linear template amplifications were removed and pooled before purification. The purified concentration for the linear template pool sample was 27.8ng/µl. Similarly, the bands from the circular template amplifications were pooled before purification. Once purified the circular template pool sample had a concentration of 91.8ng/µl. Due to the difference in concentration I now needed to decide if the increased concentration from the circular template sample was worth the risk of using it for GA.

A

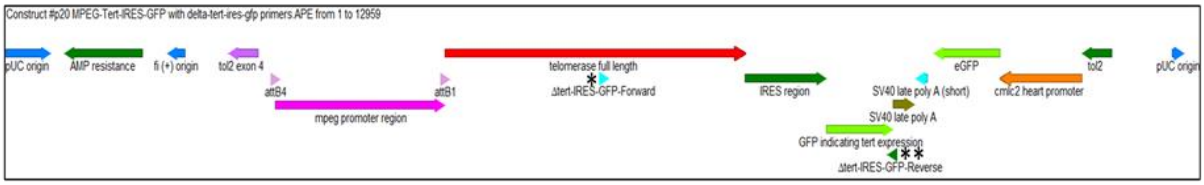

B

Primer name	5' – 3' sequence
Δtert-IRES-GFP-Reverse	ttatcatgtctggatcatcatcgatCATCGATTGTATAATAAAG TTGGAAAAAACCTCCC
Δtert-IRES-GFP-Forward	caaaacaagtttgATGAAGGGCCAGTGGAGGCC

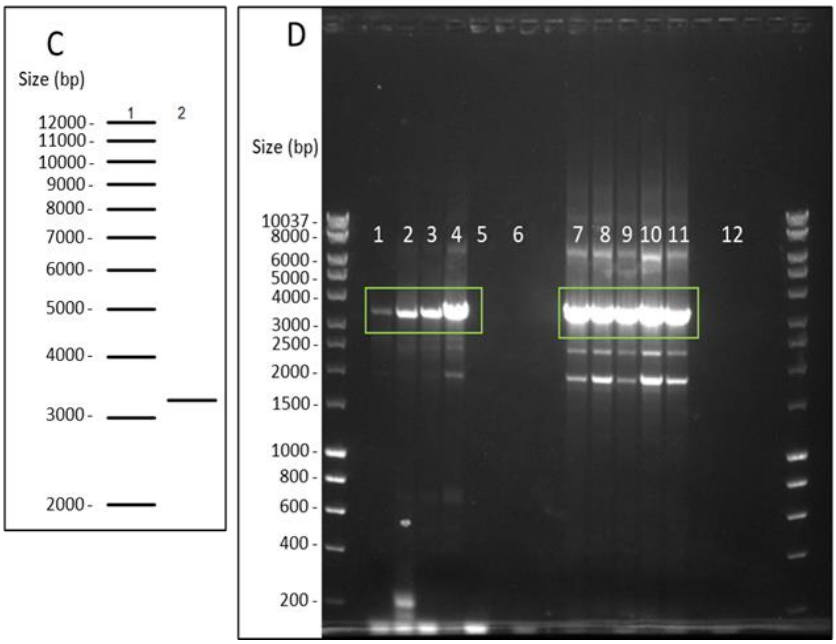

Figure 3.2.6: Generating the *Δtert-ires-gfp* region for production of the transgenic construct. **A.** Linear map of the construct used as the template for the PCR amplification of the *Δtert-ires-gfp* segment indicating forward* and reverse** primer sites. **B.** Forward and reverse primer sequences. **C.** Predicted position of the band for amplified *Δtert-ires-gfp* at 3180bp. **D.** Optimisation of primer annealing temperature, lanes 1-5 using linear construct, lanes 7-11 using circular construct, lanes 6 and 12 are relative negative controls: lane 1 and lane 7, 73°C, lane 2 and lane 8, 72.4°C, lane 3 and lane 9, 71.5°C, lane 4 and lane 10, 69.8°C, lane 5 and lane 11, 68.2 °C. Non-specific amplification bands can be observed at the bottom of the gel.

3.2.7 Production of the *mpeg1.1:Δtert-gfp* construct using Gibson assembly.

Having produced the *mpeg1.1* region, the *Δtert-gfp* region, and the *tol2* region in sufficient concentrations I attempted GA of the *mpeg1.1:Δtert-gfp* construct. The GA reaction ligates several sections of DNA together to produce the desired construct as described in section 3.2.1. I decided that to determine initially if a construct had the desired structure, I would use two diagnostic digests on a purified aliquot. Therefore, I used APE software to predict the banding pattern of the *mpeg1.1:Δtert-gfp* construct if it were produced in the correct orientation and digested using Xcm1 and Nco1 as one diagnostic digest, and Xho1 as a second diagnostic digest. If the banding patterns produced by the diagnostic digests were the same as those predicted by APE then I would take that construct forward to for further analysis.

3.2.7.1 Generating the *mpeg1.1:Δtert-gfp* construct using the *Δtert* region and *tol2* produced using PCR amplification.

Initially I attempted to produce the *mpeg1.1:Δtert-ires-gfp* construct (Fig. 3.2.7.1.A) using the *Δtert* region produced using PCR, and the *tol2* region produced using PCR. Despite the low concentration of the *tol2* using these regions mitigated the chance of circular template crossover during the GA reaction and subsequent transformation. I performed the GA using the *Δtert* region at 0.031pmol/µl, the *mpeg1.1* region at 0.404pmol/µl, and the *tol2* region produced using PCR at 0.00491pmol/µl. Both *Δtert* and the *mpeg1.1* region had suitable concentrations however the *tol2* region was below the recommended concentration of 0.02pmols/µl. Digesting and running the constructs produced on an agarose gel, I could not see a sample that had the predicted diagnostic digest pattern (Fig.3.2.7.1.B, C, D), so none were taken forward.

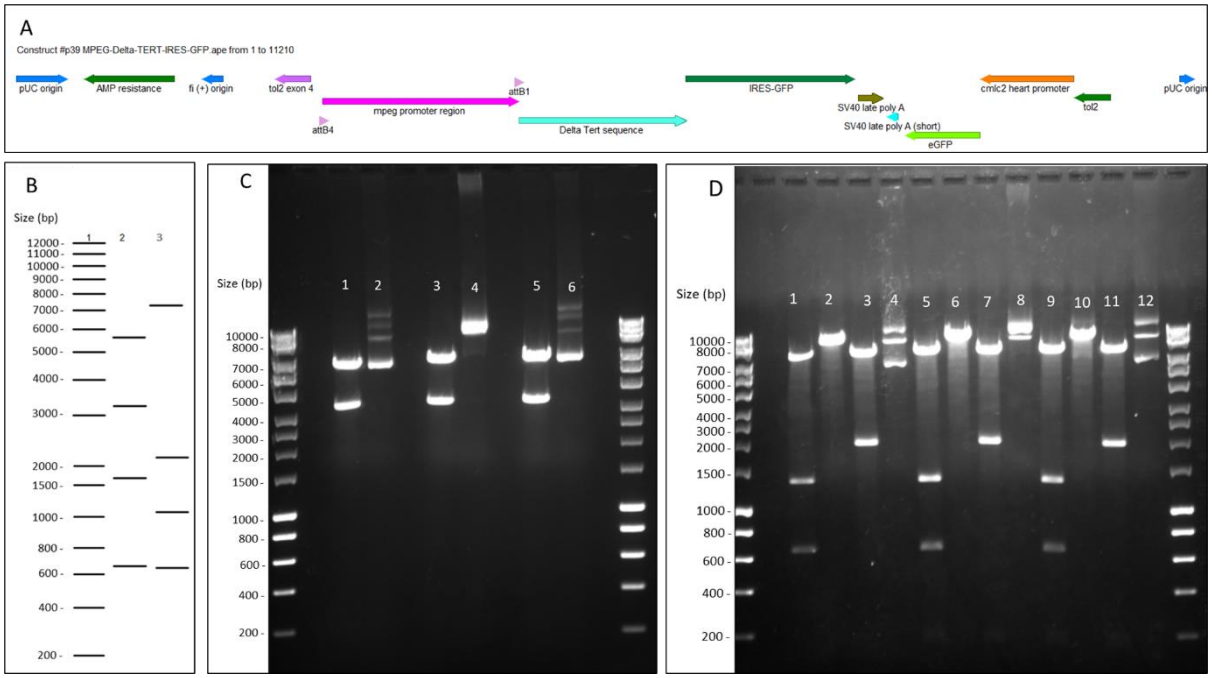

Figure 3.2.7.1: Production of the *mpeg1.1:Δtert-gfp* construct using PCR amplified regions. **A.** Theoretical linear map of the desired construct. **B.** Predicted banding patterns for enzymatic digest of desired construct: lane 1, DNA-weight ladder, lane 2, Xcm1 plus Nco1, lane 3, Xho1. **C.** Diagnostic digest of potential constructs using Xho1: lane 1, lane 3 and lane 5 are digests of potential constructs, lane 2, lane 4, and lane 6 are circular template controls using the same potential constructs. **D.** Banding pattern from potential constructs using Xcm1 and Nco1: lane 1, lane 5, and lane 9 are double digests, lane 2, lane 6, and lane 10 are Xcm1 only, lane 3, lane 7, and lane 11 are Nco1 only, lane 4, lane 8, and lane 12 are circular template positive controls.

3.2.7.2 Generating the *mpeg1.1:Δtert-gfp* construct using the *Δtert-gfp* region and *tol2* produced using enzymatic digestion.

As the first attempt at producing the *mpeg1.1:Δtert-gfp* construct had not worked I decided instead to the use *Δtert-gfp* region produced using PCR, and the *tol2* region produced using enzymatic digestion, as these had higher concentrations than the samples used in the first attempt. I performed GA again using the *Δtert-gfp* region at 0.0133pmol/µl, the *mpeg1.1* promoter at 0.095pmol/µl, and the tol2 region at 0.0154pmol/µl which was much closer to the recommended 0.02pmol/µl. Digesting and running the potential constructs using Xho1 produced on an agarose gel, I could see four samples that potentially had the correct diagnostic digest pattern (Fig.3.2.7.2.A). I ran a digest using Xcm1 and Nco1 on constructs 10, 11, 17, and 21 to confirm that the banding patterns seen were the same as those predicted (Fig. 3.2.7.1.B) and found that constructs 11, 17, and 21 had the appropriate patterns but that sample 10 had a top band that was not at the predicted weight so was not taken forward.

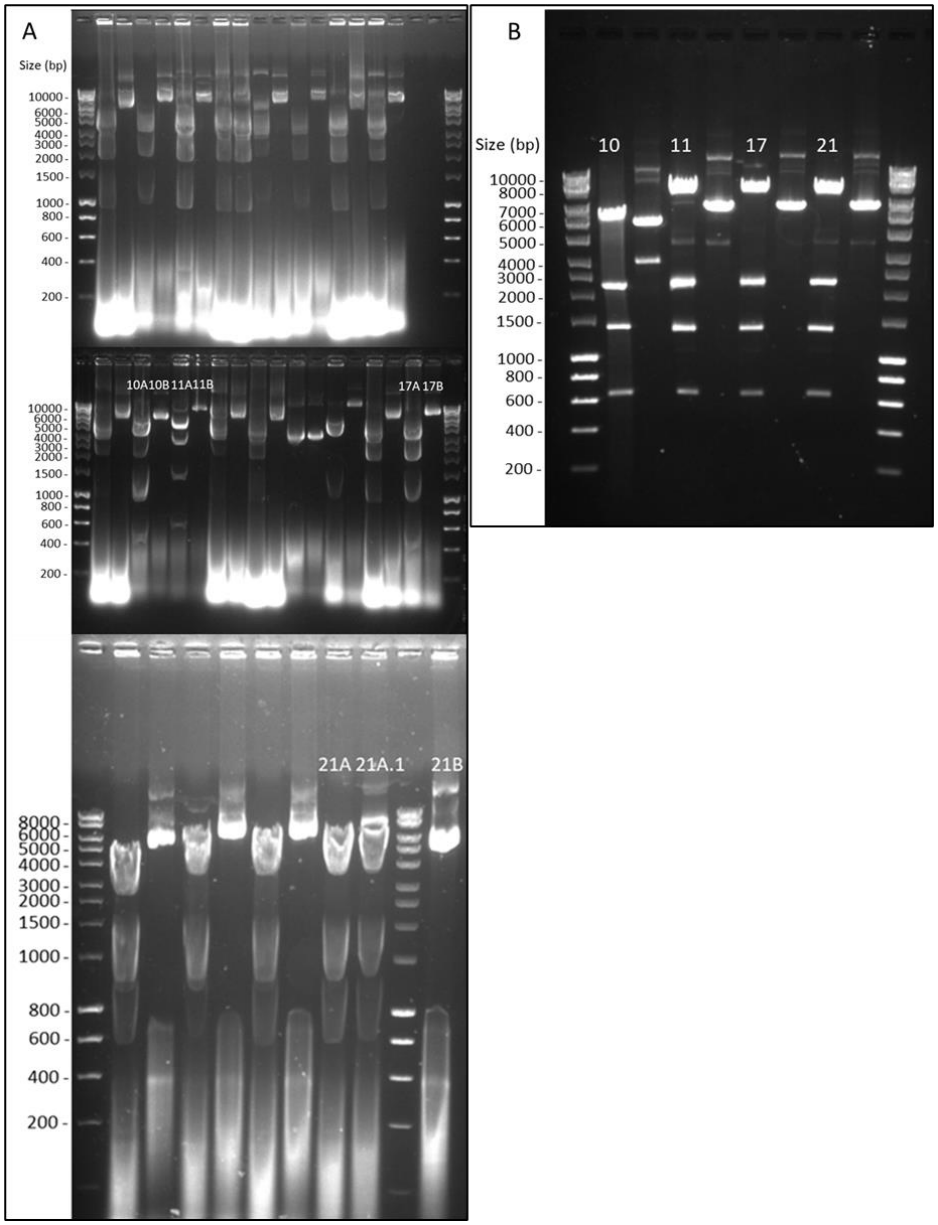

Figure 3.2.7.2: Production of the *mpeg1.1:Δtert-gfp* construct using regions produced using PCR and digestion of existing constructs. **A.** Diagnostic digest using Xho1 of potential constructs, each sample (e.g., 10A) was run next an undigested control of itself (e.g., 10B). **B.** Confirmatory double digest using Xcm1 and Nco1 of promising constructs 10, 11, 17 and 21 run next to undigested positive controls of themselves.

3.2.7.3 Sequencing of the *Δtert* region of the potential *mpeg1.1:Δtert-gfp* constructs. To confirm the *Δtert* region of the potential constructs had not been mutated during GA and bacterial transformation I had the *Δtert* region of each of the potential constructs sequenced. I used APE software to compare the sequence of the *Δtert* regions of the GA produced constructs to our predicted *in silico* sequence of the *Δtert* region (Fig. 3.2.7.3). I found that construct 17 had an unknown base pair at position 54 (Fig. 3.2.7.3.A), construct 11 had a base pair deletion at position 544 (Fig. 3.2.7.3.B) and construct 21 had multiple mismatches and unknown base pairs (Fig. 3.2.7.3.C). Examining the electropherometry plots in APE of construct 17 indicated that the unknown base pair at position 54 was an Adenine (Fig. 3.2.7.3.D) which matched the base pair at the opposite position in the predicted construct sequence. Therefore, construct 17 was not observed to have any detectable mutations and was taken forward to be used to produce the *mpeg1.1:Δtert-gfp* transgenic line.

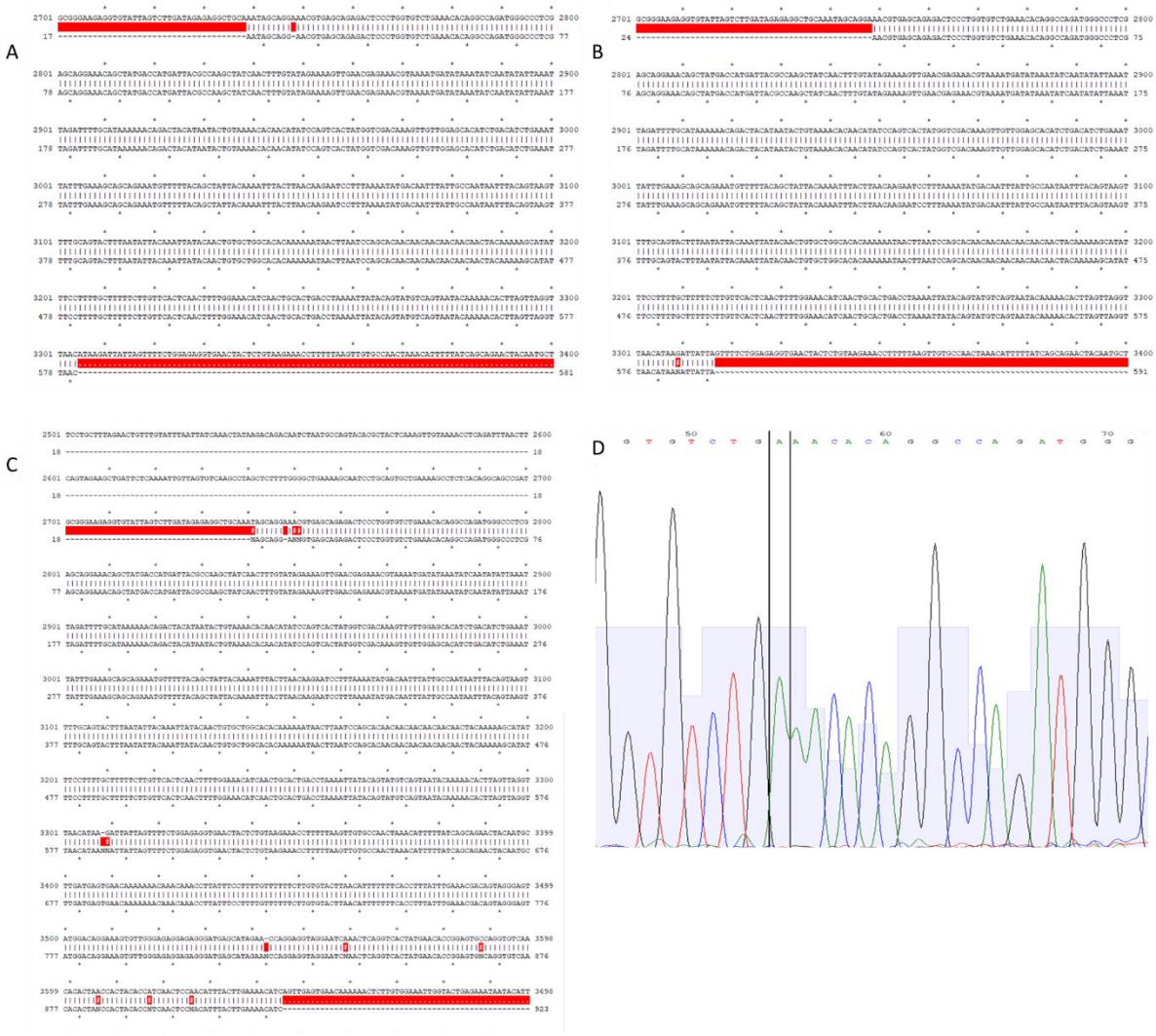

Figure 3.2.7.3: Sequencing the *Δtert* region of the *mpeg1.1:Δtert-gfp* construct. **A.** Sequencing of *Δtert* region of construct 17 compared against hypothetical *Δtert* region. **B.** Sequencing of *Δtert* region of construct 11 compared against hypothetical *Δtert*. **C.** Sequencing of *Δtert* region of construct 21 compared against hypothetical *Δtert* region. **D.** Unknown point from potential construct 17 shown to be an adenine base in electropherometry plot of sequence.

3.2.8 Breeding the transgenic zebrafish fish lines.

To study the canonical and non-canonical functions of telomerase in this project it was necessary to generate two transgenic zebrafish lines, one containing the transgene *mpeg1.1:tert-gfp* and the other the transgene *mpeg1.1:Δtert-gfp*. To study the effects these transgenes had on the prematurely aged *mpeg1.1*$^{+}$ cells found in the zebrafish gut the transgenes would need to be expressed in a prematurely aged zebrafish line. The prematurely aged zebrafish would be *tert*$^{-/-}$*:mpeg1.1:mCherry*$^{+}$ as well as either *mpeg1.1:tert-gfp*$^{+}$ or *mpeg1.1:Δtert-gfp*$^{+}$ depending on the injected transgene. To characterise the two lines I determined if the transgene was being expressed in *mpeg1.1:mCherry*$^{+}$ cells using fluorescence immunohistochemistry. I then used whole genome sequencing to establish the insertion site of the transgenes to ensure that their insertion would not affect the transgenic zebrafish' biology by disrupting other genes.

3.2.8.1 Breeding the *mpeg1.1:tert-gfp* transgenic line.

Based on the utilisation of the hu3430 line and the insertion of the transgene in a manner that would follow mendelian inheritance I designed a breeding programme to generate the desired *tert*$^{-/-}$*;mpeg1.1:mCharry.caax;mpeg1.1:tert-gfp* transgenic fish to study (Fig. 3.2.8.1). To breed the *mpeg1.1:tert-gfp* transgenic line I used eight potential founders that has been injected with the transgene before I joined the Henriques lab. These potential founders had been injected with the *mpeg1.1:tert-gfp* transgene at the single cell fertilised egg stage before being selected as transgenic due to their expression of the *cmcl2:egfp* expression and grown up. Therefore, the G_o generation are considered to be chimeras as the transgene may not be inserted into every cell. Using breeding and counting of the number of GFP^{+} fry compared to the number of GFP^{-} fry I determined three potential founders. The offspring of these potential founders were inheriting the *cmcl2:egfp* reporter, and therefore hypothetically the entire *mpeg1.1:tert-gfp* transgene, in a mendelian manner as half of the offspring had GFP^{+} hearts and half had GFP^{-} hearts. This indicated that the transgene was inserted into the germline, and that only one copy of the transgene was inserted, as if two

copies were inserted we would expect all of the offspring to have GFP^{+} hearts. The three potential founders were designated A1, A2, and C1. I then commenced with the breeding of these potential founders using the breeding plan from Fig. 3.2.8.1. GFP^{+} fish were selected and used to further characterise the expression and function of the *mpeg1.1:tert-gfp* transgene to validate the line.

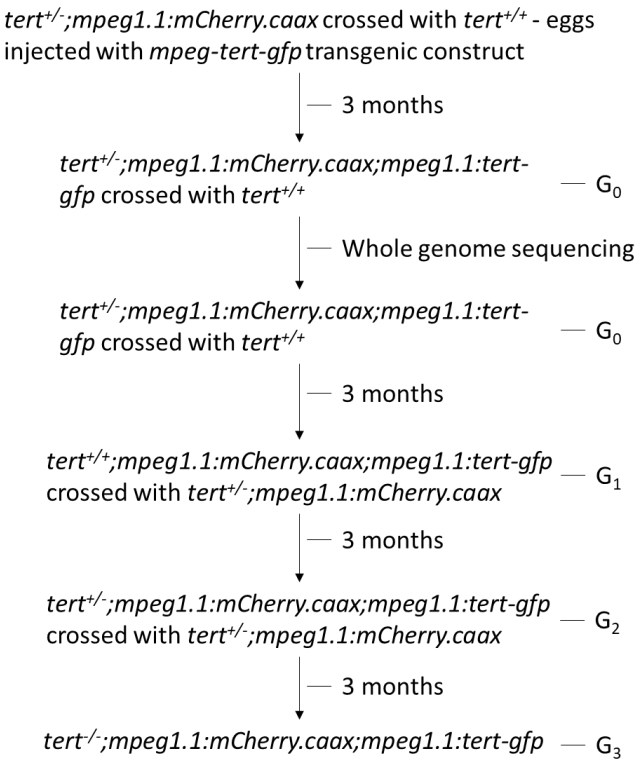

Figure 3.2.8.1: Breeding plan to for the *mpeg1.1:tert-gfp* line.

3.2.8.2 Breeding the *mpeg1.1:Δtert-gfp* transgenic line.

To breed the *mpeg1.1:Δtert-gfp* line I injected single cell fertilised embryos with the transgene. These embryos were selected for GFP$^+$ hearts as the *cmcl2:eGFP* reporter will be expressed during heart development and indicate the expression of the transgene (Fig. 3.2.8.A). I identified eight potential founders which were taken forward for breeding to determine which had a stable insertion of the *mpeg1.1:Δtert-gfp* transgene in their germ line. A stable insertion was again determined by the mendelian inheritance of the *cmcl2:eGFP* reporter. Three potential lines were identified to have a stable insertion and designated B7, C1A, and C1B. These three lines were taken forward for the *mpeg1.1:Δtert-gfp* breeding plan in Figure 3.2.8.2.B.

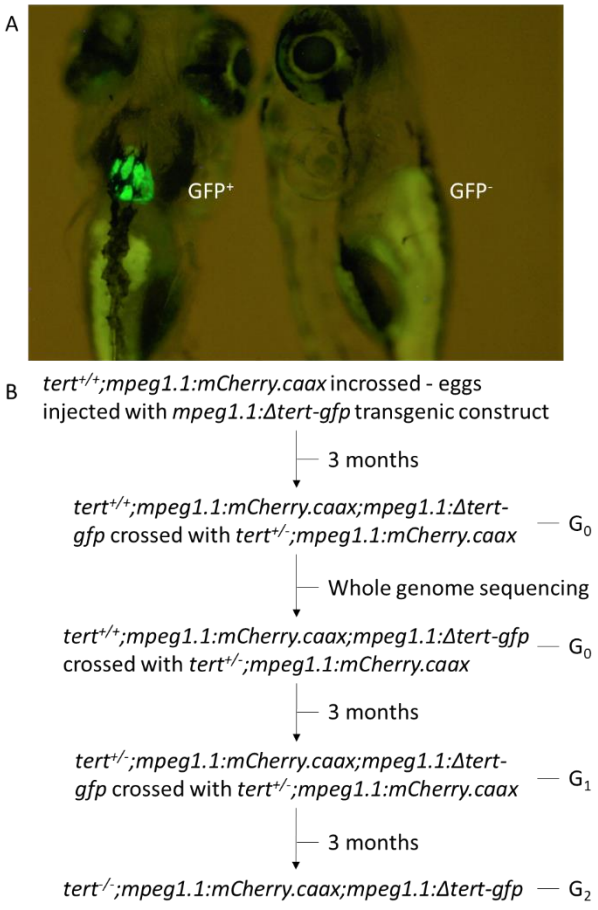

Figure 3.2.8.2: Breeding plan for the *mpeg1.1:Δtert-gfp* transgenic line. **A.** Representative image of zebrafish fry 3 days post-fertilisation (dpf), fry on left has GFP$^+$ heart indicating insertion of the transgene via expression of *cmcl2:egfp*, fry on the right has a GFP$^-$ heart so has no transgene insertion. **B.** Breeding plan to for the

3.2.9 Validating the expression of the *mpeg1.1:tert-gfp* transgene in potential founders by detecting expression of GFP and mCherry using fluorescence microscopy.

Having bred potential founders for the *mpeg1.1:tert-gfp* line I aimed to determine if they were expressing the transgene in *mpeg1.1:mCherry.caax*$^{+}$ cells by examining cryosections of intestinal villi using fluorescence microscopy. The expression of mCherry would indicate that the transgene was being expressed in *mpeg* utilising cells that may be B-cells, dendritic cells, or macrophages (185, 234). GFP expression would indicate that the *mpeg1.1:tert-gfp trans*gene was being expressed. Co-expression of mCherry and GFP would indicate that the *mpeg1.1:tert-gfp* transgene was being expressed in *mpeg1.1*$^{+}$ cells.

I used fluorescence microscopy to examine cryosections (Fig.3.2.9, A, B, C) of gut villi taken from the siblings (n = 3) of four potential G_1 founders (*tert*$^{+/-}$*;mpeg1.1:mCherry.caax;mpeg1.1:tert-gfp*), designated A1, A2, C1 (Fig. 3.2.9.D). Founder siblings were culled at 6mo, genotyped for endogenous *tert* as *tert*$^{+/-}$, and screened at 3dpf for a GFP heart to confirm the expression of the *cmcl2:eGFP* reporter indicating expression of the *mpeg1.1:tert-gfp* transgene. For the control I used *tert*$^{+/+}$*;mpeg1.1:mCherry.caax* (n=1) aged matched (6mo) to the potential founders siblings. For each fish I averaged the number of cells that were double positive for GFP and mCherry and performed a One-way Analysis of Variance (ANOVA) test to determine if there was a statistically significant difference between the potential founders and the control (Fig. 3.2.9.D). All potential founders were indicated to have statistically significant numbers of double positive cells compared to the negative control (Fig. 3.2.9.D). Therefore, this preliminary indicator of the expression of the *mpeg1.1:tert-gfp* transgene in potential founder lines indicated its expression in all three lines. The number of biological replicates in the control group was limited to n=1 due to the need for age matched fish available at the time point required of this experiment.

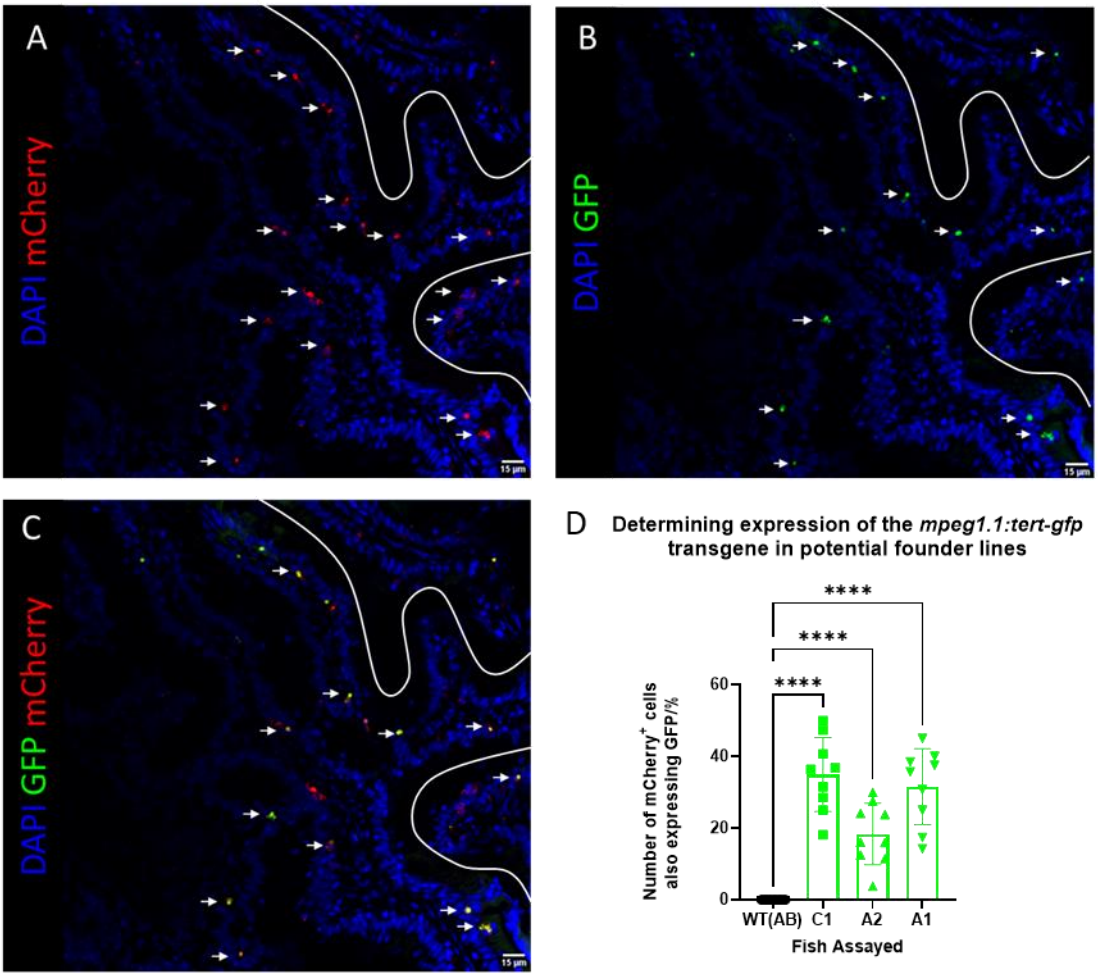

Figure 3.2.9: Determining the expression of the *mpeg1.1:tert-gfp* transgene by fluorescence imaging in potential founders. **A.** Representative images of DAPI and native fluorescence imaging indicating mCherry positive cells in zebrafish gut cryosections of *mpeg1.1:tert-gfp* founder siblings (6mo). **B.** DAPI and native fluorescence imaging indicating GFP positive cells in zebrafish gut cryosections of *mpeg1.1:tert-gfp* founder siblings. **C.** DAPI and native fluorescence imaging indicating GFP expression in mCherry^{+} cells in zebrafish gut cryosections of *mpeg1.1:tert-gfp* founder siblings. **D.** Quantification of double positive (GFP^{+} mCherry^{+}) cells in potential founder sibling gut sections (N=3 for potential founders, N=1 for negative control). **** = $p < 0.0001$

3.2.10 Sequencing of founder genomes from the *mpeg1.1:tert-gfp* transgenic zebrafish line.

Fluorescence microscopy imaging of potential founders indicated that the *mpeg1.1:tert-gfp* transgene was being expressed. However, the tol2 transposon inserts the transgene at a random position. Therefore, the genomes of the three potential founders were sequenced. Sequencing the genomes of potential founders would enable me to determine where in the genome the transgenic sequence was inserted. Additionally, determining the insertion site of the transgene would indicate if it's insertion would have unforeseen effects on the transgenic zebrafish' physiology for example via a frameshift mutation resulting from the insertion of the transgene into another gene.

3.2.10.1 Optimising the extraction of genomic DNA from zebrafish fin clips suitable for whole genome sequencing.

I had not previously performed extraction of DNA from a tail fin clip for the purpose of whole genome sequencing so decided to optimise the extraction of DNA for this purpose so that I could provide the best quality DNA sample for sequencing. The quality of the sample was determined by the concentration, the 260/280 (Fig. 3.2.10.A, B) value, and the 260/230 value. The 260/280 value is the ratio of 260nm wavelength light absorbance to 280nm wavelength light absorbance. DNA absorbs light at 260nm whereas protein contaminants will absorb light at 280nm. Therefore, the ratio of the two measures is an indicator of protein contamination in the sample. The 260/230 value is the ratio of 260nm wavelength light absorbance to 230nm wavelength light absorbance. Measuring the absorbance of 230nm light is an indicator of biological and chaotropic contaminants that may affect hydrogen bonds between atoms. Disrupting hydrogen bonding in the sample will affect the structure of the DNA and therefore the final quality of the sample.

I used two different methods for isolating genomic DNA from a zebrafish tail fin-clip. One method utilised the Monarch Genomic DNA extraction and purification kit from New England Bioscience, and the other was a protocol that utilises the Fermentas DNA extraction kit. I found that the Fermentas kit gave better concentrations of DNA that had less contaminants as assessed by the 260/280 and 260/230 values (Fig. 3.2.10.C). Therefore, I

proceeded with the Fermentas Kit to purify DNA for whole genome sequencing (Fig. 3.2.10.D).

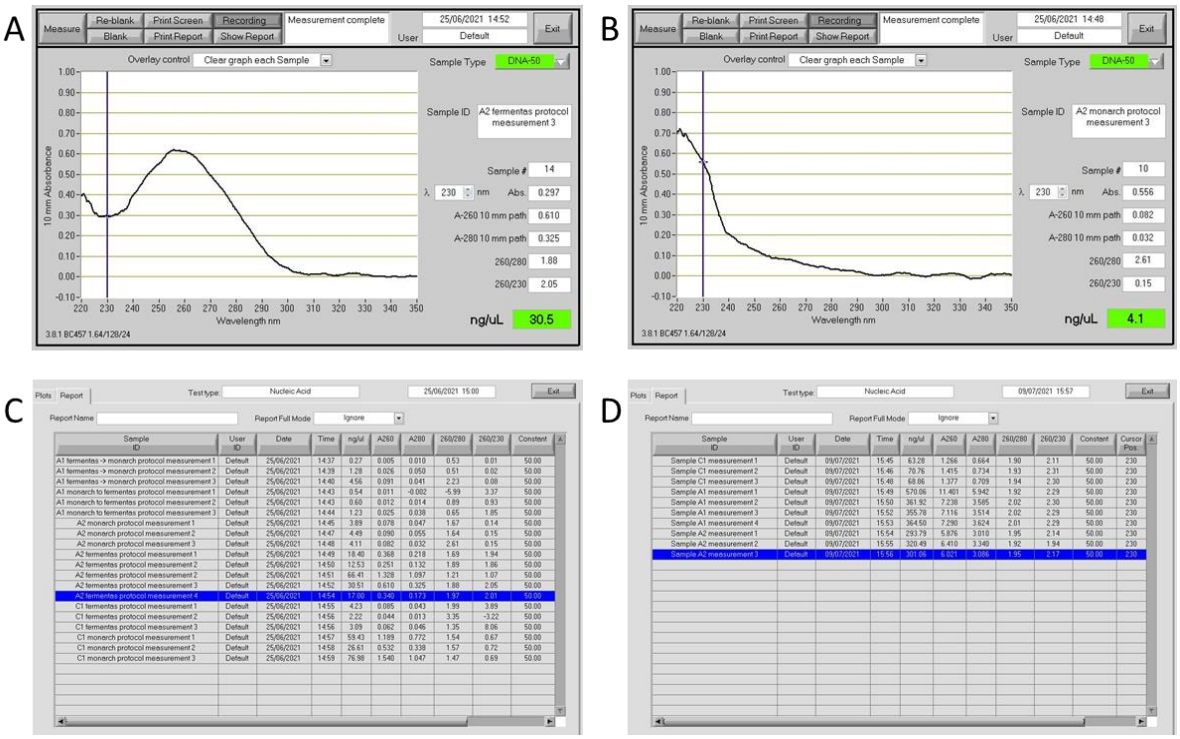

Figure 3.2.10.1: Optimising extraction of DNA suitable for whole-genome sequencing. **A.** Representative absorbance plot of DNA extracted from potential founder A2 using Fermentas protocol. **B.** Representative absorbance plot of DNA extracted from potential founder A2 using Monarch protocol. **C.** Extracted DNA concentrations comparing Monarch and Fermentas protocols. **D.** Extracted DNA readings from all founders using Fermentas protocol for samples sent for sequencing.

3.2.10.2 Variant analysis of sequenced *mpeg1.1:tert-gfp* founder genomes

To determine where in the genome the *mpeg1.1:tert-gfp* transgenes were inserted whole genome sequencing was performed on potential founders. The sequences were then aligned to an artificial *mpeg1.1:tert-gfp* chromosome, and the clipped end read sequences determined. The clipped end read sequences flank either end of the inserted transgene. By determining the sequences of the clipped end read sequences and using Basic Local Alignment Search Tool (BLAST) to search for sequences and matching them to a gene I can determine the insertion site of the transgene as well as how its insertion may affect the transgenic zebrafish' phenotype in ways other than those intended.

Whole genome sequencing of the potential founders for the *mpeg1.1:tert-gfp* line indicated that all three had the transgene inserted in its entirety. Founder A2 had the most comprehensive read coverage (Supp. Fig. 1.B), followed by founder C1 (Supp. Fig. 1.C) and A1 (Supp. Fig. 1.A). Using the BLAST online software from the National Library of Medicine I conducted searches to determine where the clipped-end reads matched the zebrafish genome. Clipped end reads are sequences of DNA that do not match the reference sequence but form part of the 150bp read that partially matches a section of the reference sequence. Therefore, the clipped end reads match partially to the reference sequence provided by me for the *mpeg1.1:tert-gfp* transgene, and partially to the zebrafish reference genome.

Interestingly the *mpeg1.1:tert-gfp* transgenes for both founder A1 and A2 were found to be inserted in the same place in chromosome 21 from position 41,004,589 to 41,004,708 (Supp. Fig. 1A, B). This places the *mpeg1.1:tert-gfp* transgene into the untranslated exon sequence of *larsb*. The gene *larsb* is predicted to code for a protein with leucine-tRNA ligase activity involved in leucyl-tRNA aminoacylation an important component of protein synthesis whereby leucine is ligated to tRNA(253). Recently *Inoue et al.* generated a *larsb*$^{-/-}$ zebrafish line to study the molecular mechanism of the disease state Infantile Liver Failure Syndrome type 1 (ILFS1) that occurs with *larsb* homologue mutations in humans(253). *Inoue et al.* found that the *larsb*$^{-/-}$ mutation resulted in death within 12 days post fertilization of the embryos(253). Therefore, we may hypothesise that despite the insertion of the *mpeg1.1:tert-gfp* transgene into the *larsb* untranslated exon the insertion is having little to

no effect on the phenotype of the A1 and A2 founders due to them developing to full maturity.

Sequencing of the *mpeg1.1:tert-gfp* transgenic founder C1 indicated that the transgene had been inserted into chromosome 11 from position 24,906,202 to 24,906,258 (Supp. Fig. 1.E). This insertion site is part of the intron region for the gene *sla2a* which is predicted to have 1-phosphatidylinositol-3-kinase regulator activity and be involved in phosphatidylinositol phosphorylation. A homologue of this gene is found in humans (*sla2)* which encodes the protein src-like-adapter 2 (SLAP2). SLAP2 has been indicated to impair antigen-receptor mediated signalling events in human B-cell lines and T-cell lines(254). Therefore, if the insertion of the *mpeg1.1:tert-gfp* gene into the intron of *sla2a* affected expression of the gene it may affect antigen-receptor mediated signalling in T-cells and B-cells of the C1 founder line.

From these sequencing results I consider the A2 founder line to be the most promising line to take forward to generate experimental fish. This is due to it having the most in-depth reads of the inserted transgene, increasing the reliability that there are no mutations in the inserted transgene, and that its insertion into the Untranslated Region (UTR) of the *larsb* gene does not currently seem to affect the zebrafish phenotype.

3.2.11 Validation of the expression of the *mpeg1.1:tert-gfp* transgene in third generation transgenics using fluorescent immunohistochemistry.

To confirm that the *mpeg1.1:tert-gfp* transgene had been passed down to the generation 3 (G3) of the C1 founder line I used fluorescence immunohistochemistry to detect the expression of mCherry and GFP in paraffin fixed gut sections. By detecting mCherry I could confirm that the cell utilised the *mpeg1.1* promoter which also drives the expression of the *mpeg1.1:tert-gfp* transgene (Fig. 3.2.11.C). By detecting GFP I would confirm that the *mpeg1.1:tert-gfp* transgene was being expressed (Fig. 3.2.11.E). I used double fluorescence immunohistochemistry with one primary antibody specific to mCherry (Table 2.26.1 Antibody #1) and the corresponding secondary with a far-red fluorescent tag (Table 2.26.1 Antibody #2), and a second primary antibody specific to GFP (Table 2.26.1 Antibody #6) with the corresponding secondary in GFP (Table 2.26.1 Antibody #5). A far-red fluorophore

conjugate was used as the mCherry secondary antibody for consistency as later experiments I planned to perform would examine the effects of the transgenes on telomere length using the Telo-FISH assay which contains a red fluorescent probe and so would necessitate the use of an alternative probe for mCherry. A one-way Analysis of Variance (ANOVA) determined that the levels of GFP expression in the mCherry^{+} cells was not significant (Fig. 3.2.11.I). This indicates that the level of GFP expression detected was not enough to say with certainty that the transgene was being expressed. However, that there was any GFP expression detected in mCherry^{+} cells indicated that GFP was being expressed and that the transgene was inserted. Therefore, I would perform additional experiments to further validate that the *mpeg1.1:tert-gfp* transgene was inserted and that TERT was being expressed in an *mpeg1.1* specific manner.

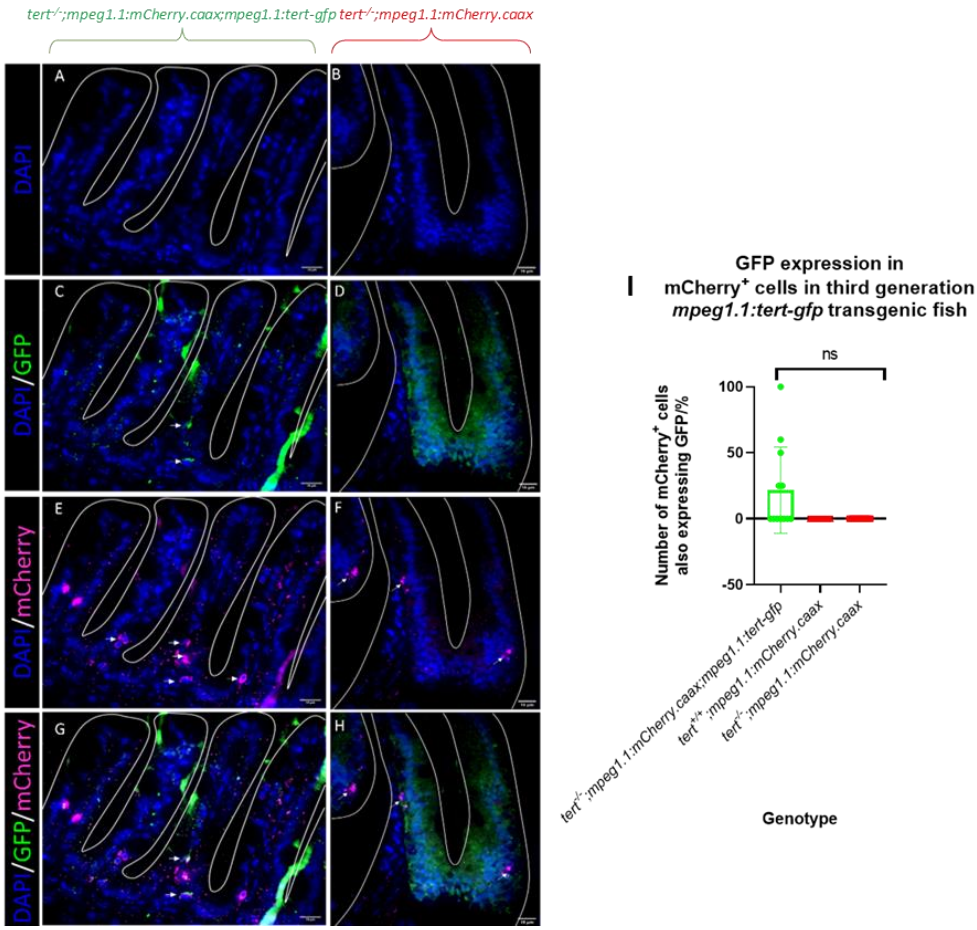

Figure 3.2.11: Determining the expression of the *mpeg1.1:tert-gfp* transgene. **A.** DAPI staining of cell nucleus in *tert*$^{-/-}$;*mpeg1.1:mCherry.caax*;*mpeg1.1:tert-gfp* fish gut. **B.** IF showing DAPI staining of cell nucleus plus anti-mCherry in *tert*$^{-/-}$;*mpeg1.1:mCherry.caax* fish gut. **C.** IF showing DAPI staining of cell nucleus plus anti-mCherry staining in *tert*$^{-/-}$;*mpeg1.1:mCherry.caax;mpeg1.1:tert-gfp* fish gut. **D.** IF showing DAPI staining of cell nucleus plus anti-GFP in *tert*$^{-/-}$;*mpeg1.1:mCherry.caax* fish gut. **E.** DAPI staining of cell nucleus plus anti-GFP staining in *tert*$^{-/-}$;*mpeg1.1:mCherry.caax*;*mpeg1.1:tert-gfp* fish gut. **F.** IF showing DAPI staining of cell nucleus plus anti-mCherry and anti-GFP in *tert*$^{-/-}$;*mpeg1.1:mCherry.caax* fish gut. **G.** IF showing DAPI staining of cell nucleus plus anti-mCherry and anti-GFP staining in *tert*$^{-/-}$;*mpeg1.1:mCherry.caax*;*mpeg1.1:tert-gfp* fish gut. **H.** IF showing DAPI staining of cell nucleus plus anti-mCherry and anti-GFP staining in *tert*$^{-/-}$;*mpeg1.1:mCherry.caax* fish gut. **I.** Quantification of double positive (anti-GFP + anti-mCherry) in *tert*$^{-/-}$;*mpeg1.1:mCherry.caax*;*mpeg1.1:tert-gfp* zebrafish gut compared to aged matched *tert*$^{-/-}$;*mpeg1.1:mCherry.caax* controls (N = 3 for each genotype). One-way ANOVA indicated non-significant, p = 0.053.

3.2.12 Characterising the effects of the *mpeg1.1:tert-gfp* gene on telomere length.

Despite seeing some expression of GFP in mCherry^{+} cells in the *mpeg1.1:tert-gfp* transgenic the p value indicated that the expression levels were not significant. Therefore, there was no statistically significant evidence that the *mpeg1.1:tert-gfp* transgene was being expressed. This led to the hypothesis that I could determine if the transgene were being expressed based on the telomere length of *tert$^{-/-}$;mpeg1.1:mCherry.caax;mpeg1.1:tert-gfp* mCherry^{+} cells. *Henriques et al* had previously reported that *tert$^{-/-}$* zebrafish have no detectable telomerase activity which leads to a premature shortening of telomeres (218). Therefore, in *tert$^{-/-}$;mpeg1.1:mCherry.caax;mpeg1.1:tert-gfp* mCherry^{+} cells we would expect to see telomeres longer than in *tert$^{-/-}$;mpeg1.1:mCherry.caax* mCherry^{+} cells. Additionally, as a byproduct of the breeding programme we generated *tert$^{+/+}$;mpeg1.1:mCherry.caax;mpeg1.1:tert-gfp* mCherry^{+} fish. I decided to include these fish in this analysis as I would also expect to see an increase in their telomere length relative to *tert$^{+/+}$;mpeg1.1:mCherry.caax* and *tert$^{-/-}$;mpeg1.1:mCherry.caax* fish. By comparing the the telomere length *tert$^{+/+}$;mpeg1.1:mCherry.caax, tert$^{-/-}$;mpeg1.1:mCherry.caax, tert$^{+/+}$;mpeg1.1:mCherry.caax;mpeg1.1:tert-gfp,* and *tert$^{-/-}$;mpeg1.1:mCherry.caax;mpeg1.1:tert-gfp* I would be able to determine if the *mpeg1.1:tert-gfp* transgene was being expressed.

To measure telomere length I used telomere fluorescence in-situ hybridisation (telo-FISH) (Fig. 3.2.12.B, E). The telo-FISH assay uses a fluorescently labelled DNA probe to hybridise with telomeric DNA. The intensity of the fluorescent signal from the telo-FISH probe is proportionate to the cell's telomere length. The *tert$^{+/+}$;mpeg1.1:mCherry.caax* acts as a positive control as it will have the telomere intensity we would expect to see with normal ageing. the *tert$^{-/-}$;mpeg1.1:mCherry.caax* acts as a negative control as it will have prematurely shortened telomeres by 9mo. Further, as the expression of the transgene is under *mpeg1.1* control we would not expect to see any expression in epithelial cells. Therefore, the telo-FISH staining of the epithelial cells can be used to normalise the telo-FISH staining of the mCherry^{+} cells to control for potential inter-sample variation in staining and imaging between sections.

I performed a one-way ANOVA to determine if there was a statistically significant difference in telo-FISH intensity between the mCherry^{+} cells from the *tert$^{-/-}$;mpeg1.1:mCherry.caax* compared to the other genotypes. As expected there was a significant difference between the *tert$^{-/-}$;mpeg1.1:mCherry.caax* and *tert$^{+/+}$;mpeg1.1:mCherry.caax* controls (Fig. 3.2.12.G). Further, analysis indicates a statistically significant difference in telo-FISH intensity between *tert$^{-/-}$;mpeg1.1:mCherry.caax* and the *tert$^{-/-}$;mpeg1.1:mCherry.caax;mpeg1.1:tert-gfp* mCherry^{+} groups indicating that the telomeres of the *tert$^{-/-}$;mpeg1.1:mCherry.caax;mpeg1.1:tert-gfp* mCherry^{+} cells were longer than those of the *tert$^{-/-}$;mpeg1.1:mCherry.caax* mCherry^{+} group. Interestingly, I observe no statistically significant difference between the *tert$^{-/-}$;mpeg1.1:mCherry.caax;mpeg1.1:mCherry.caax* mCherry^{+} group and the *tert$^{+/+}$;mpeg1.1:mCherry.caax* mCherry^{+} group indicating that the length of the telomeres in the *tert$^{-/-}$;mpeg1.1:mCherry.caax;mpeg1.1:mCherry.caax* mCherry^{+} group had been rescued to a length comparable to *tert$^{+/+}$;mpeg1.1:mCherry.caax* mCherry^{+} group (Fig. 3.2.12). I also observed a statistically significant difference between the *tert$^{+/+}$;mpeg1.1:mCherry.caax;mpeg1.1:tert-gfp* group and all other mCherry^{+} groups indicating that their telomeres may have been longer than all of the other groups (Fig. 3.2.12). Therefore, this data is evidence that the inserted *mpeg1.1:tert-gfp* transgene is being expressed and that the TERT that results from this expression is performing its canonical function of elongating telomeres. However, the quality of the staining on the slides (Fig. 3.2.12.D, E, F) was such that it was difficult to be completely certain that all of the cells that looked like mCherry^{+} were. The mCherry specific staining appeared broken or globular in some slides (Fig. 3.2.12.D, E, F). Therefore, I would repeat this experiment again to optimise the staining as well as increasing the N number for the number of slides per fish, as the quality of the staining led to N = 1 in some cases so reducing the quality of the data.

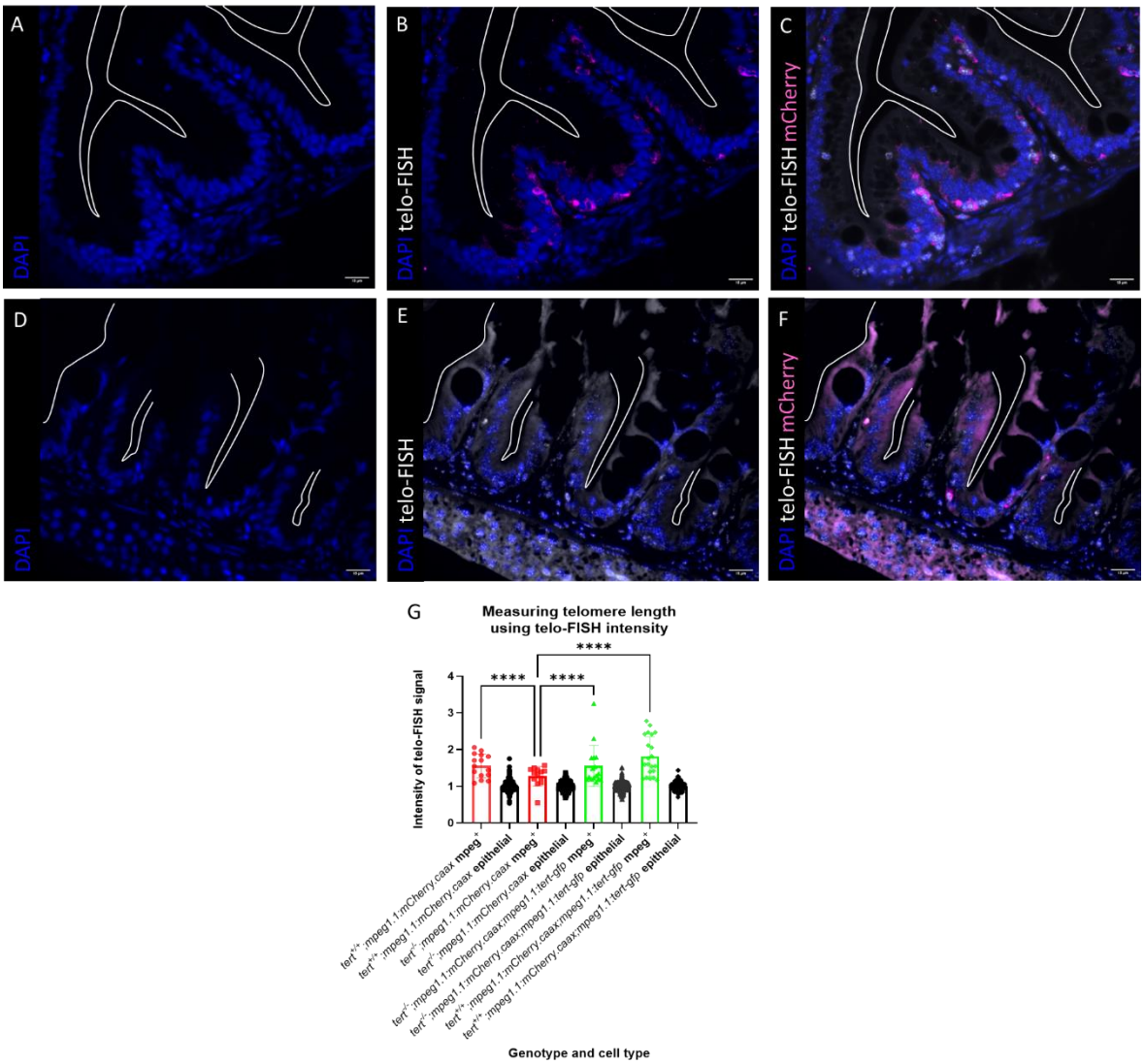

Figure 3.2.12: Determining the expression of the *mpeg1.1:tert-gfp* transgene in mCherry^{+} cells by quantifying telomere length. **A.** DAPI staining of a *tert*$^{+/+}$*;mpeg1.1:mCherry.caax;mpeg1.1:tert-gfp* gut section. **B.** IF of DAPI plus telo-FISH staining *tert*$^{+/+}$*;mpeg1.1:mCherry.caax;mpeg1.1:tert-gfp* gut section. **C.** IF of DAPI, telo-FISH, and mCherry^{+} staining of a *tert*$^{+/+}$*;mpeg1.1:mCherry.caax;mpeg1.1:tert-gfp* gut section. **D.** DAPI staining of a *tert*$^{-/-}$*;mpeg1.1:mCherry.caax;mpeg1.1:tert-gfp* gut section **E.** IF of DAPI plus telo-FISH staining *tert*$^{-/-}$*;mpeg1.1:mCherry.caax;mpeg1.1:tert-gfp* gut section. **F.** IF of DAPI, telo-FISH, and mCherry^{+} staining of a *tert*$^{-/-}$*;mpeg1.1:mCherry.caax;mpeg1.1:tert-gfp* gut section. **G.** Quantification of normalised telo-FISH staining intensity in mCherry^{+} and epithelical cells. N = 3 per group. N= 1-3 per fish. One-way ANOVA where **** $p < 0.0001$, ns = $p > 0.05$

3.2.13 Optimisation of the Telomerase Repeat Amplification Protocol for the measurement of telomerase activity in zebrafish gut.

Having obtained data indicating that TERT was active in mCherry+ cells of the *tert*$^{-/-}$*;mpeg1.1:mCherry.caax;mpeg1.1:tert-gfp* genotype (section 3.2.12) I wanted to further study the level of TERT activity to determine if it was being rescued to a level comparable to that of *tert*$^{+/+}$*;mpeg1.1:mCherry.caax* mCherry+ cells. To quantify this, I would use the Telomerase Repeat Amplification Protocol (TRAP assay). The TRAP assay uses the telomerase active in sample to elongate an artificial telomere, this translates to a colorimetric reaction where the change in colour intensity is proportional to telomerase activity. Previously it has been reported that there is no detectable telomerase activity in *tert*$^{-/-}$ zebrafish (218), therefore I used *tert*$^{+/+}$*;mpeg1.1:mCherry.caax* as the positive control and *tert*$^{-/-}$*;mpeg1.1:mCherry.caax* as the negative control. As it has been published that there is no detectable telomerase activity in *tert*$^{-/-}$ zebrafish, I can assume that any telomerase activity detected in the *tert*$^{-/}$*;mpeg1.1:mCherry.caax;mpeg1.1:tert-gfp* samples will be due to the expression of the *mpeg-tert-gfp* transgene.

Initially I isolated a population of mCherry+ cells using FACS(Fig. 3.2.13.A). My hypothesis in doing this was that isolating only mCherry+ cells improve the signal in the TRAP assay, as hypothetically all mCherry+ cells from the *tert*$^{-/}$*;mpeg1.1:mCherry.caax;mpeg1.1:tert-gfp* line would be expressing the *mpeg1.1:tert-gfp* transgene, and the TRAP signal would not be diluted by including the protein from other cells. To accurately compare the TRAP assay of each sample I needed to add the same amount of protein extract from each sample. To determine the protein concentration extracted from the cells of each sample I used the BCA assay (Fig. 3.2.13.B). The BCA assay produces a standard curve of known protein concentrations that I can then use to calculate the protein concentration in my extracted samples.

Assaying the protein concentration isolated from the FACS samples indicates that there was too little protein isolated for me to obtain an accurate measure of its concentration using the BCA curve (Fig. 3.2.13.C). Therefore, considering that the *tert*$^{-/-}$ fish have been reported to have no detectable telomerase activity (218) I decided to use whole gut lysate with the TRAP assay to determine the telomerase activity in the *tert*$^{-/--}$

;mpeg1.1:mCherry.caax;mpeg1.1:tert-gfp transgenic as this would provide me with a much higher concentration of protein and therefore more telomerase.

Initially I tested different amounts of protein from a *tert*$^{+/+}$*;mpeg1.1:mCherry.caax* control to determine the telomerase activity I would expect to see using difference amounts of protein (Fig. 3.2.13.C). I also added an additional positive control of HT1080 cells, an immortalised cell line with constitutive telomerase expression. The data indicates detectable telomerase activity in 3µg, 1.5µg, and 0.5µg *tert*$^{+/+}$*;mpeg1.1:mCherry.caax* protein samples(Fig. 3.2.13.C).

I decided to use 3µg of protein isolate from zebrafish whole gut to determine telomerase activity in the transgenic as this would maximise the amount of TERT added to the sample and therefore maximise the amount of telomerase activity. To determine the telomerase activity in the *tert*$^{-/-}$*;mpeg1.1:mCherry.caax;mpeg1.1:tert-gfp* transgenic I used *tert*$^{+/+}$*;mpeg1.1:mCherry.caax* as a positive control as well as HT1080 cell isolate as second positive control and *tert*$^{-/-}$*;mpeg1.1:mCherry.caax* isolate as the negative control. Fresh protein aliquots were isolated from zebrafish gut and 3µg of protein was used from each isolate. Both the *tert*$^{-/-}$*;mpeg1.1:mCherry.caax* and the *tert*$^{-/-}$*;mpeg1.1:mCherry.caax;mpeg1.1:tert-gfp* had negative values for their telomerase activity measurements indicating a lack of any detectable telomerase activity (Fig. 3.2.13.D).

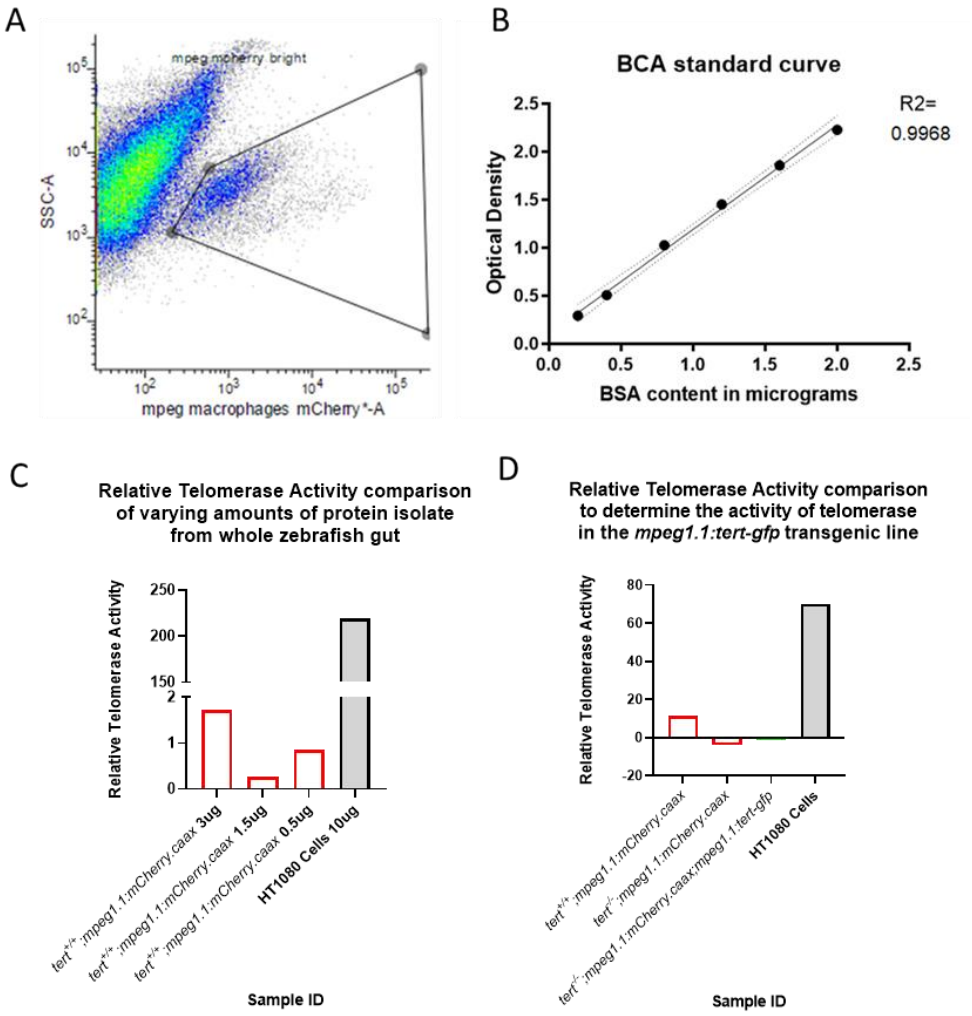

Figure 3.2.13: Quantifying the activity of telomerase expressed by the *mpeg1.1:tert-gfp* transgenic line. **A.** Representative gating for the sorting of mCherry+ cells from the *tert*$^{+/+}$*;mpeg1.1:mCherry.caax* zebrafish gut. **B.** Example BCA standard curve generated to detect protein concentration from cell lysates. **C.** Telomerase activity measured using the TRAP assay from differing protein concentrations. **D.** Telomerase activity of different genotypes measured using the TRAP assay.

3.2.14 Quantification of the expression of *mpeg1.1:Δtert-gfp* in mCherry positive cells in potential founders using fluorescent immunohistochemistry.

To determine if potential G_1 founders of the *mpeg1.1:Δtert-gfp* transgene had been inserted I determined to use fluorescent immunohistochemistry to detect the expression of GFP in mCherry+ cells. Detecting the GFP would indicate that the *mpeg1.1:Δtert-gfp* was being expressed due to the GFP reporter. Additionally, fluorescent immunohistochemistry would detect GFP and mCherry in paraffin fixed sections and fixing the sections in paraffin would allow us to keep the sections for longer to perform other experiments on them such as the telo-FISH assay. Both GFP and mCherry transgene are under the control of the *mpeg1.1* promoter, so any cell that was $mCherry^+$ should also hypothetically be GFP+.

Using fluorescent immunohistochemistry to detect GFP and mCherry I counted the number of cells that were both GFP^+ and $mCherry^+$ in sections of fixed zebrafish gut where N=3 for the number of zebrafish and n = 3 for the number of sections of gut. I founder almost no cells expressing GFP and mCherry despite finding $mCherry^+$ positive cells (Fig. 3.2.14.C). This was unexpected as the potential transgenic founders had GFP positive hearts, indicating the insertion and expression of the *cmcl2:eGFP* section of the transgene. It is possible that only the *cmcl2:eGFP* section of the transgene inserted and so it is this that is being inherited from generation to generation instead of the entire *mpeg1.1:Δtert-gfp* transgene. Despite having little evidence that the *mpeg1.1:Δtert-gfp* transgene was inserted I decided to continue with breeding to the point of the G_3 generation due to the presence of the fluorescent green hearts indicating that a transgene was being inherited, and then repeat this experiment in the *mpeg1.1:Δtert-gfp* G_3 generation.

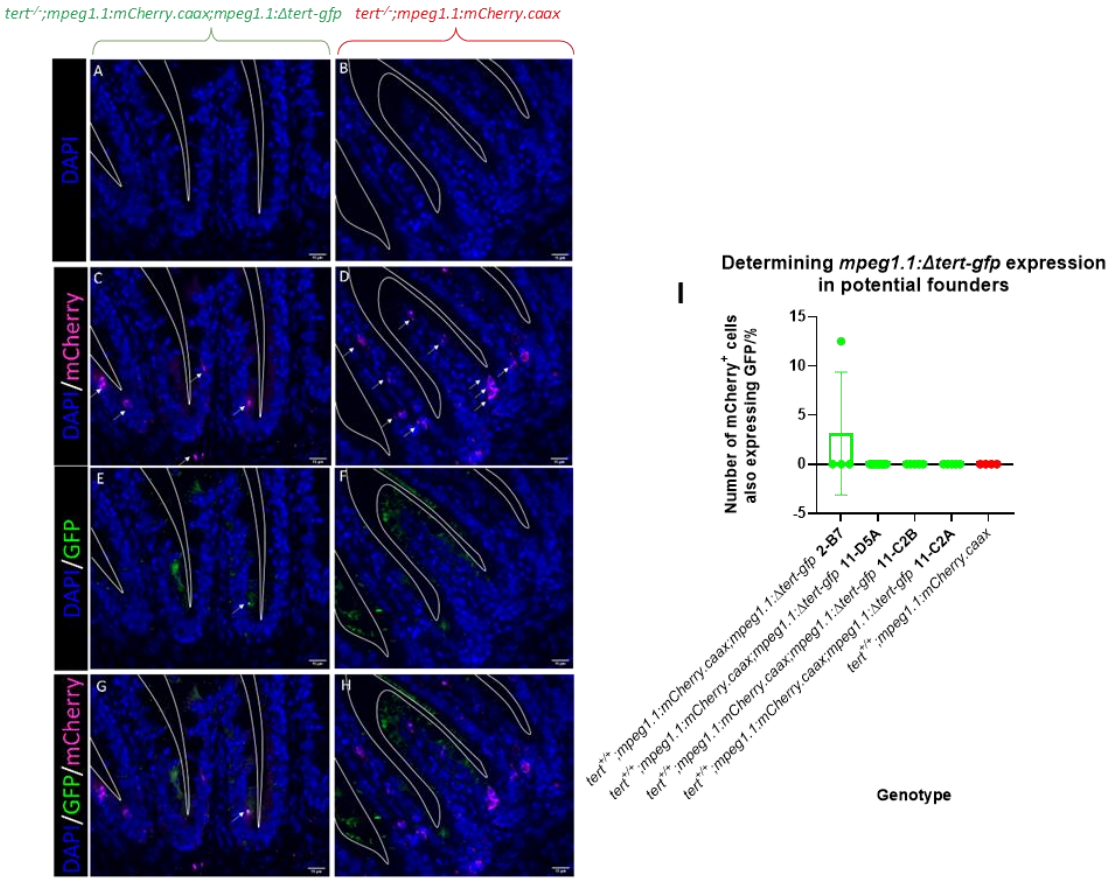

Figure 3.2.14: Quantifying the expression of the *mpeg1.1:Δtert-gfp* transgene in potential founders. **A.** DAPI staining of cell nucleus in *tert*$^{+/-}$ *mpeg1.1:mCherry.caax;mpeg1.1:Δtert-gfp* potential founder sibling gut. **B.** IF showing DAPI staining of cell nucleus in *tert*$^{+/-}$*;mpeg1.1:mCherry.caax* gut. **C.** IF showing DAPI staining of cell nucleus plus anti-mCherry in *tert*$^{+/}$*;mpeg1.1:mCherry.caax;mpeg1.1:Δtert-gfp* potential founder sibling gut. **D.** IF showing DAPI staining of cell nucleus plus anti-mCherry in *tert*$^{+/-}$*;mpeg1.1:mCherry.caax* gut. **E.** DAPI staining of cell nucleus plus anti-GFP in *tert*$^{+/-}$*;mpeg1.1:mCherry.caax;mpeg1.1:Δtert-gfp* potential founder sibling gut. **F.** IF showing DAPI staining of cell nucleus plus anti-GFP in *tert*$^{+/-}$*;mpeg1.1:mCherry.caax* gut. **G.** IF showing DAPI staining of cell nucleus plus anti-mCherry and anti-GFP in *tert*$^{+/-}$*;mpeg1.1:mCherry.caax;mpeg1.1:Δtert-gfp* potential founder sibling gut. **H.** IF showing DAPI staining of cell nucleus plus anti-mCherry and anti-GFP in *tert*$^{+/-}$*;mpeg1.1:mCherry.caax* gut. **I.** Quantification of double positive (anti-GFP + anti-mCherry) in *tert*$^{+/-}$*;mpeg1.1:mCherry.caax;mpeg1.1:Δtert-gfp* potential founder sibling fish gut compared to aged matched *tert*$^{+/-}$*;mpeg1.1:mCherry.caax* controls (n = 3 for each genotype).

3.2.15 Variant analysis of sequenced *mpeg1.1:Δtert-gfp* founder genomes

Previously I found evidence that the G3 generation of the *mpeg1.1:Δtert-gfp* were expressing GFP indicating insertion and expression of the transgene. However, I had also previously found that the G1 generation had very little evidence of the expression of the *mpeg1.1:Δtert-gfp.* To determine where the *mpeg1.1:Δtert-gfp* transgene was inserted in the genome, I decided to have the founders' genomes sequenced. This would also allow me to determine where in the genome the transgene was inserted. By determining the insertion site, I may be able to ascertain why the expression differed from G1 and G3.

Whole genome sequencing was carried out by Source Bioscience. I isolated samples of DNA isolated from zebrafish tail fin-clips with appropriate concentrations and purity. This allowed me to determine the presence of any transgene, and by using the BLAST software, to determine its insertion site which would indicate how the insertion of the transgene may affect zebrafish physiology in ways that would not be immediately apparent with more specific experiments such as fluorescent immunohistochemistry.

Sequencing of the B7 potential *mpeg1.1:Δtert-gfp* founder indicated an insertion site on chromosome 16 at position 19,790,508 to 19,790,589 (Supp. Fig. 2.A, D). This places the transgene in a non-coding region of chromosome 16. The nearest upstream gene of this site is *abcb5* which is predicted to code for an Adenosine Triphosphatase (ATPase)-coupled transmembrane transporter involved in the detoxification of mercury ions. If this genes expression was altered by the insertion of the *mpeg1.1:Δtert-gfp* via upstream signalling disruption we may expect to see less survivability of the embryos of this line, as the orthologue *abcb4* has been shown to provide protection against toxins in the environment(255). The nearest downstream gene to the insertion site of the transgene is *macc1* has been reported to function in development of zebrafish craniofacial structure as well brain development (256). Therefore, any effects of the transcription of this gene would become immediately apparent as the transgenic zebrafish developed. Currently, we do not observe any problems with zebrafish embryo survival or craniofacial development, therefore we may hypothesise currently that the changes observed due to the insertion of the *mpeg1.1:Δtert-gfp* are solely due to the effects of the transgene.

Sequencing of the C2A and C2B potential *mpeg1.1:Δtert-gfp* founders indicated that there was no detectable insertion of the insertion of the whole transgene but that the *mpeg1.1* region, the *GFP* region and the *cmcl2:eGFP* region may been inserted (Supp. Fig. 2.B, C). This may explain the observation of GFP expression in the heart during development for these founders. However, as the whole transgene is not inserted these lines will be terminated here and not taken forward for further study.

3.2.16 Quantification of the expression of *mpeg1.1:Δtert-gfp* in mCherry positive cells in paraffin zebrafish gut using fluorescent immunohistochemistry

The potential *mpeg1.1:Δtert-gfp* line was bred to the G_3 generation with the expression of the *cmcl2:eGFP* reported being recorded to be expressed and inherited in a mendelian manner indicating expression and inheritance of the *mpeg1.1:Δtert-gfp* would also follow a mendelian pattern. Fluorescent immunohistochemistry was used to validate that the *mpeg1.1:Δtert-gfp* transgene was being expressed in the G_3 fish (n = 3) (Fig. 3.2.16). A one-way ANOVA indicated a no significant difference in the number of double positive cells present ($mCherry^+$ and GFP^+) in the *mpeg1.1:Δtert-gfp* potential founder (Fig. 3.2.16.I). However, double positive cells were observed (Fig. 3.2.16.G) indicating that the *mpeg1.1:Δtert-gfp* transgene was being expressed and that further characterisation and validation of this line should be performed.

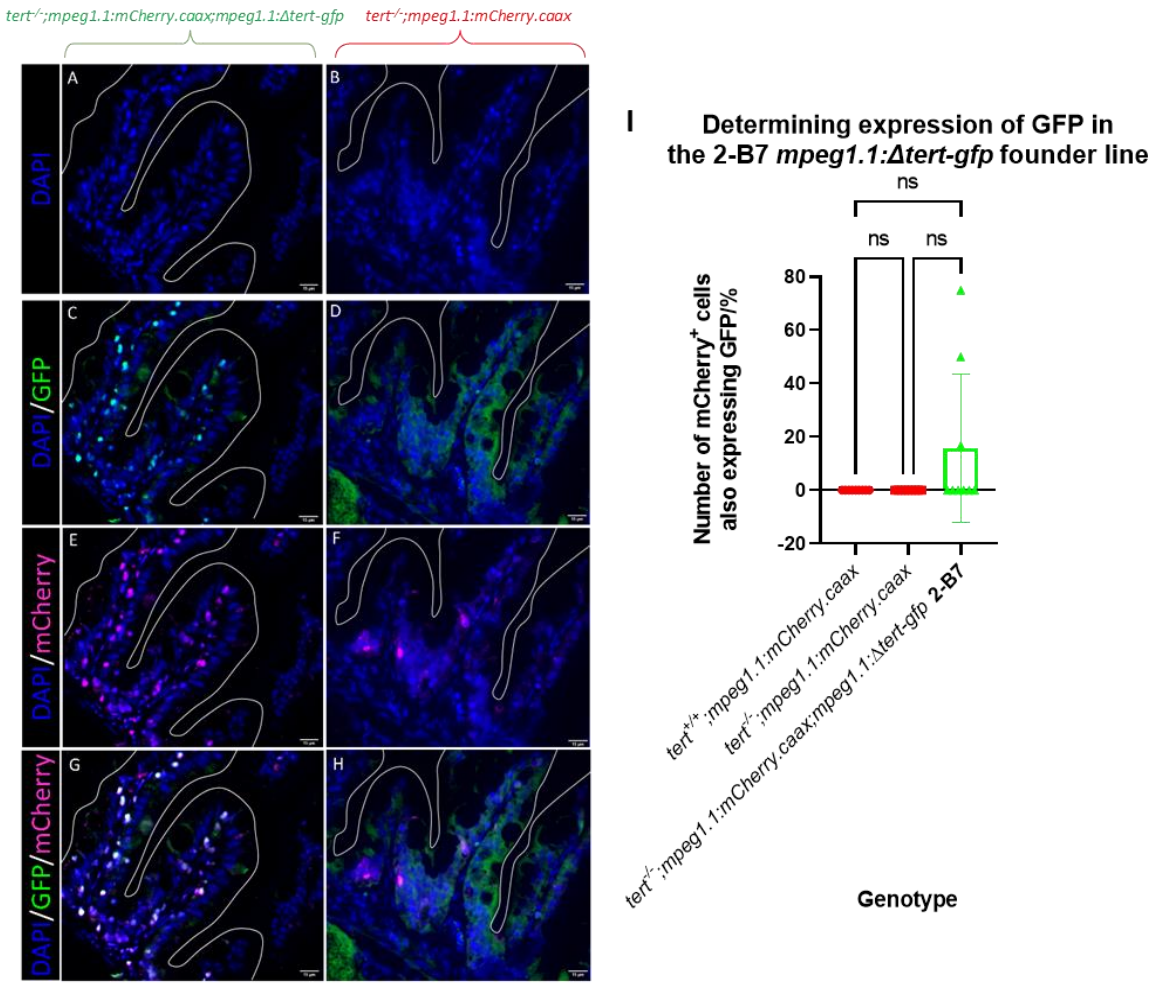

Figure 3.2.16: Quantification of the expression of the *mpeg1.1:Δtert-gfp* transgene in third generation transgenics. **A.** DAPI staining of cell nucleus in *tert*$^{-/-}$*;mpeg1.1:mCherry.caax;mpeg1.1:Δtert-gfp* gut. **B.** IF showing DAPI staining of cell nucleus in *tert*$^{-/-}$*;mpeg1.1:mCherry.caax* gut. **C.** IF showing DAPI staining of cell nucleus plus anti-mCherry in *tert*$^{-/-}$*;mpeg1.1:mCherry.caax;mpeg1.1:Δtert-gfp* gut. **D.** IF showing DAPI staining of cell nucleus plus anti-mCherry in *tert*$^{-/-}$*;mpeg1.1:mCherry.caax* gut. **E.** DAPI staining of cell nucleus plus anti-GFP in *tert*$^{-/-}$*;mpeg1.1:mCherry.caax;mpeg1.1:Δtert-gfp* gut. **F.** IF showing DAPI staining of cell nucleus plus anti-GFP in *tert*$^{-/-}$*;mpeg1.1:mCherry.caax* gut. **G.** IF showing DAPI staining of cell nucleus plus anti-mCherry and anti-GFP in *tert*$^{-/-}$*;mpeg1.1:mCherry.caax;mpeg1.1:Δtert-gfp* gut. **H.** IF showing DAPI staining of cell nucleus plus anti-mCherry and anti-GFP in *tert*$^{-/-}$*;mpeg1.1:mCherry.caax* gut. **I.** Quantification of double positive (anti-GFP + anti-mCherry) in *tert*$^{-/-}$*;mpeg1.1:mCherry.caax;mpeg1.1:Δtert-gfp* gut compared to aged matched *tert*$^{-/-}$*;mpeg1.1:mCherry.caax*. N = 3 for each genotype, N = 3 per fish, ns = p>0.05.

3.2.17 Discussion of the generation and validation of the two transgenic lines

3.2.17.1 Characterisation and validation of the *mpeg1.1tert-gfp* line

The work carried out in this chapter provides preliminary evidence that the *mpeg1.1:tert-gfp* transgenic line has been successfully produced via insertion of the *mpeg1.1:tert-gfp* transgene with tol2 mediated transgenesis. Further, evidence in this chapter suggests that *mpeg1.1:tert-gfp* transgene is expressed in an *mpeg1.1* specific manner, and that the TERT resulting from this expression is performing its non-canonical function of elongating telomeres (Fig. 3.2.12).

Figure 3.2.12 indicates the expression of TERT in the *tert*$^{-/-}$ *;mpeg1.1:mCherry.caax;mpeg1.1tert-gfp* line in an *mpeg1.1* specific manner. However, figure 3.2.11 indicates that GFP is not being reliably expressed in the *mpeg1.1:tert-gfp* transgenic line. Therefore, I can hypothesise that the IRES region may not be functioning as intended. This is supported by section 3.2.10 where the genomic sequencing data indicates that the *mpeg1.1tert-gfp* transgene has been successfully inserted in its entirety including the IRES and GFP regions. Therefore, it is a reasonable to hypothesise that the IRES region has not been a reliable method for separating the *tert* and *gfp* exons in this case. One explanation may be that the ribosome is failing to bind to the IRES region leading to a lack of GFP translation. Further investigation and characterisation of the *mpeg1.1:tert-gfp* line was warranted to determine why variable expression of GFP is observed. Using both native fluorescence (section 3.2.9) and fluorescence immunohistochemistry (section 3.2.11) the expression of GFP has been evidenced. Therefore, future experiments may utilise proteomic methods to quantify the translation of GFP in the transgenic line. For example, using a western blot to determine the level of GFP expression in *tert*$^{-/-}$ *;mpeg1.1:mCherry.caax;mpeg1.1:tert-gfp* mCherry^{+} cells compared to TERT in the same genotype may illuminate if both are being translated at equal levels or if the TERT is being translated and the GFP not. Further to this, the commissioning of a zebrafish TERT specific antibody would be required as at the time writing the Henriques lab has not found a suitable TERT-specific antibody that works in zebrafish. Making use of a zebrafish TERT

specific antibody discussed above would enable further investigation into the level of TERT expression that results from the insertion of the *mpeg1.1:tert-gfp* transgene. A zebrafish TERT specific antibody would enable the detection of TERT via western blotting, providing additional evidence that TERT is being expressed. Further, it would enable quantification of the expression of the TERT protein from the *mpeg1.1:tert-gfp*. This could be used to determine if the expression level of TERT in the *mpeg1.1:tert-gfp* transgenic is expressed to a level comparable to a $tert^{+/+}$ and indicate its activity level.

Future analysis of telomere length using telo-FISH staining may also investigate using a centromere FISH probe as this would provide a cell-specific control that the telo-FISH signal could be normalised to. A centromere FISH control was not included in the experiments discussed in this thesis due to the number of fluorophores included preventing any additional fluorescent wavelengths being included. Repeating the experiment could utilise the following fluorophores: DAPI for the nucleus, a GFP labelled centromere FISH probe, a red labelled telo-FISH probe, and a far-red labelled mCherry secondary antibody.

Analysis of telomere length using the telo-FISH assay indicated that telomere length was being rescued in $tert^{-/-}$*;mpeg1.1:mCherry.caax;mpeg1.1:tert-gfp* $mCherry^{+}$ cells to a level comparable to $tert^{+/+}$*;mpeg1.1:mCherry.caax* $mCherry^{+}$ cells (Fig. 3.2.12). However, due to the quality of the staining in this assay further optimisation of the protocol is required. While $mCherry^{+}$ cells can clearly be observed in some sections, in other sections the quality of the mCherry specific staining is not of a quality that means we can be certain that a specific cell is $mCherry^{+}$. This may be due to the high temperature required for the telo-FISH probe staining section of the protocol denaturing the antibody-fluorophore conjugate. If the protocol is affecting the staining due to antibody-conjugate denaturing this may provide an alternative explanation of the lack of GFP^{+} staining we are observing in the transgenic fish. Future optimisation may investigate performing the telo-FISH and fluorescence immunohistochemistry on separate sections. However, without the mCherry specific staining it would not be possible to determine the telo-FISH staining in specific cell types. Therefore, an alternative method for determining telomere length in these transgenic animals may be investigated. One method may be to perform Terminal Restriction Fragment (TRF) southern blot analysis(257). However, to use this method on specific cell subsets would require a sufficient population of the desired cells to be separated from a

heterogenous population via a method such as FACS. A second method for quantifying telomere length may be the use of quantitative PCR(258). However, while potentially less labour intensive than using TRF southern blot analysis, it would also require in the case of this experiment the isolation of the cell population of interest via a method such as FACS. The isolation of a sufficient population of cells of interest would also potentially require further optimisation.

It was not possible to quantify the level of telomerase activity in these cells using the TRAP assay. Interestingly, when quantifying the *tert*$^{+/+}$*;mpeg1.1:mCherry.caax* samples the 1.5µg sample had less telomerase activity than the 0.5µg. The protein concentration is calculated based on the BCA assay, but this does not take into account the TERT content of the protein isolate. Therefore, this may be due to the variation in TERT content of the isolated protein samples. The lack of telomerase activity from the *tert*$^{-/-}$*;mpeg1.1:mCherry.caax;mpeg1.1:tert-gfp* sample may indicate that the transgene is not being expressed or the concentration of the transgenic TERT expression may be so low in the whole gut isolate that too little is being carried over in the protein isolate for the TRAP assay to detect its activity. In future optimisation I would suggest using FACS to sort the mCherry^{+} populations of several *tert*$^{+/+}$ zebrafish guts into a pool and determining the telomerase activity of this pool as a standard. The experiment could then be conducted using pools from *tert*$^{+/+}$*;mpeg1.1:mCherry.caax*, *tert*$^{-/-}$*;mpeg1.1:mCherry.caax, tert*$^{-/-}$*;mpeg1.1:mCherry.caax;mpeg1.1:tert-gfp* fish gut.

Interestingly, the calculated telomerase activity of the positive controls was not directly related to its calculated concentration. A relative telomerase activity of 225 was measured from 10µg of HT1080 protein (Fig. 3.2.11.C) whereas a relative telomerase activity of 70 was measured from 3µg of isolated protein (Fig. 3.2.11.D). Therefore, with the HT1080 protein the change in protein amount if was proportional to the change in relative telomerase activity. In contrast a proportionate change in activity was not observed from the zebrafish gut cell lysate. For example, the 3µg *tert*$^{+/+}$*;mpeg1.1:mCherry.caax* sample in Fig. 3.2.11.C was calculated to have a relative telomerase activity of 1.8, whereas the *tert*$^{+/+}$*;mpeg1.1:mCherry.caax* sample in Fig. 3.2.11.D has a calculated relative telomerase activity of 15. This indicates that the TRAP assay is reliable when utilised to measure telomerase activity in cells expressing high levels of telomerase such as the HT1080 cell

culture but is not as reliable when measuring telomerase activity in zebrafish tissue samples and so may not be a suitable assay for characterising the generated transgenic lines moving forward. However, future work should continue to optimise the TRAP assay protocol to accurately measure telomerase activity in mCherry^{+} cells. Further optimisation of the TRAP assay would involve pooling the FACS of mCherry^{+} cell samples from to provide an increased concentration of TERT. Further, FACS sorting mCherry^{+} cells directly into TRAP assay lysis buffer may better preserve the TERT protein as it would lyse cells before they could undergo apoptosis.

By fully characterising the *mpeg1.1:tert-gfp* transgenic we may better understand if it is an appropriate control for the canonical functions of telomerase. Sequencing of *mpeg1.1:tert-gfp* founders indicates that the *mpeg1.1:tert-gfp* is inserted into the untranslated region of *larsb* in founders A1 and A2, and into the *sla2a* gene of founder C1 (Fig. 3.2.12.1.D, E). Further investigation into the how this affects zebrafish phenotype should be conducted to determine if the insertion of the *mpeg1.1:tert-gfp* affects the genes it is inserted into. This may preliminarily take the form of real-time quantitative polymerase chain reaction (RT-qPCR) to determine if transcription of *larsb* or *sla2a* is affected. If this is the case then the transgenic line should not be considered suitable for further experiments as the observations cannot reliably be considered to be a result of the expression of the *mpeg1.1:tert-gfp* transgene. Currently whole genome sequencing is not standard practice when a new transgenic zebrafish is generated using the tol2 system. I believe that this may be a short-sighted approach to generating transgenic lines in the zebrafish community that could lead to complications with the established transgenic models in later experiments due to the random nature of transgene insertion when using the tol2 system. If I were to generate novel transgenics in future studies using tol2 I believe that whole genome sequencing and analysis would be an invaluable tool for determining the insertion sites of the transgenes. Without knowing the insertion sites of transgenes and how this may affect zebrafish physiology, we cannot know that the effects observed in transgenic lines are due to the inserted transgene and not due to the disruption of the genome caused by the transgene.

During the breeding of the transgenic lines developments in the literature indicated that the *mpeg1.1* promoter was not macrophage specific as had previously been reported (226) but

was expressed also in B-cells and Natural killer (NK)-like cells(234, 237). Further to this there is evidence that the *mpeg1.1:mCherry.caax* transgene had not been adequately characterised due to the variation in fluorescence observed in the FACS populations in section 3.2.13. However, by detecting mCherry it was still possible to confirm that a cell utilised the *mpeg1.1* promoter and therefore may be a macrophage, B-cell, or NK-like cell.

3.2.17.2 Characterisation of the *mpeg1.1:Δtert-gfp* line

This chapter has detailed the method of production of the *mpeg1.1:Δtert-gfp* transgenic line, as well as illustrating preliminary data on characterising the insertion sites and expression of the *mpeg1.1:Δtert-gfp* transgene. Initial validation of the *mpeg1.1:Δtert-gfp* transgenic line has indicated that the full *mpeg1.1:Δtert-gfp* transgene is inserted (section 3.2.15). Further, the expression of GFP from the transgene has been indicated in mCherry^{+} cells (Fig. 3.2.16) indicating that the transgene is being expressed under the *mpeg1.1* promoter. Whole genome sequencing (section 3.2.15) demonstrated that *mpeg1.1:Δtert-gfp* was inserted in its entirety into the B7 founder line, but that only the *mpeg, GFP,* and *cmcl2:eGFP* segments of the transgene had been inserted in the C2A and C2B founder lines. This demonstrates the need for whole genome sequencing when using multiple reporters as without sequencing GFP expression may still have been observed indicating the expression of the inserted transgene. Conversely this also highlights the need for further validation of this line. Further validation would include quantification of the telomere length *tert$^{-/-}$;mpeg1.1:mCherry.caax;mpeg1.1:Δtert-gfp mCherry^{+}* cells as has been performed for the *tert$^{-/-}$;mpeg1.1:mCherry.caax;mpeg1.1:tert-gfp* line to determine if the insertion of the *mpeg1.1:Δtert-gfp* transgene is rescuing the function of telomerase. The *Δtert* is designed so that its expression should not rescue telomerase function, but this needs to be verified. Further, the production of a custom antibody that is specific to *Δtert* would enable the quantification of its expression level via western blotting. This would provide data on the comparability of the expression level of *Δtert* gene compared to the native *tert* in *tert$^{+/+}$;mpeg1.1:mCherry.caax* controls.

The *tol2* transposon is a widely characterised tool used for transgenesis in zebrafish (251, 252). Further, transgenes introduced using *tol2* as a vector are reported to be reliable expressed without silencing from the host (259). However, *tol2* is not a perfect tool as it has been reported to be promiscuous in its target site selection leading to unpredictable

insertions (259). Further to this, *tol2* has been indicated to preferentially insert into AT-rich and transcriptional regulatory regions (259). Considering both the advantages and disadvantages of the *tol2* vector it was still a logical option for use in generating these transgenic lines due to its wide use on generating zebrafish transgenics. However, the downsides noted here acted as a motivator for the whole genome sequencing of the generated transgenic lines.

A potential explanation for the variable expression of both the *mpeg1.1:tert-gfp* and the *mpeg1.1:Δtert-gfp* gene is the variation in utilisation of the *mpeg1.1* promoter in zebrafish immune cells. The effect of premature ageing on zebrafish immune cells has not been fully characterised. While some literature suggests that *mpeg1.1* is utilised in both $tert^{+/+}$ and $tert^{-/-}$ gut associated immune cells further work must be undertaken to further explore the effects of premature ageing on the zebrafish immune system(185). Literature indicates that ageing affects both macrophage and B-cell function(185, 260, 261). Considering the normal function of the *mpeg1.1* in perforin expression, its utilisation may hinge on the polarisation, tissue of residence, current cytokine or chemokine signalling, or response to infection, we can hypothesise that prematurely ageing the zebrafish immune system may have a similar effect, or indeed affect immune cells in a way that has not yet been characterised. Therefore, the use of *mpeg1.1* as an immune cell marker in ageing cells requires further investigation.

Chapter 4: Optimising the isolation of a zebrafish gut dissociation for Single-cell RNA sequencing

4.1 Introduction

Chapter 3 detailed the generation of two novel zebrafish transgenic models, the *mpeg1.1:tert-gfp* line and the *mpeg1.1:Δtert-gfp* line. One of the aims of this PhD was to use these lines to study the non-canonical functions of telomerase in *mpeg1.1*$^{+}$ cells. Single-cell RNA sequencing was considered an appropriate method for studying the effects of the *mpeg1.1:tert-gfp* transgene on zebrafish physiology due to both the amount of data this would provide and that it had previously been used to study zebrafish (234, 262-267). However, the literature had highlighted the difficulty with producing a sample suitable for single-cell RNA sequencing from zebrafish, particularly in reference to the low number of immune cells isolated (234). As this project is focusing on gut immune cell populations due to the gut being one of the fastest ageing organs the mCherry^{+} the single-cell population would be isolated from the zebrafish gut. Therefore, it was expected that the low number of immune cells problem reported in the literature would be exacerbated due to the harsh conditions found in the gut leading to a higher level of cell loss during sample preparation and that any carryover of intestinal contents may lead to issues with single-cell RNA sequencing library preparation. Therefore, it was appropriate to optimise a protocol that would provide a sample with a high number of live single cells while removing the harsh digestive components of the lysate (Fig. 4.1). Additionally, the sample had to be suitable for use with a 10x Genomics Chromium controller. To be suitable the sample needed a high viability (≥90%) to optimise the sample size and have as little clumping as possible due to the library preparation stage relying on a droplet-based barcode system from 10x Genomics. The 10x Genomics Chromium controller uses an eight well chip with each well holding a maximum of 20,000 cells in a maximum volume of 40µl/well. However, the 10x Genomics Chromium controller can sequence a maximum of 10,000 cells per well. Therefore, adding more than 10,000 cells to a well will increase the likelihood of doublets. However, adding more than 10,000 cells also increases the likelihood that the maximum 10,000 cells will be sequenced. As such, to maximise the number of cells sequenced, my target was a 40µl sample with a concentration of 500 cells/µl with a viability of ≥90%. Further, to perform single-cell RNA sequencing the sample would have little to no clumping to prevent blocking of the 10x Genomics Chromium controller and to alleviate the number of doublets.

To perform single-cell RNA sequencing on mCherry^{+} cells the cells would be isolated from a suspension of lysed zebrafish whole gut (Fig. 4.1). Expression of the mCherry fluorophore would indicate the cell was utilising the *mpeg1.1* promoter. If the cell was utilising the *mpeg1.1* promoter then hypothetically the cell would also be expressing the *mpeg1.1:tert-gfp* transgene if it were derived from the *mpeg1.1:tert-gfp* transgenic line. FACS would be used to produce a sample suitable for single-cell RNA sequencing to separate the mCherry^{+} population from the mCherry^{-} cells. FACS was chosen as it would enable the sorting of specific cells (in this case mCherry^{+}) and a specific number of cells.

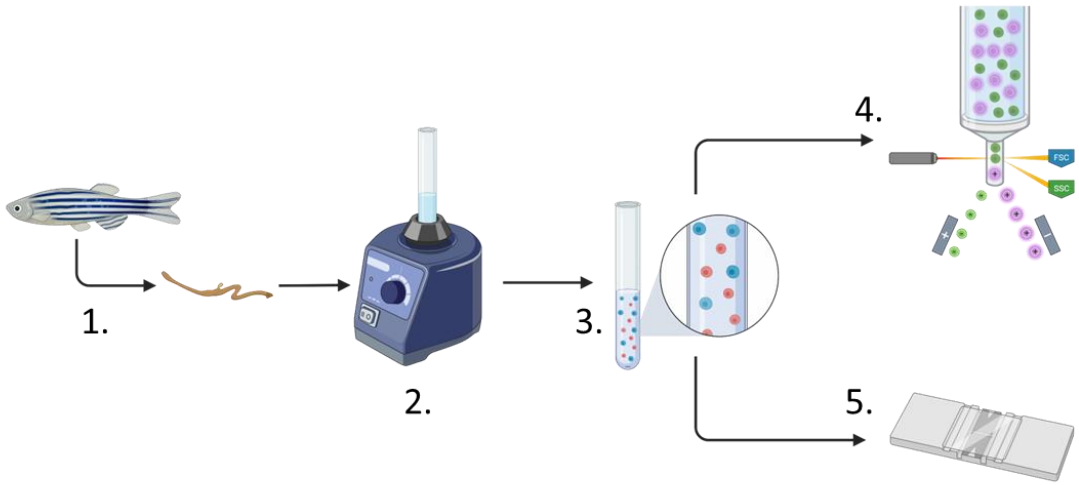

Figure 4.1: Representative illustration of the steps and potential methods for preparing samples for single-cell RNA-sequencing. Moving from zebrafish gut excision after the fish has been culled (1.), to the dissociation of the gut via the action of enzymatic digestion, stirring, and heat (2.), to produce a cell suspension (3.) which is used to perform experiments to determine if FACS (4.) or using a haemocytometer (5.) is a better method for producing a sample for single-cell RNA-sequencing.

4.2 Results

4.2.1 Isolating an mCherry^{+} population of cells from whole zebrafish gut dissociation using FACS.

Initially the gating used to isolate an mCherry^{+} population from a lysed zebrafish gut cell suspension would be optimised. Fish from the *tert*$^{+/+}$*;mpeg1.1:mCherry.caax* line were used to optimise the gating for an mCherry^{+} population as they would eventually act as healthy ageing control in the single-cell RNA sequencing experiment. WT(AB) zebrafish were used as a control for autofluorescence. The far-red wavelength fluorescent stain TO-PRO-3 was used to indicate apoptotic and dead cells. TO-PRO-3 cannot enter living cells but will move through the damaged cell membranes indicating that a cell is dead or in the process of dying and so should not be included in the sort of live cells.

FACS gating (Fig. 4.2.1) was used to isolate a population of mCherry^{+} cells from the lysed gut of a *tert*$^{+/+}$*;mpeg1.1:mCherry.caax* (Fig. 4.2.1.C) using gates that had previously been designated by the Henriques lab to select 'bright' and 'dim' mCherry^{+} cells. However, using the same gating strategy with the WT(AB) sample (Fig. 4.2.1.D) indicated that the 'dim' gate included autofluorescent (Fig. 4.2.1.D). In the WT(AB) zebrafish gut dissociation sort of 100,000 cells, 522 cells were counted in the mCherry 'dim' gate and 140 cells in the mCherry 'bright' gate (Fig. 4.2.1.D). In the *tert*$^{+/+}$*;mpeg1.1:mCherry.caax* zebrafish gut dissociation sort of 100,000 cells 1192 cells were present in the mCherry 'dim' gate and 3322 cells in the mCherry 'bright' gate (Fig. 4.2.1.C). This indicates a potential contamination of 15.3% of the sample as autoflourescent cells. Therefore, this gating strategy required further optimisation to reduce the contamination of autoflourescent cells in the mCherry^{+} gates.

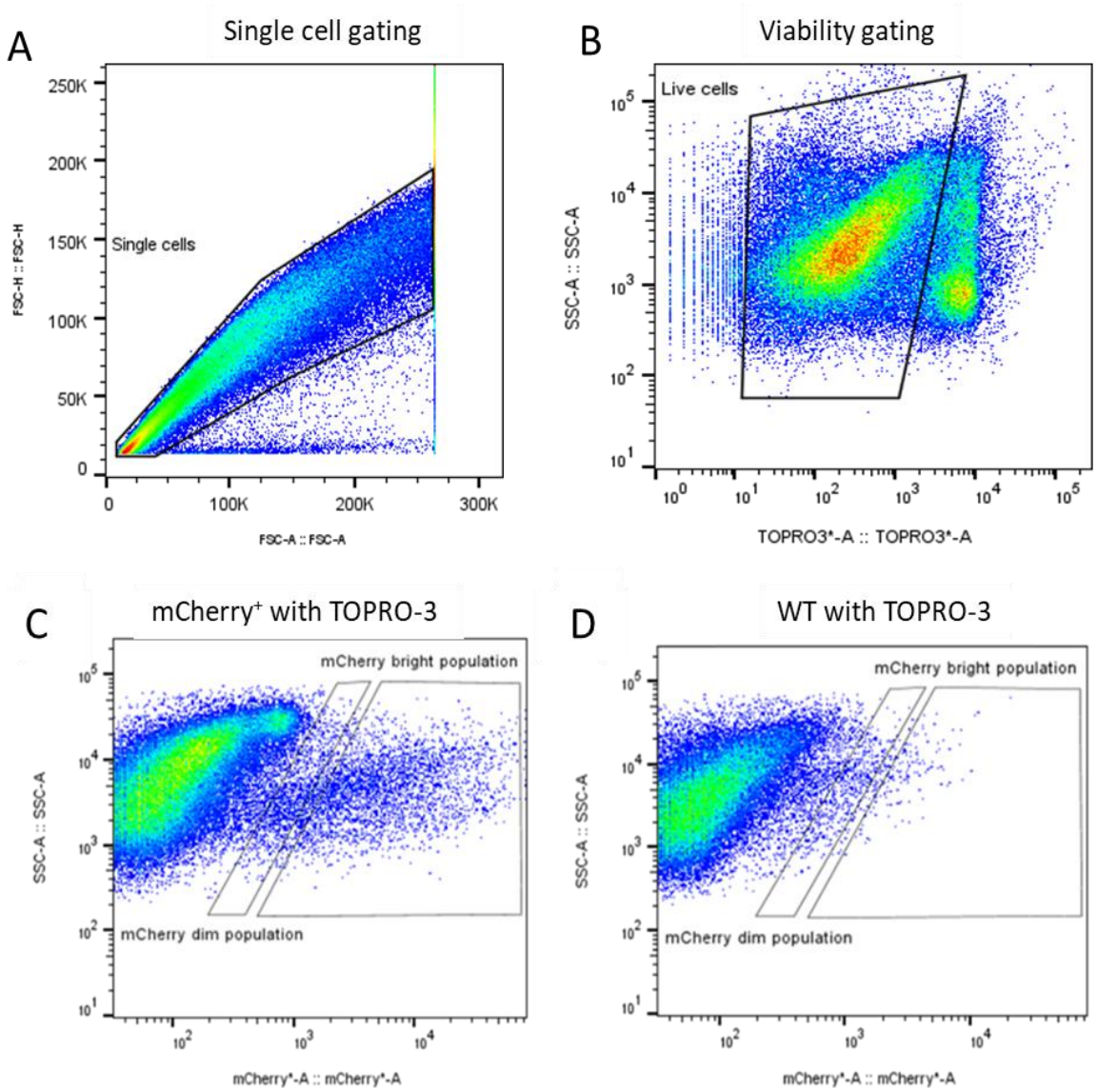

Figure 4.2.1: Optimising the FACS of an mCherry^{+} population from zebrafish gut. A. Representative gating of single cells to removed doublets. **B.** Representative gating of live cells. **C.** Initial gating for mCherry+ 'bright' and 'dim' populations on a *tert*$^{+/+}$*;mpeg1.1:mCherry.caax* gut dissociation, N = 1. **D.** Gating for mCherry^{+} 'bright' and 'dim' populations on a WT(AB) gut dissociation, N = 1.

4.2.2 Optimising a reduction in autofluorescent cell contamination in the mCherry^{+} population gating strategy.

The previous gating strategy (Fig. 4.2.1) used two gates to isolate two populations of mCherry^{+} cells but was indicated to include a contaminating population of autofluorescent cells. To produce a sample suitable for single-cell RNA sequencing using FACS it was necessary to optimise gating to produce a single population of mCherry^{+} cells without autofluorescent cell contamination. Additionally, the previous gating method (Fig. 4.2.1) used two gates, leading to the loss of a small population of mCherry^{+} cells that fell between the two gates. Therefore, a single gate that encompassed the entire mCherry^{+} population was a logical solution to isolate the maximum number of mCherry^{+} cells while eliminating any autofluorescent contamination.

Sorting a cell-suspension from a *tert*$^{+/+}$*;mpeg1.1:mCherry.caax* gut dissociation (Fig. 4.2.2) enabled the gating of an mCherry^{+} population indicating a population of 6068 mCherry^{+} cells from a sort of 100,000 cells (Fig. 4.2.2.C). Utilising the same gate for the WT(AB) gut dissociation indicated a sort of 1,093 mCherry^{+} cells from a population of 100,000 cells (Fig. 4.2.2.D). This indicates that 18% of the mCherry^{+} population may be a contaminating population of autofluorescent cells. Therefore, considering almost one fifth of the population of mCherry^{+} cells may be contamination from mCherry^{-} further optimisation was required.

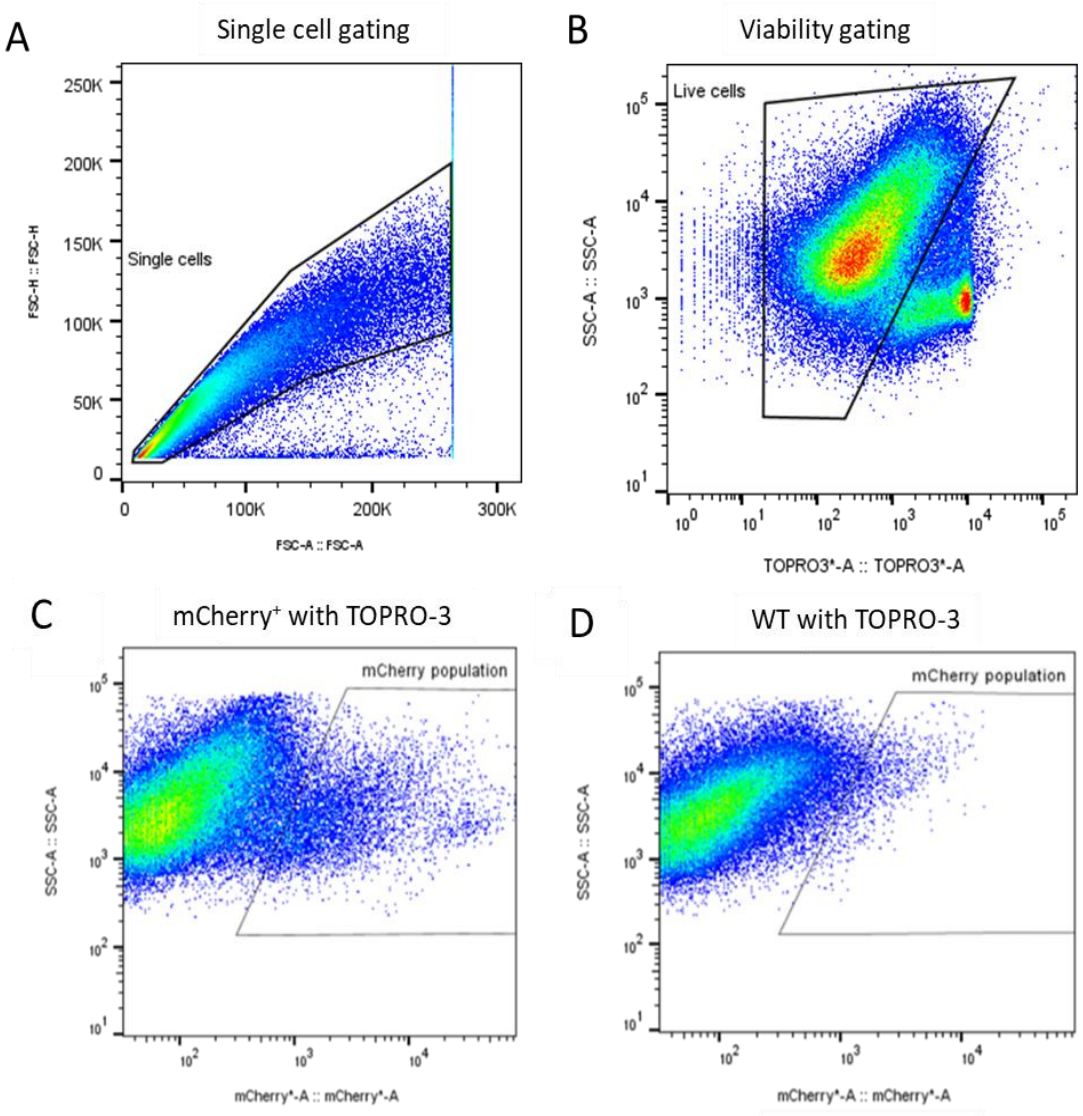

Figure 4.2.2: Optimising the FACS of an mCherry^{+} population from zebrafish gut. **A.** Representative gating of single cells to removed doublets. **B.** Representative gating of live cells. **C.** Gating for entire mCherry^{+} population on a *tert*$^{+/+}$*;mpeg1.1:mCherry.caax* gut dissociation, N = 1. **D.** Gating for entire mCherry^{+} population on WT(AB) gut lysis, N = 1.

4.2.3 Optimising the detection of a GFP$^+$/mCherry$^+$ double positive population from zebrafish gut dissociation using FACS.

The *mpeg1.1:tert-gfp* transgenic line contains a GFP reporter indicating the expression of the transgene. It was hypothesised that a double positive (mCherry$^+$ and GFP$^+$) population of cells could be isolated from the transgenic gut to reduce the autoflourescent contamination. Gating for both mCherry$^+$ and GFP$^+$ cells was based on literature published by *Nguyen-chi et al.* that utilised FACS to identify macrophages in *mpeg1.1:mCherry;tnfa:eGFP* transgenic zebrafish(227). One gate was mCherry$^+$ specific, the second was GFP$^+$ specific, and the third was a double-positive gate designed to detect cells expressing both mCherry and GFP (Fig. 4.2.3).

Gut dissociations from three genotypes underwent FACS using the new gates, WT(AB), *tert$^{+/+}$;mpeg1.1:mCherry.caax*, and *tert$^{+/-}$;mpeg1.1:mCherry.caax;mpeg1.1:tert-gfp* (Fig. 4.2.3). From the sort of the WT(AB) gut dissociation 29 cells were detected in the mCherry$^+$ gate, 7 GFP$^+$ cells were detected in the GFP$^+$ gate, and 194 cells in the double$^+$ gate from a total of 96,000 cells (Fig. 4.2.3.C). From the sort of the *tert$^{+/+}$;mpeg1.1:mCherry.caax* gut dissociation 1600 cells were mCherry$^+$, 56 were GFP$^+$ cells, and 680 were double$^+$ cells from a total of 113,000 cells (Fig. 4.2.3.D). From the sort of the *tert$^{+/-}$;mpeg1.1:mCherry.caax;mpeg1.1:tert-gfp* gut dissociation 37 mCherry$^+$ cells were detected, 63 GFP$^+$ cells were detected, and 941 double$^+$ cells were detected from a total of 235,000 cells (Fig. 4.2.3.E).

The contamination of the double$^+$ gate may be explained by the expression of mCherry causing crossover into the double$^+$ gate in the *tert$^{+/+}$;mpeg1.1:mCherry.caax* sample (Fig. 4.2.3.D). However, in the double$^+$ gate from the *tert$^{+/-}$;mpeg1.1:mCherry.caax;mpeg1.1:tert-gfp* sample a distinct double$^+$ population is observed (Fig. 4.2.3.E). However, this data does indicate that contamination of the double$^+$ gate is occurring with autofluorescent and mCherry$^+$ only cells which may equate up to 72% of the double$^+$ population in the *tert$^{+/-}$;mpeg1.1:mCherry.caax;mpeg1.1:tert-gfp* sort. Therefore, further optimisation of the gating strategy is required if FACS is to be used to produce a sample that is suitable for single-cell RNA sequencing.

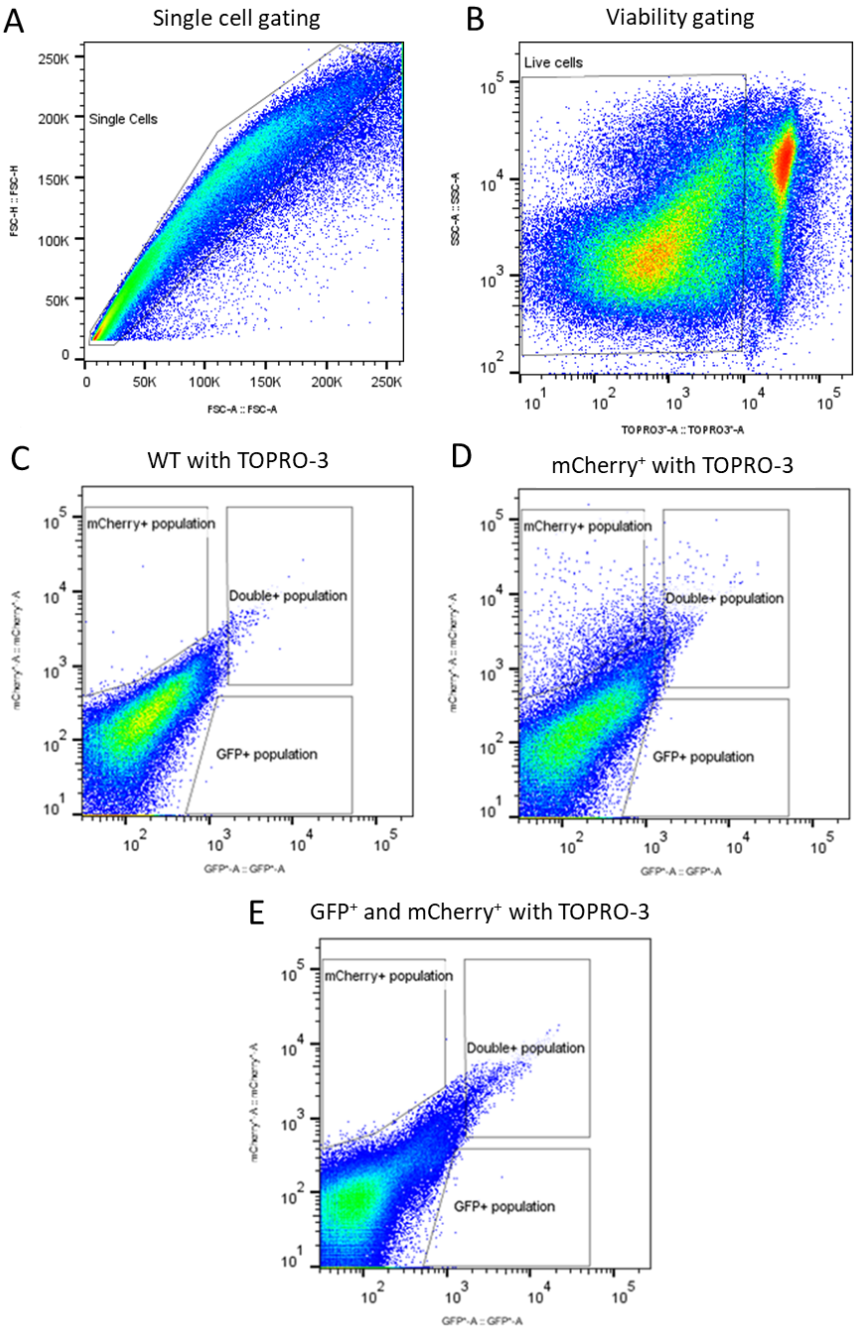

Figure 4.2.3: Optimising the gating of a double positive (GFP$^+$/mCherry$^+$) population from zebrafish gut dissociation. **A.** Representative gating of single cells to removed doublets. **B.** Representative gating of live cells. **C.** Representative gating of GFP$^+$, mCherry$^+$, and double$^+$ cells from WT(AB) zebrafish gut dissociation, N = 1. **D.** Representative gating of GFP$^+$, mCherry$^+$, and double positive cells from *tert*$^{+/-}$*;mpeg1.1:mCherry.caax* zebrafish gut dissociation, N = 1. **E.** Representative gating of GFP$^+$, mCherry$^+$, and double positive cells from *tert*$^{+/-}$*;mpeg1.1:mCherry.caax;mpeg1.1:tert-gfp* zebrafish gut dissociation, N =

4.2.4 Determining the different cell populations present in the FACS mCherry^{+} population.

At the start of the project the published literature detailing the production of the *mpeg1.1:mCherry.caax* line indicated that the *mpeg1.1:mCherry.caax* transgene was a macrophage specific reporter(226). However, more recent literature was published that demonstrated in adult zebrafish the *mpeg1.1:mCherry.caax* transgene is expressed in both populations of macrophages and B-cells in the zebrafish gut(234). Therefore, it was important to determine the phenotype of cells being selected for by the *mpeg1.1:mCherry.caax* gene as this would also indicated which cells were potentially expressing the *mpeg1.1:tert-gfp* transgene.

FACS of an *tert*$^{+/+}$*;mpeg1.1:mCherry.caax* gut dissociation was used to determine the cells that made up the heterogenous mCherry^{+} population alongside a method described by *Lugo-villarino et al.*(268). An mCherry^{+} population was sorted onto glass discs coated with poly-D lysine and incubated to allow cells to adhere. The disks were then fixed the with the cells before staining with wright-giemsa stain. However, upon inspection using a light microscope (Fig. 4.2.4.A, B) the cells had lysed during the protocol indicating that further optimisation would be required. Therefore, and alternative method was used to determine heterogenous cell types that constituted the mCherry^{+} population.

The alternative method for determining the heterogenous cells that constituted the mCherry^{+} population replicated a gating strategy reported by *Ferero et al.*(234) that uses the side-scatter and forward-scatter of the sorted cells to determine their phenotype. Using a WT(AB) zebrafish gut dissociation as a negative control for the mCherry^{+} signal indicated 14 cells had been selected by the mCherry^{+} gate (Fig. 4.2.4.C). From a *tert*$^{+/+}$*;mpeg1.1:mCherry.caax* gut dissociation found 2020 mCherry^{+} cells were sorted (Fig. 4.2.4.E). Using the gating strategy described by *Ferero et al*(234) (Fig. 4.2.4.D, F) it was determined that the mCherry^{+} cell population was made up of both lymphocyte and myelomonocyte populations as well as additional un-characterised cells. Therefore, the mCherry^{+} population is indicated to be a heterogenous mix of cell types that hypothetically all would use the *mpeg1.1* promoter and therefore may all express the *mpeg1.1:tert-gfp* transgene.

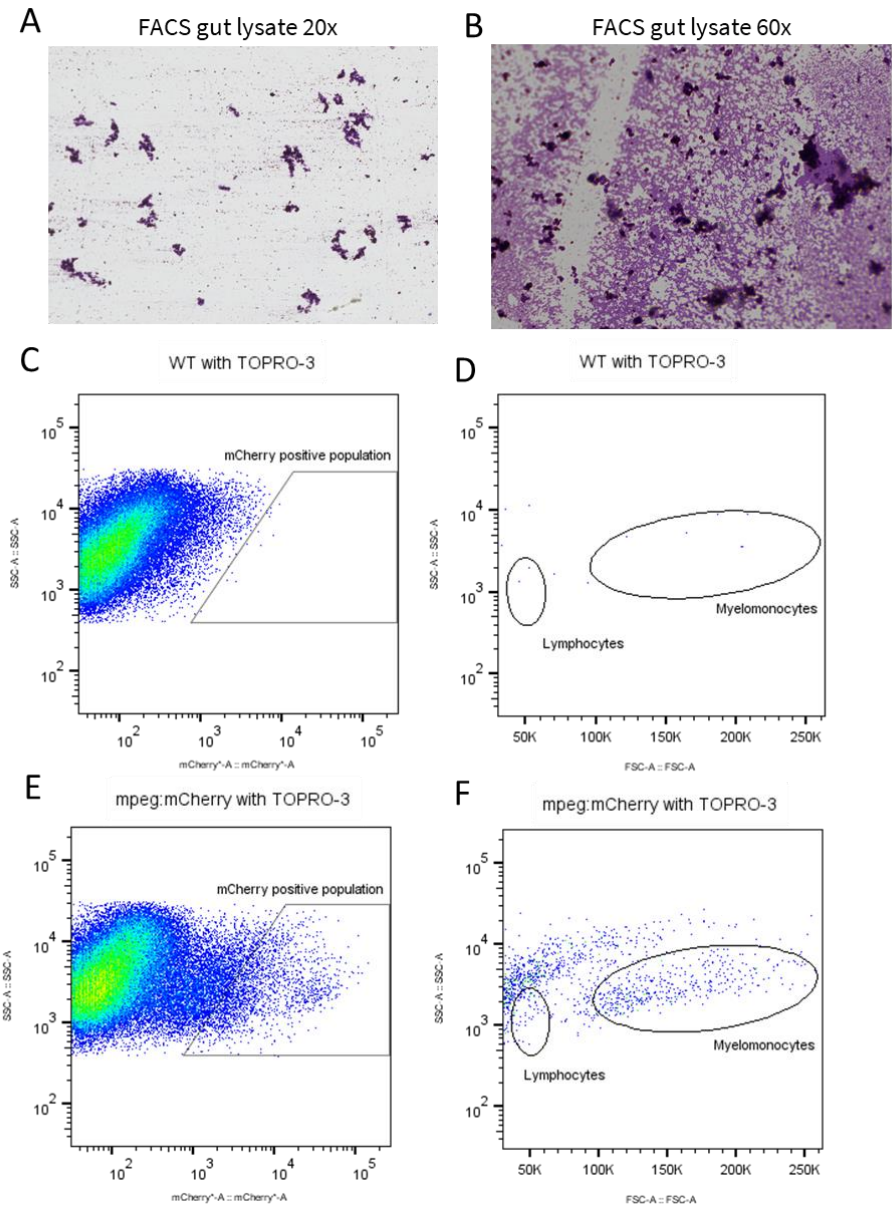

Figure 4.2.4: Determining the cell phenotypes present in the mCherry^{+} population. **A.** Representative figure of 20x imaging of wright-giemsa stained FACS of gut lysate fixed using methanol. **B.** Representative figure of 60x imaging of wright-giemsa stained FACS of gut lysate fixed using PFA. **C.** Representative gating of mCherry^{+} population from a WT(AB) zebrafish gut dissociation, N = 1. **D.** Representative gating of Myelomonocyte and Lymphocyte populations derived from mCherry^{+} gate from a WT(AB) zebrafish gut dissociation. **E.** Representative gating of mCherry^{+} population from a *tert*$^{+/+}$*;mpeg1.1:mCherry.caax* zebrafish gut dissociation, N = 2. **F.** Representative gating of Myelomonocyte and Lymphocyte populations derived from mCherry^{+} gate from a *tert*$^{+/+}$*;mpeg1.1:mCherry.caax* zebrafish gut dissociation.

4.2.5 Determining the effects of FACS on cell viability.

To further determine if FACS was a suitable method for preparing a sample for single-cell RNA sequencing it was necessary to determine how FACS affected cell viability. A 90% sample viability was the target, based on recommendation from 10x Genomics guidelines, to produce high-quality single-cell RNA sequencing data. To assess the effect of FACS on cell viability the viability of the sample would be determined after dissociation before FACS and during FACS.

Dissociated samples of one WT(AB) control (Fig. 4.2.5.A) and three *tert*$^{+/+}$*;mpeg1.1:mCherry.caax* (Fig. 4.2.5.B, C, D) were prepared then split, one half for viability and cell counting using a microscope and trypan blue staining, the other half for FACS. Trypan blue is a stain used to selectively stain dead or dying cells. Trypan blue cannot enter a cell with an intact membrane. However, trypan blue will enter a cell with a damaged membrane, so indicating that the cell is dead or undergoing apoptosis and should not be considered as a live cell. Comparing the cell counts from the FACS to the haemocytometer we see a higher range in the number of cells counted on the FACS ranging from 52-263/µl (Fig. 4.2.5.E) compared to those counted on the haemocytometer ranging from 63-73/µl per sample (Fig. 4.2.5.E). Therefore, there is more variation in the FACS cell counts than the haemocytometer. Using FACS to observe the cell viability indicated that the viability of the WT(AB) sample and the three *tert*$^{+/-}$*;mpeg1.1:mCherry.caax* samples ranged from 60.89% - 79.3% indicating that they would not have sufficient viability to meet the 90% threshold for use in single-cell RNA sequencing (Fig. 4.2.5.F). Using the haemocytometer to determine cell viability indicated that the WT(AB) sample had a viability of 76% and *tert*$^{+/-}$*;mpeg1.1:mCherry.caax* sample 1 had a viability of 69% (Fig. 4.2.5.F) also indicating that they would not meet the 90% viability threshold for use in single-cell RNA sequencing. Data for the *tert*$^{+/-}$*;mpeg1.1:mCherry.caax* samples 2 and 3 using the haemocytometer is unavailable due to human error. Interestingly the viability assessment of the FACS samples using TOPRO-3 indicates that as time progresses the number of cells taking up TOPRO-3 increase (Fig. 4.2.5.A, B, C, D). As TOPRO-3 is added to the sample a set time before it is loaded into the FACS machine this increased uptake cannot be accounted for by increased incubation time in the presence of TOPRO-3. This then may indicate that as the samples are waiting to be loaded, cells are entering apoptosis. Considering this, and the fact that undertaking the

FACS element of the protocol adds a great deal of time to the protocol for preparing a single-cell RNA sequencing sample, it made practical sense to eliminate the FACS element of the protocol and focus on optimising the production of a sample suitable for single-cell RNA sequencing using the gut dissociation protocol only.

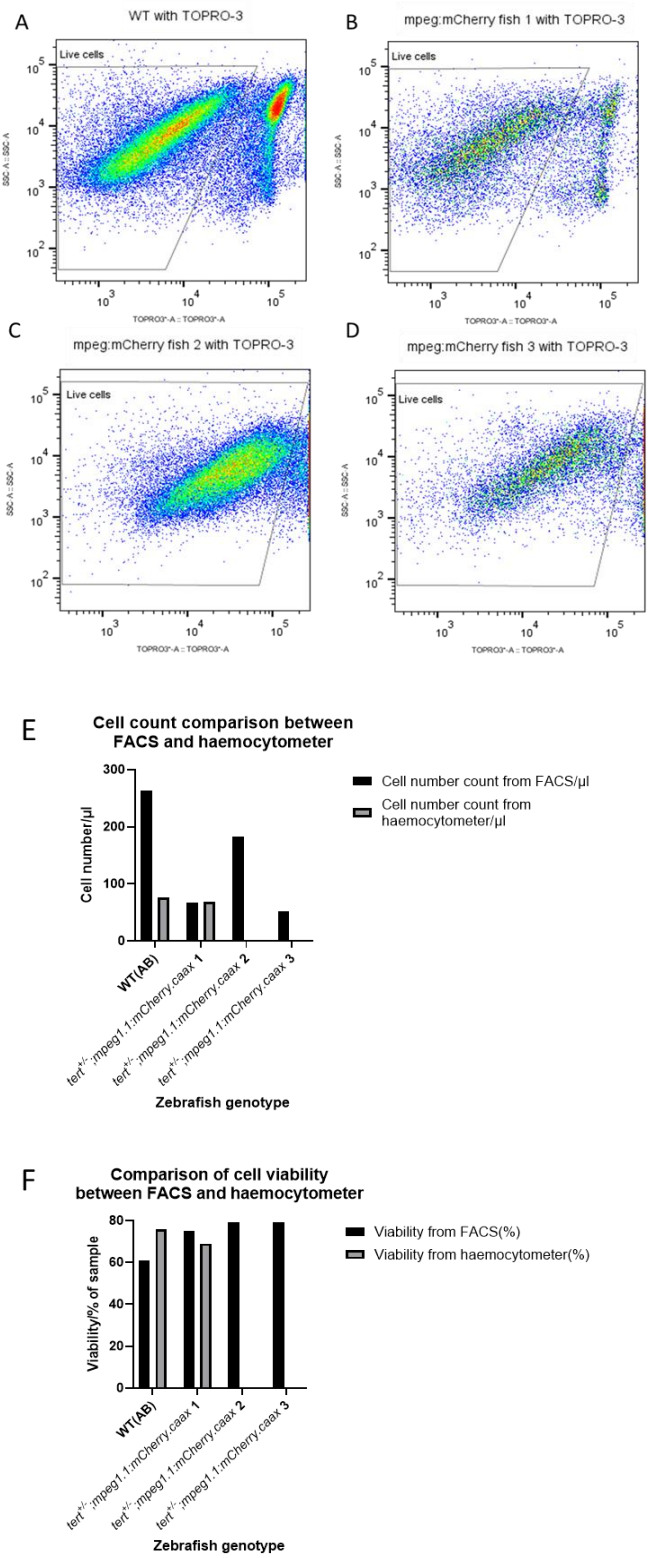

Figure 4.2.5: Determining how FACS affects cell viability. **A.** Viability count from WT(AB), N = 1. **B.** Viability count from *tert*$^{+/-}$*;mpeg1.1:mCherry.caax* 1. **C.** Viability count from *tert*$^{+/-}$*;mpeg1.1:mCherry.caax* 2. **D.** Viability count from *tert*$^{+/-}$*;mpeg1.1:mCherry.caax* 3. **E.** Comparing cell counts from FACS and haemocytometer. **F.** Comparing viability from FACS and haemocytometer.

4.2.6 Determining the efficacy of using a cell suspension from zebrafish gut dissociation for use in single-cell RNA sequencing with methanol fixation.

To optimise the protocol for preparing a suitable sample for single-cell RNA-sequencing the viability and cell number was determined when our general gut dissociation protocol was used. This would provide preliminary information on the effectiveness of isolating a single-cell suspension using this protocol and inform the steps that could be taken optimise the process. Three samples using *tert*$^{+/-}$*;mpeg1.1:mCherry.caax* zebrafish guts were prepared and their viability and the cell number assessed. Viability ranged from 62-83% indicating that an optimisation to increase viability would be required (Fig. 4.2.6.A). Cell number ranged from 178-198/µl (Fig. 4.2.6.B) indicating a sufficient cell number in all samples for single-cell RNA sequencing. Determining the number of clumps (≥2 cells together) in a sample indicated a range of 1-6/5µl (Fig. 4.2.6.C) indicating that further optimisation to reduce clumping would be beneficial, as the fewer clumps the less chance of multiple cell libraries being prepared in the same droplet and better data quality.

An alternative method provided by 10x Genomics for preparing a sample for use with the 10x Genomics chromium controller is to fix the cells that you wish to sequence using a methanol fixation process. To determine if this was a viable method for preparing a single-cell RNA sequencing sample from zebrafish gut dissociation half of each sample was fixed according to the 10x Genomics methanol fixation protocol. The cell number and clumping of each sample was then assessed and comparisons made between before and after methanol fixation (Fig. 4.2.6, B, C). Cell number was reduced in each sample and to a range of 65-168/µl indicating that up to 35% of the cells from a single sample could be lost during methanol fixation (Fig. 4.2.6.B). The number of clumps in the sample had increased after methanol fixation to a range of 2-9 clumps/5µl (Fig. 4.2.6.C).

The variation in cell number be due to the methanol fixation protocol may be due to the methanol causing some cells to lyse. Additionally, there is an indication that the methanol fixation leads to additional clumping, although this may also be due to the fact that the cells have spent longer in media as well. However, the data indicates that the methanol fixation process negatively affects the quality of the sample by increasing the number of clumps and

decreasing the number of single cells (Fig. 4.2.6). Therefore, it does not appear that this would be a viable method to produce a single-cell RNA sequencing sample.

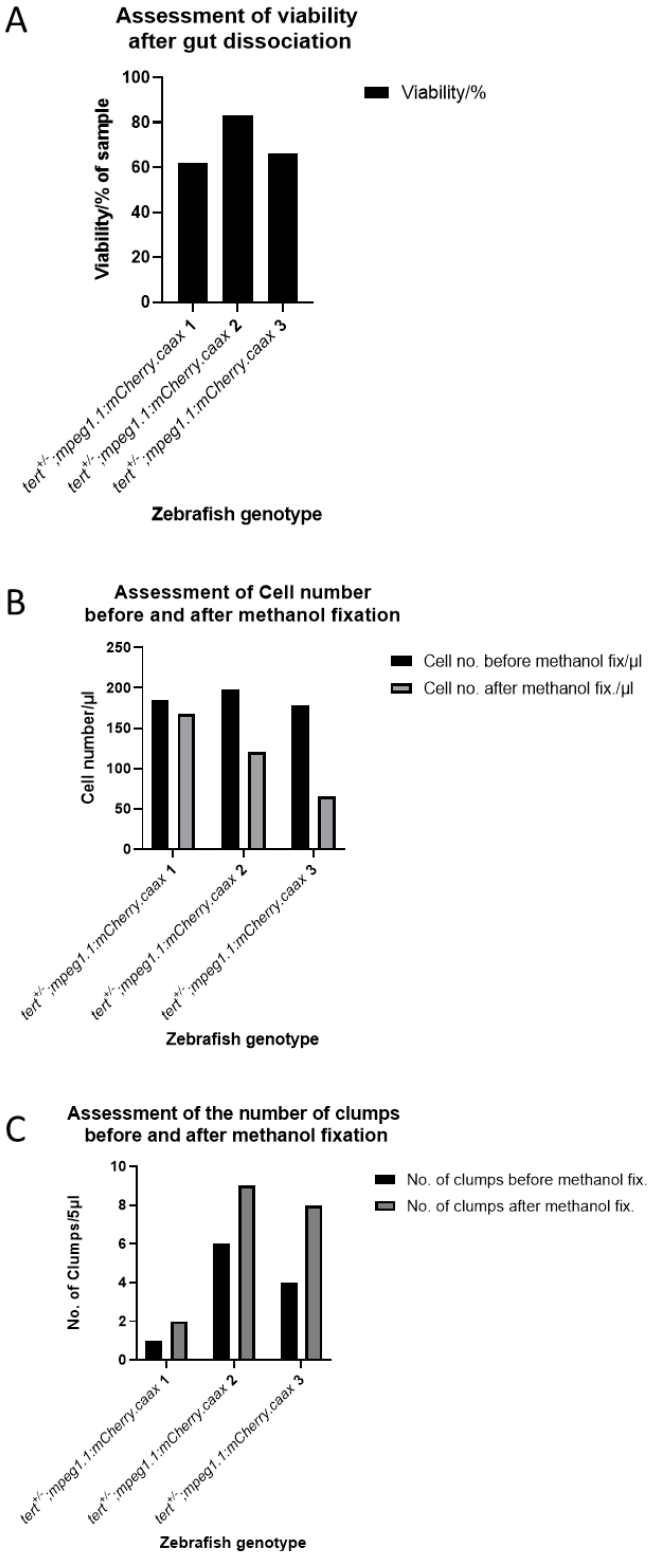

Figure 4.2.6: Determining the efficacy of using a single-cell suspension from zebrafish gut dissociation for use in single-cell RNA sequencing. **A.** Sample viability after gut dissociation. **B.** Cell number before and after methanol fixation. **C.** Number of clumps observed before and after methanol fixation.

4.2.7 Optimising the protocol to produce a sample suitable for single-cell RNA sequencing from a whole zebrafish gut lysate.

To produce a sample suitable for single-cell RNA sequencing using the 10x Genomics Chromium controller it was necessary to optimise the protocol to maximise cell concentration and viability and minimise clumping.

4.2.7.1 Optimising the protocol to increase final cell concentration.

The protocol to prepare a sample for single-cell RNA sequencing included three washes to optimise the isolation of live cells from zebrafish gut. It was hypothesised that during these wash steps cells were being lost. To test this two lysed gut samples, one WT(AB) and one *tert*$^{+/-}$*;mpeg1.1:mCherry.caax* were produced with the number of cells being calculated using a haemocytometer between washes (Fig. 4.2.7.1.A). The calculated cell number counts indicated that the number of cells did not decrease with subsequent washes demonstrating that cells were not being lost (Fig. 4.2.7.1.A). However, the counts had high variation from sample to sample ranging from 570-1,430/µl for the WT(AB) and 215-750/µl for *tert*$^{+/-}$*;mpeg1.1:mCherry.caax* potentially indicating inefficient resuspension (Fig. 4.2.7.1.A).

Further to determining cell number between washes, viability was also determined (Fig. 4.2.7.1.B). Viability declined in the WT(AB) sample from 90.48% to 75.9% over the course of the washes (Fig. 4.2.7.1.B). Further, the viability of the *tert*$^{+/-}$*;mpeg1.1:mCherry.caax* sample declined from 93.33% to 80% (Fig. 4.2.7.1.B). This indicated that cells were dying during the time it took to perform the washes so reducing the quality of the final sample (Fig. 4.2.7.1.B).

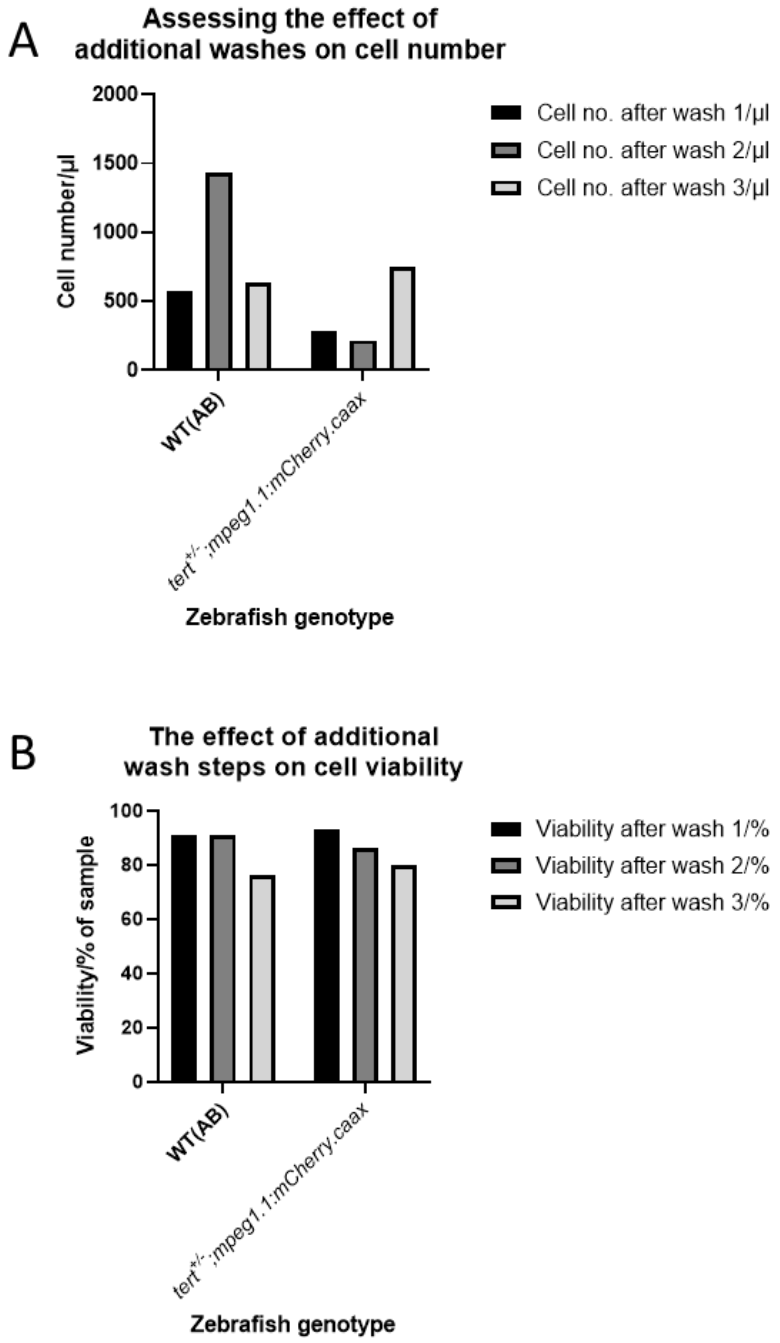

Figure 4.2.7.1: Determining how cell viability and number is affected through the washing steps. **A.** Cell number counts between washes. **B:** Viability assessments between washes.

4.2.7.2 Optimising the protocol to reduce cell clumping.

Section 4.2.6 indicated that an increase in the number of clumps may be occurring over time which would be detrimental to the quality of the single-cell RNA sequencing data. Additionally, there was a concern that a large clump of cells in the sample for single-cell RNA sequencing could cause a blockage. Therefore, the protocol was optimised to reduce the clumping of cells. The alterations to the protocol to reduce clumping were an additional 40µm filtration step or the addition of different concentrations of EDTA. EDTA chelates free Calcium and Magnesium ions so preventing intercellular bonds forming so preventing the cells from clumping.

Three samples were prepared from *tert*$^{+/-}$*;mpeg1.1:mCherry* zebrafish gut to test the effect of adding an additional filtration step to the protocol. Additional filtering led to a decrease in cell numbers in the sample *tert*$^{+/-}$*;mpeg:mCherry* 1 where the count significantly decreased from 185/µl to 83/µl. However, cell numbers for samples *tert*$^{+/-}$*;mpeg:mCherry* 2 and *tert*$^{+/-}$*;mpeg:mCherry* 3 increased slightly (Fig. 4.2.7.2.A). Sample *tert*$^{+/-}$*;mpeg:mCherry* 3 demonstrated a significant decrease in the number of clumps with additional filtering (Fig. 4.2.7.2.B). However, the number of clumps in sample *tert*$^{+/-}$*;mpeg:mCherry* 1 and *tert*$^{+/-}$*;mpeg:mCherry* 2 could not be accurately measured.

Three gut dissociations from *tert*$^{+/-}$*;mpeg:mCherry.caax* were produced to investigate the effects of adding 0.1mM EDTA. The number of clumps with and without additional EDTA was measured as well as the viability of the samples. Measuring the viability of the samples with and without EDTA indicated that there was no significant negative or positive effect on the viability (Fig. 4.2.7.2.C) as viability was observed at ≥90% for each sample. Determining the number of clumps seen with and without the addition of EDTA indicated a significant decrease in the number of clumps in sample *tert*$^{+/-}$*;mpeg:mCherry* 2 and a slight decrease in sample *tert*$^{+/-}$*;mpeg:mCherry* 2 (Fig. 4.2.7.2.D). However, a slight increase in sample *tert*$^{+/-}$*;mpeg:mCherry* 3 was observed (Fig. 4.2.7.2.D).

Further optimisation of the protocol was tested to determine if the addition of a high concentration of EDTA would further alleviate clumping. Two samples of zebrafish gut dissociation from *tert*$^{+/-}$*;mpeg:mCherry.caax* were prepared and the effect of adding 10mM EDTA determined. Viability did not significantly differ between the samples with and without the additional 10mM EDTA (Fig. 4.2.7.2.E) indicating that the increased

concentration was not significantly affecting cell viability. Comparing the number of clumps with and without the increased EDTA concentration indicated a significant reduction in the number of clumps in the samples with the EDTA (Fig. 4.2.7.2.F). Therefore, this data indicates that the increased EDTA concentration is alleviating the clumping issue. Further, the viability in the trials was consistently above ≥90% indicating samples with a viability appropriate for single-cell RNA sequencing.

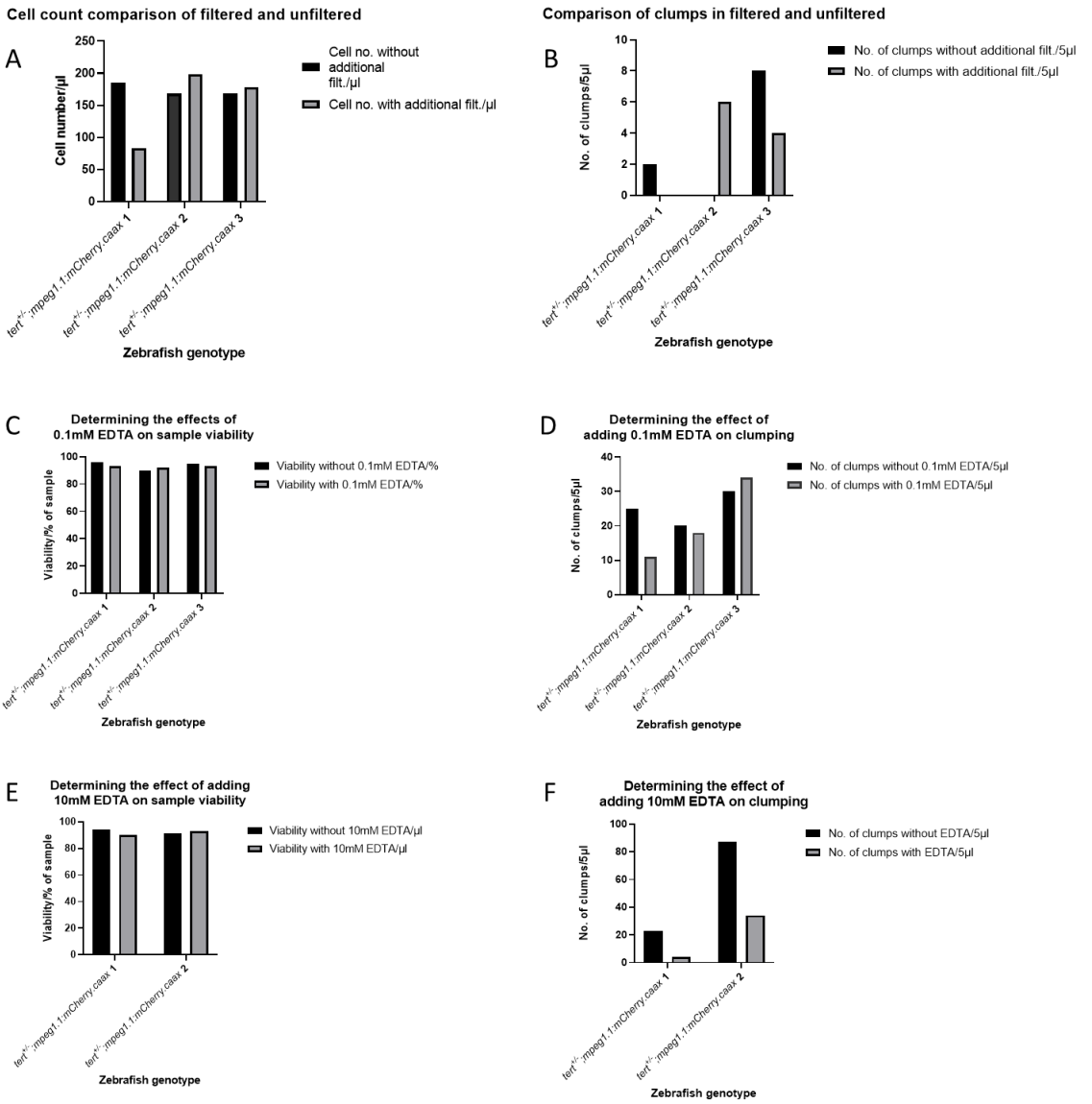

Figure 4.2.7.2: Optimising the method for producing a sample suitable for single-cell RNA-sequencing. **A.** Comparison of cell numbers with and without additional filtering step. **B.** Comparison of clumps with and without additional filtering step. **C.** Measuring the effect of adding EDTA on cell viability. **D.** Measuring the effect of increasing EDTA on clumping. **E.** Determining the effect on viability of adding an increased concentration of EDTA. **F.** Determining the effect on clumping of adding an increased concentration of

4.2.8 Discussion

The aim of this chapter was to optimise a protocol for producing a sample that met the parameters for single-cell RNA sequencing using the 10x Genomics Chromium controller. Here I have demonstrated the optimisation of a method for the preparation of a heterogeneous dissociation of zebrafish gut to a quality suitable for single-cell RNA-sequencing.

Initial gating using the 'dim' and 'bright' gates established by the Henriques lab. indicated that there was a contaminating population of autofluorescent cells. The 'dim' and 'bright' gates indicated a wide range in the levels of the mCherry fluorophore from the *mpeg1.1:mCherry.caax* line. This range may be due to the natural differential regulation of the *mpeg1.1* gene, it may be due to the *mpeg1.1:mCherry.caax* gene having an unknown number of insertions, or it may be due to the insertion site of the *mpeg1.1:mCherry.caax* gene. Therefore, further study of the *mpeg1.1:mCherry.caax* line should be performed to better characterise its effects on the zebrafish phenotype, adding weight to the point from section 3.2.17.2 that whole genome sequencing of novel transgenic lines should be more commonplace.

Further to issues with the levels of mCherry fluorescence, a contaminating population of potentially autofluorescent cells was determined from WT(AB) gut dissociations. These cells were present in gates designed to identify mCherry^{+} cells and so would dilute the specificity of RNA-seq. performed on an mCherry^{+} sample if they were included. One hypothesis for the contaminating cells being present in the mCherry^{+} gate is that zebrafish goblet cells found in the gut excrete digestive enzymes into vesicles that can then be autofluorescent. As this can prove problematic in fluorescence microscopy, it is also possible that it is causing an issue with the specific of FACS of zebrafish gut dissociation.

Further analysis of the mCherry^{+} population from FACS demonstrated that it was possible to determine a heterogenous population of mCherry^{+} cells, that included both lymphoid and myeloid derived cells, present in the *mpeg1.1:mCherry.caax* line used to generate the *mpeg1.1:tert-gfp* and *mpeg1.1:Δtert-gfp* transgenic. The identification heterogenous cell types constituting the mCherry^{+} population supports the use of single-cell RNA sequencing to investigate the different cell types that have been reported to utilise the *mpeg1.1*

promoter and the effects of the *mpeg1.1:tert-gfp* transgene, as other methods such as bulk RNA sequencing would not have cell specificity.

Additionally, section 4.2.5 indicated that viability was decreasing in the FACS of the samples as their viability plots appear to shift to the right in proportion to how long the sample was waiting on ice before it was loaded (Fig. 4.2.5.) indicating an increase in apoptotic cells. In WT(AB) and *tert*$^{+/-}$*;mpeg1.1:mCherry.caax* sample 1 a clear population of viable cells is observed inside the viable gate (Fig. 4.2.5.A, B). However, for *tert*$^{+/-}$*;mpeg1.1:mCherry.caax* samples 2 and 3 the population shifts to the right (Fig. 4.2.5.C, D) indicating an increase in the number of apoptotic cells. The FACS samples were run chronologically starting with WT(AB), then *tert*$^{+/-}$*;mpeg1.1:mCherry.caax* 1, 2 and 3. Therefore, one hypothesis would be that the increase in TOPRO-3 uptake of the populations may be occurring due to the cells membranes becoming permeable as the samples are waiting to be loaded, despite the samples being stored at 4°C. This indicates that time is of the essence when preparing the samples for single-cell RNA sequencing even with proper storage. Further, that if FACS were to be used for the preparation of a single-cell RNA sequencing sample that the increase in time would be detrimental to the sample quality.

The change in viability observed with FACS samples led to concerns that the time taken to perform FACS may also lead to alterations of gene expression in the cells which would affect the RNA sequencing data. Therefore, a method for preparing a sample suitable from single-cell RNA sequencing from whole zebrafish gut lysate was optimised (Fig. 4.2.8). This protocol would have the advantage of being much shorter without the FACS step. However, a potential disadvantage would be that the sample would not be *mpeg1.1*$^{+}$ cell specific as had been the aim with FACS. However, this may be considered an advantage as sequencing a whole gut would enable the study of many distinct cell types. Further to this was the practical considerations of performing the single-cell RNA sequencing experiment. The University of Sheffield lacking a single-cell RNA sequencing facility and the closest viable option was the University of York. This required us to take the experimental fish to the University of York live and to prepare the samples on the day that their libraries were going to be prepared. Adding the process of FACS to producing the samples would have extended the time of the protocol to the point that it would be very impractical to prepare the samples and have their libraries prepared the same day. Section 4.2.6 details the test of the

methanol fixation protocol suggested as an alternative to moving zebrafish to the University of York. However, data indicated that with methanol fixation clumping was greatly increased (Fig. 4.2.6.C) which may lead to a low-quality sample. This was supported by the cell concentration decreasing after methanol fixation (Fig. 4.2.6.B) potentially due to cells aggregating into clumps. An additional concern was that the RNA expression of the cells would alter due to methanol fixation, although this would not change once the cell had been fixed. However, the clumping and loss of concentration led to a halt in testing the methanol fixation protocol.

The focus of the protocol was to maximise viability and concentration while reducing clumping to prevent doublets and blockages of the machine. Initial considerations were to quantify how cell numbers and viability were changing through the protocol to determine how it may be improved (section 4.2.7.1). Data indicated viability decreased steadily with each wash step (Fig. 4.2.7.1.B) however the data on cell concentration did not paint a clear picture on how concentration was changing throughout the protocol (Fig. 4.2.7.1.A). However, clumping was noted throughout the protocol despite washes indicating that this required further optimisation. It was then hypothesised that adding an additional step filtering the sample through a 40µm strainer would eliminate large clumps. However, testing this (Fig. 4.2.7.2.B) led to no clear quantifiable indication that an additional filtering step led to less clumps in the final sample. An alternative method to prevent clumping would be the addition of a reagent to the sample that may prevent clumping. Both RNA and DNA released from apoptotic cells can be causes of clumping, however adding DNAse or RNAse would be undesirable as they may interfere with the library preparation step the sample was being prepared for. Therefore, the addition of EDTA was deemed a suitable solution. EDTA works by chelating free metal ions preventing their use by the cells for intracellular adhesion. Increasing concentrations of EDTA demonstrated a quantifiable decrease in clumping (Fig. 4.2.7.2.D, F) while viability was maintained at a suitable level (Fig. 4.2.7.2.C, E). While 0.1mM led to slightly less clumping (Fig. 4.2.7.2.D) 10mM EDTA provided a more noticeable difference in the number of clumps (Fig. 4.2.7.2.F). Hence, 10mM EDTA was determined to be a more suitable concentration for single-cell RNA sequencing sample preparation based on the results observed in these experiments.

Optimising a protocol for the isolation of zebrafish whole gut suspension suitable for single-cell RNA sequencing will enable the study of the effects of the *mpeg1.1:tert-gfp* transgene in the *tert*$^{-/-}$*;mpeg1.1:mCherry.caax* background in a zebrafish gut context. Further, sequencing whole gut dissociation will produce a single-cell RNA sequencing landscape of the zebrafish gut. This will enable the study of differences in RNA expression in many cell types, providing clues as to how rescuing the expression of TERT in *mpeg1.1*$^{+}$ cells affects the ageing gut as whole.

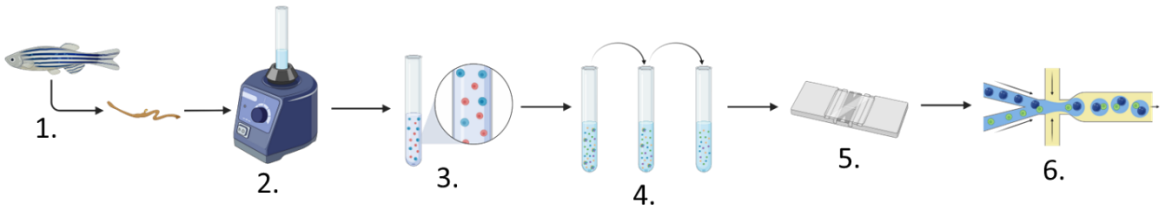

Figure 4.2.8: Representative illustration of the final process for preparing a sample for single-cell RNA-sequencing. Initially the zebrafish is sacrificed, and the intestine removed (1.), which is then dissociated (2.). This produces a cell suspension (3.) which is then filtered several times (4.) to remove clumps. The cell number and viability are checked using a hemocytometer (5.) before the sample is diluted to an appropriate concentration and loaded into the 10x Chromium device which then uses a droplet-based method to isolate single-cells (6.).

Chapter 5: Determining the effects of the *mpeg1.1:tert-gfp* transgene on *tert*$^{-/-}$*;mpeg1.1:mCherry.caax;mpeg1.1:tert-gfp* intestinal cell physiology using single-cell transcriptomics

5.1 Introduction

Characterising the aged zebrafish gut using single-cell RNA-seq. would be provide useful and novel data on how ageing affects gene expression in several different cell subsets within the zebrafish gut, indicating how it affects the organ as a whole. Further to this, characterising the gut in the transgenic *tert*$^{-/-}$*;mpeg1.1:mCherry.caax;mpeg1.1:tert-gfp* line would provide additional data on how rescuing TERT expression in *mpeg1.1*$^{+}$ immune cell subsets affects intestinal ageing.

With the advent of increasingly accessible Single-cell RNA sequencing it is possible to create atlases of cell transcripts that provide in-depth knowledge of the transcription occurring in the cell at the time of sequencing(262). Single-cell RNA is being used with increasing frequency in the zebrafish model organism to perform in depth studies of RNA expression. Understanding the alterations that occur in RNA expression in a cell provides the basis for further research. For example, if we can determine the gene that the RNA is being transcribed from we may be able to determine which signalling pathways regulate that genes expression and so extrapolate which pathways are being affected by the experimental conditions. Further to this, if the RNA codes for a protein and we can determine which protein that is we can design experiments to quantify the levels of that protein that being expressed and its function in the different experimental conditions. This forms the basis for planning future experiments that will test different aspects of the alterations observed in the model organisms. For example, *Wagner et al.* performed single-cell RNA sequencing on using zebrafish embryos to map gene expression and cell lineage in the developing zebrafish up to 24 hours post-fertilisation (hpf) providing an atlas of genes that may be investigated in future developmental genetics work that tries to understand genetic diseases that affect foetal development (266). *Farnsworth et al.* used Single-cell RNA-sequencing of 44,012 cells from developing zebrafish up to 5dpf to produce a zebrafish developmental atlas that captured rare cell types such as Putative Germ Cells (PGCs) that may be studied in future work looking at stem cell regeneration(264). Additionally *Farnsworth et al's* study enabled the tracking of changes in RNA-expression over the first five days of the zebrafishes development, which may enable future research into proteins that we now know are integral to the advancement of the zebrafish lifecycle thanks to their work(264).

The zebrafish is a widely accepted *in vivo* model with its use in the field of biogerontology growing steadily(213, 218, 219, 269). Previously, I have detailed the two novel transgenic models I have created to allow us to determine the role of telomerase in macrophage biology and discriminate between the canonical versus the non-canonical functions that may make up this role (section 3). The aim of creating these models is to determine how the non-canonical functions of TERT affect *mpeg1.1*$^{+}$ cell physiology. To determine this I would use single-cell RNA-sequencing to examine the altered gene expression between *tert*$^{+/+}$*;mpeg1.1:mCherry.caax* and *tert*$^{-/-}$*;mpeg1.1:mCherry.caax* to provide an overview of significant transcriptional differences observed between the two which would represent the difference between a healthy and prematurely aged gut phenotype. I would then utilise single-cell RNA-sequencing to determine how the insertion of the *mpeg1.1:tert-gfp* transgene affected gene expression in the *tert*$^{-/-}$*;mpeg1.1:mCherry.caax;mpeg1.1:tert-gfp* line.

Single-cell RNA sequencing was performed on 12 month old fish as it is at this age that *tert*$^{-/-}$ fish are considered to be prematurely aged and begin exhibiting the aged phenotype we see at 30 months in *tert*$^{+/+}$(220). By comparing 12-month-old *tert*$^{-/-}$*;mpeg1.1:mCherry.caax* to age matched *tert*$^{+/+}$*;mpeg1.1:mCherry.caax* I aimed to highlight the transcriptomic differences seen between the aged *mpeg*$^{+}$ in *tert*$^{-/-}$*;mpeg1.1:mCherry.caax* and the young macrophages observed in the *tert*$^{+/+}$*;mpeg1.1:mCherry.caax* line. Additionally, to determine how the *mpeg-tert-gfp* transgene affected the gene expression of the *tert*$^{-/-}$*;mpeg1.1:mCherry.caax;mpeg1.1:tert-gfp* I would compare the single-cell RNA sequencing data from *tert*$^{-/-}$*;mpeg1.1:mCherry.caax;mpeg1.1:tert-gfp* line to that of the *tert*$^{-/-}$*;mpeg1.1:mCherry.caax*.

However, there are limitations to single-cell RNA sequencing. When sequencing populations of single cells, unless the population has been selected using processes such as FACS, the population will be heterogeneous and require profiling sequencing. Further to this, the single cell population being sequenced will contain cells at different stages of the cell cycle that may affect gene expression levels, as well potentially apoptotic cells. Apoptotic cells will need to be filtered out of the data post-sequencing during the data quality control step or during the data analysis step. Additionally, the experiment must be designed to reduce batch effect. Batch effect occurs when the variation observed between samples occurs due

to the technical arrangement of the experiment rather than the change in biological factors you intend to observe the effects of(270). We designed our single cell RNA sequencing experiment with the aim of reducing batch effect. We used the 10x Chromium controller for single cell partitioning and barcoding so were limited to eight samples per run due to the design of the machine. As the experiment consisted of eighteen samples total and the samples had to be prepared on the day to we decided that six samples be loaded each day over the course of three days. Additionally, each day one of each sex (male or female) would be loaded per genotype (*tert*$^{-/-}$*;mpeg1.1:mCherry.caax*, *tert*$^{+/+}$*;mpeg1.1:mCherry.caax*, *tert*$^{-/-}$*;mpeg1.1:mCherry.caax;mpeg1.1:tert-gfp*) to control for variation between sex.

5.2 Elimination of apoptotic cells using a tailored panel of apoptosis related genes

To produce high-quality single-cell transcriptional data guts were isolated from six fish per genotype following the protocol optimise in the previous chapter. To control for variation of transcript profiles due to sex each group constituted three females and three males. To control for batch variation, six dissociations were sequenced per sequencing run, 1x *tert*$^{+/+}$*;mpeg1.1:mCherry.caax* male, 1x *tert*$^{+/+}$*;mpeg1.1:mCherry.caax* female, 1x *tert*$^{-/-}$*;mpeg1.1:mCherry.caax* male, 1x *tert*$^{-/-}$*;mpeg1.1:mCherry.caax* female, 1x *tert*$^{-/-}$*;mpeg1.1:mCherry.caax;mpeg1.1:tert-gfp* male, 1x *tert*$^{-/-}$*;mpeg1.1:mCherry.caax;mpeg1.1:tert-gfp* female. The combined total number of cells was 115,731 (*tert*$^{+/+}$*;mpeg1.1:mCherry.caax* 44,366 cells, *tert*$^{-/-}$*;mpeg1.1:mCherry.caax* 39,119 cells, *tert*$^{-/-}$*;mpeg1.1:mCherry.caax;mpeg1.1:tert-gfp* 32,246 cells(Table 5.2)), with the median number of gene reads being 3,304 and the mean feature number being 325.

To ensure that apoptotic cells were not included in the single-cell RNA sequencing analysis a list of genes the expression of which was reported to be upregulated after organismal death and expressed during apoptosis was used to remove apoptotic cells(271). The list of genes consisted of: *Caspase apoptosis-related cysteine peptidase (Casp3b), Inhibitor of apoptosis-binding mitochondrial protein a* (*Diabloa*), *Diablob* and *alkaline ceramidase 3* (*Acer3*). Apoptotic cells were grouped, and their UMI's exported as a Comma Separated Values (CSV) file. This file was then used to remove apoptotic cells during the Loupe browser processing pipeline from the *tert*$^{+/+}$*;mpeg1.1:mCherry.caax*, *tert*$^{-/-}$*;mpeg1.1:mCherry.caax*, and *tert*$^{-/-}$*;mpeg1.1:mCherry.caax;mpeg1.1:tert-gfp* single-cell RNA-sequencing samples. Using these genes to remove apoptotic cells a total of 7,154 cells from the grouped samples: 1,879 from the *tert*$^{-/-}$*;mpeg1.1:mCherry.caax* aggregate, 2,661 from the *tert*$^{-/-}$*;mpeg1.1:mCherry.caax;mpeg1.1:tert-gfp* aggregate, and 2,614 from the *tert*$^{+/+}$*;mpeg1.1:mCherry.caax* aggregate (Table 5.2).

Genotype group	Total cell number of group	Number of apoptotic cells removed from group	Percentage of group that was removed (%)
tert$^{-/-}$*;mpeg1.1:mCherry.caax*	32,246	1,879	5.8
tert$^{+/+}$*;mpeg1.1:mCherry.caax*	39,119	2,614	6.7
tert$^{-/-}$*;mpeg1.1:mCherry.caax;mpeg1.1:tert-gfp*	44,366	2,661	6

Table 5.2: Apoptotic cells removed from each sequenced genotype

5.3 Identification of *mpeg1.1*$^{+}$ cell populations and characterisation of the differential gene expression between genotypes.

In humans *mpeg1* acts as a promoter for perforin-2 that is expressed as part of the innate immune response to bacterial infection(272, 273). Previous work by *Ellet et al.* indicated *mpeg1.1* to be macrophage specific in zebrafish, however more recent work has indicated that zebrafish lymphoid cells also utilise *mpeg1.1(226, 227, 234, 237)*. The *mpeg1.1:tert-gfp* transgene was designed so that *mpeg1.1* utilising cells would express TERT in an *mpeg1.1* dependent manner. Therefore, any cell that utilises the *mpeg1.1* promoter would also express the inserted *mpeg1.1:tert-gfp* transgene. By identifying *mpeg1.1*$^{+}$ populations I can isolate the cells that the *mpeg1.1:tert-gfp* transgene will be expressed in in the transgenic line. I can then compare the *mpeg1.1*$^{+}$ population from the *tert*$^{+/+}$*;mpeg1.1:mCherry.caax* to the *mpeg1.1*$^{+}$ group from the *tert*$^{-/-}$*;mpeg1.1:mCherry.caax* group and determine which genes are differentially expressed. This will indicate the difference in gene expression between a healthy population and a prematurely aged population. I can then compare the *tert*$^{-/-}$*;mpeg1.1:mCherry.caax;mpeg1.1:tert-gfp mpeg1.1*$^{+}$ population to the *tert*$^{-/-}$*;mpeg1.1:mCherry.caax mpeg1.1*$^{+}$ population to determine how rescuing TERT expression under control of the *mpeg1.1* promoter affects their gene expression and if there are similarities that can be drawn between the *tert*$^{+/+}$*;mpeg1.1:mCherry.caax* and *tert*$^{-/-}$*;mpeg1.1:mCherry.caax;mpeg1.1:tert-gfp mpeg1.1*$^{+}$ populations.

5.3.1 Ontological analysis of differentially expressed genes in the *tert*$^{-/-}$*;mpeg1.1:mCherry.caax;mpeg1.1:tert-gfp* and *tert*$^{+/+}$*;mpeg1.1:mCherry.caax mpeg1.1*$^{+}$ populations

Identifying populations of *mpeg1.1*$^{+}$ cells in each group aggregate I found 157 *mpeg1.1*$^{+}$ cells from the *tert*$^{+/+}$*;mpeg1.1:mCherry.caax* group, 48 cells from the *tert*$^{-/-}$*;mpeg1.1:mCherry.caax* group, and 91 cells from the *tert*$^{-/-}$*;mpeg1.1:mCherry.caax;mpeg1.1:tert-gfp*. Considering the total number of cells in each

group (Table 5) the numbers of *mpeg1.1*$^{+}$ were much lower than expected, as in the literature *Ellis et al.* reported between ten and twenty percent of zebrafish intestinal cells were *mpeg1.1*$^{+}$ (185).

To further understand how the insertion of the *mpeg1.1:tert-gfp* transgene may be affecting *mpeg1.1*$^{+}$ cell physiology the ontology of the differentially expressed genes was determined (Fig. 5.3.1). Initially, the differentially regulated genes between the *tert*$^{-/-}$*;mpeg1.1:mCherry.caax* (homozygous tert mutant) and the *tert*$^{+/+}$*;mpeg1.1:mCherry.caax* (WT) *mpeg1.1*$^{+}$ populations were determined. These were then compared to the differentially regulated genes between *tert*$^{-/-}$*;mpeg1.1:mCherry.caax;mpeg1.1:tert-gfp* (homozygous tert mutant with *mpeg1.1:tert-gfp* transgene inserted) and the *tert*$^{+/+}$*;mpeg1.1:mCherry.caax mpeg1.1*$^{+}$ populations using Venny (Fig. 5.3.1.A). The *tert*$^{-/-}$*:mpeg1.1:mCherry.caax* line was used as a comparison for both the *tert*$^{-/-}$*;mpeg1.1:mCherry.caax;mpeg1.1:tert-gfp* line and the *tert*$^{+/+}$*;mpeg1.1:mCherry.caax.* The working hypothesis is that genes differentially regulated between the *tert*$^{-/-}$*;mpeg1.1:mCherry.caax* and the *tert*$^{+/+}$*;mpeg1.1:mCherry.caax* will be differentially regulated due to the effects of telomerase dependent ageing. Further, the genes differentially regulated between the *tert*$^{-/-}$*:mpeg1.1:mCherry.caax* line and the *tert*$^{-/-}$*;mpeg1.1:mCherry.caax;mpeg1.1:tert-gfp* line would be so due to the effects of the inserted *mpeg1.1:tert-gfp* transgene. I could then compare the genes differentially regulated in each comparison (Fig. 5.3.1.A) and the genes differentially regulated in only the yellow circle would be as a result of the *mpeg1.1:tert-gfp* transgene. This indicated sixty-four genes that were differentially regulated in the *tert*$^{-/-}$*;mpeg1.1:mCherry.caax;mpeg1.1:tert-gfp* that were not differentially regulated in either of the other genotypes (Fig. 5.3.1.A). Therefore, it was assumed that these genes were differentially regulated due to the effects of inserting the *mpeg1.1:tert-gfp* transgene.

The software ShinyGO was used to determine the ontology of the sixty-four genes that were differentially regulated in the *tert*$^{-/-}$*;mpeg1.1:mCherry.caax;mpeg1.1:tert-gfp* (Fig. 5.3.1.B, C, D, E)(245). ShinyGO was used in conjunction with the Kyoto Encyclopaedia of Genes and Genomes (KEGG) database and the Gene Ontology database to gain a broader understanding of the data. Specifically, the KEGG database is designed as a database that links genes to biological functions in cells(274). Using the KEGG database then indicates that

the genes also have known biological functions in the cell. The Gene Ontology database is used as it has three groups that can be utilised (molecular function, cellular component, and biological process) that indicate how differentially regulated genes relate to organismal function on three levels giving a wider understanding of how they interact and may affect an organisms health(275, 276). Initial analysis using the KEGG database indicated that the differentially regulated genes are involved in the regulation of apoptosis, cytokine receptor interactions, actin cytoskeleton regulation, the formation of the phagosome and the lysosome, and oxidative phosphorylation (Fig. 5.3.1.B). This was intriguing as previous work by *Ellis et al.* had indicated a subset of *mpeg1.1*$^{+}$ macrophages present in zebrafish gut had impaired phagocytosis with ageing that occurred in line with telomerase-dependent molecular alterations(185). Additionally, non-canonical functions of TERT in mitochondrial function have been reported (section 1.4.2.2)(132, 139, 145). Therefore, observing a change in gene expression associated with mitochondrial function indicates we may be rescuing mitochondrial in the *tert*$^{-/-}$*;mpeg1.1:mCherry.caax;mpeg1.1:tert-gfp* genotype. Analysis with the Gene Ontology Biological Processes (GOBP) database indicated differential regulation of pathways involved in the immune response to bacteria and the cellular response to superoxide free radicals (Fig. 5.3.1.C). Analysis using the Gene Ontology Cellular Components (GOCC) database indicated differential regulation of pathways involved in respiration and the cytochrome complex as well as formation of ribosomes (Fig. 5.3.1.D). Further, analysis using the Gene Ontology Molecular Functions (GOMF) database indicated differential regulation of pathways involved in chromatin binding, cytochrome and electron transfer activity, and peroxidase activity (Fig. 5.3.1.E). Overall, this is an indication that insertion of the *mpeg1.1:tert-gfp* transgene is causing differential regulation of genes that play a part in the regulation of mitochondrial structure, respiration, ribosome formation and structure, and the immune response (Fig. 5.3.1).

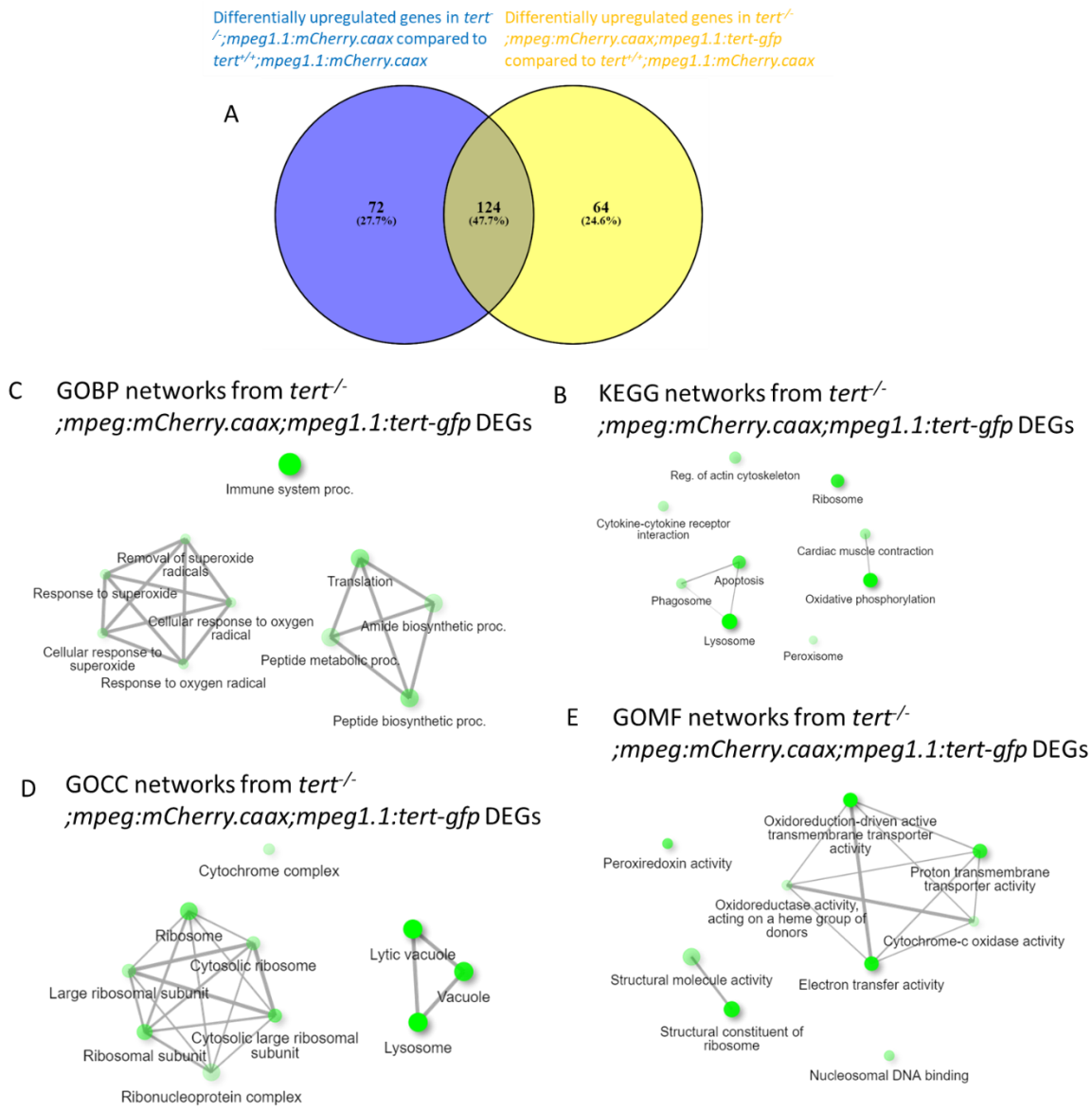

Figure 5.3.1: Upregulated genes from each *mpeg1.1*$^{+}$ population and their associated pathways. **A.** Venn diagram of the differentially regulated genes between the t*ert*$^{-/-}$*;mpeg1.1:mCherry.caax;mpeg1.1:tert-gfp* and *tert*$^{+/+}$*;mpeg1.1:mCherry.caax mpeg1.1*$^{+}$ population (yellow) compared to the t*ert*$^{-/-}$*;mpeg1.1:mCherry.caax* and *tert*$^{+/+}$*;mpeg1.1:mCherry.caax mpeg1.1*$^{+}$ population (blue) with genes that upregulated in both populations indicated in the shaded centre. **B.** Gene ontology analysis of the differentially regulated genes from the KEGG database. **C.** Gene ontology analysis of the differentially regulated genes from the GOBP database. **D.** Gene ontology analysis of the differentially regulated genes from the GOCC database. **E.** Gene ontology analysis of the differentially regulated genes from the GOMF

5.3.2 Exploring the effects of the insertion of the *mpeg1.1:tert-gfp* transgene on rescuing gene expression towards *tert*$^{+/+}$*;mpeg1.1:mCherry.caax* levels.

To determine if insertion of the *mpeg1.1:tert-gfp* transgene rescues the ageing phenotype of *mpeg1.1*$^{+}$ cells I compared the ten most upregulated genes in the *tert*$^{+/+}$*;mpeg1.1:mCherry.caax* compared to the ten most upregulated genes in the *tert*$^{-/-}$*;mpeg1.1:mCherry.caax;mpeg1.1:tert-gfp* using the *tert*$^{-/-}$*;mpeg1.1:mCherry.caax* as the baseline. Comparing the population of *mpeg1.1*$^{+}$ cells from *tert*$^{+/+}$*;mpeg1.1:mCherry.caax* to the population from *tert*$^{-/-}$*;mpeg1.1:mCherry.caax* indicated several upregulated genes in the *tert*$^{+/+}$*;mpeg1.1:mCherry.caax* population, the ten most significant of which were: *BX855618.1*, *claudin b (cldnb)*, *zgc:193726*, *epithelial cell adhesion molecule (epcam)*, *si:ch211-137i24.10*, *si:dkeyp-110c12.3*, *BX908782.2*, *keratin 15 (krt15)*, *krt91*, and *krt4*(Fig. 5.3.2).

Currently the gene *zgc:193726* is predicted to be protein coding however the function has yet to be investigated. The genes *krt15, krt91*, and *krt4* code for keratin that forms part of the intermediate filament. The *BX855618.1* codes for a section of zebrafish chromosome 4 that contains the *dopamine receptor D4 (drd4)* gene which is predicted to have G protein-coupled receptor activity and dopamine neurotransmitter activity. Further, the gene *si:dkeyp-110c12.3* is predicted to encode a Guanosine Trypohosphate-ase (GTP-ase), *cldnb* which is predicted to be involved in sodium ion transport, and *epcam* which is a cell adhesion molecule. The expression of these genes is important to the continued maintenance of cell physiology, and their dysregulation in the prematurely aged phenotype is consistent with the prematurely aged phenotypes gut atrophy. The region *BX908782.2* is indicated to contain the genes *Lymphocyte antigen 97, tandem duplicate 2 (ly97.2)* and *Sodium channel, voltage gated, type XII, alpha a (scn12aa)*. *Ly97.2* is indicated to bind to exhibit LPS binding activity and therefore is involve in the defence response to gram-negative bacteria and LPS. *Scn12aa* is predicted to have voltage-gated sodium channel activity and to be expressed in the nervous system and to be involved in heart contraction regulation.

To determine how the effects of the *mpeg1.1:tert-gfp* transgene affects gene expression in the prematurely aged *mpeg1.1*$^{+}$ population examined the differential expression of genes between *mpeg1.1*$^{+}$ cells from the *tert*$^{-/-}$*;mpeg1.1:mCherry.caax* group to that of the *tert*$^{-/-}$*;mpeg1.1:mCherry.caax;mpeg1.1:tert-gfp* group. From this analysis the ten most significant genes upregulated in *tert*$^{-/-}$*;mpeg1.1:mCherry.caax;mpeg1.1:tert-gfp mpeg1.1*$^{+}$ positive cells include *apolipoprotein A-II (apoa2)*, *apolipoprotein A-Ib (apoa1b)*, *zgc:193726*, *fatty acid binding protein 11a (fabp11a)*, *ferritin, heavy polypeptide-like 28 (fthl28)*, *tumor necrosis factor b (tnfb)*, *CABZ011124091.1*, *XLOC_025423*, *si:dkey-203a12.9*, and *BX323596.2* (Fig. 5.3.2). Initially we can see that *apoa2*, *apoa1b*, and *fabp11a* are involved in lipid and cholesterols metabolism. This is interesting as it has been reported human macrophages process cholesterol and fat in both the liver and in atherosclerotic plaques (100) and that *apoa* acts in a similar manner in zebrafish(277). Therefore, this may indicate that the expression of the *mpeg1.1:tert-gfp* transgene is contributing to change in the processing of fatty acids and cholesterol. This would be in-line with the observations of *Gizard et al.* whereby the induction of TERT expression was observed in macrophages present in atherosclerotic plaques(146). The gene *fthl28* is predicted to have ferric ion binding activity and therefore may be involved in iron homeostasis. This is intriguing as it is reported that iron homeostasis is linked to macrophage function phenotype via NF-κB signalling, DNA methylation, and histone modification(278). The upregulation of *tnfb* (in humans known as lymphotoxin-α) is interesting as the tumour necrosis family of proteins has been reported to be a regulator of the macrophage and B-cell physiology(279). *CABZ011124091.1* is predicted to encode a copy of the zebrafish *mucin* gene *muc2.4* which is expressed to produce mucin which protects cells from the harsh environment of the gut. The gene *si:dkey-203a12.9* is predicted to encode a serine peptidase inhibitor responsible for the cleaving of peptide bonds in proteins, however further detail is not available at this time. Additionally, while *zgc:193726* is registered gene it has not yet been studied to the point that any conclusions can be made about its function. Further, *XLOC_025423* has also yet to be characterised to the point that its function is understood. Therefore, this initial evidence indicates that expression of the *mpeg1.1:tert-gfp* transgene is rescuing the expression of genes important to normal macrophage and B-cell function and the maintenance of their physiology (*apoa2, apoa1b, fabp11a*). Further, it suggests that it is affecting their inflammatory signalling pathway via *tnfb* signalling potentially altering their inflammatory state. While this analysis

provides some interesting preliminary insights into the effects of the *mpeg1.1:tert-gfp* transgene on *mpeg1.1*$^{+}$ cells, further investigation into specific cell subsets is required to increase the specificity of the analysis in terms of its effects on cell physiology.

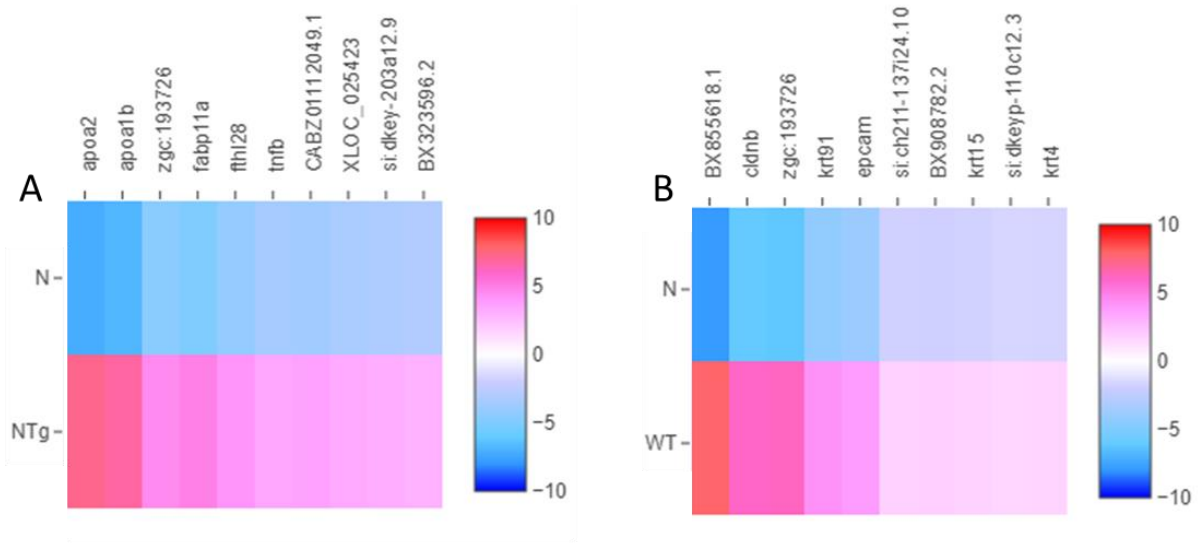

Figure 5.3.2: The ten most differentially upregulated genes in *mpeg1.1*$^{+}$ populations. **A.** Upregulated genes from *tert*$^{+/+}$*;mpeg1.1:mCherry.caax* (abbreviated to WT) (n=157) versus *tert*$^{-/-}$*;mpeg1.1:mCherry.caax* (abbreviated to N) (n=48) *mpeg1.1*$^{+}$ populations. **B.** Upregulated genes from *tert*$^{-/-}$*;mpeg1.1:mCherry.caax;mpeg1.1:tert-gfp* (abbreviated to NTg) (n=91) compared to *tert*$^{-/-}$*;mpeg1.1:mCherry.caax* (n=48) *mpeg1.1*$^{+}$ populations.

5.3.2.1 Exploring the commonly upregulated genes between *tert*$^{+/+}$*;mpeg1.1:mCherry.caax* and *tert*$^{-/-}$*;mpeg1.1:mCherry.caax;mpeg1.1:tert-gfp mpeg1.1*$^{+}$ populations

As there was no correlation between the ten most significantly upregulated genes in the *mpeg1.1* populations I determined to broaden the search and ascertain if there were any upregulated genes in the top fifty upregulated genes (Fig. 5.3.2.1). This analysis indicated eleven genes were upregulated in both the *tert*$^{+/+}$*;mpeg1.1:mCherry.caax* and the *tert*$^{-/-}$*;mpeg1.1:mCherry.caax;mpeg1.1:tert-gfp mpeg1.1*$^{+}$ populations (Fig. 5.3.2.1.A). These genes were: *Metallothionein 2 (mt2)*, *mitochondrial Cytochrome b (mt-cyb), mitochondrial Nicotinamide adenine dinucleotide (NADH)-ubiquinone oxidoreductase chain 3 (mt-nd3), mt-nd4, md-nd5, mitochondrial Cytochrome c oxidase subunit 1 (mt-co1), mt-co2, mt-co3, mitochondrial ATP-synthase subunit a (mt-atp6), krt4,* and *si:ch211-39i22.1* which is predicted to be a CD99-like molecule. Ontological analysis of this data indicates that insertion of the *mpeg1.1:tert-gfp* transgene has led to an upregulation of genes involved in ATP synthesis via oxidative phosphorylation (Fig. 5.3.2.1.B). Further, protein interaction network analysis indicates that the proteins encoded by the upregulated genes interaction (Fig. 5.3.2.1.C). Specifically, we can see that *mt-nd3, mt-nd4, mt-nd5, mt-atp6, mt-cyb, mt-co1, mt-co2,* and *mt-co3* form an interaction network. Therefore, this data indicates that insertion of *mpeg1.1:tert-gfp* transgene may have rescued mitochondrial function in *tert*$^{-/-}$*;mpeg1.1:mCherry.caax mpeg1.1*$^{+}$ cells towards the expression levels of *tert*$^{+/+}$*;mpeg1.1:mCherry.caax mpeg1.1*$^{+}$ cells.

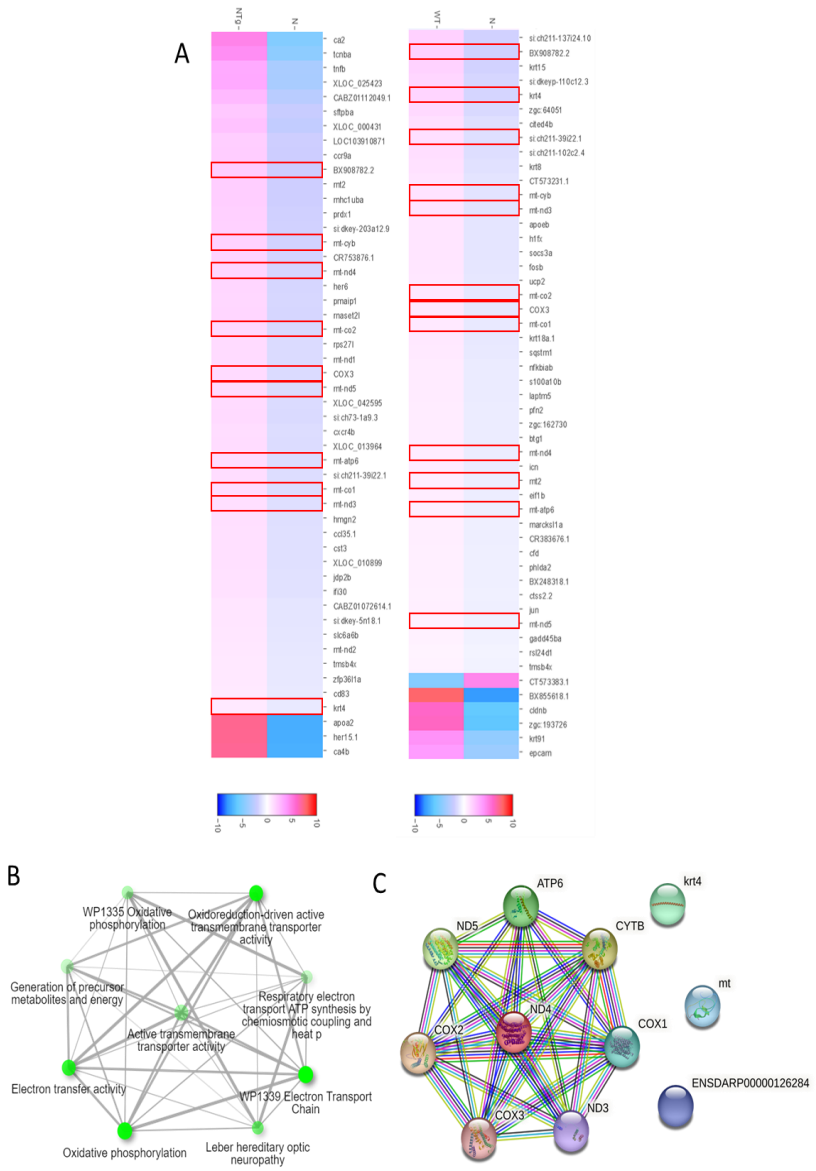

Figure 5.3.2.1: A comparison of genes upregulated in both *tert*$^{+/+}$*;mpeg1.1:mCherry.caax* and *tert*$^{-/-}$*;mpeg1.1:mCherry.caax;mpeg1.1:tert-gfp mpeg1.1*$^{+}$ populations. **A.** Comparison of the top fifty upregulated genes in each genotype with genes commonly upregulated indicated by a red box. **B.** Ontology analysis of the commonly upregulated genes. **C.** Interaction network of the proteins encoded by the upregulated genes Interactions are identified by STRING using text-mining (yellow), experiments previously performed (pink), databases (light blue), co-expression (black), neighbourhood in the genome (green), gene fusion (red) and co-occurrence in publications (dark blue).

5.3.3 Determining the cell subsets that constitute the *mpeg1.1*$^{+}$ cell population.

As discussed in the introduction to section 5.1, the *mpeg1.1* promoted has been identified to be utilised in both zebrafish macrophages and B-cells(226, 234, 236). Therefore, I wanted to determine the cell subsets that constituted the *mpeg1.1*$^{+}$ cells from my zebrafish gut dissociation single-cell RNA sequencing data. I would expect there to be a population of B-cells and macrophages, however additional populations may also be present.

To determine the cell subsets the *mpeg1.1*$^{+}$ population from all groups underwent unsupervised clustering (Fig. 5.3.3.A). This produced four distinct clusters (Fig. 5.3.3.A). The upregulated genes from cluster were compared to determine which genes were uniquely upregulated in each cluster (Fig. 5.3.3.B). The uniquely upregulated genes from each cluster were then used as markers to determine which cells were mostly likely in each cluster. From the sixty-three genes unique to cluster 1 markers were identified primarily indicating precursors to blood cells, immune cells, and subsets of immune cells including monocytes and B-cells (Fig. 5.3.3.C). From the seventy-one genes from cluster 2, predominantly macrophage markers are identified, with other immune cell subsets markers such as those for neutrophils and monocytes (Fig. 5.3.3.D). From the sixty-four genes from cluster 3 a wide variety of markers are identified indicating a mix of cells including microglia, enterocytes, and brush border cells (Fig. 5.3.3.E). From the one hundred and fifteen genes from cluster 4 several markers are identified for epidermal and epithelial cells (Fig. 5.3.3.F). Therefore, several cell subsets are identified as potentially being part of the *mpeg1.1*$^{+}$ group. Considering the literature, we would expect to see macrophages and B-cells indicated, which we do (Fig. 5.3.3.C, D)(226, 234). However, the data also indicates markers for non-immune cells including epidermal and epithelial cells (Fig. 5.3.3.F). Therefore, further investigation into the expression of *mpeg1.1* in other zebrafish cell subsets may be warranted.

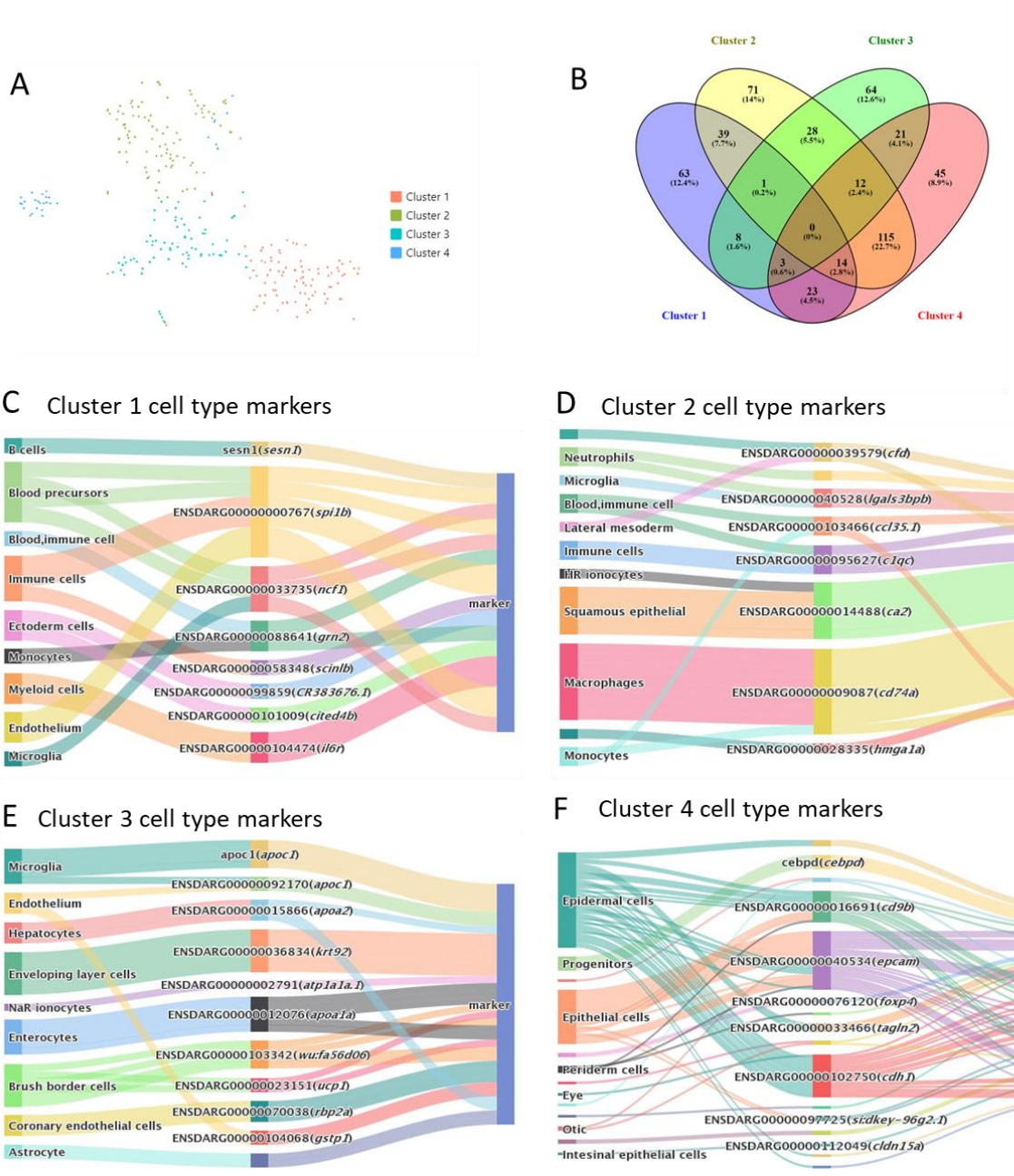

Figure 5.3.3: Unsupervised clustering of the *mpeg1.1*$^{+}$ populations from all genotypes indicates four distinct clusters. **A.** Four clusters that are determined using unsupervised clustering of the *mpeg1.1*$^{+}$ population from all genotypes. **B.** Upregulated genes from each cluster are compared to determine the genes unique to each cluster. **C.** Cluster 1 cell type markers. **D.** Cluster 2 cell type markers. **E.** Cluster 3 cell type markers. **F.** Cluster 4 cell type markers.

5.4 Exploring the effects of the *mpeg1.1:tert-gfp* gene on macrophages

The *mpeg1.1* gene was initially identified as being a macrophage specific gene and I have identified a macrophage population in the *mpeg1.1*$^{+}$ cluster (Fig.5.3.2.D)(226). Therefore, the *mpeg1.1:tert-gfp* transgene will hypothetically be expressed in gut resident macrophages in the transgenic line I have generated. To determine how the expression of the *mpeg1.1:tert-gfp* transgene affects gut resident macrophage physiology I used a tailored panel of genes to isolate the *tert*$^{+/+}$*;mpeg1.1:mCherry.caax* and *tert*$^{-/-}$*;mpeg1.1:mCherry.caax;mpeg1.1:tert-gfp* macrophage populations. The tailored panel of genes included: *Colony stimulating factor 1 receptor a* (*CSF1ra*), *CSF1rb*, *Marco*, M*acrophage stimulating 1* (*MST1*), *Monocyte to macrophage differentiation 1* (*MMD1*), *MMD2a*, *MMD2b*, *microfibrillar-associated protein 4 (mfap4)* based on previous publications characterising zebrafish immune cell subsets(234, 280, 281).

5.4.1 Analysis of pathways differentially expressed genes are involved in for macrophages.

To better understand how the insertion of the *mpeg1.1:tert-gfp* transgene may be affecting macrophage physiology, the ontology of the differentially regulated genes was determined (Fig. 5.4.1). Initially, the differentially regulated genes between the *tert*$^{-/-}$*;mpeg1.1:mCherry.caax* and the *tert*$^{+/+}$*;mpeg1.1:mCherry.caax* macrophage populations were determined. These were then compared to the differentially regulated genes between *tert*$^{-/-}$*;mpeg1.1:mCherry.caax;mpeg1.1:tert-gfp* and the *tert*$^{+/+}$*;mpeg1.1:mCherry.caax* macrophage populations using Venny (Fig. 5.4.1.A). This indicated sixty-two differentially regulated genes from the *tert*$^{-/-}$*;mpeg1.1:mCherry.caax;mpeg1.1:tert-gfp* macrophage population that were not differentially regulated in either of the other genotypes (Fig. 5.4.1.A). Therefore, it was assumed that these genes were differentially regulated due to the effects of inserting the *mpeg1.1:tert-gfp* transgene.

The ontology of the sixty-two differentially regulated genes was determined using ShinyGO (Fig. 5.4.1.B). Ontological analysis indicated that the upregulated genes were involved

protein processing, endocytosis, the spliceosome, Mitogen Activated Protein Kinase (MAPK) signalling, the adipocytokine signalling pathway, and salmonella infection (Fig. 5.4.1.B). Upregulation of genes involved in endocytosis indicates that insertion of the *mpeg1.1:tert-gfp* transgene is leading to an increase in endocytic processes. In gut associated macrophages this may play a role in immunogenic sensing of the local microenvironment. Further, as phagocytosis is a form of endocytosis, this may indicate that insertion of the *mpeg1.1:tert-gfp* transgene is leading to an upregulation of genes that play a role in the immune functions of the macrophages. This is supported by data from Fig. 5.4.1 that indicates the phagocytic function of *mpeg*$^{+}$ cells was upregulated (Fig. 5.4.1.B). Additionally, upregulation of the MAPK pathways I also interesting as this pathway is linked to the regulation of several internal kinase cascades that regulate proliferation, differentiation, and inflammation.

To more specifically examine how the expression of the *mpeg1.1:tert-gfp* transgene was affecting macrophage physiology ontological analysis was performed on the differentially regulated genes from the *tert*$^{-/-}$*;mpeg1.1:mCherry.caax:mpeg1.1:tert-gfp* macrophages(Fig. 5.4.1.B, C, D). From the GOBP database analysis there is indication of the differential regulation of genes associated with the regulation of the innate immune response, the regulation of antigen processing and presentation, and the regulation of the actin cytoskeleton (Fig. 5.4.1.B). From the GOMF, we can observe the differential regulation of genes associated with RNA-binding, chromatin binding, and the regulation of endopeptidase activity (Fig. 5.4.1.C). From the GOCC analysis, we can see the differential regulation of genes associated with mitochondrial respiration, chromatin binding, major histocompatibility complex (MHC) class 1, and ribosome formation (Fig. 5.4.1.D). Therefore, this data indicates that insertion of the *mpeg1.1:tert-gfp* transgene is leading to the differential regulation of pathways associated with mitochondrial respiration, ribosome structure and function, chromatin binding, and the function of the innate immune response in macrophages (Fig. 5.4.1). This provides additional evidence that telomerase may have non-canonical roles in the regulation of cellular respiration via the mitochondria, translation of mRNA, and the immune response.

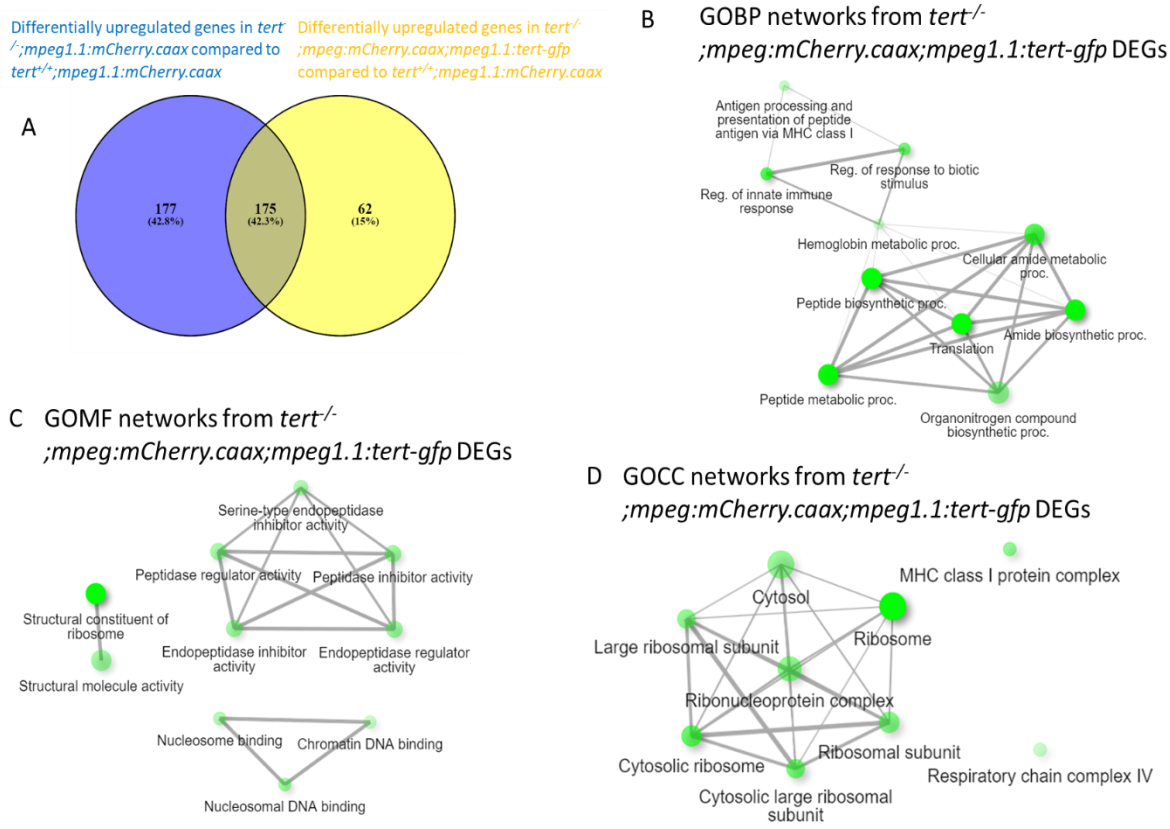

Figure 5.4.1: Exploring differentially regulated pathways of the *tert*$^{-/-}$ *;mpeg1.1:mCherry.caax;mpeg1.1:tert-gfp* macrophage population. **A.** Venn diagram of the differentially regulated genes between the *tert*$^{-/-}$ *;mpeg1.1:mCherry.caax;mpeg1.1:tert-gfp* and *tert*$^{+/+}$*;mpeg1.1:mCherry.caax* macrophage population compared to the *tert*$^{-/-}$*;mpeg1.1:mCherry.caax* and *tert*$^{+/+}$*;mpeg1.1:mCherry.caax* macrophage population. **B.** Gene ontology analysis of the differentially regulated genes from the GOBP database. **C.** Gene ontology analysis of the differentially regulated genes from the GOMF database. **D.** Gene ontology analysis of the

5.4.2 Exploring the differentially expressed genes in the *tert$^{-/-}$;mpeg1.1:mCherry.caax;mpeg1.1:tert-gfp* macrophages.

To determine the effects of the insertion of the *mpeg1.1:tert-gfp* gene in the *tert$^{-/-}$;mpeg1.1:mCherry.caax* background I determined the ten most upregulated genes when comparing *tert$^{+/+}$;mpeg1.1:mCherry.caax* to *tert$^{-/-}$;mpeg1.1:mCherry.caax*, and the ten most upregulated genes when comparing *tert$^{-/-}$;mpeg1.1:mCherry.caax;mpeg1.1:tert-gfp* to *tert$^{-/-}$;mpeg1.1:mCherry.caax* in macrophages.

The *tert$^{+/+}$;mpeg1.1:mCherry.caax* macrophage population displays significantly upregulated expression of the genes *vitellogenin 1 (vtg1)*, *vitellogenin 2 (vtg2)*, *vitellogenin (vtg4)*, *vitellogenin (vtg6)*, *vitellogenin (vtg7)*, *somatostatin 2 (sst2)*, *CR556712.1, si:dkeyp-75b4.10, si:dkey-203a12.2,* and *CABZ01058647.1* (Fig. 5.4.2). Interestingly, we see five members of the vitellogenin family in the ten most significantly upregulated genes in the *tert$^{+/+}$;mpeg1.1:mCherry.caax* macrophage population. The vitellogenin family is involved in the modulation of lipid metabolism. Therefore, in the *tert$^{+/+}$;mpeg1.1:mCherry.caax* macrophages we may be observing an increased regulation of lipid sensing and metabolism. This is perhaps unsurprising considering the well documented role of macrophages in regulating lipid levels(282, 283). I also observe the upregulation of *sst2* which is involved in the regulation of cell migration, and *CR556712.1* which encodes a region containing several genes from the *krt* family, indicating that the macrophage population is producing keratin as part of the cytoskeleton. Together, the upregulation of these genes may indicate that *tert$^{+/+}$;mpeg1.1:mCherry.caax* macrophages have increased cell migration compared to *tert$^{-/-}$;mpeg:mCherry.caax* macrophages. The *si:dkeyp-75b4.10* region is predicted to have carbohydrate binding activity. Both *si:dkey-203a12.2* and *CABZ01058647.1* have not been characterised to the point that I can comment on their function. However, overall this data suggests that *tert$^{+/+}$;mpeg1.1:mCherry.caax* macrophages have a higher expression of genes associated with nutrient sensing compared to *tert$^{-/-}$;mpeg1.1:mCherry.caax* macrophages.

The genes upregulated in the *tert$^{-/-}$;mpeg1.1:mCherry.caax;mpeg1.1:tert-gfp* population include *CR556712.1*, *High mobility group nucleosomal binding domain 2 (hmgn2)*, *Hairy and enhancer of split-related 15 tandem duplicate 1 (her15.1), her6, High mobility group box 2a (hmgb2a), hmgb2b, si:ch73-1a9.3, XLOC_000431, XLOC_013964,* and *BX908782.2*.

Interestingly we see that *CR556712.1* is significantly upregulated in both the *tert*$^{+/+}$*;mpeg1.1:mCherry.caax* macrophage population and the *tert*$^{-/-}$*;mpeg1.1:mCherry.caax;mpeg1.1:tert-gfp* macrophage population to the same level (Fig. 5.4.2). This may indicate that the expression of the *krt* genes in this region are linked to telomerase length or TERT expression as insertion of the *mpeg1.1:mCherry.caax* has rescued the expression of *CR556712.1* in the *tert*$^{-/-}$*;mpeg1.1:mCherry.caax* macrophages to a level comparable to the *tert*$^{+/+}$*;mpeg1.1:mCherry.caax* macrophages. Both *her6* and *her15.1* are predicted to be involved in mitogenic signalling and the Notch pathway and therefore are reported to take part neural development and bone regeneration(284-286). We also observed upregulation of *hmgb2a* and *hmgb2b*. Both *hmgb2a* and *hmgb2b* are indicated to be involved in the positive regulation of transcription via interaction with RNA-polymerase II. Additionally, both are indicated to be involved in the positive regulation of the innate immune response(287). *Si:ch73-1a9.3* has not been extensively characterised however it may be associated with *hmgn1b*. If so, *hmgn1b* is predicted to have chromatin binding activity as is *hmgn2*. The region BX908782.2 is indicated to contain the genes *ly97.2* and *scn12aa*. *Ly97.2* is indicated to bind to exhibit LPS binding activity and therefore is involve in the defence response to gram-negative bacteria and LPS. *Scn12aa* is predicted to have voltage-gated sodium channel activity and to be expressed in the nervous system and to be involved in heart contraction regulation. Unfortunately, *XLOC_000431* and *XLOC_013964* have not yet been characterised to the point that I can comment on how their upregulation may affect macrophage biology.

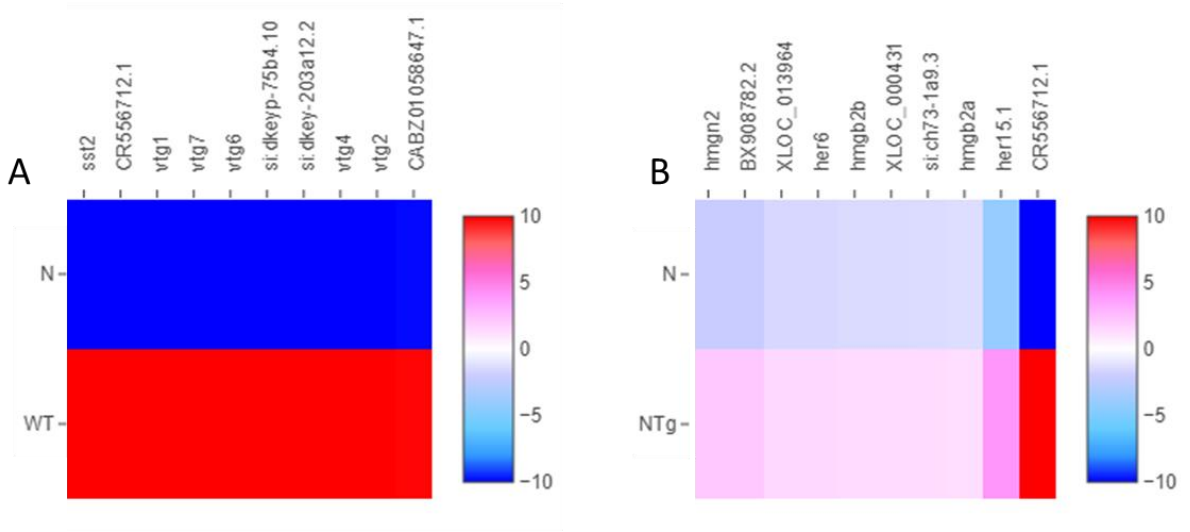

Figure 5.4.2: The ten most significantly upregulated genes in each macrophage population. **A.** Upregulated genes from *tert*$^{+/+}$*;mpeg1.1:mCherry.caax* (n = 641) versus *tert*$^{-/-}$*;mpeg1.1:mCherry.caax* (n = 538) macrophage populations. **B.** Upregulated genes from *tert*$^{-/-}$*;mpeg1.1:mCherry.caax;mpeg1.1:tert-gfp* (n = 819) compared to *tert*$^{-/-}$*;mpeg1.1:mCherry.caax* (n = 538) macrophage populations.

5.4.2.1 Exploring the similarities in upregulated genes to determine if insertion of the *mpeg1.1:tert-gfp* genes rescues macrophage function

To further explore how insertion of the *mpeg1.1:tert-gfp* gene was affecting gene expression in *tert*$^{-/-}$*;mpeg1.1:mCherry.caax;mpeg1.1tert-gfp* macrophages I determined I determined the fifty most upregulated genes when comparing *tert*$^{+/+}$*;mpeg:mCherry.caax* to *tert*$^{-/-}$*;mpeg:mCherry.caax*, and the fifty most upregulated genes when comparing *tert*$^{-/-}$*;mpeg:mCherry.caax;mpeg1.1:tert-gfp* to *tert*$^{-/-}$*;mpeg:mCherry.caax*. These lists were then compared using Venny (Fig.5.4.2.1.A) and nine genes were indicated to be significantly upregulated in both populations. These genes were: *CR556712.1, XLOC_010899, zgc:193726, Proenkephalin a precursor (penka), Prothymosin alpha (si:ch211-222l21.1), prothymosin alpha-a (ptma-α), hmgb2b, her6,* and *hmgn2* (Fig.5.4.2.1). STRING analysis of these genes indicates and link in the function of *si:ch211-222l21.1* and *ptma-α* (Fig. 5.4.2.1.B). Interestingly, *Emmanouilidou et al* demonstrated that knockdown of *ptma-α* led to increased rates of cell death in head and tail regions during embryo development in conjunction with an increase in the active form of caspase-3 indicating increased apoptosis levels(288). Further, *Pai et al* indicated that overexpression of *ptma-α* in zebrafish skin epidermis led to a resistance to the apoptosis inducing effects of Ultraviolet B (UVB) radiation via the increased expression of *bcl2*(289). Therefore, the increased expression of *ptma-α* may indicate an increase in anti-apoptosis signalling in *tert*$^{-/-}$*;mpeg1.1:mCherry.caax;mpeg1.1:tert-gfp* macrophages towards levels observed in *tert*$^{+/+}$*;mpeg1.1:mCherry.caax* macrophages (Fig. 5.4.2.1.A). This may indicate that insertion of the *mpeg1.1:tert-gfp* transgene is leading to less apoptosis which is an indicator that the premature ageing phenotype is being rescued, to an extent, in macrophages.

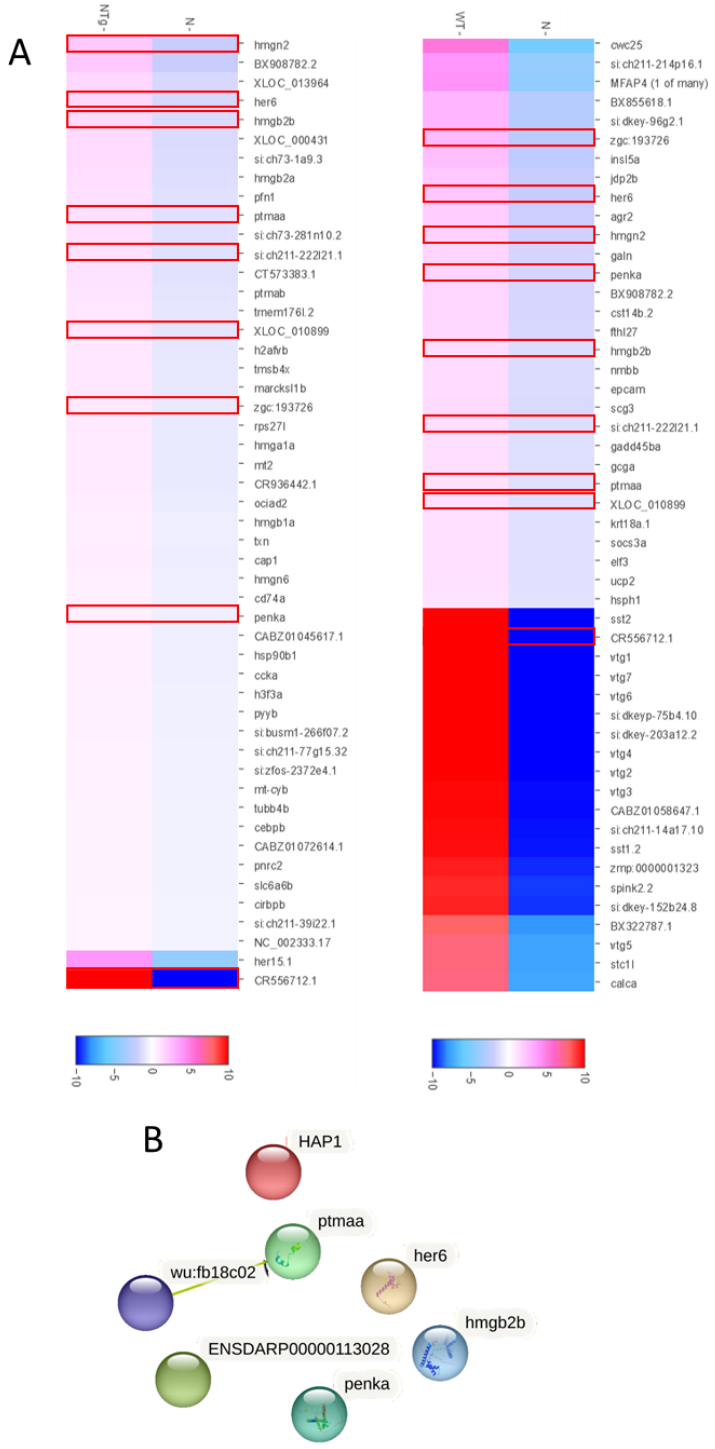

Figure 5.4.2.1: A comparison of genes upregulated in both *tert*$^{+/+}$*;mpeg1.1:mCherry.caax* and *tert*$^{-/-}$*;mpeg1.1:mCherry.caax;mpeg1.1:tert-gfp* macrophages. **A.** Comparison of the top fifty upregulated genes in each genotype with genes commonly upregulated indicated by a red box. **B.** Ontology analysis of the commonly upregulated genes using the GOMF database. **C.** Ontological analysis of the upregulated genes from the *tert*$^{-/-}$*;mpeg1.1:mCherry.caax;mpeg1.1:tert-gfp* using the KEGG database.

5.5 Exploring the differentially expressed genes in the *tert*$^{-/-}$*;mpeg1.1:mCherry.caax;mpeg1.1:tert-gfp* B-cell populations.

Recent literature has demonstrated that zebrafish B-cells utilise the *mpeg1.1* promoter(234). Therefore, we can hypothesise that the *mpeg1.1:tert-gfp* transgene will be expressed in the zebrafish gut B-cell population in the *mpeg1.1:tert-gfp* transgenic line characterised in Chapter 3. To determine if insertion of the *mpeg1.1:tert-gfp* transgene affects the physiology of the B-cell population a tailored panel of B-cell specific genes was used to identify B-cell populations from in the single-cell RNA sequencing aggregate populations. B-cell populations were identified using the genes *CD22, CD79a, CD79b, CD74a, CD74b, B cell linker (Blnk),* and *Paired box 5 (Pax5)*(234, 280).

5.5.1 Differentially regulated gene pathways from the *tert*$^{-/-}$*;mpeg1.1:mCherry.caax;mpeg1.1:tert-gfp* B-cell population.

To further understand how the insertion of the *mpeg1.1:tert-gfp* transgene may be affecting B-cell physiology the ontology of the differentially genes was determined (Fig. 5.5.1). Initially, the differentially regulated genes between the *tert*$^{-/-}$*;mpeg1.1:mCherry.caax* and the *tert*$^{+/+}$*;mpeg1.1:mCherry.caax* B-cell populations were determined. These were then compared to the differentially regulated genes between *tert*$^{-/-}$*;mpeg1.1:mCherry.caax;mpeg1.1:tert-gfp* and the *tert*$^{+/+}$*;mpeg1.1:mCherry.caax* B-cell populations using Venny (Fig. 5.5.1.A). This indicated forty-eight genes that were differentially regulated in the *tert*$^{-/-}$*;mpeg1.1:mCherry.caax;mpeg1.1:tert-gfp* that were not differentially regulated in either of the other genotypes (Fig. 5.5.1.A). Therefore, it was assumed that these genes were differentially regulated due to the effects of inserting the *mpeg1.1:tert-gfp* transgene.

To determine how the insertion of the *mpeg1.1:tert-gfp* transgene affects gene regulation in *tert*$^{-/-}$*;mpeg1.1:mCherry.caax;mpeg1.1:tert-gfp* B-cells physiology, the ontology of the forty-eight differentially regulated genes was determined using Shiny GO (Fig. 5.5.1.B, C, D). Analysis using the KEGG database indicated the differential regulation of genes associated with the phagosome, apoptosis, oxidative phosphorylation, and the regulation of the actin

cytoskeleton (Fig. 5.5.1.B). Further analysis using the GOMF database indicates that differential expression of genes involved in antigen binding, oxidoreductase activity, and the regulation of endopeptidase activity (Fig. 5.5.1.C). Additionally, analysis using the GOBP database indicates that genes associated with the negative regulation of endopeptidase activity, the electron transport chain, the activation of the complement pathway, and the immune response to viruses were differentially regulated (Fig. 5.5.1.D). The differential regulation of genes associated with these pathways is further evidence that telomerase may have non-canonical functions associated with the regulation of metabolism, autophagy (via endopeptidase activity), and the immune response.

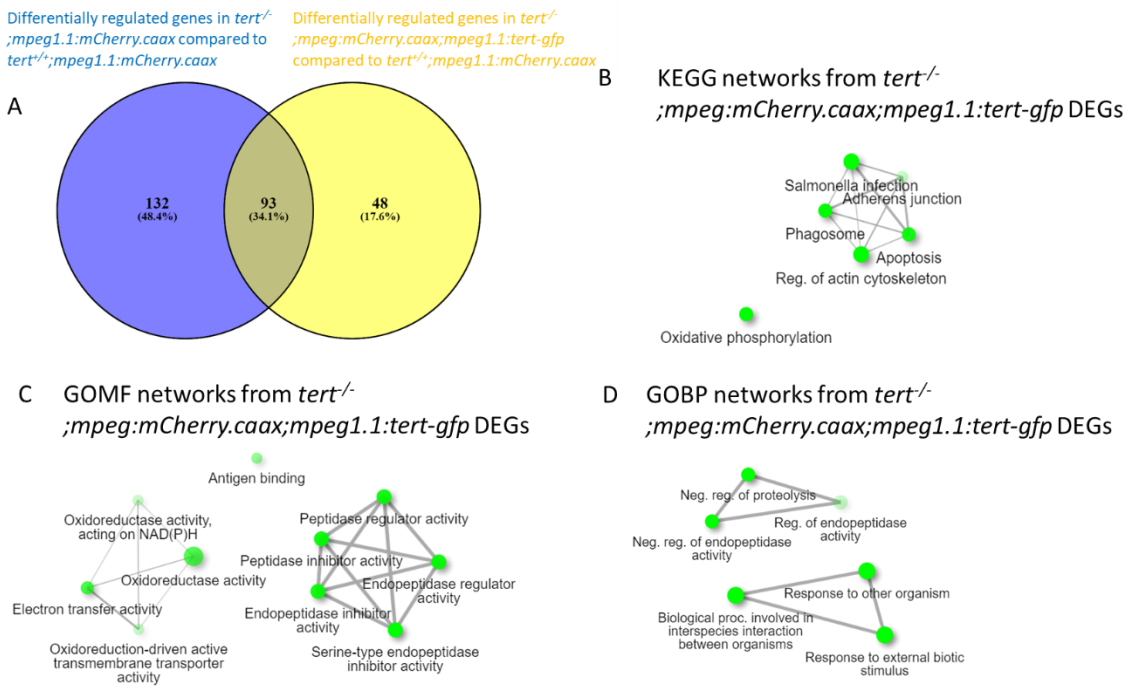

Figure 5.5.1: Exploring differentially regulated pathways of the *tert*$^{-/-}$*;mpeg1.1:mCherry.caax;mpeg1.1:tert-gfp* B-cell population. **A.** Venn diagram of the differentially regulated genes between the t*ert*$^{-/-}$*;mpeg1.1:mCherry.caax;mpeg1.1:tert-gfp* and *tert*$^{+/+}$*;mpeg1.1:mCherry.caax* B-cell population compared to the t*ert*$^{-/-}$*;mpeg1.1:mCherry.caax* and *tert*$^{+/+}$*;mpeg1.1:mCherry.caax* B-cell population. **B.** Gene ontology analysis of the differentially regulated genes from the KEGG database. **C.** Gene ontology analysis of the differentially regulated genes from the GOMF database. **D.** Gene ontology analysis of the differentially regulated genes from the GOBP

5.5.2 Differentially expressed genes between the B-cell populations.

To explore the effects of the insertion of the *mpeg1.1:tert-gfp* gene in the *tert*$^{-/-}$*;mpeg1.1:mCherry.caax* background I determined the ten most upregulated genes when comparing *tert*$^{+/+}$*;mpeg1.1:mCherry.caax* to *tert*$^{-/-}$*;mpeg1.1:mCherry.caax*, and the ten most upregulated genes when comparing *tert*$^{-/-}$*;mpeg1.1:mCherry.caax;mpeg1.1:tert-gfp* to *tert*$^{-/-}$*;mpeg1.1:mCherry.caax* in B-cell populations.

In the *tert*$^{+/+}$*;mpeg1.1:mCherry.caax* I observe differential upregulation of the genes *Cathepsin S tandem duplicate 2 (ctss2.2)*, *Heat shock 105/110 protein 1 (hsph1)*, *serine peptidase inhibitor kazal type 2 tandem duplicate 2 (spink2.2)*, *Ferritin heavy polypeptide like 27 (fthl27)*, *anterior gradient 2 (agr2)*, *zgc:64051*, *BX855618.1*, *si:dkey-96g2.1*, *si:dkey-203a12.2*, and *si:dkeyp-75b4.10(Fig.5.5.2.A)*. *Ctss2.2* is predicted to be involved in the regulation of the immune response via proteolysis and the lysosome. *Hsph1* is part of the heat shock protein family so is predicted to have ATP binding capacity. *Spink2.2* is predicted to have serine-type endopepotidase inhibitor activity. Additionally, *si:dkey-203a12.2* is associated with *spink2.7* indicating it may have a similar function. *Fthl27* is predicted to have ferric ion binding activity and so be involved in the sequestering on intracellular iron ions. *Agr2* is indicated to act either upstream or within intestinal epithelial cell differentiation(290, 291). *Zgc:64051* is predicted to be involved in plasma membrane structure. *Si:dkeyp-75b4.10* is predicted to have carbohydrate binding activity and to be orthologous to human *Regenerating family member 1 alpha (Reg1a).* Unfortunately, *BX855618.1* and *si:dkey-96g2.1* have not been characterised to the point that I can comment on their effects on macrophage biology.

In the *tert*$^{-/-}$*;mpeg1.1:mCherry.caax;mpeg1.1:tert-gfp* I observe upregulation of the genes *mmp13a*, *pyyb*, *il1b*, *zgc:172053*, *si:dkeyp-75b4.10*, *si:dkey-102g19.3*, *si:ch1073-67j19.1*, *LOC110437886, beta-microseminoprotein-like LOC110437731* (*LOC110437731*), and *BX322787.1(Fig. 5.5.2.B)*. Upregulation of the *mmp13a* gene indicates that the *tert*$^{-/-}$*;mpeg1.1:mCherry.caax;mpeg1.1:tert-gfp* B-cell population is upregulating metalloendopeptidase activity which can influence cell migration, remodelling of the extracellular matrix, and wound healing(292). *Pyyb* is involved in regulating feeding behaviour indicating there may be some alteration in nutrient sensing as a results of the insertion of *mpeg1.1:tert-gfp.* Further to this, Both *zgc:172053* and *si:dkeyp-75b4.10* are

both indicated to be involved in the regulation of nutrient sensing and have human orthologs in the Islet of Langerhans Regenerating Protein (REG) family. *Il1b* is involved in regulation of the immune response, and oxidative stress, its upregulation in the *mpeg1.1:tert-gfp* transgenic indicates we may be observing a rescue of B-cell function or a polarisation of transgenic B-cells as a consequence of the transgenes insertion. This may potentially be in a coordination axis with macrophages(293). The gene *LOC110437731* is predicted to code for a beta-microseminoprotein like protein, which in humans is indicated to have inhibin like properties and bind to immunoglobulin. The region *BX322787*.1 contains four genes: *DNA-activate protein kinase catalytic subunit (prkdc)*, *SMAD family member 3b (smad3b)*, *ATP-binding cassette sub-family F member 2b (abcf2b)*, and *chondroitin polymerizing factor 2 (chpf2)*. Most interestingly, *prkdc* codes for a DNA-dependent protein kinase with serine/threonine kinase activity that acts as part of B-cell differentiation and V(D)J recombination. In conjunction with *prkdc* upregulation we see an upregulation of SMAD3b, a DNA-binding transcription factor. Further, we see upregulation of abcf2b, an ATP-binding cassette sub-family member that will increase energy release, and chondroitin polymerizing factor 2 involved in chondroitin biosynthesis. Therefore, we may be seeing the upregulation of a pathway that influences B-cell differentiation and expansion due to the effects of the *mpeg1.1:tert-gfp* transgene. Unforturnately *si:dkey-102g19.3* and *si:ch1073-67j19.1* have not yet been characterised to the point that I can comment on the effects of their upregulation.

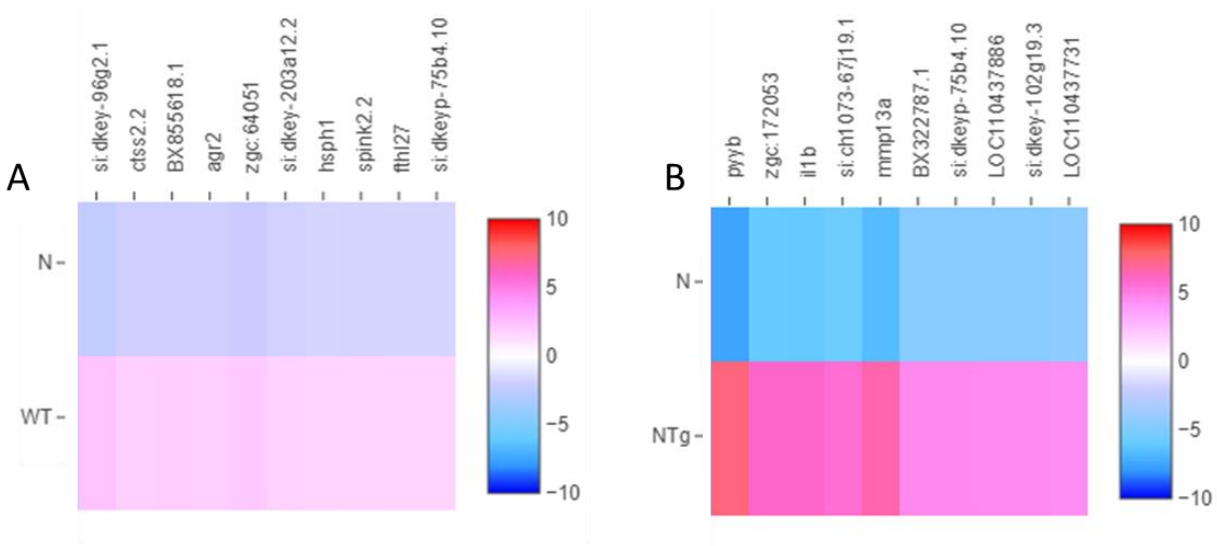

Figure 5.5.2: The ten most differentially upregulated genes in the tert$^{+/+}$*;mpeg1.1:mCherry.caax* and *tert*$^{-/-}$*;mpeg1.1:mCherry.caax;mpeg1.1:tert-gfp* B-cell populations. **A.** Upregulated genes from *tert*$^{+/+}$*;mpeg1.1:mCherry.caax* (n = 1,946) versus *tert*$^{-/-}$*;mpeg1.1:mCherry.caax* (n = 473) B-cell populations. **B.** Upregulated genes from *tert*$^{-/-}$*;mpeg1.1:mCherry.caax;mpeg1.1:tert-gfp* (n = 1,201) compared to *tert*$^{-/-}$*;mpeg1.1:mCherry.caax* (n = 473) B-cell populations.

5.5.2.1 Further exploration of the rescue of B-cell gene expression in the *tert*$^{-/-}$*;mpeg1.1:mCherry.caax;mpeg1.1:tert-gfp* B-cell population

To further understand how insertion of the *mpeg1.1:tert-gfp* transgene affected B-cell gene expression I determined the fifty most upregulated genes in both *tert*$^{+/+}$*;mpeg1.1:mCherry.caax* and *tert*$^{-/-}$*;mpeg1.1:mCherry.caax;mpeg1.1:tert-gfp* B-cells when compared to *tert*$^{-/-}$*;mpeg1.1:mCherry.caax* B-cells (Fig. 5.5.2.1.A). Comparing these upregulated gene sets indicated fifteen genes upregulated in both populations (Fig. 5.5.2.1.A). These genes included: *si:dkey-96g2.1, si:ch211-39i2.2, hmgn2, Profilin-1 (Pfn1), XLOC_010899, Beta thymosin-like protein 4x (Tmsb4x), ptma-α*, *Suppressor of cytokine signaling 3a (Socs3a)*, *Ferritin heavy-polypeptide like (fthl27), Proline-rich nuclear receptor coactivator 2 (pnrc2), Anterior gradient protein 2 (agr2), CCAAT/enhancer binding protein(C/EBP) beta (Cebpb)*, *Si:dkeyp-75b4.10*, *Serine protease inhibitor kazal-type 2 (spink2.2)*, and *Si:dkey-203a12.2*. Interestingly, we see and upregulation of *ptma-α* in the macrophage population (Fig. 5.4.2.1) as well as here in the B-cell population (Fig. 5.5.1.1.B). This correlation may indicate that in both cell populations, the insertion of the *mpeg1.1:tert-gfp* transgene is potentially leading to a rescue of the premature ageing phenotype in *mpeg1.1*$^{+}$ immune cells. Further to this, the upregulation of *Socs3a* and *Cebpb* (Fig. 5.5.2.1.B) indicates the activation of STAT3, an important component in zebrafish immune cell function, potentially indicating a rescue of immune cell function in the *tert*$^{-/-}$*;mpeg1.1:mCherry.caax;mpeg1.1:tert-gfp* B-cell population(294).

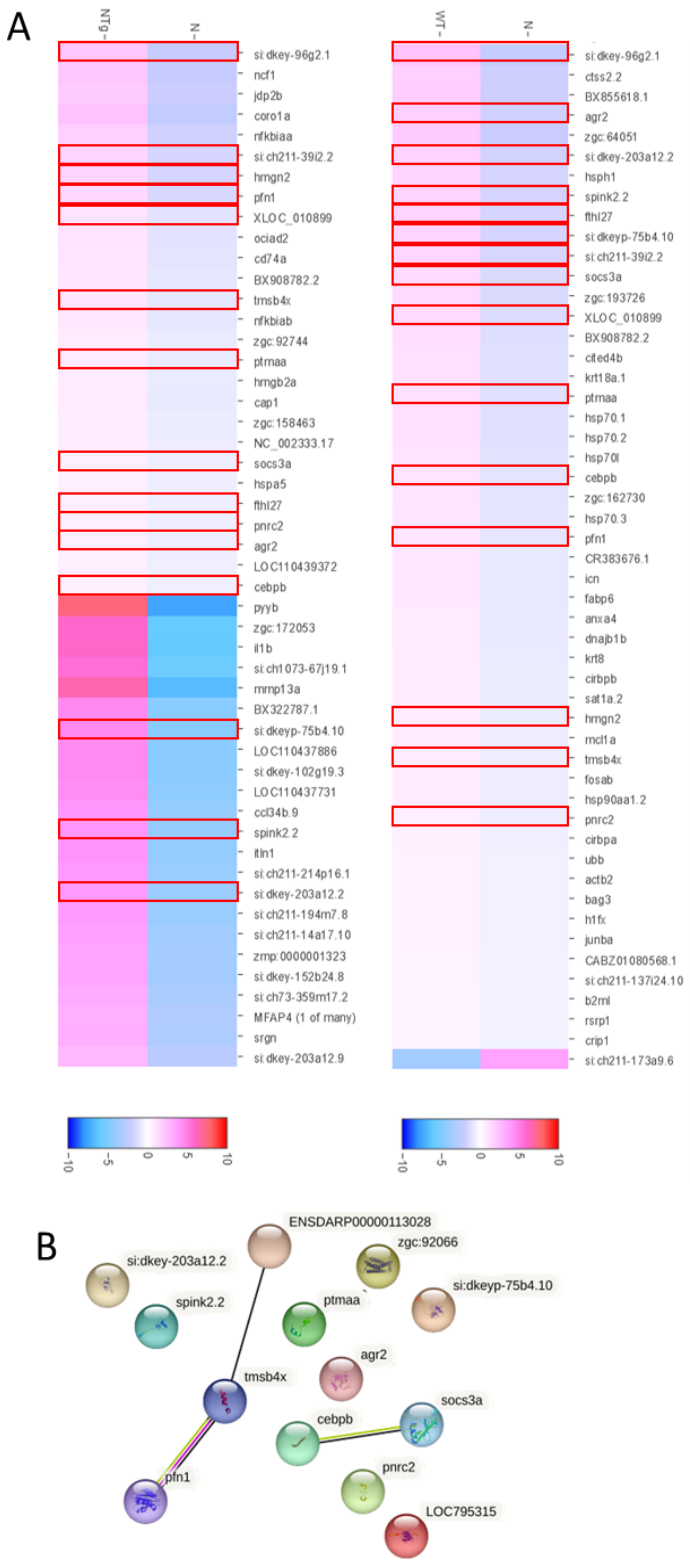

Figure 5.5.2.1: A comparison of genes upregulated in both *tert*$^{+/+}$*;mpeg1.1:mCherry.caax* and *tert*$^{-/-}$*;mpeg1.1:mCherry.caax;mpeg1.1:tert-gfp* B-cells. **A.** Comparison of the top fifty upregulated genes in each genotype with genes commonly upregulated indicated by a red box. **B.** Ontology analysis of the commonly upregulated genes.

5.6 Identification of immune cell populations and differential gene expression within them between *tert*$^{-/-}$*;mpeg1.1:mCherry.caax* and *tert*$^{+/+}$*;mpeg1.1:mCherry.caax*

As both macrophages and B-cells have roles in regulating the immune response via interactions with other immune cell subtypes I decided to investigate the gene expression of other immune cell populations found in the zebrafish gut. If the *mpeg1.1:tert-gfp* gene were altering the physiology of macrophages and B-cells then a consequence of this alteration may be changes in communication with other immune cell subtypes via either via cell-to-cell interactions or via intercellular signalling molecules such as cytokines. Macrophages are documented to interact with T-cells, Neutrophils, and NK cells(295-297). B-cells interact with T-cells and NK cells(298, 299). Therefore, it is logical to hypothesise that T-cells, NK cells, and neutrophils may have an altered physiology based on their interactions with *tert*$^{-/-}$*;mpeg1.1:mCherry.caax;mpeg1.1:tert-gfp* macrophages and B-cells compared to *tert*$^{-/-}$*;mpeg1.1:mCherry.caax* populations.

To characterise how *tert*$^{-/-}$*;mpeg1.1:mCherry.caax;mpeg1.1:tert-gfp* macrophages and B-cells were affecting the physiology of other gut resident immune cell populations I would examine the differentially regulated genes in the single-cell RNA sequencing data. I would characterise normal T-cell, NK cell, and Neutrophil populations by analysing the differentially regulated genes between the *tert*$^{+/+}$*;mpeg1.1:mCherry.caax* populations and the *tert*$^{-/-}$*;mpeg1.1:mCherry.caax* populations. I would then explore how the presence of the *mpeg1.1:tert-gfp* in macrophage and B-cell populations affected *tert*$^{-/-}$*;mpeg1.1:mCherry.caax;mpeg1.1:tert-gfp* T-cell, NK, and neutrophil populations.

5.6.1 Does insertion of the *mpeg1.1:tert-gfp* gene rescue T-cell gene expression in the *tert$^{-/-}$;mpeg1.1:mCherry.caax;mpeg1.1-tert-gfp* phenotype.

T-cell populations were identified using the marker genes: *CD28, CD4, CD8, si:dkey-11f4.2, and T-cell receptor detal (trdc)(300, 301).* Comparing the *tert$^{-/-}$;mpeg1.1:mCherry.caax;mpeg1.1:tert-gfp* and *tert$^{+/+}$;mpeg1.1:mCherry.caax* aggregate T-cell populations to the *tert$^{-/-}$;mpeg1.1:mCherry.caax;mpeg1.1:tert-gfp* T-cell population provided a list of differentially regulated genes. To determine if inserting the *mpeg1.1:tert-gfp* transgene had rescued T-cell gene expression in the *tert$^{-/-}$;mpeg1.1:mCherry.caax;mpeg1.1-tert-gfp* population such that it was comparable to the *tert$^{+/+}$;mpeg1.1:mCherry.caax* population I compared the top ten most upregulated genes in each T-cell population (Fig. 5.6.1).

Exploring the differentially regulated genes between the *tert$^{-/-}$;mpeg1.1:mCherry.caax* and *tert$^{+/+}$;mpeg1.1:mCherry.caax* T-cell populations I can see that *vtg1*, *lysozyme (lyz), vtg4, vtg5, serine peptidase inhibitor Kazal type 2 tandem duplicate 5 (spink2.5)*, *CABZ01058647.1*, *keratin 91 (krt91)*, *si:dkey-203a12.7*, *BX908782.2*, and *transcobalamin beta a (tcnba)* are all upregulated in the *tert$^{+/+}$;mpeg1.1:mCherry.caax* group. The genes *vtg1*, *vtg4*, and *vtg5* code for variants of vitellogenin which is indicated to act as part of the cellular response to an oestrogen stimulus(302). *Vtg1* also exhibits antioxidant activity and has been indicated to be an integral membrane component(303). *Vtg4* and *Vtg5* are further indicated to have lipid transport capabilities(303). *Lyz* codes for the lysozyme enzyme that forms part of the of the immune response to bacteria, whereby lysozyme acts to degrade the peptidoglycan cell wall of the bacteria. The BX908782.2 region contains *ly97.2* and *scn12aa*. *Spink2.5* codes for a serine-type endopeptidase inhibitor and *si:dkey-203a12.7* is indicated to act as a regulator of transcription by RNA Polymerase II. Additionally, *tcnba* is indicated to be a transcobalamin transporter and so may form part of the digestive response to the uptake of vitamin B12.

Genes alternatively regulated in the transgenic include *lyz*, *npsn*, *leukocyte cell derived chemotaxin 2 (lect2l)*, *mmp13a*, *si:ch1073-67j19.1*, *CABZ01058647.1*, *purine nucleoside phosphorylase 5a (pnp5a)*, *LOC110437886*, *il1b*, *zgc:172053*. Upregulation of *lyz* potentially

indicates an upregulated immune response to gram negative bacteria. This may be a result of interactions with macrophages initiating a more sensitive state to infection. Additionally, it is interesting that *lyz* is upregulated in the *tert*$^{-/-}$*;mpeg1.1:mCherry.caax;mpeg1.1:tert-gfp* T-cell population to the same level as that observed in the *tert*$^{+/+}$*;mpeg1.1:mCherry.caax* population. This may indicate that the *mpeg-tert-gfp* gene is altering the physiology of B-cell and macrophage populations to induce the expression of *lyz* in T-cells. Further, upregulation of *lect2l* indicates an increased sensitive to leukocyte chemotaxis signalling. This is in conjunction with the upregulation of *il1b* which also acts to sensitive T-cells to leukocyte chemotaxis signalling. Therefore, the changes in physiology in macrophages and B-cells due to the *mpeg1.1:tert-gfp* gene's insertion may be leading to an increase in intercellular communication and an altering of the physiology of T-cells to be pro inflammatory**.** Interestingly, we also see upregulation of the metalloendopeptidase *mmp13a* and the metalloendopeptidase activity regulator *npsn* indicating increased metal ion regulation and sensitivity. Further metabolic change is indicated by the upregulation of *pnp5a* which plays a role in purine metabolism feeding into the production ATP so indicating an increase in metabolic processes. This is supported by upregulation of *zgc:172053* which is orthologues to human REG1A so is indicated in insulin signalling and that IL1-β is involved in the regulation of energy metabolism.

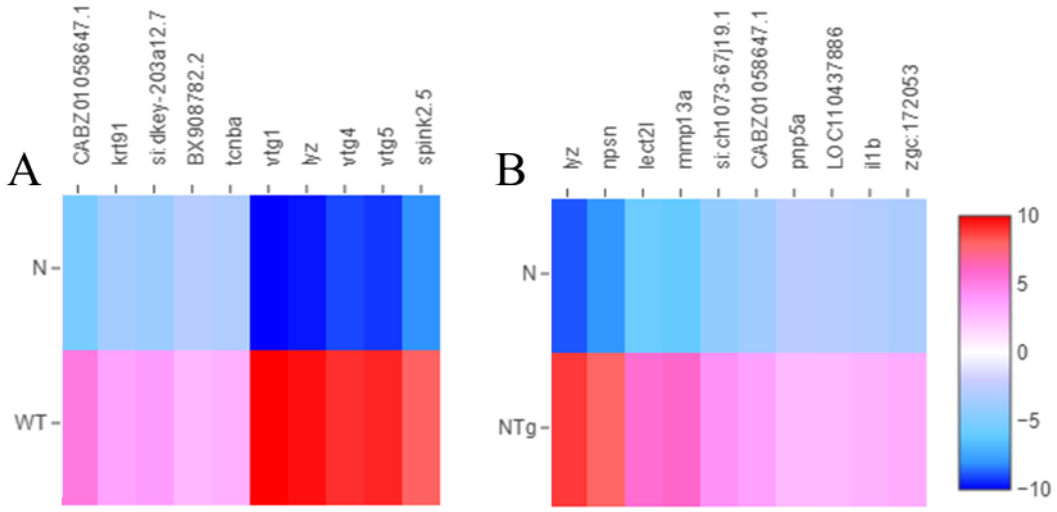

Figure 5.6.1: The ten most differentially upregulated genes in the *tert*$^{+/+}$*;mpeg1.1:mCherry.caax* and *tert*$^{-/-}$*;mpeg1.1:mCherry.caax;mpeg1.1:tert-gfp* T-cell populations. **A.** Upregulated genes from *tert*$^{+/+}$*;mpeg1.1:mCherry.caax* (n = 428) versus *tert*$^{-/-}$*;mpeg1.1:mCherry.caax* (n = 314) T-cell populations. **B.** Upregulated genes from *tert*$^{-/-}$*;mpeg1.1:mCherry.caax;mpeg1.1:tert-gfp* (n = 708) compared to *tert*$^{-/-}$*;mpeg1.1:mCherry.caax* (n = 314) T-cell populations.

5.6.1.1 Exploring the upregulated pathways in the *tert$^{-/-}$;mpeg1.1:mCherry.caax;mpeg1.1:tert-gfp* and *tert$^{+/+}$;mpeg1.1:mCherry.caax* T-cell populations

As there was no correlation between the ten most upregulated pathways in both the *tert$^{-/-}$;mpeg1.1:mCherry.caax;mpeg1.1:tert-gfp* and *tert$^{+/+}$;mpeg1.1:mCherry.caax* T-cell populations I wanted to explore the pathways the upregulated genes in each population were part of (Fig. 5.6.1.1). This would enable further exploration of how the insertion go the *mpeg1.1:tert-gfp* gene had affected T-cell gene expression in a prematurely aged phenotype.

Using ShinyGO software I determined the ten pathways that were most significantly upregulated in the *tert$^{-/-}$;mpeg1.1:mCherry.caax;mpeg1.1:tert-gfp* T-cell population (Fig. 5.6.1.1.A). I found that these ten pathways were split into two groups of five by the ShinyGO software (Fig. 5.6.1.1.A). The top group indicated the upregulation of pathways involved in myeloid cell development, myeloid differentiation, and thymus development (Fig. 5.6.1.1.A). Therefore, this may indicate an upregulation of genes involved in T-cell cell development and differentiation. Additionally, it may indicate upregulation of myeloid lineage genes in T-cells, which are from a lymphoid lineage. In the bottom group we can see an upregulation of pathways involved in enterocytes, epithelial cells, lipid localisation and absorption, and basement membrane formation (Fig. 5.6.1.1.A). This may indicate that the insertion of the *mpeg1.1:tert-gfp* gene is leading to the upregulation of genes involved in lipid metabolism and the differentiation of enterocytes even in a T-cell population.

Using ShinyGO software I determined the ten pathways that were most significantly upregulated in the *tert$^{+/+}$;mpeg1.1:mCherry.caax* T-cell population (Fig. 5.6.1.1.B). Pathways involved in T-cell differentiation and thymus development were upregulated, as well as pathways involve in lymphoid progenitor cell differentiation, and haematopoiesis (Fig. 5.6.1.1.B). This indicates that in *tert$^{+/+}$;mpeg1.1:mCherry.caax* cells we see an upregulation of genes involved in T-cell differentiation and development when compared to *tert$^{-/-}$;mpeg1.1:mCherry.caax* T-cells.

To determine which pathways were upregulated in both *tert$^{-/-}$;mpeg1.1:mCherry.caax;mpeg1.1:tert-gfp* and *tert$^{+/+}$;mpeg1.1:mCherry.caax* T-cells I used Venny to compare the significantly upregulated genes in both populations (Fig. 5.6.1.1.B).

This indicated 51 genes shared between populations (Fig. 5.6.1.1.C). By examining the genes shared between the populations I can determine a set of genes that would be upregulated in a healthy T-cell population compared to a prematurely aged population but that were also upregulated in the transgenic T-cell population, indicating that their expression had been rescued by the *mpeg1.1:tert-gfp* transgene. To further explore the pathways these 51 genes were involved in I used ShinyGO to determine the ten most upregulated pathways (Fig. 5.6.1.1.D). This indicated upregulation in pathways associated with T-cell differentiation in the thymus, myeloid cell development, microglial cell development, chemoattractant and cytokine activity, and hematopoietic cell differentiation (Fig. 5.6.1.1.D). Overall, these results indicate that the insertion of the *mpeg1.1:tert-gfp* transgene is affecting T-cell gene expression. Further, that the expression of a specific subset of genes in the T-cell population derived from *tert*$^{-/-}$*;mpeg1.1:mCherry.caax;mpeg1.1:tert-gfp* gut is being rescued towards an expression level comparable to the *tert*$^{+/+}$*;mpeg1.1:mCherry.caax* T-cell population.

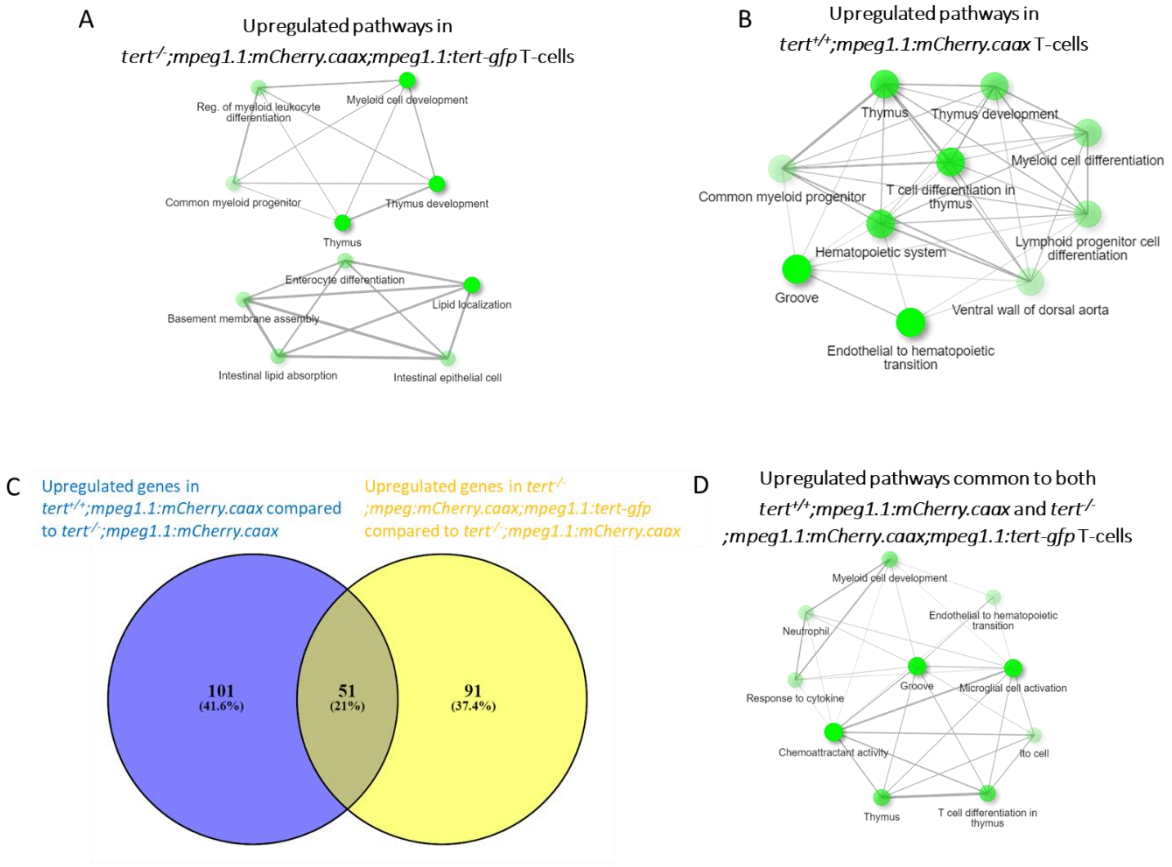

Figure 5.6.1.1: Exploring upregulated pathways of the *tert*$^{-/-}$*;mpeg1.1:mCherry.caax;mpeg1.1:tert-gfp* and *tert*$^{+/+}$*;mpeg1.1:mCherry.caax* T-cell populations. **A.** The ten most upregulated pathways from the *tert*$^{-/-}$*;mpeg1.1:mCherry.caax;mpeg1.1:tert-gfp* T-cell population. **B.** The ten most upregulated pathways from the *tert*$^{+/+}$*;mpeg1.1:mCherry.caax* T-cell population. **C.** Venn diagram comparing the upregulated genes in the *tert*$^{+/+}$*;mpeg1.1:mCherry.caax* T-cell population (blue) to the upregulated genes in the *tert*$^{-/-}$*;mpeg1.1:mCherry.caax;mpeg1.1:tert-gfp* T-cell population (yellow). **D.** The ten most upregulated pathways from the genes upregulated in both T-cell populations.

5.6.2 Neutrophils

As both B-cells and macrophages interact with neutrophils I hypothesised that changes in the physiology of *tert*$^{-/-}$*;mpeg1.1:mCherry;mpeg1.1:tert-gfp* macrophage and B-cell groups may affect the physiology of neutrophils via intercellular interactions(304). To determine these changes I isolated the neutrophil populations from the *tert*$^{-/-}$*;mpeg1.1:mCherry;mpeg1.1:tert-gfp* and *tert*$^{+/+}$*;mpeg1.1:mCherry.caax* populations and examined the differential regulation of genes between them and the *tert*$^{-/-}$*;mpeg1.1:mCherry.caax* population. I identified Neutrophil populations using the differential expression of the gene *Six-cysteine containing astacin protease 1 (C6ast1)* and *Myeloid-specific peroxidase (Mpx)*(305).

This group includes the genes *sst2, sst1.2, calca, lyz, stc1l, spink2.2, CR556712.1, si:dkeyp-75b4.10, si:dkeyp-203a12.2,* and *zmp:0000001323* (Fig. 5.6.2). *Sst2* encodes the somatostatin receptor gene and acts to regulate cell migration and activity. *Sst2* has homologs in humans that have been indicated in the induction of pancreatic cancer due to a single point mutation(306). *Sst1.2* has also been indicated to regulate cell migration. *Calca* encodes the peptides calcitonin, calcitonin gene-related peptide and katacalcin, with the final peptide expressed being determined by tissue-specific alternative RNA splicing of gene transcripts and cleavage of inactive precursor proteins. Due to this variability, *calca* may be involved in calcium ion regulation or anti-microbial activity. *Stc1l* is also indicated to be involved in calcium ion regulation and the negative regulation of gene transcription. *Lyz* encodes the lysozyme enzyme, part of the innate immune defence against pathogenic bacteria. *Spink2.2m* is linked to male fertility in humans and is required for the normal development of spermatozoa via its action as a trypsin and acrosin inhibitor. *si:dkeyp-75b4.10* is predicted to have carbohydrate binding activity and be involved in the regulation of insulin levels. *si:dkeyp-203a12.2* is indicated to have Adenosine Triphosphate (ATP) binding activity and so be involved in intracellular signalling. *zmp:0000001323* encodes microfibril associated protein 4.6 (mfap4.6) in zebrafish, a protein involved in the maintenance of elastic fibres as well as regulating cell-to-cell adhesion. *CR556712.1* has not yet been studied in detail to the point that its function may be determined.

Transgenic genes include *si:dkeyp-75b4.10*, *zgc:172053*, *si:dkey-203a12.2*, *itln1*, *spink2.2*, *ccl34b.9*, *zmp:00000001323*, *si:ch211-14a17.10*, *si:dkey-152b24.8*, and *npsn*. In this we see a change in the regulation of several genes involved in metabolic processes including *si:dkeyp-75b4.10*, *itln1*, *zgc:172053*, *spink2.2*, and *si:dkey-152b24.8*. As a group, the differential regulation of these genes indicates a change in nutrient sensing to both lipids and carbohydrates such that they both may be utilised as an energy source. Further, upregulated expression of *si:ch211-14a17.10*, which is predicted to have ubiquitin ligase activity, potentially indicates increased turn-over of proteins/increased autophagy. Most interestingly we see and upregulation of *ccl34b.9* and *npsn*. Where *ccl34b.9* is predicted to be a chemokine receptor and so will regulate responses to leukocyte chemotaxins, cytokines, and the extracellular signal-regulated kinases (ERK) cascade. In conjunction *npsn* is predicted to be involved in the immune response to bacteria and its upregulation may indicate a more sensitised state that has occurred in response to the upregulation of *ccl34b.9*. Unfortunately, the regions zmp:00000001323 and si:dkey-203a12.2 have not been sufficiently characterised that I may determine how their differential regulation affects cell physiology.

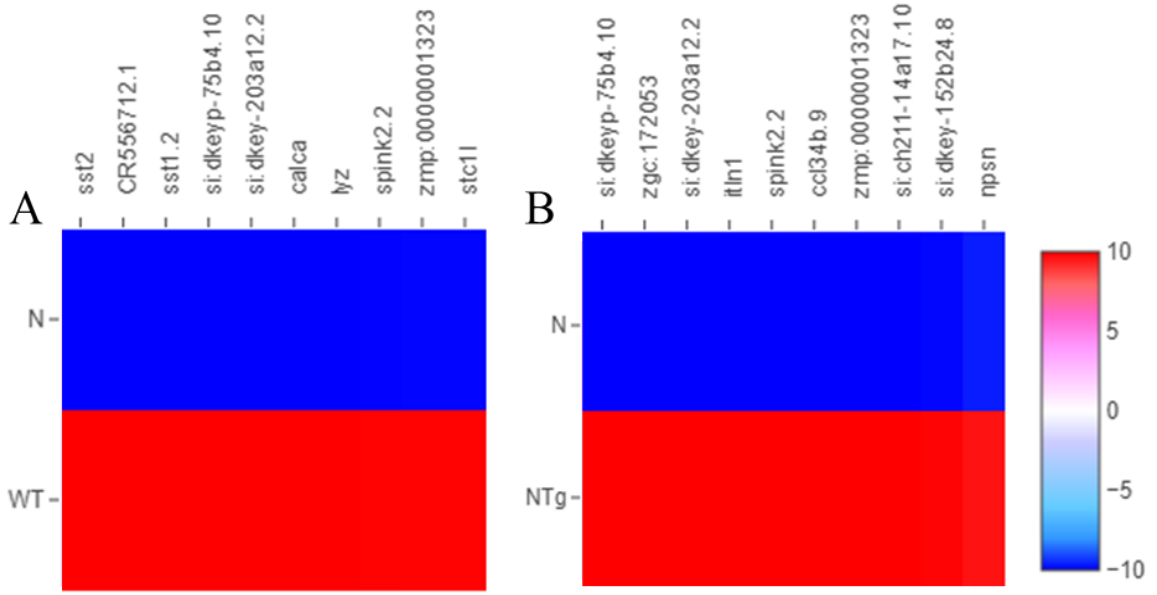

Figure 5.6.2: The ten most differentially upregulated genes in the *tert*$^{-/-}$*;mpeg1.1:mCherry;mpeg1.1:tert-gfp* and *tert*$^{+/+}$*;mpeg1.1:mCherry.caax* neutrophil populations. **A.** Upregulated genes from *tert*$^{+/+}$*;mpeg1.1:mCherry.caax* (n = 268) versus *tert*$^{-/-}$*;mpeg1.1:mCherry.caax* (n = 232) neutrophil populations. **B.** Upregulated genes from *tert*$^{-/-}$*;mpeg1.1:mCherry.caax;mpeg1.1:tert-gfp* (n = 296) compared to *tert*$^{-/-}$*;mpeg1.1:mCherry.caax* (n = 232) neutrophil populations.

5.6.2.1 Exploring the upregulated pathways in the *tert*$^{-/-}$*;mpeg1.1:mCherry.caax;mpeg1.1:tert-gfp* and *tert*$^{+/+}$*;mpeg1.1:mCherry.caax* neutrophil populations.

To further explore the pathways affected by the upregulated genes in the *tert*$^{-/-}$*;mpeg1.1.mCherry.caax;mpeg1.1:tert-gfp* and *tert*$^{+/+}$*;mpeg1.1:mCherry.caax* populations I used ShinyGO software(Fig. 5.6.2.1). Initially, I determined the 10 pathways that were most significantly upregulated in the *tert*$^{+/+}$*;mpeg1.1:mCherry.caax* neutrophil population (Fig. 5.6.2.1.A). This analysis indicated that the 10 most significantly upregulated genes in the *tert*$^{+/+}$*;mpeg1.1:mCherry.caax* neutrophils were all involved in mitochondrial health and ATP production (Fig. 5.6.2.1.A). This indicates that the *tert*$^{+/+}$*;mpeg1.1:mCherry.caax* neutrophils have increased expression of genes associated with the regulation of mitochondria and energy release when compared to the *tert*$^{-/-}$*;mpeg1.1:mCherry.caax* neutrophils.

Using ShinyGO I then determined the ten most upregulated gene pathways in the *tert*$^{-/-}$*;mpeg1.1:mCherry.caax;mpeg1.1:tert-gfp* neutrophil population compared to the *tert*$^{-/-}$*;mpeg1.1:mCherry.caax* population (Fig. 5.6.2.1.B). The 10 most upregulated pathways were shown in include neutrophil activation and response to cytokines, leukocyte differentiation and migration, immune cell development and granulocyte migration (Fig. 5.6.2.1.B). This indicates that insertion of the *mpeg1.1:tert-gfp* transgene is leading to an upregulation of several genes involved with neutrophil function leading to increased response to cytokine signalling, increased cell migration, and potentially influencing neutrophil differentiation (Fig. 5.6.2.1.B).

To investigate if insertion of the *mpeg1.1:tert-gfp* transgene rescues the *tert*$^{-/-}$*;mpeg1.1:mCherry.caax;mpeg1.1:tert-gfp* towards *tert*$^{+/+}$*;mpeg1.1:mCherry.caax* expression levels I used Venny to determine which genes were upregulated in both neutrophil populations indicating 73 genes in common (Fig. 5.6.2.1.C). To determine which pathways these genes were part of I used ShinyGO to determine the 10 most significantly upregulated pathways (Fig. 5.6.2.D). This analysis indicated an upregulation in both neutrophil populations of pathways involved in lipid absorption, basement membrane assembly, and intestinal epithelial cell function (Fig. 5.6.2.D).

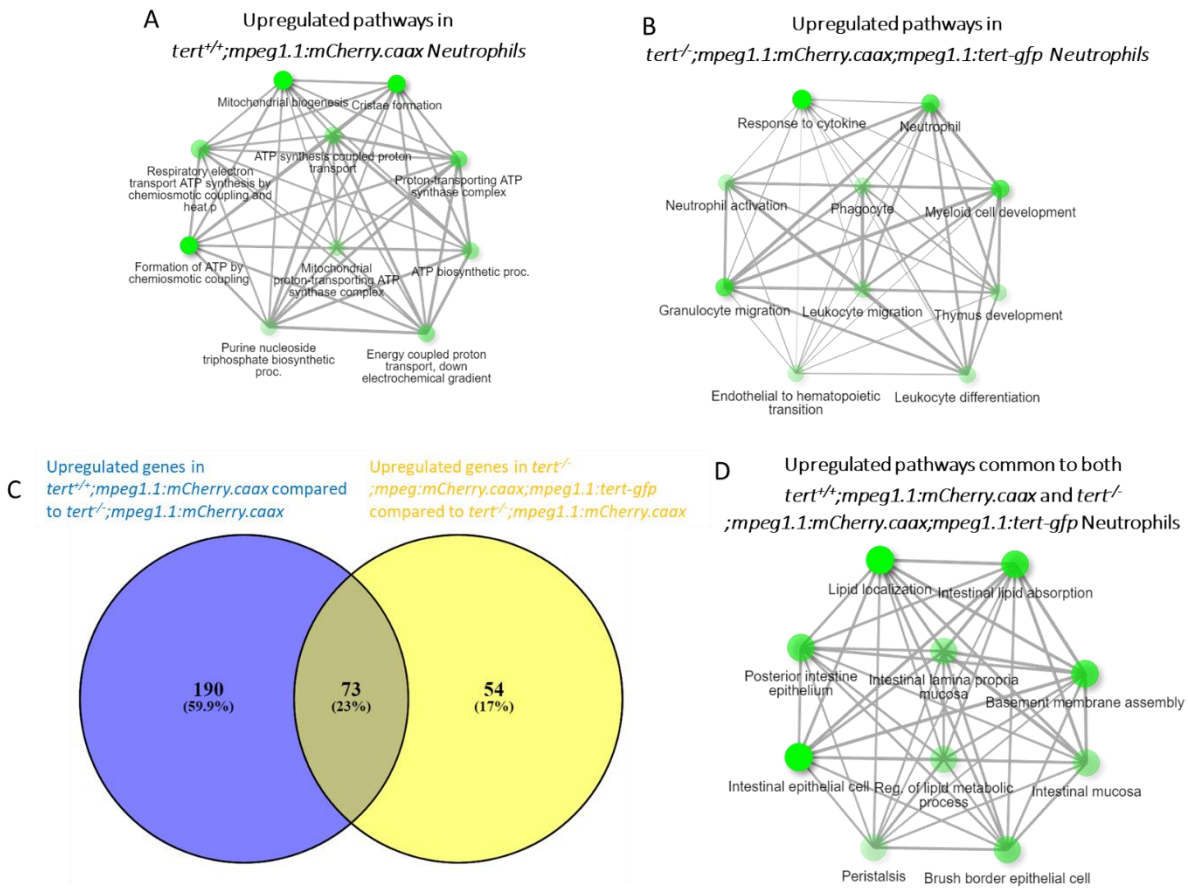

Figure 5.6.2.1: Exploring upregulated pathways of the *tert*$^{-/-}$*;mpeg1.1:mCherry.caax;mpeg1.1:tert-gfp* and *tert*$^{+/+}$*;mpeg1.1:mCherry.caax* neutrophils. **A.** The ten most upregulated pathways from the *tert*$^{-/-}$*;mpeg1.1:mCherry.caax;mpeg1.1:tert-gfp* neutrophil population. **B.** The ten most upregulated pathways from the *tert*$^{+/+}$*;mpeg1.1:mCherry.caax* neutrophil population. **C.** Venn diagram comparing the upregulated genes in the *tert*$^{+/+}$*;mpeg1.1:mCherry.caax* neutrophil population (blue) to the upregulated genes in the *tert*$^{-/-}$*;mpeg1.1:mCherry.caax;mpeg1.1:tert-gfp* neutrophil population (yellow). **D.** The ten most upregulated pathways from the genes upregulated in both neutrophil populations.

5.6.3 Natural Killer cells

Due to NK cells interacting with macrophages it was logical to determine how NK cell physiology may have been altered due to the change macrophage physiology due to the *mpeg1.1:tert-gfp* transgene insertion. Therefore, I determined the populations of NK cells (Fig. 5.6.3) in order to explore the differentially regulated genes between the *tert*$^{-/-}$*;mpeg1.1:mCherry.caax* and *tert*$^{-/-}$*;mpeg1.1:mCherry.caax;mpeg1.1:tert-gfp* genotypes, and the *tert*$^{-/-}$*;mpeg1.1:mCherry.caax* and *tert*$^{+/+}$*;mpeg1.1:mCherry.caax* genotypes. NK cell populations were determined using the gene *Zinc finger and BTB domain containing 32* (*zbtb32*)(305).

The differentially upregulated genes from the *tert*$^{+/+}$*;mpeg1.1:mCherry.caax* genotype includes *CT573383.1, nucleoside diphosphate kinase 2b tandem duplicate 2 (nme2b.2), epithelial cell adhesion molecule (epcam), Jun dimerization protein 2b (jdp2b), heat shock protein alpha-crystallin-related 1 (hspb1), cd74a, chitinase acidic 6 (chia.6), si:ch730343g19.4, zgc:193726,* and *BX855618.1*. The *CT573383.1* region contains the *ice2* gene which is predicted to be involved in the positive regulation of gene transcription, indicating the upregulation of RNA polymerase activity. Further *jdp2b* is also predicted to be involved in transcription factor activity and to regulate histone deacetylation and modification. Therefore, we may be seeing that the *tert*$^{-/-}$*;mpeg1.1:mCherry.caax* genotype has decreased RNA transcription. Upregulation of *nme2b.2* indicates increased use of Guanosine triphosphate (GTP) potentially indicating increased energy use for genetic translation as a consequence of the upregulated transcription. Upregulation of *hspb1* indicates a more sensitive autophagy response due to its chaperone protein activity. Upregulation of *chia. 6* may indicate an upregulated sensitivity to certain pathogen associated molecular patterns (PAMPs) (307). The hypothesis of increased immune sensitive in the *tert*$^{+/+}$*;mpeg1.1:mCherry.caax* population is supported by the upregulation of CD74a which is involved in the activation of T-cells. The region *BX855618.1* contains several genes the function of which has not yet been determined, however it also contains the gene *dopamine receptor D4 related sequence (drd4-rs)* which is predicted to have dopamine receptor activity. This further indicates a crosstalk between immune cells and neural cells in the zebrafish gut. Unfortunately, the regions *si:ch730343g19.4* and *zgc:193726* have not

been studied to the point that I can comment on how their upregulation may affect NK cell physiology.

The differentially upregulated genes from the *tert*$^{-/-}$*;mpeg1.1:mCherry.caax;mpeg1.1:tert-gfp* population include *si:ch211-214p16.1, si:dkeyp-75b4.10, LOC110437731, BX332787.1, tnfb, si:dkey-152b24.8, pglyrp5, spink2.2, fthl28*. The gene *si:dkeyp-75b4.10*, is predicted to have carbohydrate binding activity, potentially indicating a shift in regulating the metabolism of carbohydrates. The region LOC110437731 is predicted to be a beta-microseminoprotein-like protein an immunoglobulin that is indicated to have inhibin-like properties therefore potentially affecting growth regulation. Upregulation of *tnfb* is interesting as it has a wide range of regulatory effects on mechanisms including cell proliferation, apoptosis, and lipid metabolism. Therefore, in the upregulation of *tnfb* we may be observing a factor that is influencing the upregulation of other genes such as *si:dkey-152b24.8* which is predicted to be involved in the lipid metabolic processes. Upregulation of *spink2.2* may indicate an increased regulation endopeptidase activity. Upregulation of *fthl28* may indicate an increase in the cells ability to regulate iron ion homeostasis. Upregulation of *pglyrp5* indicates an increase in the regulation of the response to bacterial immunogenic stimulation. This is interesting in the context of NK cells as they are part of the innate immune system and so are responsible for the early response to infection. In the gut we expect to see a more tolerogenic environment so upregulation of a protein responsible for modulating the defence response to bacteria may indicate a heightened state of responsiveness to potential pathogenic threats. Additionally, if this is occurring due to the effects of the expression of *mpeg1.1:tert-gfp* in the macrophages and B-cells then I may be observing a link between the effects of TERT on immune cell physiology and the immune response. Unfortunately, regions *si:ch211-214p16.1* and *BX332787.1* have not been studied to the point that I may determine how they would affect physiology.

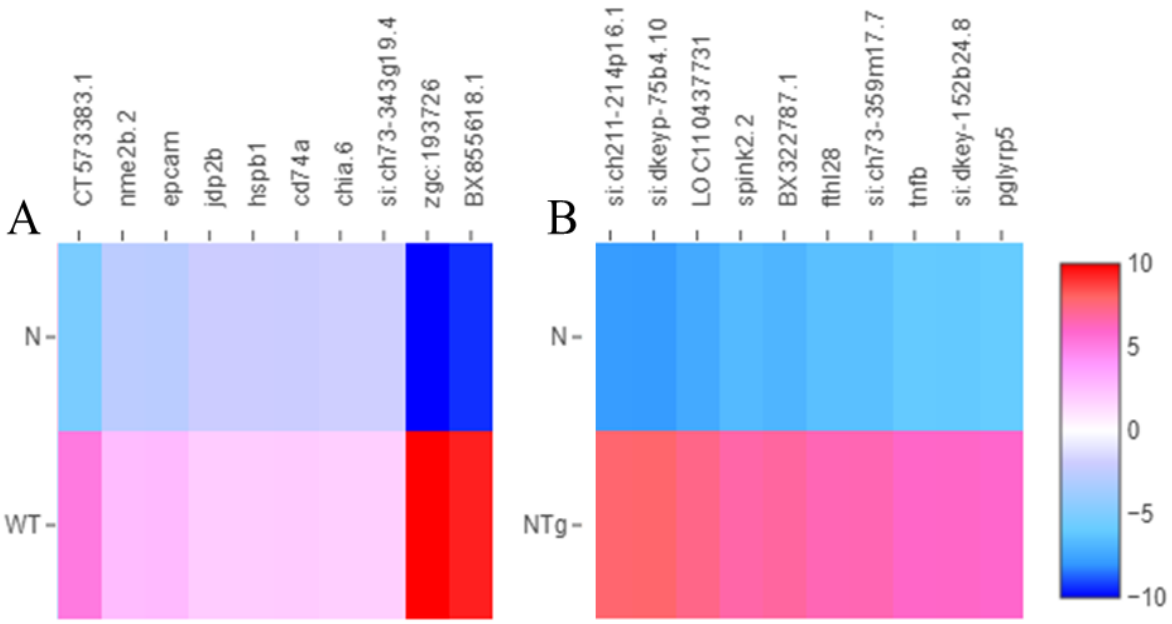

Figure 5.6.3: The ten most differentially upregulated genes in the *tert*$^{-/-}$*;mpeg1.1:mCherry.caax;mpeg1.1:tert-gfp* and *tert*$^{+/+}$*;mpeg1.1:mCherry.caax* Natural Killer cell populations. **A.** Upregulated genes from *tert*$^{+/+}$*;mpeg1.1:mCherry.caax* (n = 20) versus *tert*$^{-/-}$*;mpeg1.1:mCherry.caax* (n = 29) NK cell populations. **B.** Upregulated genes from *tert*$^{-/-}$*;mpeg1.1:mCherry.caax;mpeg1.1:tert-gfp* (n = 22) compared to *tert*$^{-/-}$*;mpeg1.1:mCherry.caax* (n = 29) NK cell populations.

5.6.3.1 Exploring the upregulated pathways in the *tert$^{-/-}$;mpeg1.1:mCherry.caax;mpeg1.1:tert-gfp* and *tert$^{+/+}$;mpeg1.1:mCherry.caax* NK cell populations

To further investigate how the insertion of the *mpeg1.1:tert-gfp* transgene had affected NK cell gene expression, and if it had rescued gene expression in *tert$^{-/-}$;mpeg1.1:mCherry.caax;mpeg1.1:tert-gfp* cells to *tert$^{+/+}$;mpeg1.1:mCherry.caax* cell levels I wanted to explore the pathways upregulated in both populations (Fig. 5.6.3.1). Using ShinyGO software I performed gene enrichment analysis and determined the ten pathways that were most significantly upregulated in the *tert$^{-/-}$;mpeg1.1:mCherry.caax;mpeg1.1:tert-gfp* NK cell population (Fig. 5.6.3.1.A). The pathways were divided into two groups, one of six connected pathways and one of four connected pathways (Fig. 5.6.3.1.A). The group of six related pathways were indicated to be involved in protein folding, the formation of cataracts, and kidney structure formation. The separate group of four indicated an upregulation of genes involved in pathways involved in myeloid and leukocyte development and differentiation, as well as neutrophil mediated immunity.

Using ShinyGO software I determined the ten pathways that were most significantly upregulated in the *tert$^{+/+}$;mpeg1.1:mCherry.caax* NK cell population (Fig. 5.6.3.1.B). I found the upregulated pathways separated into three groups (Fig. 5.6.3.1.B). The first group constituted pathways involved in cellular response to growth stimuli and ethanol metabolism, the second of pathways involved in protein chaperoning and folding, and the third of pathways that formed part of the electron transport chain (Fig. 5.6.3.1.B).

To further explore how insertion of the *mpeg1.1:tert-gfp* gene affected NK cell gene expression I used Venny to determine the genes that were upregulated in both *tert$^{-/-}$;mpeg1.1:mCherry.caax;mpeg1.1:tert-gfp* and *tert$^{+/+}$;mpeg1.1:mCherry.caax* NK cells (Fig. 5.6.3.1.C). This indicated fifty-one genes that were shared between the two NK cell populations (Fig. 5.6.3.1.C). Using ShinyGO I determined the ten most upregulated pathways these genes were part of (Fig. 5.6.3.1.D). This analysis indicated that eight of the ten pathways were involved in the regulation of immune cell differentiation and response to chemokine signalling (Fig. 5.6.3.1.D). Two of the pathways, groove and ventral wall of dorsal aorta, were pathways regulating anatomical structure (Fig. 5.6.3.1.D).Overall, this data indicates that *tert$^{-/-}$;mpeg1.1:mCherry.caax;mpeg1.1:tert-gfp* NK cell gene expression is

altered such that the expression of genes involved in protein folding and chaperoning was upregulated to level comparable to *tert*$^{+/+}$*;mpeg1.1:mCherry.caax* NK cells. Further, that both *tert*$^{-/-}$*;mpeg1.1:mCherry.caax;mpeg1.1:tert-gfp* and *tert*$^{+/+}$*;mpeg1.1:mCherry.caax* NK cells exhibit an upregulation of genes involved in immune cell response to chemoattractant signalling, differentiation, and development. However, this data is constrained by the small sample size of NK cells extracted from the RNA sequencing groups. Therefore, it may be considered preliminary data indicating an avenue for further investigation into premature ageing affects NK cell gene expression.

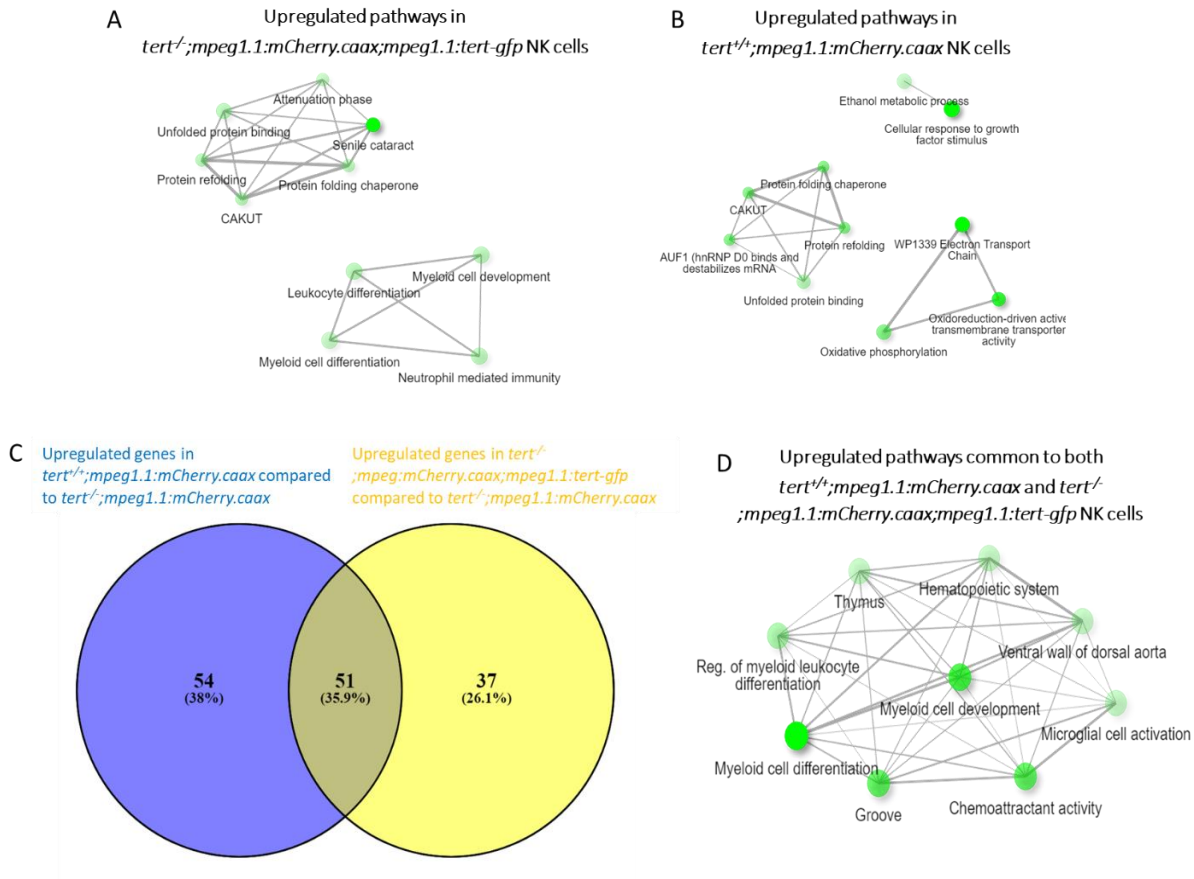

Figure 5.6.3.1: Exploring upregulated pathways of the *tert*$^{-/-}$*;mpeg1.1:mCherry.caax;mpeg1.1:tert-gfp* and *tert*$^{+/+}$*;mpeg1.1:mCherry.caax* NK cells. **A.** The ten most upregulated pathways from the *tert*$^{-/-}$*;mpeg1.1:mCherry.caax;mpeg1.1:tert-gfp* NK cell population. **B.** The ten most upregulated pathways from the *tert*$^{+/+}$*;mpeg1.1:mCherry.caax* NK cell population. **C.** Venn diagram comparing the upregulated genes in the *tert*$^{+/+}$*;mpeg1.1:mCherry.caax* NK cell population (blue) to the upregulated genes in the *tert*$^{-/-}$*;mpeg1.1:mCherry.caax;mpeg1.1:tert-gfp* NK cell population (yellow). **D.** The ten most upregulated pathways from the genes upregulated in both NK cell populations.

5.7 Investigating the effects of *mpeg1.1:tert-gfp* transgene on tissue ageing in non-immune zebrafish gut populations.

Both macrophages and B-cells interact with their resident tissue(308). Therefore, I wanted to explore how the insertion of the *mpeg1.1:tert-gfp* gene affected other intestinal cell groups where we would not expect the transgene to be expressed. The three groups we decided to study were epithelial cells, neural cells, and stem cells, as they have all been indicated to interact with macrophages or B-cells or both in tissues throughout the zebrafish model organism(281, 309).

5.7.1 Exploring the differential gene regulation of epithelial cells between the three genotypes.

Epithelial cell populations were determined using the genes *fatty acid binding protein 2 (fabp2)*, *apolipoprotein A-1a (apoa1a)*, *apolipoprotein A-4a (apoa4a)*, and *vil1 (vil1)*. Altered gene expression in the *tert*$^{+/+}$*;mpeg1.1:mCherry.caax* included *fatty acid binding protein 6* (*fabp6*), *ferritin heavy polypeptide-like 27* (*fthl27*), *anterior gradient 2* (*agr2*), *mitochondrial NADH dehydrogenase 2* (*mt-nd2*), *mitochondrial cytochrome c oxidase 3* (*cox3*), *mitochondrial NADH dehydrogenase 4* (*mt-nd4*), *mitochondrial cytochrome c oxidase 2* (*mt-co2*), *mitochondrial cytochrome b* (*mt-cyb*), *NC_002333.4* and *NC_002333.17* (regions of the *D. rerio* mitochondrial genome) (Fig. 5.7.1). Upregulation of *fabp6* indicates that the *tert*$^{+/+}$*;mpeg1.1:mCherry.caax* epithelial cell population has an increased uptake of fatty-acids compared to the *tert*$^{-/-}$*;mpeg1.1:mCherry.caax* epithelial cell population. Upregulation of the ferritin gene *fthl27* indicates an increase in intracellular iron storage of *tert*$^{+/+}$*;mpeg1.1:mCherry.caax* epithelial cells. A decrease in the regulation of intracellular iron storage has been indicated as a factor in age related pathologies such as Alzheimer's disease and dysregulated bone resorption(310) Therefore, observing a significant difference in the zebrafish intestinal epithelial cells expression of a ferritin gene between a healthy and premature aged phenotype potentially indicates that dysregulation of iron homeostasis begins in the gut. Upregulation of *agr2* is interesting due anterior gradient 2 being predicted to act within intestinal epithelial cell differentiation, indicating that its upregulation in the

tert$^{+/+}$*;mpeg1.1:mCherry.caax* epithelial cell population may be influencing their differentiation. I also observe differential regulation of five specific mitochondrial genes as well as two regions of the zebrafish mitochondrial genome all of which are indicated to act as part of the electron transport chain production of Adenosine Triphosphate (ATP). Therefore, this indicates that the *tert*$^{+/+}$*;mpeg1.1:mCherry.caax* epithelial cell population has increased ATP production and potentially healthier mitochondria compared to the *tert*$^{-/-}$*;mpeg1.1:mCherry.caax* population. This is interesting as there have been several papers detailing the non-canonical functions of TERT in mitochondrial biology and the *tert*$^{-/-}$*;mpeg1.1:mCherry.caax* genotype exhibits premature ageing due to a mutation in its TERT gene(132, 218)

Altered gene expression in the *tert*$^{-/-}$*;mpeg1.1:mCherry.caax;mpeg1.1:tert-gfp* included *XLOC_00431*, *BX908782.2*, *BX004857.1*, *Ictacalcin* (*icn*), *XLOC_010899*, *High mobility group nucleosomal binding domain 2* (*hmgn2*), *Ovarian Cancer Immunoreactive Antigen domain containing 2* (*ociad2*), *fabp6*, *CT57338.1*, and *agr2*. Initially it is interesting to see that both *fabp6* and *agr2* are upregulated in the *tert*$^{-/-}$*;mpeg1.1:mCherry.caax*;*mpeg1.1:tert-gfp* population compared to the *tert*$^{-/-}$*;mpeg1.1:mCherry.caax* population as both of these are also observed to be upregulated in the *tert*$^{+/+}$*;mpeg1.1:mCherry.caax* population compared to the *tert*$^{-/-}$*;mpeg1.1:mCherry.caax* (Fig. 5.7.1). Therefore, this may indicate that rescuing the expression of TERT in *mpeg1.1*$^{+}$ cells altering their physiology leading to an altering of the physiology of the epithelial cells via extracellular interactions or excretions. The protein coded by the gene *ociad2* is indicated to be involved in endocytosis and the Janus Kinase-Signal Transducer and activator of Transcription proteins (JAK-STAT) pathway, therefore this may indicate that the epithelial cells have an increased endocytic uptake. Upregulation of *icn2* indicates increased regulation of calcium ions as ictacalcin is predicted to enable calcium-dependent protein binding activity. The gene *hmgn2* encodes a protein that is predicted to enable chromatin binding and organisation; therefore, upregulation of this gene may indicate a chromatin reorganisation. In mice High Mobility Group Nucleosome-binding 2 (HMGN2) has been found to maintain chromatin accessibility at promoter regions (311) indicating it's expression has the ability to alter the expression of genes involved in cellular development (311). Further, *BX004857.1* encodes a region containing si:ch211-217i17.1 predicted to be involved in chromosome segregation potentially indicating

additional regulation of gene transcription. The region BX908782.2 encodes *ly97.2* which enables LPS binding and the calcium ion channel *scn12aa*. Unfortunately, the genes *XLOC_010899, XLOC_00431,* and *CT57338.1* have not been studied to the extent that I can comment on how they may affect epithelial cell physiology.

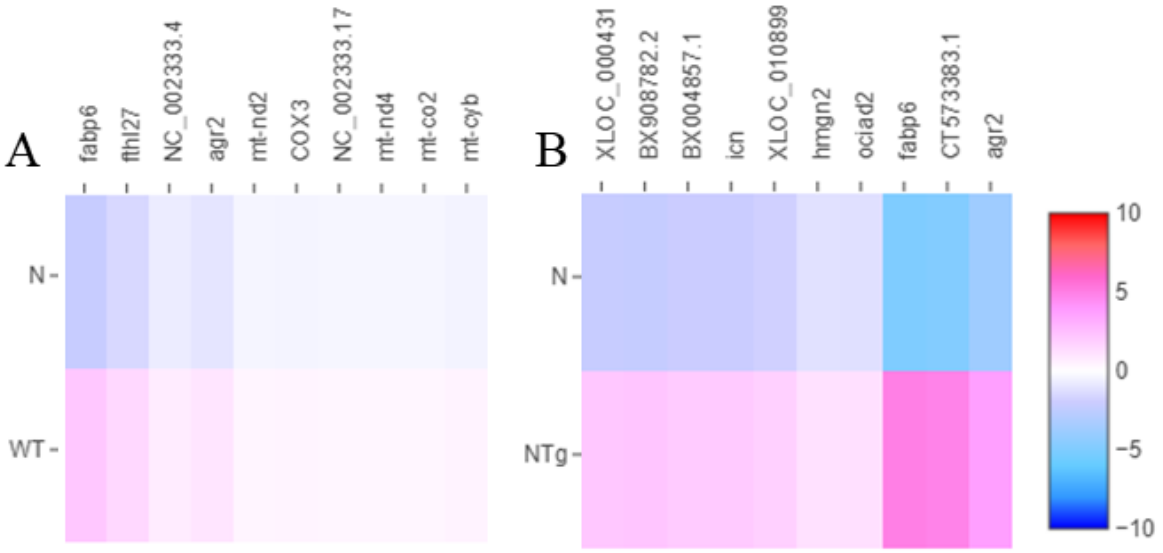

Figure 5.7.1: The ten most differentially upregulated genes in the *tert*$^{-/-}$*;mpeg1.1:mCherry.caax;mpeg1.1:tert-gfp* and *tert*$^{+/+}$*;mpeg1.1:mCherry.caax* epithelial cell populations. **A.** Upregulated genes from *tert*$^{+/+}$*;mpeg1.1:mCherry.caax* (n = 30,018) versus *tert*$^{-/-}$*;mpeg1.1:mCherry.caax* (n = 20,158) epithelial cell populations. **B.** Upregulated genes from *tert*$^{-/-}$*;mpeg1.1:mCherry.caax;mpeg1.1:tert-gfp* (n = 20,158) compared to *tert*$^{-/-}$*;mpeg1.1:mCherry.caax* (n = 25,616) epithelial cell populations.

5.7.1.1 Exploring the upregulated pathways in both *tert*$^{-/-}$*;mpeg1.1:mCherry.caax;mpeg1.1:tert-gfp* and *tert*$^{+/+}$*;mpeg1.1:mCherry.caax* epithelial cells

To further determine how the insertion of the *mpeg1.1:tert-gfp* gene affects epithelial cell gene expression via their interaction with *mpeg1.1*$^{+}$ cells I determined the genes that were upregulated in the *tert*$^{-/-}$*;mpeg1.1:mCherry.caax;mpeg1.1:tert-gfp* and *tert*$^{+/+}$*;mpeg1.1:mCherry.caax* epithelial cell populations. Upregulated genes in the *tert*$^{+/+}$*;mpeg1.1:mCherry.caax* population would indicate which cells were upregulated in a healthy gut. Upregulated genes in the *tert*$^{-/-}$*;mpeg1.1:mCherry.caax;mpeg1.1:tert-gfp* population would indicate which genes were upregulated due to the effects of the insertion of the *mpeg1.1:tert-gfp* gene. This would not be due to the expression of the transgene in the epithelial cells. Rather, it would be downstream effects of the expression of the transgene in *mpeg1.1*$^{+}$ cells.

Cluster analysis indicated twenty-three significantly upregulated genes in the *tert*$^{+/+}$*;mpeg1.1:mCherry.caax* population and twenty-seven significantly upregulated genes in the *tert*$^{-/-}$*;mpeg1.1:mCherry.caax;mpeg1.1:tert-gfp* population. Analysis using Venny software indicated thirteen genes were upregulated in both populations. As these genes are upregulated in a healthy epithelial cell population they can be thought of as characteristic of a healthy gut. As they are upregulated in the *tert*$^{-/-}$*;mpeg1.1:mCherry.caax;mpeg1.1:tert-gfp* population as well, hypothetically they are being rescued to a level comparable to that in the healthy gut. Ontological analysis of these genes indicates that they are predominantly involved in ATP generation and the electron transport chain (Fig. 5.7.1.1.B, C, D, E). Therefore, this data indicates that epithelial cells derived from the *tert*$^{-/-}$*;mpeg1.1:mCherry.caax;mpeg1.1:tert-gfp* gut have increased expression of metabolism related genes comparable to epithelial cells derived from the *tert*$^{+/+}$*;mpeg1.1:mCherry.caax* population.

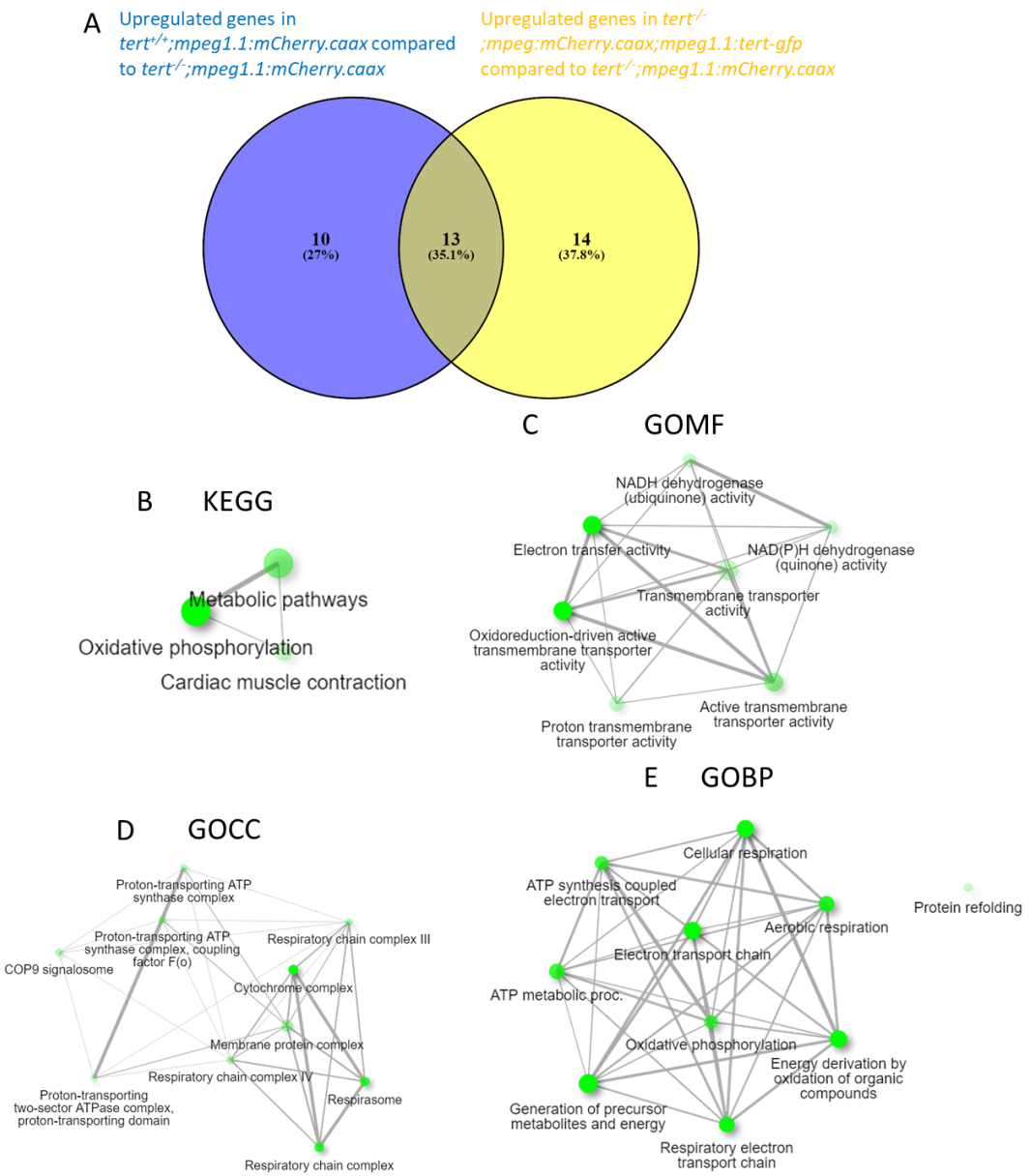

Figure 5.7.1.1: Exploring differentially regulated pathways of the *tert*$^{-/-}$*;mpeg1.1:mCherry.caax;mpeg1.1:tert-gfp* and *tert*$^{+/+}$*;mpeg1.1:mCherry.caax* epithelial cell populations. **A.** Venn diagram displaying the upregulated genes in the *tert*$^{-/-}$*;mpeg1.1:mCherry.caax;mpeg1.1:tert-gfp* and *tert*$^{+/+}$*;mpeg1.1:mCherry.caax* epithelial cell populations and the genes upregulated in both genotypes **B.** Gene ontology analysis of the common upregulated genes from the KEGG database. **C.** Gene ontology analysis of the common upregulated genes from the GOMF database. **D.** Gene ontology analysis of the common upregulated genes from the GOCC database. **E.** Gene ontology analysis of the common upregulated genes from the GOBP database.

5.7.2 Exploring the differential gene regulation of neural cells between the three genotypes.

Neural cell populations were determined using the genes *Nerve Growth Factor Receptor (NGFR), Kinesin-like calmodulin-binding protein (zwi),* and *embryonic lethal abnormal vision-like 3 (elavl3).* Upregulated genes from the *tert*$^{+/+}$*;mpeg1.1:mCherry.caax* genotype include *icn, BX004816.2, BX908782.2, krt18a.1, her6, si:ch211-214p16.3, tmem176l.2, pyyb, agr2, fabp6*. The upregulation of the gene *icn* indicates an increase in expression of the ictacalcin protein which is predicted to have calcium ion binding activity so may indicate increased regulation of calcium ion levels. The gene *her6* is predicted to enable RNA-polymerase II activity upstream of neural cell development and the Notch signalling pathway. As Notch signalling promotes proliferation, upregulation of *her6* may indicate increased proliferative signalling in the *tert*$^{+/+}$*;mpeg1.1:mCherry.caax* compared to the *tert*$^{-/-}$*;mpeg1.1:mCherry.caax* population. The gene *tmem176l.2* which codes for a transmembrane protein involved in cellular differentiation. The gene *ppyb* allows for the regulation of type 2 neuropeptide Y receptor binding activity and is predicted to be involved in feeding behaviour. Differential regulation of genes associated with feeding behaviour may further indicate why we see reduced nutrient sensing in the aged gut. The genes *agr2* and *fabp6* have also been shown to be upregulated in epithelial cells (section 5.7.1). These genes are essential to intestinal cell development and differentiation and nutrient sensing. Therefore, their repeated differential regulation in different cell populations may indicate a link between them and the physiological changes we see with the ageing gut. The region *si:ch211-214p16.3* is associated with the *plb1* gene which is involved in phospholipid metabolism. The region BX004816.2 is indicated to code for a large section of chromosome 3 making it difficult to determine how its upregulation may affect the physiology of the cell. The region BX908782.2 contains both the *lyz97* gene and the *scn12aa* gene. *lyz97* exhibits lipopolysaccharide binding activity and so is involved in responding to gram negative bacteria, and *scn12aa* is predicted to have voltage gated sodium ion channel activity which may indicate in the context of neural cells the healthy maintenance of an action potential.

Upregulated genes from the *tert*$^{-/-}$*;mpeg1.1:mCherry.caax*;*mpeg1.1:tert-gfp* genotype include *BX908782.2, CABZ01072614.1, NC_002333.4, NC_002333.17, mt-cyb, mt2, zgc:158463, wu:fb18f06, Cytochrome c oxidase subunit III (COX3), rps27l*. Interestingly, we see *BX908782.2* upregulated in both the *tert*$^{+/+}$*;mpeg1.1:mCherry.caax* neural cell population and the *tert*$^{-/-}$*;mpeg1.1:mCherry.caax*;*mpeg1.1:tert-gfp* population, potentially indicating that the *mpeg1.1:tert-gfp* transgene is rescuing the expression of the genes in this region although not to the same level of expression as is observed in the *tert*$^{+/+}$*;mpeg1.1:mCherry.caax* population (Fig. 5.7.2). The region *BX908782.2* codes for both the *scn12aa* and the *ly97.2* genes. The gene *ly97.2* is part of the response to lipopolysaccharide. Upregulation of *ly97.2* may indicate a tolerogenic response to commensal gram-negative bacteria in the zebrafish gut. Upregulation of the *scn12aa* gene may indicate a regulation of calcium as part of the nutrient absorbing process. The gene *rps27l* codes for a ribosomal protein therefore it's upregulation may indicate an increase translation or an increase in ribosomal turnover. Interestingly, *mt-cyb, mt2, COX3, NC_002333.4*, and *NC_002333.17* are all genes associated with the mitochondria or regions of the mitochondria associated with the production of ATP via oxidative phosphorylation. Upregulation of these in the *tert*$^{-/-}$*;mpeg1.1:mCherry.caax*;*mpeg1.1:tert-gfp* may indicate that the expression of the *mpeg1.1:tert-gfp* gene is causing a change in metabolism. This hypothesis is supported by literature that reports TERT as being shuttled to mitochondria and having non-canonical functions that improve mitochondrial health (139). Unfortunately, *CABZ01072614.1* and *zgc:158463* have not been studied to the point that I can comment on how their upregulation may affect neural cell physiology.

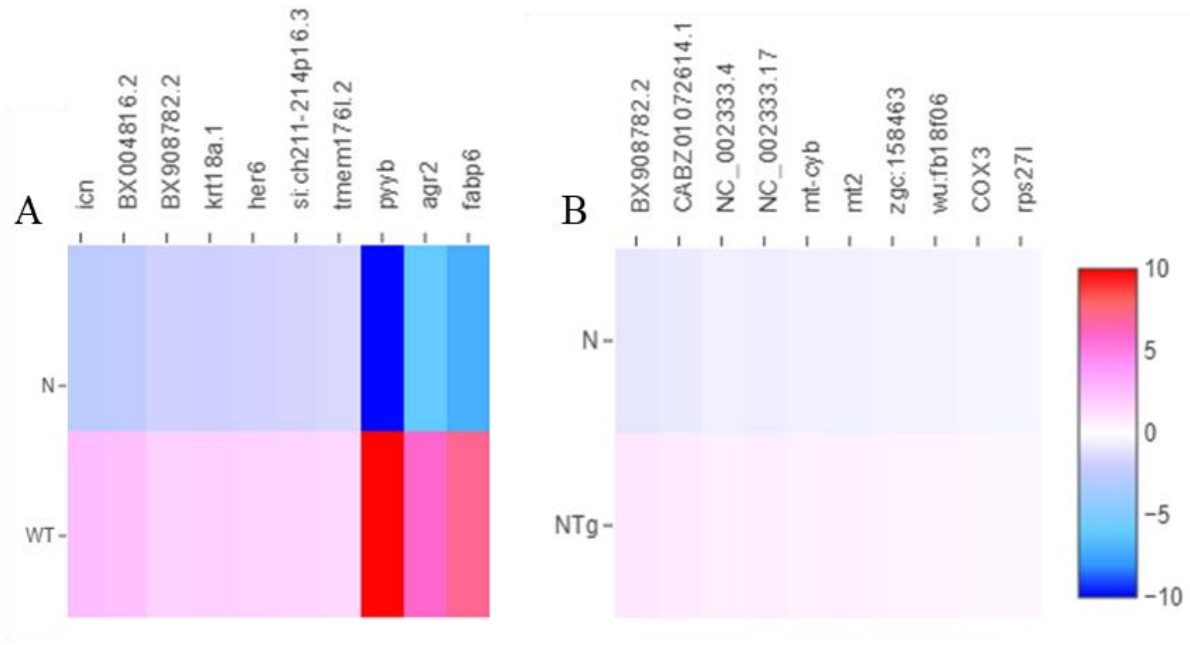

Figure 5.7.2: The ten most differentially upregulated genes in the *tert*$^{-/-}$*;mpeg1.1:mCherry;mpeg1.1:tert-gfp* and *tert*$^{+/+}$*;mpeg1.1:mCherry.caax* neural cell populations. **A.** Upregulated genes from *tert*$^{+/+}$*;mpeg1.1:mCherry.caax* (n = 297) versus *tert*$^{-/-}$*;mpeg1.1:mCherry.caax* (n = 266) Neural cell populations. **B.** Upregulated genes from *tert*$^{-/-}$*;mpeg1.1:mCherry.caax;mpeg1.1:tert-gfp* (n = 296) compared to *tert*$^{-/-}$*;mpeg1.1:mCherry.caax* (n = 266) Neural cell populations.

5.7.2.1 Further exploration of the effects of the neural cell gene expression in *tert*$^{+/+}$*;mpeg1.1:mCherry.caax* and *tert*$^{-/-}$*;mpeg1.1:mCherry.caax;mpeg1.1:tert-gfp* intestinal neural cell populations.

To further investigate how the insertion of the *mpeg1.1.:tert-gfp* transgene may be affecting gene expression in neural cells I determined the genes that had been upregulated in both *tert*$^{+/+}$*;mpeg1.1:mCherry.caax* and *tert*$^{-/-}$*;mpeg1.1:mCherry.caax;mpeg1.1:tert-gfp* neural cells (Fig. 5.7.2.1.A). This analysis indicated one-hundred and six upregulated genes were present in both populations (Fig. 5.7.2.1.A). Ontological analysis of these genes against the KEGG database indicates an upregulation of pathways involved in oxidative phosphorylation, regulation of the actin cytoskeleton, and protein processing (Fig. 5.7.2.1.B). Upregulation of pathways involved in ATP production and respiration are also indicated in analysis using the GOCC database and the GOBP database (Fig. 5.7.2.1.D, E). Analysis against the GOMF database indicates and upregulation of pathways involved in RNA binding and translation (Fig. 5.7.2.1.C). Upregulation of pathways involved in translation, RNA splicing, and mRNA processing are also indicated in analysis using the GOBP database (Fig. 5.7.2.1.E). Therefore, this data indicates that insertion of the *mpeg1.1:tert-gfp* transgene is leading to a rescue in the expression of genes involved mRNA translation, gene expression, and metabolism in prematurely aged gut neural cells.

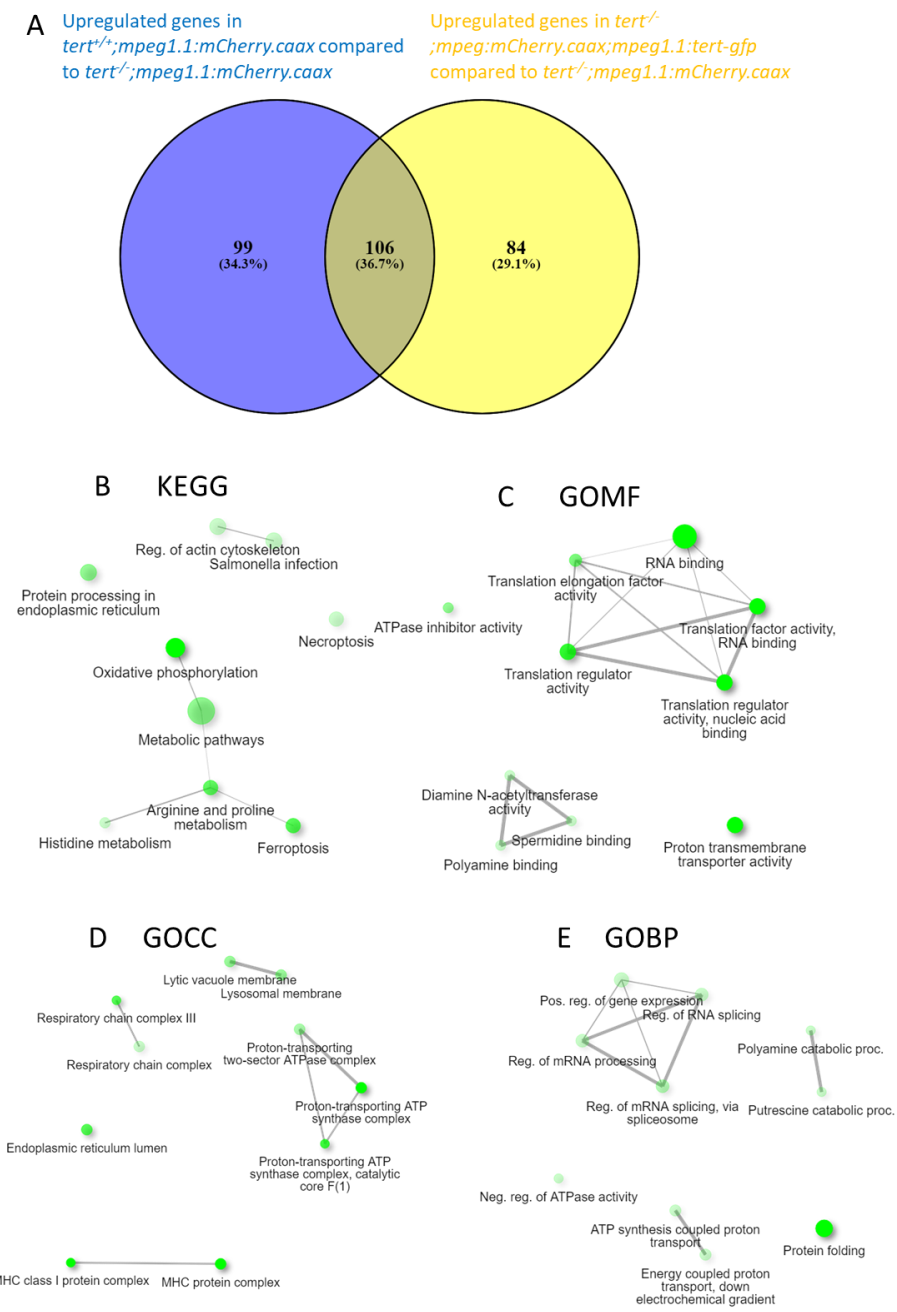

Figure 5.7.2.1: Exploring differentially regulated pathways of the *tert*$^{-/-}$*;mpeg1.1:mCherry.caax;mpeg1.1:tert-gfp* and *tert*$^{+/+}$*;mpeg1.1:mCherry.caax* neural cell populations. **A.** Venn diagram displaying the upregulated genes in the t*ert*$^{-/-}$*;mpeg1.1:mCherry.caax;mpeg1.1:tert-gfp* and *tert*$^{+/+}$*;mpeg1.1:mCherry.caax* neural cell populations and the genes upregulated in both genotypes **B.** Gene ontology analysis of the common upregulated genes from the KEGG database. **C.** Gene ontology analysis of the common upregulated genes from the GOMF database. **D.** Gene ontology analysis of the common upregulated genes from the GOCC database. **E.** Gene ontology analysis of the common upregulated genes from the GOBP database.

5.7.3 Exploring the differential gene regulation of stem cells between the three genotypes.

I wanted to determine how a change in intestinal environment resulting from introduction of the *mpeg1.1:tert-gfp* transgene affected stem cell biology. To isolate the stem cell population, I used the differential upregulation of the *protein arginine methyl transferase (prmt1)* gene(312). Upregulated genes from *tert*$^{+/+}$*;mpeg1.1:mCherry.caax* include *vtg5, insl5a, sst2, sst1.2, vtg6, vtg2, vtg7, vtg1, CR556712.1, vtg4*. Interestingly, we see upregulation of the majority of the *vtg* family, similar to the differentially regulated genes observed in the macrophage population (section 5.3.1). The *vtg* family regulates the response of the cell to lipid metabolism and antioxidant activity as well as playing a role in determining egg quality. Therefore, increased expression in stem cells may indicate a healthy regulation of lipid processing. Upregulated expression of the *sst* in the stem cell population may indicate a response to growth hormone signalling or cell mitosis signalling. In the context of stem cells this may be a signal to continue division and expansion. Upregulation of *insl5a* indicates a potential increase in G-protein coupled receptor binding activity. Upregulation of the *CR556712.1* may lead to an increase in keratin expression as this region contains the keratin genes *krt98, krt99,* and *krt15*.

Upregulated genes from the transgenic include si:zfos-2372e4.1, spink2.2, si:dkey-203a12.2, si:dkeyp-75b4.10, BX322787.1, CT573383.1, XLOC_010899, ociad2, hmgn2, BX004857.1. As *spink2.2* is a serine-type endopeptidase inhibitor its upregulation would indicate an increase in serine-type endopeptidase inhibitor activity. This is further supported by the upregulation of *si:dkey-203a12.2* which codes for spink2.7 Upregulation of *ociad2* may indicate better regulation of the stem cell population's homeostasis as it has been predicted to be a regulator of the JAK-STAT pathway. Interestingly *hmgn2* is a chromatin binding factor hence its upregulation may indicate epigenetic changes in the stem cell population that are occurring as a result of the effects of the *mpeg1.1:tert-gfp* transgene. This is supported by the upregulated expression of *CT573383.1* which codes for *Interactor Of Little Elongation Complex ELL Subunit 2* (ICE2). ICE2 is predicted to be involved in the positive regulation of RNA polymerase II mediated gene transcription. Hence chromatin remodelling followed by increased gene transcription would be an elegant indicator of the gene transcription non-canonical function of TERT. The gene *si:dkeyp-75b4.10* is predicted to be orthologues to

human REG1A and so is predicted to have carbohydrate binding activity. This is an interesting contrast to the upregulation of the vitellogenin family we see in the *tert*$^{+/+}$*;mpeg1.1:mCherry.caax* population potentially indicating the *mpeg-tert-gfp* is affecting the metabolism of the cell in a more specific way than rescuing overall physiological health. The region BX322787.1 contains the genes *chpf2, samrd3b, and prkdc* all of which are involved in the regulation and activity of the cytoskeleton. The region *BX004857.1* contains the gene *si:ch211-217i17.1* which is predicted to have serine/threonine kinase activity and be involved in chromosomal segregation potentially indicating altered cell-cycle regulation. Unfortunately, the region *XLOC_010899* has not been characterised to the point that I can comment on how it may affect cell physiology.

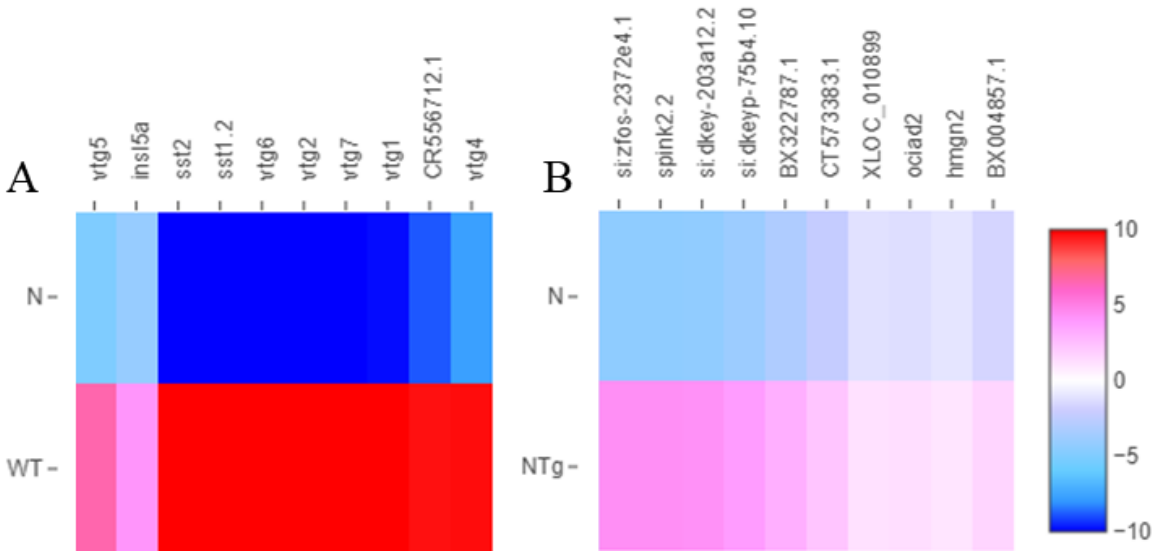

Figure 5.7.3: The ten most differentially upregulated genes in the *tert*$^{-/-}$*;mpeg1.1:mCherry;mpeg1.1:tert-gfp* and *tert*$^{+/+}$*;mpeg1.1:mCherry.caax* stem cell populations. **A.** Upregulated genes from *tert*$^{+/+}$*;mpeg1.1:mCherry.caax* (n = 1,875) versus *tert*$^{-/-}$*;mpeg1.1:mCherry.caax* (n = 1,702) stem cell populations. **B.** Upregulated genes from *tert*$^{-/-}$*;mpeg1.1:mCherry.caax;mpeg1.1:tert-gfp* (n = 1,702) compared to *tert*$^{-/-}$*;mpeg1.1:mCherry.caax* (n = 1,925) stem cell populations.

5.7.3.1 Further exploration of the effects of stem cell gene expression in *tert*$^{+/+}$*;mpeg1.1:mCherry.caax* and *tert*$^{-/-}$*;mpeg1.1:mCherry.caax;mpeg1.1:tert-gfp* intestinal stem cell populations.

To further investigate how the insertion of the *mpeg1.1:tert-gfp* transgene affects stem cell gene expression I compared the upregulated genes in *tert*$^{-/-}$*;mpeg1.1:mCherry.caax;mpeg1.1:tert-gfp* and *tert*$^{+/+}$*;mpeg1.1:mCherry.caax* stem cell populations (Fig. 5.7.3.1.A). This indicated one-hundred and twenty-two genes that were upregulated in both populations (Fig. 5.7.3.1.A). To determine how the upregulation of these genes would affect stem cell biology I used ShinyGO to perform ontological analysis on the pathways these genes are part of. Analysis using the KEGG database indicated upregulation of genes involved in protein processing, bile acid synthesis, phagocytosis, and response to pathogenic infection (Fig. 5.7.3.1.B). Analysis using the GOMF database indicated an upregulation of genes associated with transcription and translation, as well as pathways involved in protein folding (Fig. 5.7.3.1.C). Utilising the GOCC database indicated upregulation of pathways involved in protein processing in the endoplasmic reticulum (Fig. 5.7.3.1.D). Finally, analysis using the GOBP further indicated the upregulation of protein folding and chaperone pathways (Fig. 5.7.3.1.E). Therefore, this data indicates that insertion of the *mpeg1.1:tert-gfp* transgene as led to an upregulation of the expression of genes associated with protein folding, as well as DNA transcription and translation in prematurely aged stem cells that may rescue them towards a healthy state.

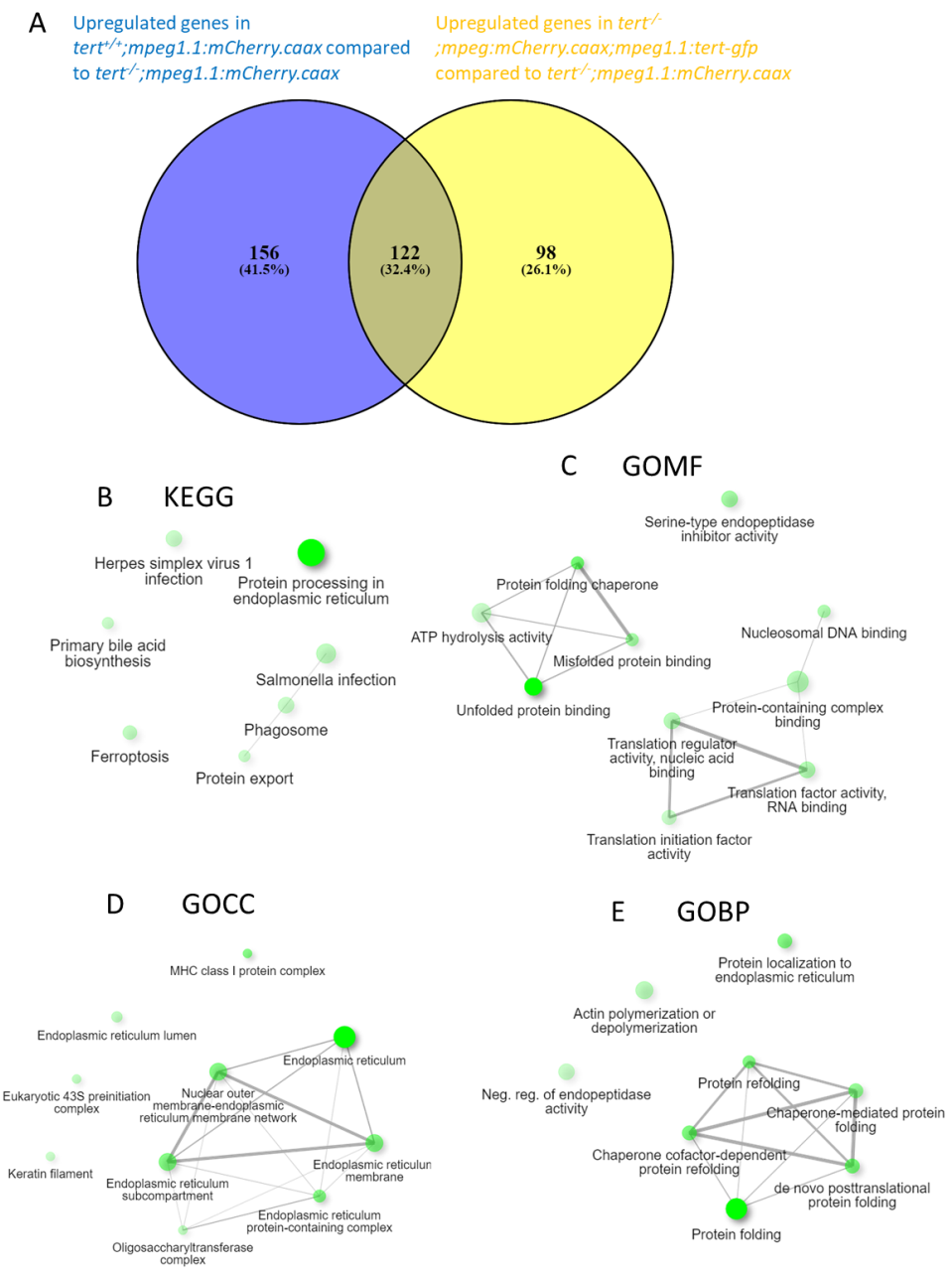

Figure 5.7.3.1: Exploring differentially regulated pathways of the *tert*$^{-/-}$*;mpeg1.1:mCherry.caax;mpeg1.1:tert-gfp* and *tert*$^{+/+}$*;mpeg1.1:mCherry.caax* stem cell populations. **A.** Venn diagram displaying the upregulated genes in the t*ert*$^{-/-}$*;mpeg1.1:mCherry.caax;mpeg1.1:tert-gfp* and *tert*$^{+/+}$*;mpeg1.1:mCherry.caax* stem cell populations and the genes upregulated in both genotypes **B.** Gene ontology analysis of the common upregulated genes from the KEGG database. **C.** Gene ontology analysis of the common upregulated genes from the GOMF database. **D.** Gene ontology analysis of the common upregulated genes from the GOCC database. **E.** Gene ontology analysis of the common upregulated genes from the GOBP database.

5.8 Conclusion

Here I have demonstrated the use of single-cell RNA sequencing in characterising zebrafish intestinal physiology on a cellular level. Gene enrichment analysis has been performed on healthy *tert*$^{+/+}$*;mpeg1.1:mCherry.caax*, prematurely aged *tert*$^{-/-}$*;mpeg1.1:mCherry.caax*, and transgenic *tert*$^{-/-}$*;mpeg1,1:mCherry.caax;mpeg1.1:tert-gfp* intestinal cell subsets. Further, data has been produced indicating how the insertion of the *mpeg1.1:tert-gfp* transgene into a premature ageing background has affected intestinal cell gene expression.

Initially I determined populations of cells that had upregulated expression of *mpeg1.1*. Initially, examining the upregulated genes in the *tert*$^{-/-}$*;mpeg1.1:mCherry.caax;mpeg1.1:tert-gfp* population indicated an upregulation of pathways involved ATP production and response to ROS that resulted from the insertion of the *mpeg1.1:tert-gfp* gene (Fig.5.3.1). This indicates that insertion of the transgene was potentially rescuing one of the non-canonical functions of TERT which is its shuttling to the mitochondria to protect mitochondrial DNA from ROS(132, 145). Further, this data suggests that insertion of the *mpeg1.1:tert-gfp* transgene led to increased mitochondrial function via upregulation of genes associated with ATP production, potentially indicating further research should be undertaken to determine how this may affect the prematurely aged immune cell. Further, it has already been reported by *Hu et al* that TERT localisation to the mitochondria improves wound healing outcomes(141). Therefore, I can hypothesise that the insertion of the *mpeg1.1:tert-gfp* transgene may also lead to improved wound healing outcomes and that these may occur as result of the increased mitochondrial function indicated in section 5.3.1 and 5.3.1.1.

Unsupervised clustering of the *mpeg1.1* populations indicated four distinct clusters. These clusters were indicated to be macrophages, B-cells, epithelial cells, and a mix of different cell types (Fig.5.3.2). I would expect both B-cells and macrophages to be expressing the *mpeg1.1* gene as this has previously been reported in the literature(226, 234). The presence of epithelial cells in the *mpeg1.1* population was unexpected as this has not been previously reported in the literature to my knowledge at this point. One explanation for the presence of upregulated *mpeg1.1* expression in previously uncharacterised cells may be the *mpeg1.1:mCherry.caax* transgene being expressed, as its insertion site has not been

characterised. Alternatively, it may be that further investigation of the *mpeg1.1* clusters is required to better identify the constitutive cell types.

Observing the alterations in macrophage gene expression between *tert*$^{-/-}$*;mpeg1.1:mCherry.caax* and *tert*$^{+/+}$*;mpeg1.1:mCherry.caax* populations the most significant differentially regulated genes were those involved in nutrient sensing as part of the vitellogenin family indicating a change in nutrient sensing and inflammatory state. In observing the alterations in macrophage gene expression between the *tert*$^{-/-}$*;mpeg1.1:mCherry.caax* and *tert*$^{-/-}$*;mpeg1.1:mCherry.caax;mpeg1.1:tert-gfp* cells I found that genes involved in neural cell interaction, inflammatory state, and nutrient sensing. Additionally, I determined that genes involved in mitochondrial health and the generation of ATP were rescued in the *tert*$^{-/-}$*;mpeg1.1:mCherry.caax;mpeg1.1:tert-gfp* genotype towards the levels of *tert*$^{+/+}$*;mpeg1.1:mCherry.caax* macrophages indicating that the *mpeg1.1:tert-gfp* gene was rescuing mitochondrial function as had been observed in the *tert*$^{+/+}$*;mpeg;mCherry.caax* and the *tert*$^{-/-}$*;mpeg1.1:mCherry.caax;mpeg1.1:tert-gfp mpeg1.1* populations.

Observing differentially regulated genes in B-cell physiology between the *tert*$^{-/-}$*;mpeg1.1:mCherry.caax* and *tert*$^{+/+}$*;mpeg1.1:mCherry.caax* populations indicated an upregulation of genes associated with response to oxidative stress as well as response to growth hormone and chemotaxis signalling. Differential gene regulation between the *tert*$^{-/-}$*;mpeg1.1:mCherry.caax;mpeg1.1:tert-gfp* and *tert*$^{-/-}$*;mpeg1.1:mCherry.caax* populations indicated the upregulation genes associated with increased mitochondrial function as well as response to chemotactic signalling and B-cell subset differentiation. This may indicate that the insertion of the *mpeg1.1:tert-gfp* transgene is affecting mitochondrial health in the *tert*$^{-/-}$*;mpeg1.1:mCherry.caax;mpeg1.1:tert-gfp* B-cell population as it is indicated to do in the macrophage population. Further, it may be affecting the regulation of B-cells into B1 or B2 populations.

I have also observed the effects of the *tert*$^{-/-}$*;mpeg1.1:mCherry.caax;mpeg1.1:tert-gfp* macrophage and B-cell populations on intestinal cell populations that do not utilise the *mpeg* promoter and therefore we would not expect the expression of the *mpeg1.1:tert-gfp* transgene. In these populations I have observed alterations in nutrient sensing, inflammatory pathways, growth and differentiation signalling. This indicates that the

insertion of the *mpeg1.1:tert-gfp* transgene is altering the physiology of B-cells and macrophages in the *tert*$^{-/-}$*;mpeg1.1:mCherry.caax;mpeg1.1:tert-gfp* group such that they are then going on to alter their interactions with other intestinal tissue cell populations.

In the T-cell population I see an upregulation of genes associated with T-cell differentiation and thymus development in the *tert*$^{-/-}$*;mpeg1.1:mCherry.caax;mpeg1.1:tert-gfp* population (Fig. 5.6.1.1). This may indicate that the changes to gene expression in *mpeg1.1* cell subsets is leading to altered regulation of T-cell development and differentiation potentially via cytokine signalling. I also observe the upregulation of genes involved in neutrophil activation in the *tert*$^{-/-}$*;mpeg1.1:mCherry.caax;mpeg1.1:tert-gfp* indicating neutrophil gene expression and activation state may also be altered due to the effects of inserting the *mpeg1.1:tert-gfp* transgene. Future work may look to determine the specific genes that are upregulated in the transgenic T-cell and neutrophil populations and how they may be regulated by signals from other immune cells that utilise *mpeg1.1* and so may be expressing the *mpeg1.1:tert-gfp* transgene. In both the T-cell population and the neutrophil population I observed the upregulation of pathways that indicated potential contamination with other cell types (sections 5.6.1, 5.6.2). In T-cells I observed the upregulation of pathways associated with microglia and neutrophils. In the neutrophil population enrichment analysis indicated the upregulation of pathways associated with epithelial cells and thymus development potentially indicating some contaminating cells being present. Therefore, future analysis may look to optimising the T-cell and neutrophil specific markers.

Enrichment analysis of NK cells from the *tert*$^{-/-}$*;mpeg1.1:mCherry.caax;mpeg1.1:tert-gfp* population indicated the upregulation of pathways associated with the oxidative phosphorylation, protein folding, and response to mitogenic signalling (section 5.6.3). However, gene enrichment analysis of upregulated genes common to the *tert*$^{-/-}$*;mpeg1.1:mCherry.caax;mpeg1.1:tert-gfp* and the *tert*$^{+/+}$*;mpeg1.1:mCherry.caax* populations indicated upregulation of pathways involved in myeloid cell development despite NK cells being derived from the lymphoid lineage (Fig. 5.6.3.1). Therefore, we may be observing some contamination in the NK cell populations. If this were the case, due to the small sample size of the NK cell populations, we would expect the effects of the contaminating populations to be amplified which may be why I observe the upregulation of unexpected pathways in Fig. 5.6.3.1.D.

Performing further work on this data I would aim to further understand the networks that are differentially regulated in the *tert*$^{-/-}$*;mpeg1.1:mCherry.caax;mpeg1.1:tert-gfp* macrophage and B-cell populations. To do this I would determine a panel of marker genes that may be differentially regulated due to TERT expression but not due to telomere length increasing. This would enable the exploration of how insertion of the *mpeg1.1:tert-gfp* transgene has affected the expression of genes associated with the non-canonical functions of TERT. To further explore how the insertion of the *mpeg1.1:tert-gfp* transgene affected immunosenescence and tissue senescence I would aim to create a panel of genes I would expect to be upregulated in senescent cells and determine how their expression was altered between the three genotypes. Additional future work would be to determine how the *mpeg1.1:Δtert-gfp* transgene altered macrophage and B-cell gene expression using the *tert*$^{-/-}$*;mpeg1.1:mCherry.caax;mpeg1.1:Δtert-gfp* line I have developed. However, this would require performing the single-cell RNA sequencing again utilising age matched fish of all four phenotypes (*tert*$^{+/+}$*;mpeg1.1:mCherry.caax,* *tert*$^{-/-}$*;mpeg1.1:mCherry.caax,* *tert*$^{-/-}$*;mpeg1.1:mCherry.caax;mpeg1.1:tert-gfp,* *tert*$^{-/-}$*;mpeg1.1:mCherry.caax;mpeg1.1:Δtert-gfp*) so that the data is comparable. This data would then indicate if the insertion of the *mpeg1.1:Δtert-gfp* gene rescued non-canonical functions of TERT.

6. Discussion

The work carried out here has begun to establish two novel model organisms that allow the study of the non-canonical functions of telomerase in the context of immune system ageing. Further, it establishes a protocol for the isolation of a viable single-cell suspension of zebrafish gut cells which be utilised in further single-cell RNA sequencing work (Fig. 6). The single-cell RNA sequencing analysis performed here has indicated several genes are rescued in the *tert*$^{-/-}$*;mpeg1.1:mCherry.caax;mpeg1.1:tert-gfp* immune system towards levels observed in immune cells in the *tert*$^{+/+}$*;mpeg1.1:mCherry.caax* genotype. Further, analysis has indicated that insertion of the *mpeg1.1:tert-gfp* transgene has led to the rescue of functions outside of the canonical function of TERT. These functions include a rescue of genes associated with mitochondrial health, the electron transport chain, and the generation of ATP. Further, in macrophages I observed an upregulation of genes involved in macrophage polarisation and the innate immune response. In B-cells, I also observed an upregulation of genes associated with B-cell polarisation and immune response.

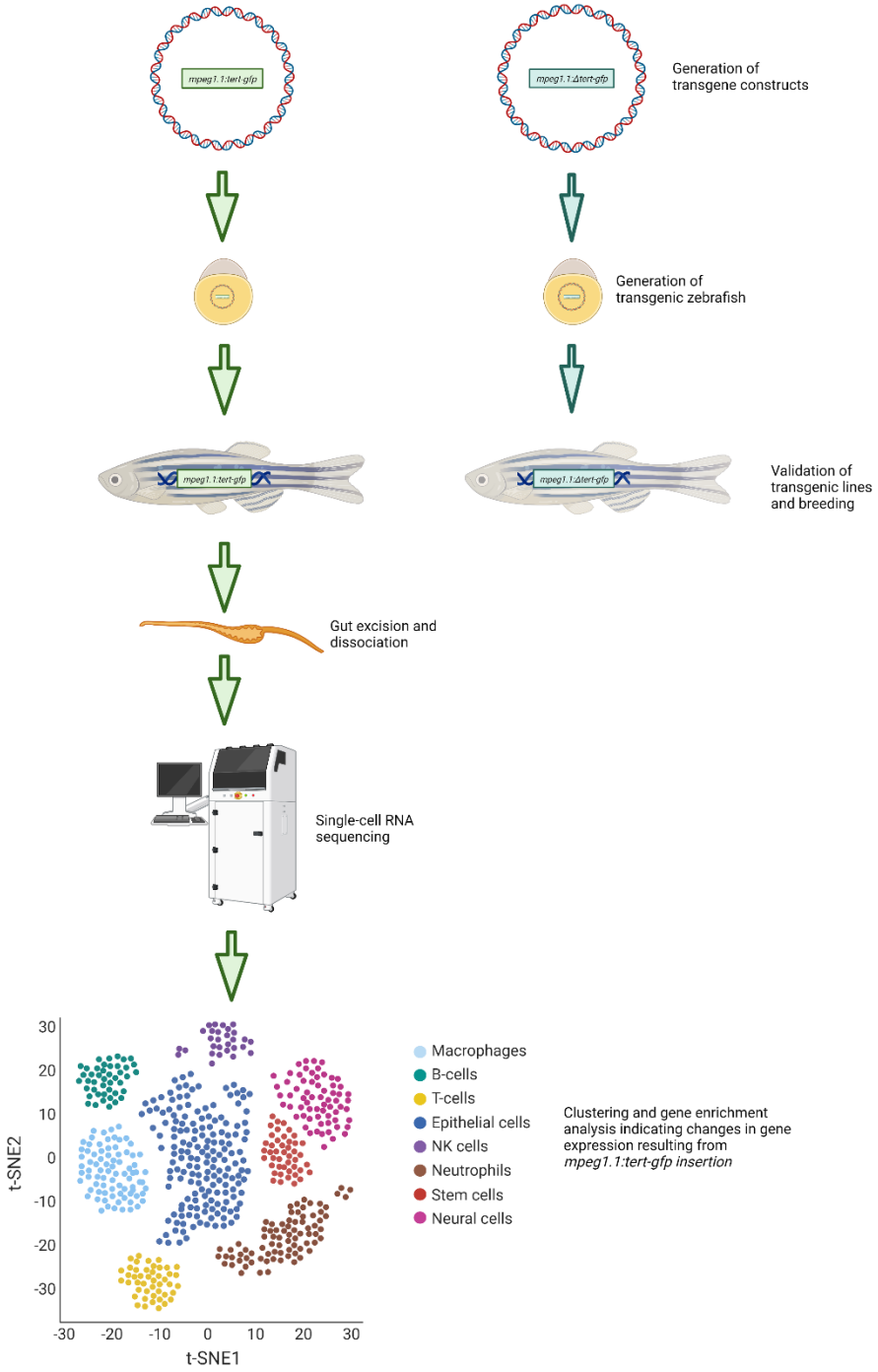

Figure 6: General representative diagram of the experiments and analysis carried out throughout this thesis.

6.1 Characterising the novel transgenic lines and their potential uses for future work.

This project demonstrated the characterisation of two novel transgenic zebrafish lines generated with the aim of studying the non-canonical functions of telomerase. The first novel transgenic line being a full-length telomerase rescue (*mpeg1.1:tert-gfp*) that expresses telomerase regulated by the *mpeg1.1* promoter. The second, a mutant telomerase rescue (*mpeg1.1:Δtert-gfp*) that expresses ΔTERT also under the regulation of the *mpeg1.1* promoter. Whole genome sequencing demonstrated that the *mpeg1.1:tert-gfp* transgene was inserted into chromosome 11 from position 24,906,202 to 24,906,258. Insertion at this position indicated insertion into the *larsb* gene but without evidence that the insertion had led to significant changes to the transgenic fish physiology. However, future work should aim to quantify the normal expression of *larsb* and compare this to the *mpeg1.1:tert-gfp* transgenic to further investigate if there are potentially uncharacterised effects of the insertion of the *mpeg1.1:tert-gfp* transgene.

Whole genome sequencing demonstrated that the *mpeg1.1:Δtert-gfp* transgene was inserted into chromosome 16 at position 19,790,508 to 19,790,589 (Sup. Fig. 2.A, D). This is a non-coding region and therefore I would not expect the insertion of the *mpeg1.1:Δtert-gfp* to affect the transgenic line in a way other to its expression. This is supported by the literature where *macc1* is reported to play a role in zebrafish development(256). Therefore, if the insertion *mpeg1.1:Δtert-gfp* were affecting *macc1* we would expect to see alterations in the transgenic lines craniofacial development which we currently do not. However, in future work I would validate that this was the case by quantifying, using southern blotting or real-time quantitative PCR, the expression of the nearest coding regions. In this case the nearest upstream coding region would be *abcb5* and the nearest downstream coding region would be *macc1*.

The tol2 transposase system was used as it has been well established as a genetic engineering tool in fish(251, 252, 259). However, future work in generating zebrafish transgenic lines may instead look to using the CRISPR/Cas9 system. The CRISPR/Cas9 system has the advantage of being able to produce more targeted mutations in germline and adult

zebrafish compared to the more random tol2 system(313, 314). In the context of this study, future work may look at using knock-out methods to remove the region of *tert* that codes for TERC binding with the aim of a generating a transgenic zebrafish that will have the non-canonical functions of TERT in all cells rather than just *mpeg1.1*$^{+}$.

A limitation of this project is that I have not quantifiably determined that insertion of the *mpeg1.1:tert-gfp* transgene is leading to increased telomerase activity in *mpeg1.1*$^{+}$ cells. I have shown data in section 3.2.12 that telomere length is increased in transgenic *mepg1.1*$^{+}$ cells which indicates that telomerase activity is increased, however additional work should be carried out to further verify if this is the case. I did attempt to optimise the use of the TRAP assay to detect telomerase activity in zebrafish gut dissociations (Section 3.2.13). This was attempted as the TRAP assay is an established method for determining telomerase activity from cell lysates. Unfortunately, using the TRAP assay kit on dissociated zebrafish gut proved difficult due the presence of false positives in the negative control indicating a contamination. I hypothesise that this is due to the presence of residual digestive enzymes from the gut lumen activating the colorimetric change that is designed to be the measure of telomerase activity. Therefore, further optimisation of using the TRAP assay to determine telomerase activity in zebrafish gut dissociation may aim to provide a cleaner preparation that has undergone more wash steps to remove residual gut contents. For example, it may be possible to use FACS to sort cells from a zebrafish gut dissociation directly into the lysis buffer.

The IF data indicates that the GFP from the *mpeg1.1:Δtert-gfp* is being expressed in some cells but not to a level that is statistically significant. However, the whole genome sequencing data demonstrates that the entirety of the *mpeg1.1:Δtert-gfp* transgene is inserted. Therefore, one hypothesis for the disparity in this data may be that the IRES region is unreliable in this model. A second hypothesis is that the insertion site of the transgene is causing the transgenes expression to be regulated either by upstream or downstream signalling. Finally, another hypothesis is that the immunofluorescent staining protocol requires further optimisation and the anti-GFP antibody requires further validation using a positive control of an established GFP transgenic. Further, characterisation of the *mpeg1.1:Δtert-gfp* line should aim to determine if the ΔTERT is elongates telomeres using

the same telo-FISH assay used to determine the canonical activity of transgenic TERT in the *mpeg1.1:tert-gfp* line.

Provided it was possible to determine that *Δtert* was not elongating telomeres, and was being expressed, it would then be possible to study the non-canonical functions of TERT in zebrafish *mpeg1.1*$^{+}$ cells. This would require using both the *mpeg1.1:tert-gfp* and the *mpeg1.1:Δtert-gfp* transgenic lines to determine which genes were being rescued in both transgenics. This may be determined using either single-cell RNA sequencing or bulk RNA sequencing. Bulk RNA sequencing would be cheaper, and the equipment needed more accessible. However, bulk-RNA sequencing would require the optimisation of the isolation of a population of mCherry^{+} cells. Additionally, the literature has demonstrated that the *mpeg1.1* promoter may be expressed in several different cell subsets(226, 234, 237). An alternative to bulk RNA sequencing is single-cell RNA sequencing as I have performed in this study. Using single-cell RNA sequencing would enable exploration of the effects of the *mpeg1.1:Δtert-gfp* transgene on prematurely aged zebrafish. A further alternative to determine the effects of the insertion and expression of the transgenes would be to determine specific genes the expression of which is reported to be altered by rescuing TERT expression or have been indicated to be influenced as a non-canonical effect of TERT. It may then be possible to quantify the expression of these genes using qPCR, or to quantify the translation of associated proteins using western blotting to determine how insertion and expression of the the transgenes have affected them.

6.2 Single-cell RNA sequencing of zebrafish lines indicates the possibility of rescuing immunosenescence in a prematurely aged phenotype.

Single-cell RNA sequencing is an effective method for studying the difference in gene expression between distinct phenotypes. This project demonstrated through single-cell RNA sequencing that the tissue resident immune cells of the zebrafish gut exhibit specific ageing characteristics a selection of which can be rescued with the expression of TERT. Future work that would expand on the findings of this project would be divided into two sections. The

first section would focus on further characterising the phenotypic changes that occur in the *mpeg1.1:tert-gfp* and *mpeg1.1:Δtert-gfp* rescue models generated as part of this project. Initially I would recommend continuing to optimise the isolation of macrophages and B-cells as individual cell populations. I would then determine if B-cells were phagocytic using phagocytosis assays already established, for example using fluorescent green beads (315). I would use live cell imaging to determine if *mpeg1.1* controlled expression of mCherry and the transgene increased in response to phagocytic stimuli. I would perform the same experiment with isolated live macrophages using both $tert^{+/+}$ and $tert^{-/-}$ phenotypes to determine how the expression of the transgenes affects phagocytosis. Further to this I would have a custom antibody produced specific to the active site of TERT so that it may be used to detect the expression of both TERT and ΔTERT. Using this antibody, I would validate the expression of the transgenes. I would then further determine if the *mpeg1.1:Δtert-gfp* transgene was affecting telomere length via Telo-FISH or if it had any canonical telomerase activity via the TRAP assay.

Data from section 5.3.2 indicates the upregulation of genes associated with mitochondrial health and the electron transport chain. Previously, it has been reported that TERT is transported into the mitochondria via Src where the transport of TERT into mitochondria led to an increase in mitochondrial function and biogenesis (145). Therefore, observing the upregulation of mitochondrial genes that are related to mitochondrial health in $mpeg1.1^{+}$ cells (Fig. 5.3.2) containing the *mpeg1.1tert-gfp* transgene may indicated that I am observing evidence of a rescue of the non-canonical functions of TERT in the $tert^{-/-}$ *;mpeg1.1:mCherry.caax;mpeg1.1:tert-gfp* line. Further to this, ontological analysis indicated that genes associated with the of Nicotinamide adenine dinucleotide (NADH) dehydrogenase were upregulated in $mpeg1.1^{+}$ cells (Fig. 5.3.2). Upregulation of genes associated with NADH dehydrogenase indicate an increase in mitochondrial respiration potentially indicating that the TERT expressed as result of the *mpeg1.1:tert-gfp* transgene is increasing respiration in $mpeg1.1^{+}$ cells. Exploring the gene enrichment data from GOBP in section 5.4 we can see insertion of the *mpeg1.1:tert-gfp* transgene is indicated to lead to the upregulation of genes associated with immune function, specifically the MHC 1 complex, and respiratory chain activity (Fig. 5.4.1.B, D). We also see and upregulation of genes associated with oxidoreduction and ATP generation in B-cell populations (Fig. 5.5.1.C).

Therefore, this data further supports the hypothesis that insertion of the *mpeg1.1:tert-gfp* transgene is leading to increased mitochondrial function and respiration. Future work may look to explore this further using mitochondrial function assays such as measures of respiration rate or membrane potential(316). For example, A future experiment to determine the difference in mitochondrial function in the *mpeg1.1:tert-gfp* transgenic line would be to determine mitochondrial respiration rate in controls (*tert*$^{+/+}$ *and tert*$^{-/-}$ cells) and the *tert*$^{-/-}$*;mpeg1.1:mCherry.caax;mpeg1.1:tert-gfp* derived *mpeg1.1*$^{+}$ cells(316).

Gene enrichment analysis of the *tert*$^{-/-}$*;mpeg1.1:mCherry.caax;mpeg1.1:tert-gfp* macrophages indicated an upregulation of genes associated with the innate immune response pathway (Fig.5.4.1.B). Further, gene enrichment analysis of the *tert*$^{-/-}$*;mpeg1.1:mCherry.caax;mpeg1.1:tert-gfp* B-cell population indicated an upregulation of genes associated with antigen binding, indicating a change in B-cell immune response activity (Fig. 5.5.1). Therefore, this data suggests that insertion of the *mpeg1.1:tert-gfp* transgene is leading to an alteration in immune cell function. Considering that in the literature the function of immune cells has been linked to telomerase activity, we may be observing the rescue of immune cell function due to an increase in the expression of TERT and increased telomerase activity(185). However, to validate this would require further validation of the *mpeg1.1:tert-gfp* transgenic line as discussed in section 6.1. Further, future experiments may be performed to examine immune cell function in the *tert*$^{-/-}$*;mpeg1.1:mCherry.caax;mpeg1.1:tert-gfp* line. For example, a phagocytosis assay can be used to determine macrophage phagocytic function as an indicator of macrophage activity(185). Considering that the phagocytosis assay may be performed *in vivo*, there is the potential to combine it with an opsonophagocytic assay or Enzyme-linked immunosorbent spot assay to assess B-cell function at the same time(317).

Gene enrichment analysis of *tert*$^{-/-}$*;mpeg1.1:mCherry.caax;mpeg1.1:tert-gfp* T-cell populations indicated an upregulation of pathways involved in T-cell differentiation and lymphoid progenitor cell differentiation (Fig. 5.6.1.1.B). One hypothesis as to why we see this is that insertion of the *mpeg1.1:tert-gfp* transgene leading to *mpeg1.1*$^{+}$ cells influencing T-cell development and differentiation via intracellular signalling as literature has been published that demonstrates the interaction of T-cells with mononuclear phagocytes in zebrafish(318). However, this hypothesis should be tested potentially by quantifying the

number of different T-cell subpopulations in *tert*$^{+/+}$*;mpeg1.1:mCherry.caax* and *tert*$^{-/-}$*;mpeg1.1:mCherry.caax* and then determining how the number of those populations change in the *tert*$^{+/+}$*;mpeg1.1:mCherry.caax;mpeg1.1:tert-gfp* line using.

Gene enrichment analysis of the *tert*$^{-/-}$*;mpeg1.1:mCherry.caax;mpeg1.1:tert-gfp* neutrophil populations indicated an upregulation of pathways involved in neutrophil activation and myeloid cell development (Fig. 5.6.2.1.B). This may indicate that gene regulation in the transgenic neutrophil population is being altered due to the insertion of the *mpeg1.1:tert-gfp* transgene. At the time of writing, I have not found literature that indicates zebrafish neutrophils utilise the *mpeg1.1* promoter. Therefore, any changes I observed in neutrophil gene expression are hypothesised to be a result of intracellular interactions with other immune cells(304). Further work may look to explore how the intracellular interactions between regulatory cells and neutrophils are affected. For example, we look to quantify the expression levels of specific cytokines that indicated to affect neutrophil activation state, such as granulocyte colony stimulating factor, tumour necrosis factor, and type 1 and 2 interferons(319). Further, as neutrophils are established phagocytes, we may also explore how their phagocytic function is affected *in vivo* utilising the *tert*$^{-/-}$*;mpeg1.1:mCherry.caax* genotype and the *tert*$^{-/-}$*;mpeg1.1:mCherry.caax;mpeg1.1:tert-gfp* lines(319)

In exploring the gene enrichment in stem cells, neural cells, and epithelial cells I aimed to determine if insertion of the *mpeg1.1:tert-gfp* gene had led to any significant changes in the prematurely aged tissue that may rescue its function towards a *tert*$^{+/+}$*;mpeg1.1:mCherry.caax* state. In both epithelial and neural cell populations I see evidence of the upregulation of genes associated with increased ATP production and use, indicating that their metabolism may have been rescued towards a *tert*$^{+/+}$*;mpeg1.1:mCherry.caax* level. In the stem cell population I see an upregulation of genes associated with protein folding and chaperoning, nucleosomal DNA binding and translation, indicating changes in the regulation of gene expression. However, further exploration of how insertion of the *mpeg1.1:tert-gfp* transgene affects tissue ageing would be to use tissue ageing biomarkers. Initially I would produce suitable populations to monitor over the course of their lives to produce a survival curve. These fish would be monitored for signs of ageing, such as weight loss and spinal curvature. This would provide data on how organismal ageing was affected by the insertion of the *mepg1.1:tert-gfp* transgene. Second

to this I would produce experimental populations of fish with which would be taken at set timepoints in their lifespan to assess their physiological health. These timepoints would be three months, six months, nine months, twelve months, fifteen months, and eighteen months (at which time we would expect to see the majority of the control *tert*$^{-/-}$*;mpeg1.1:mCherry.caax* population having died(218)). At each time point I would perform various experiments to determine both cellular and tissue health. These would include SA-β-gal staining on tissues including gut, brain, head kidney, and skin, to determine how the build-up of senescent cells was affected by the insertion of the *mpeg1.1:tert-gfp* transgene. Hypothetically, if insertion of the *mpeg1.1:tert-gfp* transgene rescues some macrophage function, we may expect to see less senescent cells in the *tert*$^{-/-}$*;mpeg1.1:mCherry.caax;mpeg1.1:tert-gfp* compared to the *tert*$^{-/-}$*;mpeg1.1:mCherry.caax* line at the same time points, as macrophages have been indicated to clear senescent cells(146, 154, 320, 321). Additionally, assessing biomarkers of ageing such as epigenetic methylation, the expression of inflammatory cytokines associated with the SASP, and telo-FISH staining to determine the maintenance of chromosomes over-time.

6.3 Additional future work and closing remarks.

As TERT has been reported to have several non-canonical functions a potential next step would be to utilise both the *mpeg1.1:tert-gfp* and *mpeg1.1:Δtert-gfp* transgenic lines to investigate these in a zebrafish model(132, 134, 322). This would require further breeding of *tert*$^{-/-}$*;mpeg1.1:mCherry.caax;mpeg1.1:Δtert-gfp* fish alongside age matched *tert*$^{-/-}$*;mpeg1.1:mCherry.caax*, *tert*$^{+/+}$*;mpeg1.1.mCherry.caax*, and *tert*$^{-/-}$*;mpeg1.1:mCherry.caax;mpeg1.1:tert-gfp* fish. However, moving forward we may look to combine breed transgenic lines together to further understand how the insertion of the *mpeg1.1:tert-gfp* or *mpeg1.1:Δtert-gfp* affects different cells subsets. For example, we may look to crossbreed the *mpeg1.1:tert-gfp* and *mpeg1.1:Δtert-gfp* with the *mpx:gfp* line which allows the identification of neutrophils in order to further understand the how insertion of the transgenes affects neutrophil biology(323). Alternatively, we may look to crossbreed with B-cell reporter lines so that we can further understand how insertion of the transgenes may affect B-cell biology(185). Therefore, future studies may look to generating more novel

transgenic lines to better understand the effects of the *mpeg1.1:tert-gfp* and *mpeg1.1:Δtert-gfp* on specific cell subsets.

To better facilitate antibody-based assays, I would commission the production of a zebrafish TERT specific antigen, that was specific to the sequence conserved between the TERT and ΔTERT transgenes, to utilise in immunohistochemistry and western blotting experiments. In immunohistochemistry a TERT specific antigen would enable the visualisation of TERT within the cell. In western blotting it would add an additional method that we could use to determine the concentration of TERT or ΔTERT that was being expressed. While this is potentially a considerable economic investment, at the time of writing I have not found a commercially available antibody that has been demonstrated to reliably identify zebrafish TERT for immunohistochemistry.

In further future work I would utilise cell culture and transgenesis to determine the non-canonical function of TERT in human cells. *Imamura et al.* previously established that human TERT functions in zebrafish cells (238). Therefore, we may expect that zebrafish TERT would function in human cells. To determine this, I would utilise the *mpeg1.1:tert-gfp* and *mpeg1.1:Δtert-gfp* transgenes transfected into human a human cell line that utilised the *mpeg1.1* promoter, such as THP-1 cells, and validate the expression of the transgene by fluorescence imaging, immunohistochemistry, and western blotting. If I did not find that TERT and ΔTERT were expressed in the human cell line I would produce novel transgenes containing human TERT and human ΔTERT that I could then utilise to study the functions of TERT in human cells. To study these functions, I would transiently induce the overexpression of TERT and ΔTERT using the transgenes mRNA, and then use bulk RNA sequencing of the cultured cells to determine how the expression profiles had changed. I would also look at the effects of the potential transgenes on non-canonical functions of TERT that have been reported(145). For example, I may look to induce mitochondrial dysfunction in the cells and then determine if induction of the transgenes protected the mitochondria from damage. Additionally, I would examine the regulation of pathways associated with TERT non-canonical functions, such as the PPAR pathway, to determine if overexpression of TERT or ΔTERT also influenced these pathways in a manner similar to that reported with endogenous TERT(324).

Finally, I would like to reiterate that with ageing a noticeable decrease in the function of the immune system is observed termed immunosenescence (84). Immunosenescence leads to a decreased ability to mount an effective response to disease and inhibits the effectiveness of vaccines. Further, immunosenescence of specific cell subsets leads to an increase in inflammation, contributing to the inflammageing phenotype(87). Therefore, it is imperative that we advance our understanding of immunosenescence and begin to understand how we may develop therapies that ameliorate the effects of immunosenescence. We are already seeing reports of the reintroduction of TERT expression using lentiviral vectors in mice(190). However, the well-founded concern of the reintroduction of TERT expression leading to increased incidence of cancer has not been completely explored. Therefore, by establishing the *mpeg1.1:tert-gfp* and *mpeg1.1:Δtert-gfp* transgenic lines I have provided additional tools with which we can study the complex interaction of TERT and telomerase in the ageing paradigm and further elucidate how rescuing TERT and ΔTERT in an immune cell specific manner may rescue immunosenescence and potentially whole organism ageing. Eventually, it is my goal that this may contribute to a novel therapy designed to alleviate the impacts of immunosenescence in the elderly based on the rescue of the non-canonical functions of TERT.

7. Bibliography

1. Fahy GM, Brooke RT, Watson JP, Good Z, Vasanawala SS, Maecker H, et al. Reversal of epigenetic aging and immunosenescent trends in humans. Aging Cell. 2019;18(6):e13028.
2. Pomatto LCD, Davies KJA. The role of declining adaptive homeostasis in ageing. J Physiol. 2017;595(24):7275-309.
3. Rudnicka E, Napierala P, Podfigurna A, Meczekalski B, Smolarczyk R, Grymowicz M. The World Health Organization (WHO) approach to healthy ageing. Maturitas. 2020;139:6-11.
4. Divo MJ, Martinez CH, Mannino DM. Ageing and the epidemiology of multimorbidity. Eur Respir J. 2014;44(4):1055-68.
5. Kingston A, Robinson L, Booth H, Knapp M, Jagger C, project M. Projections of multi-morbidity in the older population in England to 2035: estimates from the Population Ageing and Care Simulation (PACSim) model. Age Ageing. 2018;47(3):374-80.
6. Fabbri LM, Rabe KF. From COPD to chronic systemic inflammatory syndrome? Lancet. 2007;370(9589):797-9.
7. Marengoni A, Angleman S, Melis R, Mangialasche F, Karp A, Garmen A, et al. Aging with multimorbidity: a systematic review of the literature. Ageing Res Rev. 2011;10(4):430-9.
8. Bahler C, Huber CA, Brungger B, Reich O. Multimorbidity, health care utilization and costs in an elderly community-dwelling population: a claims data based observational study. BMC Health Serv Res. 2015;15:23.
9. Stokes J, Guthrie B, Mercer SW, Rice N, Sutton M. Multimorbidity combinations, costs of hospital care and potentially preventable emergency admissions in England: A cohort study. PLoS Med. 2021;18(1):e1003514.
10. Yoon J, Zulman D, Scott JY, Maciejewski ML. Costs associated with multimorbidity among VA patients. Med Care. 2014;52 Suppl 3:S31-6.
11. Rattan SIS. Biogerontology: research status, challenges and opportunities. Acta Biomed. 2018;89(2):291-301.
12. Lopez-Otin C, Blasco MA, Partridge L, Serrano M, Kroemer G. The hallmarks of aging. Cell. 2013;153(6):1194-217.
13. Garmany A, Yamada S, Terzic A. Longevity leap: mind the healthspan gap. NPJ Regen Med. 2021;6(1):57.
14. Levine ME, Lu AT, Quach A, Chen BH, Assimes TL, Bandinelli S, et al. An epigenetic biomarker of aging for lifespan and healthspan. Aging (Albany NY). 2018;10(4):573-91.
15. Morris BJ, Willcox BJ, Donlon TA. Genetic and epigenetic regulation of human aging and longevity. Biochim Biophys Acta Mol Basis Dis. 2019;1865(7):1718-44.
16. Kaeberlein M. How healthy is the healthspan concept? Geroscience. 2018;40(4):361-4.
17. Queen NJ, Hassan QN, 2nd, Cao L. Improvements to Healthspan Through Environmental Enrichment and Lifestyle Interventions: Where Are We Now? Front Neurosci. 2020;14:605.
18. Curtis E, Litwic A, Cooper C, Dennison E. Determinants of Muscle and Bone Aging. J Cell Physiol. 2015;230(11):2618-25.

19. Statistics UKOfN. National life tables - life expectancy in the UK: 2018 to 2020 2021 [Available from: https://www.ons.gov.uk/peoplepopulationandcommunity/birthsdeathsandmarriages/lifeexpectancies/bulletins/nationallifetablesunitedkingdom/2018to2020.
20. Statistics UKOfN. Health state life expectancies, UK: 2018 to 2020 2022 [updated 4/3/2022. Available from: https://www.ons.gov.uk/peoplepopulationandcommunity/healthandsocialcare/healthandlifeexpectancies/bulletins/healthstatelifeexpectanciesuk/2018to2020.
21. Rathinam VAK, Chan FK. Inflammasome, Inflammation, and Tissue Homeostasis. Trends Mol Med. 2018;24(3):304-18.
22. Zhang F, Kerbl-Knapp J, Akhmetshina A, Korbelius M, Kuentzel KB, Vujic N, et al. Tissue-Specific Landscape of Metabolic Dysregulation during Ageing. Biomolecules. 2021;11(2).
23. Hanahan D, Weinberg RA. Hallmarks of cancer: the next generation. Cell. 2011;144(5):646-74.
24. Clarke TL, Mostoslavsky R. DNA repair as a shared hallmark in cancer and ageing. Mol Oncol. 2022;16(18):3352-79.
25. Simon M, Yang J, Gigas J, Earley EJ, Hillpot E, Zhang L, et al. A rare human centenarian variant of SIRT6 enhances genome stability and interaction with Lamin A. EMBO J. 2022;41(21):e110393.
26. Pinho S, Frenette PS. Haematopoietic stem cell activity and interactions with the niche. Nat Rev Mol Cell Biol. 2019;20(5):303-20.
27. Jaiswal S, Ebert BL. Clonal hematopoiesis in human aging and disease. Science. 2019;366(6465).
28. Jaiswal S, Libby P. Clonal haematopoiesis: connecting ageing and inflammation in cardiovascular disease. Nat Rev Cardiol. 2020;17(3):137-44.
29. Kane AE, Sinclair DA. Epigenetic changes during aging and their reprogramming potential. Crit Rev Biochem Mol Biol. 2019;54(1):61-83.
30. Hannum G, Guinney J, Zhao L, Zhang L, Hughes G, Sadda S, et al. Genome-wide methylation profiles reveal quantitative views of human aging rates. Mol Cell. 2013;49(2):359-67.
31. Horvath S. DNA methylation age of human tissues and cell types. Genome Biol. 2013;14(10):R115.
32. Bocklandt S, Lin W, Sehl ME, Sanchez FJ, Sinsheimer JS, Horvath S, et al. Epigenetic predictor of age. PLoS One. 2011;6(6):e14821.
33. Higham J, Kerr L, Zhang Q, Walker RM, Harris SE, Howard DM, et al. Local CpG density affects the trajectory and variance of age-associated DNA methylation changes. Genome Biol. 2022;23(1):216.
34. Hillje R, Luzi L, Amatori S, Persico G, Casciaro F, Rusin M, et al. Time makes histone H3 modifications drift in mouse liver. Aging (Albany NY). 2022;14(12):4959-75.
35. Kugel S, Sebastian C, Fitamant J, Ross KN, Saha SK, Jain E, et al. SIRT6 Suppresses Pancreatic Cancer through Control of Lin28b. Cell. 2016;165(6):1401-15.
36. Huang M, Xu L, Liu J, Huang P, Tan Y, Chen S. Cell-Cell Communication Alterations via Intercellular Signaling Pathways in Substantia Nigra of Parkinson's Disease. Front Aging Neurosci. 2022;14:828457.
37. Hayat R, Manzoor M, Hussain A. Wnt signaling pathway: A comprehensive review. Cell Biol Int. 2022;46(6):863-77.

38. Funk MC, Zhou J, Boutros M. Ageing, metabolism and the intestine. EMBO Rep. 2020;21(7):e50047.
39. Flores EM, Nguyen AT, Odem MA, Eisenhoffer GT, Krachler AM. The zebrafish as a model for gastrointestinal tract-microbe interactions. Cell Microbiol. 2020;22(3):e13152.
40. Roberts S, Colombier P, Sowman A, Mennan C, Rolfing JH, Guicheux J, et al. Ageing in the musculoskeletal system. Acta Orthop. 2016;87(sup363):15-25.
41. Camernik K, Mihelic A, Mihalic R, Marolt Presen D, Janez A, Trebse R, et al. Increased Exhaustion of the Subchondral Bone-Derived Mesenchymal Stem/ Stromal Cells in Primary Versus Dysplastic Osteoarthritis. Stem Cell Rev Rep. 2020;16(4):742-54.
42. Zhou BO, Yue R, Murphy MM, Peyer JG, Morrison SJ. Leptin-receptor-expressing mesenchymal stromal cells represent the main source of bone formed by adult bone marrow. Cell Stem Cell. 2014;15(2):154-68.
43. Wu NN, Zhang Y, Ren J. Mitophagy, Mitochondrial Dynamics, and Homeostasis in Cardiovascular Aging. Oxid Med Cell Longev. 2019;2019:9825061.
44. Chaudhari SN, Kipreos ET. Increased mitochondrial fusion allows the survival of older animals in diverse C. elegans longevity pathways. Nat Commun. 2017;8(1):182.
45. Ham PB, 3rd, Raju R. Mitochondrial function in hypoxic ischemic injury and influence of aging. Prog Neurobiol. 2017;157:92-116.
46. Summer R, Shaghaghi H, Schriner D, Roque W, Sales D, Cuevas-Mora K, et al. Activation of the mTORC1/PGC-1 axis promotes mitochondrial biogenesis and induces cellular senescence in the lung epithelium. Am J Physiol Lung Cell Mol Physiol. 2019;316(6):L1049-L60.
47. Childs BG, Gluscevic M, Baker DJ, Laberge RM, Marquess D, Dananberg J, et al. Senescent cells: an emerging target for diseases of ageing. Nat Rev Drug Discov. 2017;16(10):718-35.
48. Baker DJ, Childs BG, Durik M, Wijers ME, Sieben CJ, Zhong J, et al. Naturally occurring p16(Ink4a)-positive cells shorten healthy lifespan. Nature. 2016;530(7589):184-9.
49. van Deursen JM. The role of senescent cells in ageing. Nature. 2014;509(7501):439-46.
50. Campisi J, d'Adda di Fagagna F. Cellular senescence: when bad things happen to good cells. Nat Rev Mol Cell Biol. 2007;8(9):729-40.
51. Hayflick L, Moorhead PS. The serial cultivation of human diploid cell strains. Exp Cell Res. 1961;25:585-621.
52. Slawinska N, Krupa R. Molecular Aspects of Senescence and Organismal Ageing-DNA Damage Response, Telomeres, Inflammation and Chromatin. Int J Mol Sci. 2021;22(2).
53. Martens UM, Chavez EA, Poon SS, Schmoor C, Lansdorp PM. Accumulation of short telomeres in human fibroblasts prior to replicative senescence. Exp Cell Res. 2000;256(1):291-9.
54. Campisi J. Aging, cellular senescence, and cancer. Annu Rev Physiol. 2013;75:685-705.
55. Childs BG, Baker DJ, Kirkland JL, Campisi J, van Deursen JM. Senescence and apoptosis: dueling or complementary cell fates? EMBO Rep. 2014;15(11):1139-53.
56. Austad SN, Hoffman JM. Is antagonistic pleiotropy ubiquitous in aging biology? Evol Med Public Health. 2018;2018(1):287-94.
57. Kritsilis M, S VR, Koutsoudaki PN, Evangelou K, Gorgoulis VG, Papadopoulos D. Ageing, Cellular Senescence and Neurodegenerative Disease. Int J Mol Sci. 2018;19(10).

58. Baker DJ, Wijshake T, Tchkonia T, LeBrasseur NK, Childs BG, van de Sluis B, et al. Clearance of p16Ink4a-positive senescent cells delays ageing-associated disorders. Nature. 2011;479(7372):232-6.
59. Baker DJ, Perez-Terzic C, Jin F, Pitel KS, Niederlander NJ, Jeganathan K, et al. Opposing roles for p16Ink4a and p19Arf in senescence and ageing caused by BubR1 insufficiency. Nat Cell Biol. 2008;10(7):825-36.
60. Carnero A. Markers of cellular senescence. Methods Mol Biol. 2013;965:63-81.
61. Marhenke S, Buitrago-Molina LE, Endig J, Orlik J, Schweitzer N, Klett S, et al. p21 promotes sustained liver regeneration and hepatocarcinogenesis in chronic cholestatic liver injury. Gut. 2014;63(9):1501-12.
62. Rodriguez JA, Marigorta UM, Hughes DA, Spataro N, Bosch E, Navarro A. Antagonistic pleiotropy and mutation accumulation influence human senescence and disease. Nat Ecol Evol. 2017;1(3):55.
63. Jia HJ, Zhou M, Vashisth MK, Xia J, Hua H, Dai QL, et al. Trifluridine induces HUVECs senescence by inhibiting mTOR-dependent autophagy. Biochem Biophys Res Commun. 2022;610:119-26.
64. Itahana K, Campisi J, Dimri GP. Methods to detect biomarkers of cellular senescence: the senescence-associated beta-galactosidase assay. Methods Mol Biol. 2007;371:21-31.
65. Terman A, Brunk UT. On the degradability and exocytosis of ceroid/lipofuscin in cultured rat cardiac myocytes. Mech Ageing Dev. 1998;100(2):145-56.
66. Song L, Wu F, Li C, Zhang S. Dietary intake of GDF11 delays the onset of several biomarkers of aging in male mice through anti-oxidant system via Smad2/3 pathway. Biogerontology. 2022.
67. Bodnar AG, Ouellette M, Frolkis M, Holt SE, Chiu CP, Morin GB, et al. Extension of life-span by introduction of telomerase into normal human cells. Science. 1998;279(5349):349-52.
68. Gemberling M, Karra R, Dickson AL, Poss KD. Nrg1 is an injury-induced cardiomyocyte mitogen for the endogenous heart regeneration program in zebrafish. Elife. 2015;4.
69. Takahashi A, Ohtani N, Yamakoshi K, Iida S, Tahara H, Nakayama K, et al. Mitogenic signalling and the p16INK4a-Rb pathway cooperate to enforce irreversible cellular senescence. Nat Cell Biol. 2006;8(11):1291-7.
70. Toussaint O, Medrano EE, von Zglinicki T. Cellular and molecular mechanisms of stress-induced premature senescence (SIPS) of human diploid fibroblasts and melanocytes. Exp Gerontol. 2000;35(8):927-45.
71. Di Micco R, Cicalese A, Fumagalli M, Dobreva M, Verrecchia A, Pelicci PG, et al. DNA damage response activation in mouse embryonic fibroblasts undergoing replicative senescence and following spontaneous immortalization. Cell Cycle. 2008;7(22):3601-6.
72. Raghuram GV, Mishra PK. Stress induced premature senescence: a new culprit in ovarian tumorigenesis? Indian J Med Res. 2014;140 Suppl:S120-9.
73. Wyld L, Bellantuono I, Tchkonia T, Morgan J, Turner O, Foss F, et al. Senescence and Cancer: A Review of Clinical Implications of Senescence and Senotherapies. Cancers (Basel). 2020;12(8).
74. Kuilman T, Michaloglou C, Vredeveld LC, Douma S, van Doorn R, Desmet CJ, et al. Oncogene-induced senescence relayed by an interleukin-dependent inflammatory network. Cell. 2008;133(6):1019-31.

75. Furukawa A, Tada-Oikawa S, Kawanishi S, Oikawa S. H2O2 accelerates cellular senescence by accumulation of acetylated p53 via decrease in the function of SIRT1 by NAD+ depletion. Cell Physiol Biochem. 2007;20(1-4):45-54.
76. Coppe JP, Patil CK, Rodier F, Sun Y, Munoz DP, Goldstein J, et al. Senescence-associated secretory phenotypes reveal cell-nonautonomous functions of oncogenic RAS and the p53 tumor suppressor. PLoS Biol. 2008;6(12):2853-68.
77. Franceschi C, Garagnani P, Vitale G, Capri M, Salvioli S. Inflammaging and 'Garb-aging'. Trends Endocrinol Metab. 2017;28(3):199-212.
78. Ferrucci L, Fabbri E. Inflammageing: chronic inflammation in ageing, cardiovascular disease, and frailty. Nat Rev Cardiol. 2018;15(9):505-22.
79. Fulop T, Larbi A, Pawelec G, Khalil A, Cohen AA, Hirokawa K, et al. Immunology of Aging: the Birth of Inflammaging. Clin Rev Allergy Immunol. 2021.
80. Biran A, Zada L, Abou Karam P, Vadai E, Roitman L, Ovadya Y, et al. Quantitative identification of senescent cells in aging and disease. Aging Cell. 2017;16(4):661-71.
81. Yao C, Guan X, Carraro G, Parimon T, Liu X, Huang G, et al. Senescence of Alveolar Type 2 Cells Drives Progressive Pulmonary Fibrosis. Am J Respir Crit Care Med. 2021;203(6):707-17.
82. Aghali A, Khalfaoui L, Lagnado AB, Drake LY, Teske JJ, Pabelick CM, et al. Cellular senescence is increased in airway smooth muscle cells of elderly persons with asthma. Am J Physiol Lung Cell Mol Physiol. 2022;323(5):L558-L68.
83. Jeon OH, Kim C, Laberge RM, Demaria M, Rathod S, Vasserot AP, et al. Local clearance of senescent cells attenuates the development of post-traumatic osteoarthritis and creates a pro-regenerative environment. Nat Med. 2017;23(6):775-81.
84. Peilin W, Songsong T, Chengyu Z, Zhi C, Chunhui M, Yinxian Y, et al. Directed elimination of senescent cells attenuates development of osteoarthritis by inhibition of c-IAP and XIAP. Biochim Biophys Acta Mol Basis Dis. 2019;1865(10):2618-32.
85. Crooke SN, Ovsyannikova IG, Poland GA, Kennedy RB. Immunosenescence: A systems-level overview of immune cell biology and strategies for improving vaccine responses. Exp Gerontol. 2019;124:110632.
86. Barbe-Tuana F, Funchal G, Schmitz CRR, Maurmann RM, Bauer ME. The interplay between immunosenescence and age-related diseases. Semin Immunopathol. 2020;42(5):545-57.
87. Pawelec G. Age and immunity: What is "immunosenescence"? Exp Gerontol. 2018;105:4-9.
88. Lewis ED, Wu D, Meydani SN. Age-associated alterations in immune function and inflammation. Prog Neuropsychopharmacol Biol Psychiatry. 2022:110576.
89. Weiskopf D, Weinberger B, Grubeck-Loebenstein B. The aging of the immune system. Transpl Int. 2009;22(11):1041-50.
90. Wagner A, Garner-Spitzer E, Jasinska J, Kollaritsch H, Stiasny K, Kundi M, et al. Age-related differences in humoral and cellular immune responses after primary immunisation: indications for stratified vaccination schedules. Sci Rep. 2018;8(1):9825.
91. Unanue ER. Antigen-presenting function of the macrophage. Annu Rev Immunol. 1984;2:395-428.
92. Alexander KA, Chang MK, Maylin ER, Kohler T, Muller R, Wu AC, et al. Osteal macrophages promote in vivo intramembranous bone healing in a mouse tibial injury model. J Bone Miner Res. 2011;26(7):1517-32.

93. Aurora AB, Porrello ER, Tan W, Mahmoud AI, Hill JA, Bassel-Duby R, et al. Macrophages are required for neonatal heart regeneration. J Clin Invest. 2014;124(3):1382-92.
94. Simkin J, Gawriluk TR, Gensel JC, Seifert AW. Macrophages are necessary for epimorphic regeneration in African spiny mice. Elife. 2017;6.
95. Hesketh M, Sahin KB, West ZE, Murray RZ. Macrophage Phenotypes Regulate Scar Formation and Chronic Wound Healing. Int J Mol Sci. 2017;18(7).
96. Pridans C, Raper A, Davis GM, Alves J, Sauter KA, Lefevre L, et al. Pleiotropic Impacts of Macrophage and Microglial Deficiency on Development in Rats with Targeted Mutation of the Csf1r Locus. J Immunol. 2018;201(9):2683-99.
97. Wallis ZK, Williams KC. Monocytes in HIV and SIV Infection and Aging: Implications for Inflamm-Aging and Accelerated Aging. Viruses. 2022;14(2).
98. Salminen A. Clinical perspectives on the age-related increase of immunosuppressive activity. J Mol Med (Berl). 2022;100(5):697-712.
99. Alves AS, Bueno V. Immunosenescence: participation of T lymphocytes and myeloid-derived suppressor cells in aging-related immune response changes. Einstein (Sao Paulo). 2019;17(2):eRB4733.
100. Childs BG, Baker DJ, Wijshake T, Conover CA, Campisi J, van Deursen JM. Senescent intimal foam cells are deleterious at all stages of atherosclerosis. Science. 2016;354(6311):472-7.
101. Eshghjoo S, Kim DM, Jayaraman A, Sun Y, Alaniz RC. Macrophage Polarization in Atherosclerosis. Genes (Basel). 2022;13(5).
102. Tyciakova S, Valova V, Svitkova B, Matuskova M. Overexpression of TNFalpha induces senescence, autophagy and mitochondrial dysfunctions in melanoma cells. BMC Cancer. 2021;21(1):507.
103. Han L, Zhang Y, Zhang M, Guo L, Wang J, Zeng F, et al. Interleukin-1beta-Induced Senescence Promotes Osteoblastic Transition of Vascular Smooth Muscle Cells. Kidney Blood Press Res. 2020;45(2):314-30.
104. Van den Bossche J, Leenen PJM. Keep your macrophages fit for healthy aging. Cell Metab. 2021;33(3):468-70.
105. Minhas PS, Latif-Hernandez A, McReynolds MR, Durairaj AS, Wang Q, Rubin A, et al. Restoring metabolism of myeloid cells reverses cognitive decline in ageing. Nature. 2021;590(7844):122-8.
106. Crooke SN, Ovsyannikova IG, Poland GA, Kennedy RB. Immunosenescence and human vaccine immune responses. Immun Ageing. 2019;16:25.
107. St Paul M, Ohashi PS. The Roles of CD8(+) T Cell Subsets in Antitumor Immunity. Trends Cell Biol. 2020;30(9):695-704.
108. Zhang M, Wang G, Ma Z, Xiong G, Wang W, Huang Z, et al. BET inhibition triggers antitumor immunity by enhancing MHC class I expression in head and neck squamous cell carcinoma. Mol Ther. 2022;30(11):3394-413.
109. Plitas G, Rudensky AY. Regulatory T Cells: Differentiation and Function. Cancer Immunol Res. 2016;4(9):721-5.
110. Atif M, Cherai M, Miyara M. Phenotypic and Functional Studies of Human Treg Cell Subpopulations. Methods Mol Biol. 2023;2559:153-69.
111. Palmer S, Albergante L, Blackburn CC, Newman TJ. Thymic involution and rising disease incidence with age. Proc Natl Acad Sci U S A. 2018;115(8):1883-8.

112. Tedeschi V, Paldino G, Kunkl M, Paroli M, Sorrentino R, Tuosto L, et al. CD8(+) T Cell Senescence: Lights and Shadows in Viral Infections, Autoimmune Disorders and Cancer. Int J Mol Sci. 2022;23(6).
113. Morris SR, Chen B, Mudd JC, Panigrahi S, Shive CL, Sieg SF, et al. Inflammescent CX3CR1+CD57+CD8+ T cells are generated and expanded by IL-15. JCI Insight. 2020;5(11).
114. Selvarani R, Mohammed S, Richardson A. Effect of rapamycin on aging and age-related diseases-past and future. Geroscience. 2021;43(3):1135-58.
115. Yousefzadeh MJ, Flores RR, Zhu Y, Schmiechen ZC, Brooks RW, Trussoni CE, et al. An aged immune system drives senescence and ageing of solid organs. Nature. 2021;594(7861):100-5.
116. Kataru RP, Jung K, Jang C, Yang H, Schwendener RA, Baik JE, et al. Critical role of CD11b+ macrophages and VEGF in inflammatory lymphangiogenesis, antigen clearance, and inflammation resolution. Blood. 2009;113(22):5650-9.
117. Riethman H. Human telomere structure and biology. Annu Rev Genomics Hum Genet. 2008;9:1-19.
118. Xin H, Liu D, Songyang Z. The telosome/shelterin complex and its functions. Genome Biol. 2008;9(9):232.
119. Levy MZ, Allsopp RC, Futcher AB, Greider CW, Harley CB. Telomere end-replication problem and cell aging. J Mol Biol. 1992;225(4):951-60.
120. Ferreira MG, Miller KM, Cooper JP. Indecent exposure: when telomeres become uncapped. Mol Cell. 2004;13(1):7-18.
121. Campisi J. The biology of replicative senescence. Eur J Cancer. 1997;33(5):703-9.
122. Lipps HJ, Rhodes D. G-quadruplex structures: in vivo evidence and function. Trends Cell Biol. 2009;19(8):414-22.
123. Ghanim GE, Fountain AJ, van Roon AM, Rangan R, Das R, Collins K, et al. Structure of human telomerase holoenzyme with bound telomeric DNA. Nature. 2021;593(7859):449-53.
124. Chan H, Wang Y, Feigon J. Progress in Human and Tetrahymena Telomerase Structure Determination. Annu Rev Biophys. 2017;46:199-225.
125. Venteicher AS, Meng Z, Mason PJ, Veenstra TD, Artandi SE. Identification of ATPases pontin and reptin as telomerase components essential for holoenzyme assembly. Cell. 2008;132(6):945-57.
126. Rubtsova M, Dontsova O. Human Telomerase RNA: Telomerase Component or More? Biomolecules. 2020;10(6).
127. Khattar E, Kumar P, Liu CY, Akincilar SC, Raju A, Lakshmanan M, et al. Telomerase reverse transcriptase promotes cancer cell proliferation by augmenting tRNA expression. J Clin Invest. 2016;126(10):4045-60.
128. Ahmed R, Roger L, Costa Del Amo P, Miners KL, Jones RE, Boelen L, et al. Human Stem Cell-like Memory T Cells Are Maintained in a State of Dynamic Flux. Cell Rep. 2016;17(11):2811-8.
129. Pech MF, Garbuzov A, Hasegawa K, Sukhwani M, Zhang RJ, Benayoun BA, et al. High telomerase is a hallmark of undifferentiated spermatogonia and is required for maintenance of male germline stem cells. Genes Dev. 2015;29(23):2420-34.
130. Cong YS, Wright WE, Shay JW. Human telomerase and its regulation. Microbiol Mol Biol Rev. 2002;66(3):407-25, table of contents.
131. Avilion AA, Piatyszek MA, Gupta J, Shay JW, Bacchetti S, Greider CW. Human telomerase RNA and telomerase activity in immortal cell lines and tumor tissues. Cancer Res. 1996;56(3):645-50.

132. Saretzki G. Extra-telomeric functions of human telomerase: cancer, mitochondria and oxidative stress. Curr Pharm Des. 2014;20(41):6386-403.
133. Jiang J, Wang Y, Susac L, Chan H, Basu R, Zhou ZH, et al. Structure of Telomerase with Telomeric DNA. Cell. 2018;173(5):1179-90 e13.
134. Martinez P, Blasco MA. Telomeric and extra-telomeric roles for telomerase and the telomere-binding proteins. Nat Rev Cancer. 2011;11(3):161-76.
135. Seimiya H, Tanji M, Oh-hara T, Tomida A, Naasani I, Tsuruo T. Hypoxia up-regulates telomerase activity via mitogen-activated protein kinase signaling in human solid tumor cells. Biochem Biophys Res Commun. 1999;260(2):365-70.
136. Kang SS, Kwon T, Kwon DY, Do SI. Akt protein kinase enhances human telomerase activity through phosphorylation of telomerase reverse transcriptase subunit. J Biol Chem. 1999;274(19):13085-90.
137. Haendeler J, Hoffmann J, Rahman S, Zeiher AM, Dimmeler S. Regulation of telomerase activity and anti-apoptotic function by protein-protein interaction and phosphorylation. FEBS Lett. 2003;536(1-3):180-6.
138. Patrick S, Gowda P, Lathoria K, Suri V, Sen E. YAP1-mediated regulation of mitochondrial dynamics in IDH1 mutant gliomas. J Cell Sci. 2021;134(22).
139. Haendeler J, Drose S, Buchner N, Jakob S, Altschmied J, Goy C, et al. Mitochondrial telomerase reverse transcriptase binds to and protects mitochondrial DNA and function from damage. Arterioscler Thromb Vasc Biol. 2009;29(6):929-35.
140. Spilsbury A, Miwa S, Attems J, Saretzki G. The role of telomerase protein TERT in Alzheimer's disease and in tau-related pathology in vitro. J Neurosci. 2015;35(4):1659-74.
141. Hu Q, Liu XM, Liu ZR, Liu ZY, Zhang HG, Zhang Q, et al. Dexmedetomidine reduces enteric glial cell injury induced by intestinal ischaemia-reperfusion injury through mitochondrial localization of TERT. J Cell Mol Med. 2022;26(9):2594-606.
142. Zhou QG, Liu MY, Lee HW, Ishikawa F, Devkota S, Shen XR, et al. Hippocampal TERT Regulates Spatial Memory Formation through Modulation of Neural Development. Stem Cell Reports. 2017;9(2):543-56.
143. Cesca F, Baldelli P, Valtorta F, Benfenati F. The synapsins: key actors of synapse function and plasticity. Prog Neurobiol. 2010;91(4):313-48.
144. Florian C, Roullet P. Hippocampal CA3-region is crucial for acquisition and memory consolidation in Morris water maze task in mice. Behav Brain Res. 2004;154(2):365-74.
145. Miwa S, Czapiewski R, Wan T, Bell A, Hill KN, von Zglinicki T, et al. Decreased mTOR signalling reduces mitochondrial ROS in brain via accumulation of the telomerase protein TERT within mitochondria. Aging (Albany NY). 2016;8(10):2551-67.
146. Gizard F, Heywood EB, Findeisen HM, Zhao Y, Jones KL, Cudejko C, et al. Telomerase activation in atherosclerosis and induction of telomerase reverse transcriptase expression by inflammatory stimuli in macrophages. Arterioscler Thromb Vasc Biol. 2011;31(2):245-52.
147. Wu XQ, Yang Y, Li WX, Cheng YH, Li XF, Huang C, et al. Telomerase reverse transcriptase acts in a feedback loop with NF-kappaB pathway to regulate macrophage polarization in alcoholic liver disease. Sci Rep. 2016;6:18685.
148. Kato M, Putta S, Wang M, Yuan H, Lanting L, Nair I, et al. TGF-beta activates Akt kinase through a microRNA-dependent amplifying circuit targeting PTEN. Nat Cell Biol. 2009;11(7):881-9.
149. Yang S, Li J, Chen Y, Zhang S, Feng C, Hou Z, et al. MicroRNA-216a promotes M1 macrophages polarization and atherosclerosis progression by activating telomerase via the Smad3/NF-kappaB pathway. Biochim Biophys Acta Mol Basis Dis. 2019;1865(7):1772-81.

150. Chen HM, Wang LQ, Wan HP, Wei HZ, Ke LC, Liu CY, et al. Study on the functions and mechanism of immune functions of human telomerase reverse transcriptase regulating dendritic cells treating sepsis. Eur Rev Med Pharmacol Sci. 2016;20(21):4500-7.
151. Edwards JR, Perrien DS, Fleming N, Nyman JS, Ono K, Connelly L, et al. Silent information regulator (Sir)T1 inhibits NF-kappaB signaling to maintain normal skeletal remodeling. J Bone Miner Res. 2013;28(4):960-9.
152. Tang BL. Sirt1 and the Mitochondria. Mol Cells. 2016;39(2):87-95.
153. Zeng C, Chen M. Progress in Nonalcoholic Fatty Liver Disease: SIRT Family Regulates Mitochondrial Biogenesis. Biomolecules. 2022;12(8).
154. Costa-Beber LC, Guma F. The macrophage senescence hypothesis: the role of poor heat shock response in pulmonary inflammation and endothelial dysfunction following chronic exposure to air pollution. Inflamm Res. 2022;71(12):1433-48.
155. Liu H, Xu S, Wang C, Deng Y, Xu B, Yang T, et al. The Beneficial Role of Sirtuin 1 in Preventive or Therapeutic Options of Neurodegenerative Diseases. Neuroscience. 2022;504:79-92.
156. Chen Y, Zhou D, Feng Y, Li B, Cui Y, Chen G, et al. Association of sirtuins (SIRT1-7) with lung and intestinal diseases. Mol Cell Biochem. 2022;477(11):2539-52.
157. Pefoyo AJ, Bronskill SE, Gruneir A, Calzavara A, Thavorn K, Petrosyan Y, et al. The increasing burden and complexity of multimorbidity. BMC Public Health. 2015;15:415.
158. Tchkonia T, Morbeck DE, Von Zglinicki T, Van Deursen J, Lustgarten J, Scrable H, et al. Fat tissue, aging, and cellular senescence. Aging Cell. 2010;9(5):667-84.
159. Jura M, Kozak LP. Obesity and related consequences to ageing. Age (Dordr). 2016;38(1):23.
160. Garg SK, Maurer H, Reed K, Selagamsetty R. Diabetes and cancer: two diseases with obesity as a common risk factor. Diabetes Obes Metab. 2014;16(2):97-110.
161. Lavie CJ, De Schutter A, Parto P, Jahangir E, Kokkinos P, Ortega FB, et al. Obesity and Prevalence of Cardiovascular Diseases and Prognosis-The Obesity Paradox Updated. Prog Cardiovasc Dis. 2016;58(5):537-47.
162. Duggal NA. Reversing the immune ageing clock: lifestyle modifications and pharmacological interventions. Biogerontology. 2018;19(6):481-96.
163. Lowder T, Padgett DA, Woods JA. Moderate exercise protects mice from death due to influenza virus. Brain Behav Immun. 2005;19(5):377-80.
164. Effros RB, Walford RL, Weindruch R, Mitcheltree C. Influences of dietary restriction on immunity to influenza in aged mice. J Gerontol. 1991;46(4):B142-7.
165. Ritz BW, Gardner EM. Malnutrition and energy restriction differentially affect viral immunity. J Nutr. 2006;136(5):1141-4.
166. Kirkland JL, Tchkonia T. Senolytic drugs: from discovery to translation. J Intern Med. 2020;288(5):518-36.
167. Hu Q, Peng J, Jiang L, Li W, Su Q, Zhang J, et al. Metformin as a senostatic drug enhances the anticancer efficacy of CDK4/6 inhibitor in head and neck squamous cell carcinoma. Cell Death Dis. 2020;11(10):925.
168. Fielder E, Wan T, Alimohammadiha G, Ishaq A, Low E, Weigand BM, et al. Short senolytic or senostatic interventions rescue progression of radiation-induced frailty and premature ageing in mice. Elife. 2022;11.
169. Short S, Fielder E, Miwa S, von Zglinicki T. Senolytics and senostatics as adjuvant tumour therapy. EBioMedicine. 2019;41:683-92.

170. Zhu Y, Tchkonia T, Pirtskhalava T, Gower AC, Ding H, Giorgadze N, et al. The Achilles' heel of senescent cells: from transcriptome to senolytic drugs. Aging Cell. 2015;14(4):644-58.
171. Abou Dalle I, Jabbour E, Short NJ, Ravandi F. Treatment of Philadelphia Chromosome-Positive Acute Lymphoblastic Leukemia. Curr Treat Options Oncol. 2019;20(1):4.
172. Xu M, Pirtskhalava T, Farr JN, Weigand BM, Palmer AK, Weivoda MM, et al. Senolytics improve physical function and increase lifespan in old age. Nat Med. 2018;24(8):1246-56.
173. Justice JN, Nambiar AM, Tchkonia T, LeBrasseur NK, Pascual R, Hashmi SK, et al. Senolytics in idiopathic pulmonary fibrosis: Results from a first-in-human, open-label, pilot study. EBioMedicine. 2019;40:554-63.
174. Hickson LJ, Langhi Prata LGP, Bobart SA, Evans TK, Giorgadze N, Hashmi SK, et al. Senolytics decrease senescent cells in humans: Preliminary report from a clinical trial of Dasatinib plus Quercetin in individuals with diabetic kidney disease. EBioMedicine. 2019;47:446-56.
175. Hickson LJ, Langhi Prata LGP, Bobart SA, Evans TK, Giorgadze N, Hashmi SK, et al. Corrigendum to 'Senolytics decrease senescent cells in humans: Preliminary report from a clinical trial of Dasatinib plus Quercetin in individuals with diabetic kidney disease' EBioMedicine 47 (2019) 446-456. EBioMedicine. 2020;52:102595.
176. Yousefzadeh MJ, Zhu Y, McGowan SJ, Angelini L, Fuhrmann-Stroissnigg H, Xu M, et al. Fisetin is a senotherapeutic that extends health and lifespan. EBioMedicine. 2018;36:18-28.
177. Mbara KC, Devnarain N, Owira PMO. Potential Role of Polyphenolic Flavonoids as Senotherapeutic Agents in Degenerative Diseases and Geroprotection. Pharmaceut Med. 2022;36(6):331-52.
178. Grosse L, Wagner N, Emelyanov A, Molina C, Lacas-Gervais S, Wagner KD, et al. Defined p16(High) Senescent Cell Types Are Indispensable for Mouse Healthspan. Cell Metab. 2020;32(1):87-99 e6.
179. Demaria M, O'Leary MN, Chang J, Shao L, Liu S, Alimirah F, et al. Cellular Senescence Promotes Adverse Effects of Chemotherapy and Cancer Relapse. Cancer Discov. 2017;7(2):165-76.
180. Triggle CR, Mohammed I, Bshesh K, Marei I, Ye K, Ding H, et al. Metformin: Is it a drug for all reasons and diseases? Metabolism. 2022:155223.
181. Egashira M, Hirota Y, Shimizu-Hirota R, Saito-Fujita T, Haraguchi H, Matsumoto L, et al. F4/80+ Macrophages Contribute to Clearance of Senescent Cells in the Mouse Postpartum Uterus. Endocrinology. 2017;158(7):2344-53.
182. Sagiv A, Biran A, Yon M, Simon J, Lowe SW, Krizhanovsky V. Granule exocytosis mediates immune surveillance of senescent cells. Oncogene. 2013;32(15):1971-7.
183. Prata L, Ovsyannikova IG, Tchkonia T, Kirkland JL. Senescent cell clearance by the immune system: Emerging therapeutic opportunities. Semin Immunol. 2018;40:101275.
184. Behmoaras J, Gil J. Similarities and interplay between senescent cells and macrophages. J Cell Biol. 2021;220(2).
185. Ellis PS, Martins RR, Thompson EJ, Farhat A, Renshaw SA, Henriques CM. A subset of gut leukocytes has telomerase-dependent "hyper-long" telomeres and require telomerase for function in zebrafish. Immun Ageing. 2022;19(1):31.

186. Tasat DR, Mancuso R, O'Connor S, Molinari B. Age-dependent change in reactive oxygen species and nitric oxide generation by rat alveolar macrophages. Aging Cell. 2003;2(3):159-64.
187. Doudna JA. The promise and challenge of therapeutic genome editing. Nature. 2020;578(7794):229-36.
188. Munoz-Lorente MA, Cano-Martin AC, Blasco MA. Mice with hyper-long telomeres show less metabolic aging and longer lifespans. Nat Commun. 2019;10(1):4723.
189. Bernardes de Jesus B, Vera E, Schneeberger K, Tejera AM, Ayuso E, Bosch F, et al. Telomerase gene therapy in adult and old mice delays aging and increases longevity without increasing cancer. EMBO Mol Med. 2012;4(8):691-704.
190. Jaijyan DK, Selariu A, Cruz-Cosme R, Tong M, Yang S, Stefa A, et al. New intranasal and injectable gene therapy for healthy life extension. Proc Natl Acad Sci U S A. 2022;119(20):e2121499119.
191. Martinez P, Blasco MA. Telomere-driven diseases and telomere-targeting therapies. J Cell Biol. 2017;216(4):875-87.
192. Bar C, Blasco MA. Telomeres and telomerase as therapeutic targets to prevent and treat age-related diseases. F1000Res. 2016;5.
193. Mojiri A, Walther BK, Jiang C, Matrone G, Holgate R, Xu Q, et al. Telomerase therapy reverses vascular senescence and extends lifespan in progeria mice. Eur Heart J. 2021;42(42):4352-69.
194. Kachroo AH, Laurent JM, Yellman CM, Meyer AG, Wilke CO, Marcotte EM. Evolution. Systematic humanization of yeast genes reveals conserved functions and genetic modularity. Science. 2015;348(6237):921-5.
195. Zimmermann A, Hofer S, Pendl T, Kainz K, Madeo F, Carmona-Gutierrez D. Yeast as a tool to identify anti-aging compounds. FEMS Yeast Res. 2018;18(6).
196. He C, Zhou C, Kennedy BK. The yeast replicative aging model. Biochim Biophys Acta Mol Basis Dis. 2018;1864(9 Pt A):2690-6.
197. Egan BM, Scharf A, Pohl F, Kornfeld K. Control of aging by the renin-angiotensin system: a review of C. elegans, Drosophila, and mammals. Front Pharmacol. 2022;13:938650.
198. Tullet JMA, Green JW, Au C, Benedetto A, Thompson MA, Clark E, et al. The SKN-1/Nrf2 transcription factor can protect against oxidative stress and increase lifespan in C. elegans by distinct mechanisms. Aging Cell. 2017;16(5):1191-4.
199. Hesp K, Smant G, Kammenga JE. Caenorhabditis elegans DAF-16/FOXO transcription factor and its mammalian homologs associate with age-related disease. Exp Gerontol. 2015;72:1-7.
200. Bayat M, Tanny RE, Wang Y, Herden C, Daniel J, Andersen EC, et al. Effects of telomerase overexpression in the model organism Caenorhabditis elegans. Gene. 2020;732:144367.
201. Adams MD, Celniker SE, Holt RA, Evans CA, Gocayne JD, Amanatides PG, et al. The genome sequence of Drosophila melanogaster. Science. 2000;287(5461):2185-95.
202. Pardue ML, DeBaryshe PG. Retrotransposons that maintain chromosome ends. Proc Natl Acad Sci U S A. 2011;108(51):20317-24.
203. Kordyukova M, Olovnikov I, Kalmykova A. Transposon control mechanisms in telomere biology. Curr Opin Genet Dev. 2018;49:56-62.

204. Biessmann H, Champion LE, O'Hair M, Ikenaga K, Kasravi B, Mason JM. Frequent transpositions of Drosophila melanogaster HeT-A transposable elements to receding chromosome ends. EMBO J. 1992;11(12):4459-69.
205. Ma M, Moulton MJ, Lu S, Bellen HJ. 'Fly-ing' from rare to common neurodegenerative disease mechanisms. Trends Genet. 2022;38(9):972-84.
206. Orr WC, Radyuk SN, Sohal RS. Involvement of redox state in the aging of Drosophila melanogaster. Antioxid Redox Signal. 2013;19(8):788-803.
207. Varga M. The Doctor of Delayed Publications: The Remarkable Life of George Streisinger (1927-1984). Zebrafish. 2018;15(3):314-9.
208. Rosa JGS, Lima C, Lopes-Ferreira M. Zebrafish Larvae Behavior Models as a Tool for Drug Screenings and Pre-Clinical Trials: A Review. Int J Mol Sci. 2022;23(12).
209. Astell KR, Sieger D. Zebrafish In Vivo Models of Cancer and Metastasis. Cold Spring Harb Perspect Med. 2020;10(8).
210. Gore AV, Pillay LM, Venero Galanternik M, Weinstein BM. The zebrafish: A fintastic model for hematopoietic development and disease. Wiley Interdiscip Rev Dev Biol. 2018;7(3):e312.
211. Shi W, Fang Z, Li L, Luo L. Using zebrafish as the model organism to understand organ regeneration. Sci China Life Sci. 2015;58(4):343-51.
212. Alestrom P, D'Angelo L, Midtlyng PJ, Schorderet DF, Schulte-Merker S, Sohm F, et al. Zebrafish: Housing and husbandry recommendations. Lab Anim. 2020;54(3):213-24.
213. Van Houcke J, De Groef L, Dekeyster E, Moons L. The zebrafish as a gerontology model in nervous system aging, disease, and repair. Ageing Res Rev. 2015;24(Pt B):358-68.
214. Goldsmith JR, Jobin C. Think small: zebrafish as a model system of human pathology. J Biomed Biotechnol. 2012;2012:817341.
215. Howe K, Clark MD, Torroja CF, Torrance J, Berthelot C, Muffato M, et al. The zebrafish reference genome sequence and its relationship to the human genome. Nature. 2013;496(7446):498-503.
216. Rafferty SA, Quinn TA. A beginner's guide to understanding and implementing the genetic modification of zebrafish. Prog Biophys Mol Biol. 2018;138:3-19.
217. Sharma P, Sharma BS, Verma RJ. CRISPR-based genome editing of zebrafish. Prog Mol Biol Transl Sci. 2021;180:69-84.
218. Henriques CM, Carneiro MC, Tenente IM, Jacinto A, Ferreira MG. Telomerase is required for zebrafish lifespan. PLoS Genet. 2013;9(1):e1003214.
219. Carneiro MC, de Castro IP, Ferreira MG. Telomeres in aging and disease: lessons from zebrafish. Dis Model Mech. 2016;9(7):737-48.
220. Carneiro MC, Henriques CM, Nabais J, Ferreira T, Carvalho T, Ferreira MG. Short Telomeres in Key Tissues Initiate Local and Systemic Aging in Zebrafish. PLoS Genet. 2016;12(1):e1005798.
221. Paramos-de-Carvalho D, Martins I, Cristovao AM, Dias AF, Neves-Silva D, Pereira T, et al. Targeting senescent cells improves functional recovery after spinal cord injury. Cell Rep. 2021;36(1):109334.
222. Anchelin M, Alcaraz-Perez F, Martinez CM, Bernabe-Garcia M, Mulero V, Cayuela ML. Premature aging in telomerase-deficient zebrafish. Dis Model Mech. 2013;6(5):1101-12.
223. Brugman S. The zebrafish as a model to study intestinal inflammation. Dev Comp Immunol. 2016;64:82-92.

224. Bailone RL, Fukushima HCS, Ventura Fernandes BH, De Aguiar LK, Correa T, Janke H, et al. Zebrafish as an alternative animal model in human and animal vaccination research. Lab Anim Res. 2020;36:13.
225. Choe CP, Choi SY, Kee Y, Kim MJ, Kim SH, Lee Y, et al. Transgenic fluorescent zebrafish lines that have revolutionized biomedical research. Lab Anim Res. 2021;37(1):26.
226. Ellett F, Pase L, Hayman JW, Andrianopoulos A, Lieschke GJ. mpeg1 promoter transgenes direct macrophage-lineage expression in zebrafish. Blood. 2011;117(4):e49-56.
227. Nguyen-Chi M, Laplace-Builhe B, Travnickova J, Luz-Crawford P, Tejedor G, Phan QT, et al. Identification of polarized macrophage subsets in zebrafish. Elife. 2015;4:e07288.
228. Whitlock B. Telomere Length and Arsenic: Improving Animal Models of Toxicity by Choosing Mice With Shorter Telomeres. Int J Toxicol. 2021;40(3):211-7.
229. Amano H, Chaudhury A, Rodriguez-Aguayo C, Lu L, Akhanov V, Catic A, et al. Telomere Dysfunction Induces Sirtuin Repression that Drives Telomere-Dependent Disease. Cell Metab. 2019;29(6):1274-90 e9.
230. Vazquez BN, Thackray JK, Serrano L. Sirtuins and DNA damage repair: SIRT7 comes to play. Nucleus. 2017;8(2):107-15.
231. Martinez P, Blasco MA. Heart-Breaking Telomeres. Circ Res. 2018;123(7):787-802.
232. Calado RT, Dumitriu B. Telomere dynamics in mice and humans. Semin Hematol. 2013;50(2):165-74.
233. Martins RR, Ellis PS, MacDonald RB, Richardson RJ, Henriques CM. Resident Immunity in Tissue Repair and Maintenance: The Zebrafish Model Coming of Age. Front Cell Dev Biol. 2019;7:12.
234. Ferrero G, Gomez E, Lyer S, Rovira M, Miserocchi M, Langenau DM, et al. The macrophage-expressed gene (mpeg) 1 identifies a subpopulation of B cells in the adult zebrafish. J Leukoc Biol. 2020;107(3):431-43.
235. Spilsbury K, O'Mara MA, Wu WM, Rowe PB, Symonds G, Takayama Y. Isolation of a novel macrophage-specific gene by differential cDNA analysis. Blood. 1995;85(6):1620-9.
236. Zakrzewska A, Cui C, Stockhammer OW, Benard EL, Spaink HP, Meijer AH. Macrophage-specific gene functions in Spi1-directed innate immunity. Blood. 2010;116(3):e1-11.
237. Moyse BR, Richardson RJ. A Population of Injury-Responsive Lymphoid Cells Expresses mpeg1.1 in the Adult Zebrafish Heart. Immunohorizons. 2020;4(8):464-74.
238. Imamura S, Uchiyama J, Koshimizu E, Hanai J, Raftopoulou C, Murphey RD, et al. A non-canonical function of zebrafish telomerase reverse transcriptase is required for developmental hematopoiesis. PLoS One. 2008;3(10):e3364.
239. Bolger AM, Lohse M, Usadel B. Trimmomatic: a flexible trimmer for Illumina sequence data. Bioinformatics. 2014;30(15):2114-20.
240. Li H, Durbin R. Fast and accurate long-read alignment with Burrows-Wheeler transform. Bioinformatics. 2010;26(5):589-95.
241. Tarasov A, Vilella AJ, Cuppen E, Nijman IJ, Prins P. Sambamba: fast processing of NGS alignment formats. Bioinformatics. 2015;31(12):2032-4.
242. Layer RM, Chiang C, Quinlan AR, Hall IM. LUMPY: a probabilistic framework for structural variant discovery. Genome Biol. 2014;15(6):R84.
243. Rausch T, Zichner T, Schlattl A, Stutz AM, Benes V, Korbel JO. DELLY: structural variant discovery by integrated paired-end and split-read analysis. Bioinformatics. 2012;28(18):i333-i9.

244. Zheng GX, Terry JM, Belgrader P, Ryvkin P, Bent ZW, Wilson R, et al. Massively parallel digital transcriptional profiling of single cells. Nat Commun. 2017;8:14049.
245. Ge SX, Jung D, Yao R. ShinyGO: a graphical gene-set enrichment tool for animals and plants. Bioinformatics. 2020;36(8):2628-9.
246. Szklarczyk D, Kirsch R, Koutrouli M, Nastou K, Mehryary F, Hachilif R, et al. The STRING database in 2023: protein-protein association networks and functional enrichment analyses for any sequenced genome of interest. Nucleic Acids Res. 2023;51(D1):D638-D46.
247. Guo C, Ye W, Shi M, Duan Y, Zhang W, Cheng Y, et al. FishSCT: a zebrafish-centric database for exploration and visualization of fish single-cell transcriptome. Sci China Life Sci. 2023.
248. Xie Z, Bailey A, Kuleshov MV, Clarke DJB, Evangelista JE, Jenkins SL, et al. Gene Set Knowledge Discovery with Enrichr. Curr Protoc. 2021;1(3):e90.
249. Hellen CU, Sarnow P. Internal ribosome entry sites in eukaryotic mRNA molecules. Genes Dev. 2001;15(13):1593-612.
250. Huang CJ, Tu CT, Hsiao CD, Hsieh FJ, Tsai HJ. Germ-line transmission of a myocardium-specific GFP transgene reveals critical regulatory elements in the cardiac myosin light chain 2 promoter of zebrafish. Dev Dyn. 2003;228(1):30-40.
251. Kawakami K. Tol2: a versatile gene transfer vector in vertebrates. Genome Biol. 2007;8 Suppl 1:S7.
252. Kwan KM, Fujimoto E, Grabher C, Mangum BD, Hardy ME, Campbell DS, et al. The Tol2kit: a multisite gateway-based construction kit for Tol2 transposon transgenesis constructs. Dev Dyn. 2007;236(11):3088-99.
253. Inoue M, Miyahara H, Shiraishi H, Shimizu N, Tsumori M, Kiyota K, et al. Leucyl-tRNA synthetase deficiency systemically induces excessive autophagy in zebrafish. Sci Rep. 2021;11(1):8392.
254. Holland SJ, Liao XC, Mendenhall MK, Zhou X, Pardo J, Chu P, et al. Functional cloning of Src-like adapter protein-2 (SLAP-2), a novel inhibitor of antigen receptor signaling. J Exp Med. 2001;194(9):1263-76.
255. Fischer S, Kluver N, Burkhardt-Medicke K, Pietsch M, Schmidt AM, Wellner P, et al. Abcb4 acts as multixenobiotic transporter and active barrier against chemical uptake in zebrafish (Danio rerio) embryos. BMC Biol. 2013;11:69.
256. Melvin VS, Feng W, Hernandez-Lagunas L, Artinger KB, Williams T. A morpholino-based screen to identify novel genes involved in craniofacial morphogenesis. Dev Dyn. 2013;242(7):817-31.
257. Kimura M, Stone RC, Hunt SC, Skurnick J, Lu X, Cao X, et al. Measurement of telomere length by the Southern blot analysis of terminal restriction fragment lengths. Nat Protoc. 2010;5(9):1596-607.
258. Lin J, Smith DL, Esteves K, Drury S. Telomere length measurement by qPCR - Summary of critical factors and recommendations for assay design. Psychoneuroendocrinology. 2019;99:271-8.
259. Sandoval-Villegas N, Nurieva W, Amberger M, Ivics Z. Contemporary Transposon Tools: A Review and Guide through Mechanisms and Applications of Sleeping Beauty, piggyBac and Tol2 for Genome Engineering. Int J Mol Sci. 2021;22(10).
260. Dunston CR, Griffiths HR. The effect of ageing on macrophage Toll-like receptor-mediated responses in the fight against pathogens. Clin Exp Immunol. 2010;161(3):407-16.
261. De Maeyer RPH, Chambers ES. The impact of ageing on monocytes and macrophages. Immunol Lett. 2021;230:1-10.

262. Jiang M, Xiao Y, E W, Ma L, Wang J, Chen H, et al. Characterization of the Zebrafish Cell Landscape at Single-Cell Resolution. Front Cell Dev Biol. 2021;9:743421.
263. Xia J, Kang Z, Xue Y, Ding Y, Gao S, Zhang Y, et al. A single-cell resolution developmental atlas of hematopoietic stem and progenitor cell expansion in zebrafish. Proc Natl Acad Sci U S A. 2021;118(14).
264. Farnsworth DR, Saunders LM, Miller AC. A single-cell transcriptome atlas for zebrafish development. Dev Biol. 2020;459(2):100-8.
265. Tambalo M, Mitter R, Wilkinson DG. A single cell transcriptome atlas of the developing zebrafish hindbrain. Development. 2020;147(6).
266. Wagner DE, Weinreb C, Collins ZM, Briggs JA, Megason SG, Klein AM. Single-cell mapping of gene expression landscapes and lineage in the zebrafish embryo. Science. 2018;360(6392):981-7.
267. Hernandez PP, Strzelecka PM, Athanasiadis EI, Hall D, Robalo AF, Collins CM, et al. Single-cell transcriptional analysis reveals ILC-like cells in zebrafish. Sci Immunol. 2018;3(29).
268. Lugo-Villarino G, Balla KM, Stachura DL, Banuelos K, Werneck MB, Traver D. Identification of dendritic antigen-presenting cells in the zebrafish. Proc Natl Acad Sci U S A. 2010;107(36):15850-5.
269. Shao X, Fu Y, Ma J, Li X, Lu C, Zhang R. Functional alterations and transcriptomic changes during zebrafish cardiac aging. Biogerontology. 2020;21(5):637-52.
270. Jia C, Hu Y, Kelly D, Kim J, Li M, Zhang NR. Accounting for technical noise in differential expression analysis of single-cell RNA sequencing data. Nucleic Acids Res. 2017;45(19):10978-88.
271. Pozhitkov AE, Neme R, Domazet-Loso T, Leroux BG, Soni S, Tautz D, et al. Tracing the dynamics of gene transcripts after organismal death. Open Biol. 2017;7(1).
272. McCormack RM, de Armas LR, Shiratsuchi M, Fiorentino DG, Olsson ML, Lichtenheld MG, et al. Perforin-2 is essential for intracellular defense of parenchymal cells and phagocytes against pathogenic bacteria. Elife. 2015;4.
273. Fields KA, McCormack R, de Armas LR, Podack ER. Perforin-2 restricts growth of Chlamydia trachomatis in macrophages. Infect Immun. 2013;81(8):3045-54.
274. Kanehisa M, Goto S. KEGG: kyoto encyclopedia of genes and genomes. Nucleic Acids Res. 2000;28(1):27-30.
275. Gene Ontology C, Aleksander SA, Balhoff J, Carbon S, Cherry JM, Drabkin HJ, et al. The Gene Ontology knowledgebase in 2023. Genetics. 2023;224(1).
276. Ashburner M, Ball CA, Blake JA, Botstein D, Butler H, Cherry JM, et al. Gene ontology: tool for the unification of biology. The Gene Ontology Consortium. Nat Genet. 2000;25(1):25-9.
277. Otis JP, Zeituni EM, Thierer JH, Anderson JL, Brown AC, Boehm ED, et al. Zebrafish as a model for apolipoprotein biology: comprehensive expression analysis and a role for ApoA-IV in regulating food intake. Dis Model Mech. 2015;8(3):295-309.
278. Xia Y, Li Y, Wu X, Zhang Q, Chen S, Ma X, et al. Ironing Out the Details: How Iron Orchestrates Macrophage Polarization. Front Immunol. 2021;12:669566.
279. James Bates RE, Browne E, Schalks R, Jacobs H, Tan L, Parekh P, et al. Lymphotoxin-alpha expression in the meninges causes lymphoid tissue formation and neurodegeneration. Brain. 2022;145(12):4287-307.
280. Jiao A, Zhang C, Wang X, Sun L, Liu H, Su Y, et al. Single-cell sequencing reveals the evolution of immune molecules across multiple vertebrate species. J Adv Res. 2023.

281. Cavone L, McCann T, Drake LK, Aguzzi EA, Oprisoreanu AM, Pedersen E, et al. A unique macrophage subpopulation signals directly to progenitor cells to promote regenerative neurogenesis in the zebrafish spinal cord. Dev Cell. 2021;56(11):1617-30 e6.
282. Sene A, Khan AA, Cox D, Nakamura RE, Santeford A, Kim BM, et al. Impaired cholesterol efflux in senescent macrophages promotes age-related macular degeneration. Cell Metab. 2013;17(4):549-61.
283. Krenkel O, Tacke F. Liver macrophages in tissue homeostasis and disease. Nat Rev Immunol. 2017;17(5):306-21.
284. Kraus JM, Giovannone D, Rydzik R, Balsbaugh JL, Moss IL, Schwedler JL, et al. Notch signaling enhances bone regeneration in the zebrafish mandible. Development. 2022;149(5).
285. Sanchez-Iranzo H, Halavatyi A, Diz-Munoz A. Strength of interactions in the Notch gene regulatory network determines patterning and fate in the notochord. Elife. 2022;11.
286. Sigloch C, Spitz D, Driever W. A network of Notch-dependent and -independent her genes controls neural stem and progenitor cells in the zebrafish thalamic proliferation zone. Development. 2023;150(7).
287. Rao Y, Su J, Yang C, Peng L, Feng X, Li Q. Characterizations of two grass carp Ctenopharyngodon idella HMGB2 genes and potential roles in innate immunity. Dev Comp Immunol. 2013;41(2):164-77.
288. Emmanouilidou A, Karetsou Z, Tzima E, Kobayashi T, Papamarcaki T. Knockdown of prothymosin alpha leads to apoptosis and developmental defects in zebrafish embryos. Biochem Cell Biol. 2013;91(5):325-32.
289. Pai CW, Chen YH. Transgenic expression of prothymosin alpha on zebrafish epidermal cells promotes proliferation and attenuates UVB-induced apoptosis. Transgenic Res. 2010;19(4):655-65.
290. Shih LJ, Lu YF, Chen YH, Lin CC, Chen JA, Hwang SP. Characterization of the agr2 gene, a homologue of X. laevis anterior gradient 2, from the zebrafish, Danio rerio. Gene Expr Patterns. 2007;7(4):452-60.
291. Lu YF, Liu DW, Li IC, Lin J, Wang CM, Chu KC, et al. Delta/Jagged-mediated Notch signaling induces the differentiation of agr2-positive epidermal mucous cells in zebrafish embryos. PLoS Genet. 2021;17(12):e1009969.
292. Li L, Zhang J, Akimenko MA. Inhibition of mmp13a during zebrafish fin regeneration disrupts fin growth, osteoblasts differentiation, and Laminin organization. Dev Dyn. 2020;249(2):187-98.
293. Wei Z, Li C, Zhang Y, Lin C, Zhang Y, Shu L, et al. Macrophage-Derived IL-1beta Regulates Emergency Myelopoiesis via the NF-kappaB and C/ebpbeta in Zebrafish. J Immunol. 2020;205(10):2694-706.
294. Xiong S, Wu J, Jing J, Huang P, Li Z, Mei J, et al. Loss of stat3 function leads to spine malformation and immune disorder in zebrafish. Sci Bull (Beijing). 2017;62(3):185-96.
295. Bouchery T, Harris N. Neutrophil-macrophage cooperation and its impact on tissue repair. Immunol Cell Biol. 2019;97(3):289-98.
296. Raveney BJ, Copland DA, Calder CJ, Dick AD, Nicholson LB. TNFR1 signalling is a critical checkpoint for developing macrophages that control of T-cell proliferation. Immunology. 2010;131(3):340-9.
297. Vivier E, Tomasello E, Baratin M, Walzer T, Ugolini S. Functions of natural killer cells. Nat Immunol. 2008;9(5):503-10.

298. Cui C, Wang J, Fagerberg E, Chen PM, Connolly KA, Damo M, et al. Neoantigen-driven B cell and CD4 T follicular helper cell collaboration promotes anti-tumor CD8 T cell responses. Cell. 2021;184(25):6101-18 e13.
299. Vos Q, Ortaldo JR, Conan-Cibotti M, Vos MD, Young HA, Anderson SK, et al. Phenotypic and functional characterization of a panel of cytotoxic murine NK cell clones that are heterogeneous in their enhancement of Ig secretion in vitro. Int Immunol. 1998;10(8):1093-101.
300. Langenau DM, Ferrando AA, Traver D, Kutok JL, Hezel JP, Kanki JP, et al. In vivo tracking of T cell development, ablation, and engraftment in transgenic zebrafish. Proc Natl Acad Sci U S A. 2004;101(19):7369-74.
301. Zhang Y, Wiest DL. Using the Zebrafish Model to Study T Cell Development. Methods Mol Biol. 2016;1323:273-92.
302. Yilmaz O, Patinote A, Nguyen T, Bobe J. Multiple vitellogenins in zebrafish (Danio rerio): quantitative inventory of genes, transcripts and proteins, and relation to egg quality. Fish Physiol Biochem. 2018;44(6):1509-25.
303. Biscotti MA, Barucca M, Carducci F, Canapa A. New Perspectives on the Evolutionary History of Vitellogenin Gene Family in Vertebrates. Genome Biol Evol. 2018;10(10):2709-15.
304. Mantovani A, Cassatella MA, Costantini C, Jaillon S. Neutrophils in the activation and regulation of innate and adaptive immunity. Nat Rev Immunol. 2011;11(8):519-31.
305. Hu CB, Wang J, Hong Y, Li H, Fan DD, Lin AF, et al. Single-cell transcriptome profiling reveals diverse immune cell populations and their responses to viral infection in the spleen of zebrafish. FASEB J. 2023;37(6):e22951.
306. Torrisani J, Bouisson M, Puente E, Capella G, Laurent-Puig P, Berger A, et al. Transcription of SST2 somatostatin receptor gene in human pancreatic cancer cells is altered by single nucleotide promoter polymorphism. Gastroenterology. 2001;120(1):200-9.
307. Elieh Ali Komi D, Sharma L, Dela Cruz CS. Chitin and Its Effects on Inflammatory and Immune Responses. Clin Rev Allergy Immunol. 2018;54(2):213-23.
308. Duong L, Radley HG, Lee B, Dye DE, Pixley FJ, Grounds MD, et al. Macrophage function in the elderly and impact on injury repair and cancer. Immun Ageing. 2021;18(1):4.
309. Wallace KL, Zheng LB, Kanazawa Y, Shih DQ. Immunopathology of inflammatory bowel disease. World J Gastroenterol. 2014;20(1):6-21.
310. Zeidan RS, Han SM, Leeuwenburgh C, Xiao R. Iron homeostasis and organismal aging. Ageing Res Rev. 2021;72:101510.
311. Gao XL, Tian WJ, Liu B, Wu J, Xie W, Shen Q. High-mobility group nucleosomal binding domain 2 protects against microcephaly by maintaining global chromatin accessibility during corticogenesis. J Biol Chem. 2020;295(2):468-80.
312. Xue L, Bao L, Roediger J, Su Y, Shi B, Shi YB. Protein arginine methyltransferase 1 regulates cell proliferation and differentiation in adult mouse adult intestine. Cell Biosci. 2021;11(1):113.
313. Klatt Shaw D, Mokalled MH. Efficient CRISPR/Cas9 mutagenesis for neurobehavioral screening in adult zebrafish. G3 (Bethesda). 2021;11(8).
314. Li M, Zhao L, Page-McCaw PS, Chen W. Zebrafish Genome Engineering Using the CRISPR-Cas9 System. Trends Genet. 2016;32(12):815-27.
315. Linehan E, Dombrowski Y, Snoddy R, Fallon PG, Kissenpfennig A, Fitzgerald DC. Aging impairs peritoneal but not bone marrow-derived macrophage phagocytosis. Aging Cell. 2014;13(4):699-708.

316. Connolly NMC, Theurey P, Adam-Vizi V, Bazan NG, Bernardi P, Bolanos JP, et al. Guidelines on experimental methods to assess mitochondrial dysfunction in cellular models of neurodegenerative diseases. Cell Death Differ. 2018;25(3):542-72.
317. Izadi N, Hauk PJ. Cellular assays to evaluate B-cell function. J Immunol Methods. 2023;512:113395.
318. Dee CT, Nagaraju RT, Athanasiadis EI, Gray C, Fernandez Del Ama L, Johnston SA, et al. CD4-Transgenic Zebrafish Reveal Tissue-Resident Th2- and Regulatory T Cell-like Populations and Diverse Mononuclear Phagocytes. J Immunol. 2016;197(9):3520-30.
319. Selders GS, Fetz AE, Radic MZ, Bowlin GL. An overview of the role of neutrophils in innate immunity, inflammation and host-biomaterial integration. Regen Biomater. 2017;4(1):55-68.
320. Guimaraes GR, Almeida PP, de Oliveira Santos L, Rodrigues LP, de Carvalho JL, Boroni M. Hallmarks of Aging in Macrophages: Consequences to Skin Inflammaging. Cells. 2021;10(6).
321. Elder SS, Emmerson E. Senescent cells and macrophages: key players for regeneration? Open Biol. 2020;10(12):200309.
322. Maida Y, Masutomi K. Telomerase reverse transcriptase moonlights: Therapeutic targets beyond telomerase. Cancer Sci. 2015;106(11):1486-92.
323. Renshaw SA, Loynes CA, Trushell DM, Elworthy S, Ingham PW, Whyte MK. A transgenic zebrafish model of neutrophilic inflammation. Blood. 2006;108(13):3976-8.
324. Zhang Q, Feng W, Wang Q, Wang J, Chai L, Chen Y, et al. PPARgamma activation inhibits PDGF-induced pulmonary artery smooth muscle cell proliferation and migration by modulating TERT. Biomed Pharmacother. 2022;152:113233.

Appendix

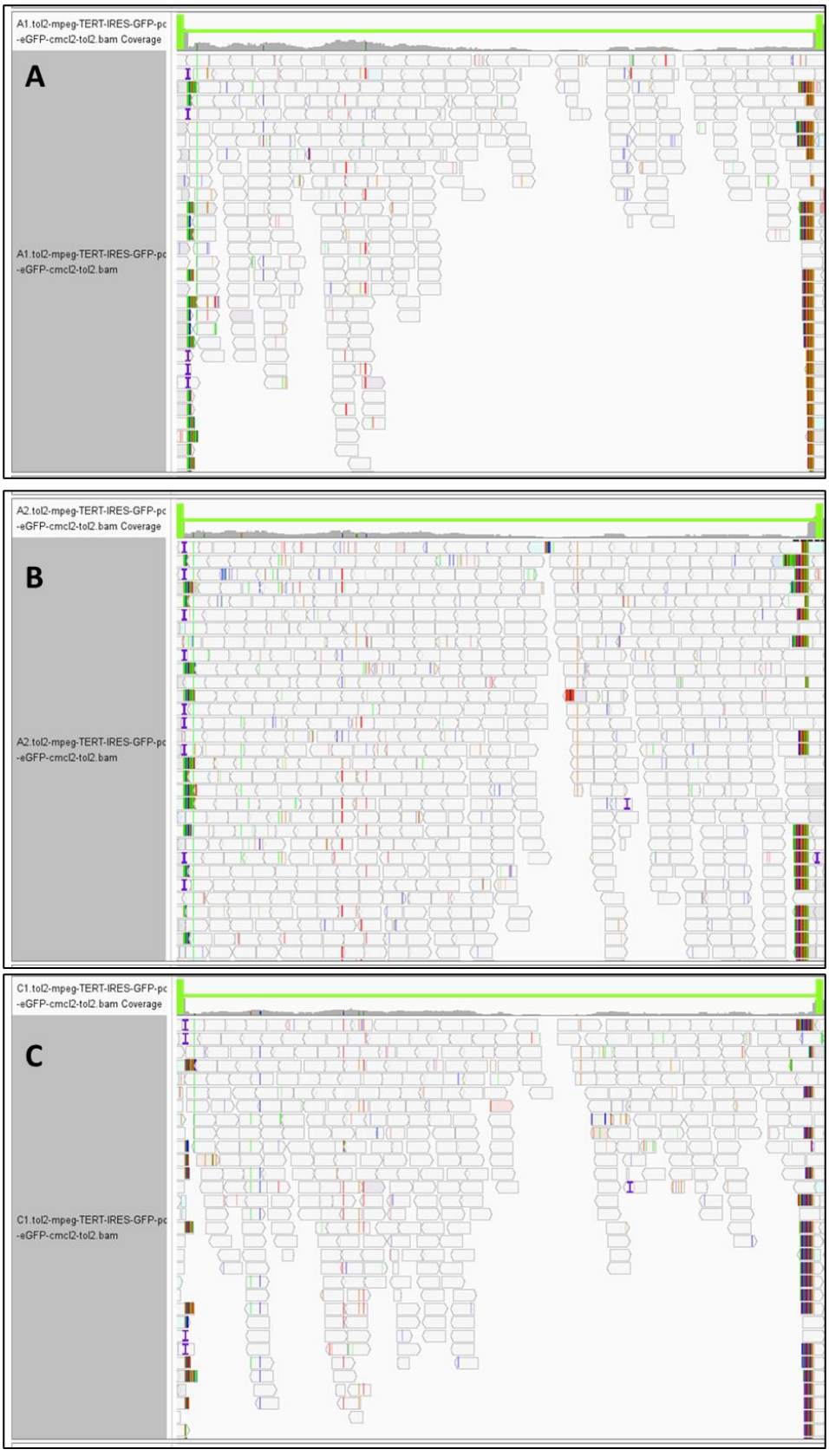
A1.tol2-mpeg-TERT-IRES-GFP-pc
-eGFP-cmcl2-tol2.bam Coverage
A
A1.tol2-mpeg-TERT-IRES-GFP-pc
-eGFP-cmcl2-tol2.bam
A2.tol2-mpeg-TERT-IRES-GFP-pc
-eGFP-cmcl2-tol2.bam Coverage
B
A2.tol2-mpeg-TERT-IRES-GFP-pc
-eGFP-cmcl2-tol2.bam
C1.tol2-mpeg-TERT-IRES-GFP-pc
-eGFP-cmcl2-tol2.bam Coverage
C
C1.tol2-mpeg-TERT-IRES-GFP-pc
-eGFP-cmcl2-tol2.bam

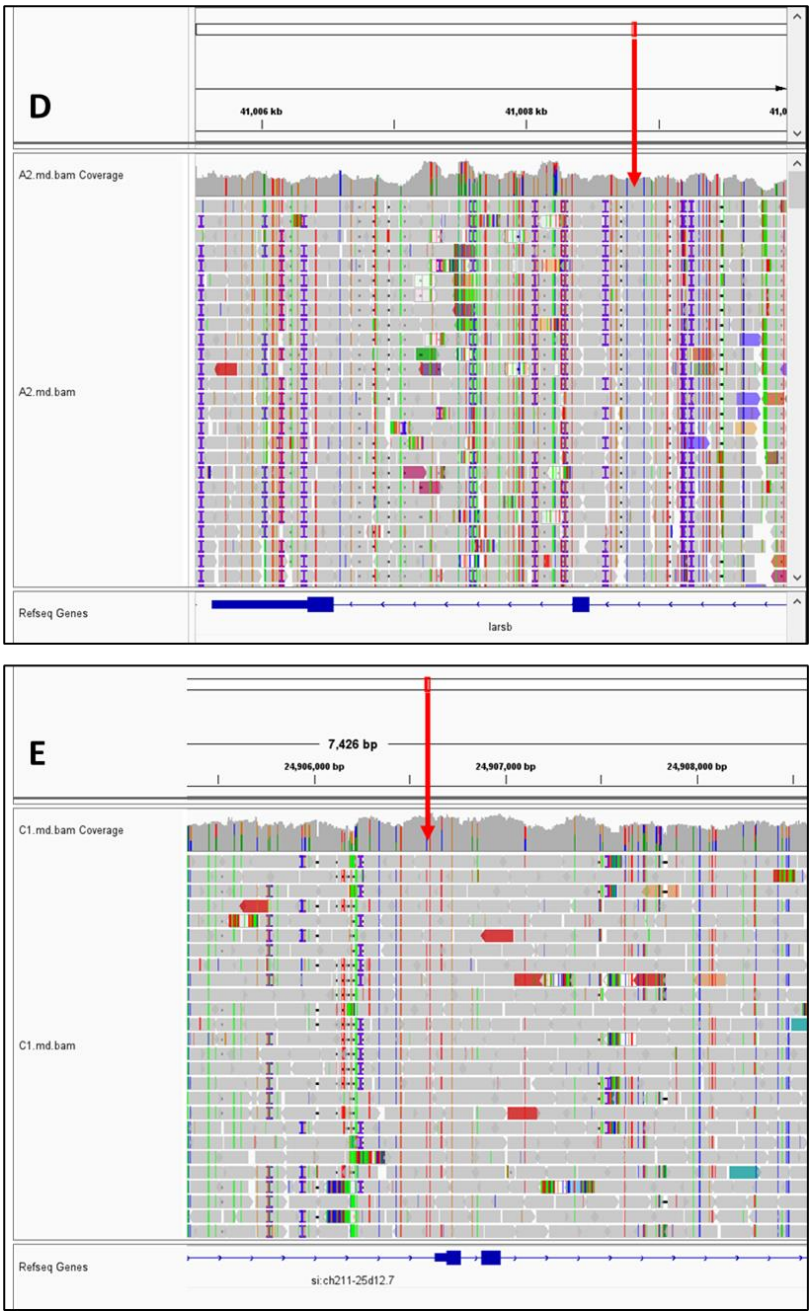

Supplementary Figure 1: A. Representative sequencing of the *mpeg-tert-IRES-GFP* inserted into the A1 potential founder line with green line indicating insertion of the *tert* region. **B.** Representative sequencing of the *mpeg-tert-IRES-GFP* inserted into the A2 potential founder line with green line indicating insertion of the *tert* region. **C.** Representative sequencing of the *mpeg-tert-IRES-GFP* inserted into the C1 potential founder line with green line indicating insertion of the *tert* region. **D.** Insertion site of the transgene in A1 and C1 *mpeg-tert-IRES-GFP* founder lines indicated by the red arrow. Refseq genes are listed along the bottom, indicating insertion into larsb. **E.** Insertion site of the transgene in the A2 *mpeg-tert-IRES-GFP* founder line indicated by the red line arrow. Refseq genes are listed along the bottom, indicating insertion into si:ch211-25d12.7.

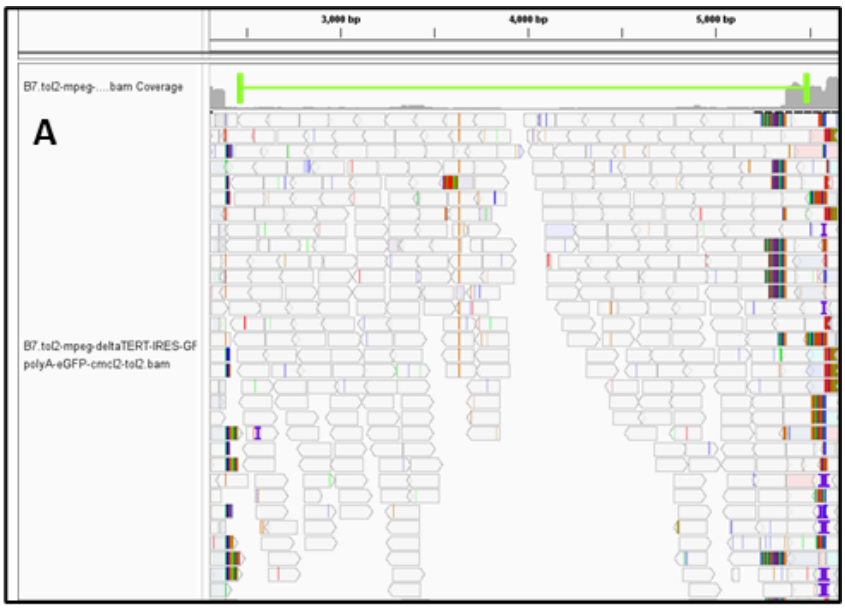
3,000 bp
4,000 bp
5,000 bp
B7.tol2-mpeg-....bam Coverage
A
B7.tol2-mpeg-deltaTERT-IRES-GF
polyA-eGFP-cmcl2-tol2.bam

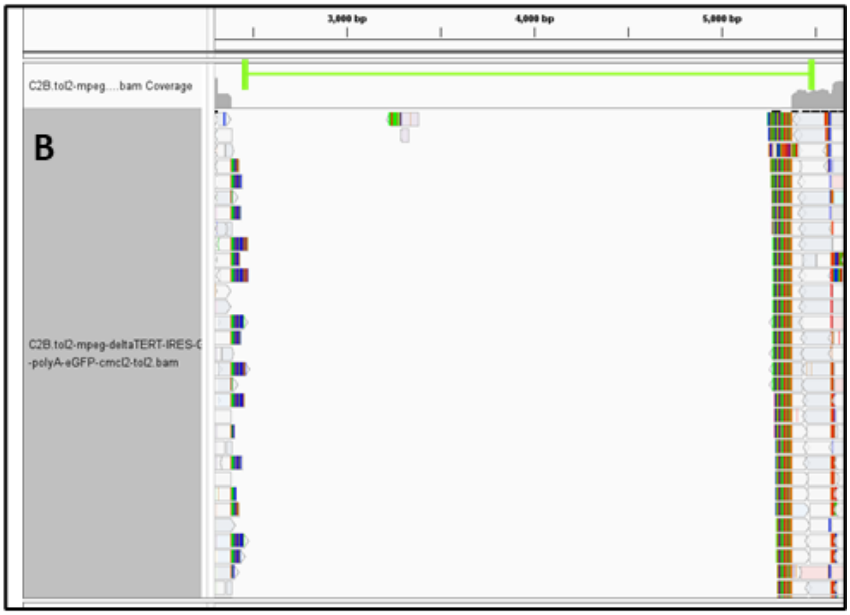
3,000 bp
4,000 bp
5,000 bp
C2B.tol2-mpeg....bam Coverage
B
C2B.tol2-mpeg-deltaTERT-IRES-(
-polyA-eGFP-cmcl2-tol2.bam

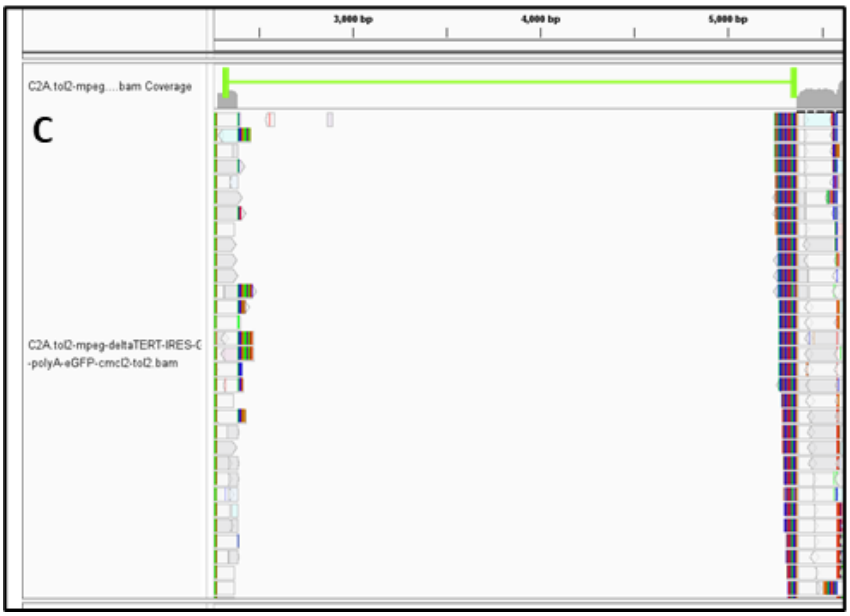
3,000 bp
4,000 bp
5,000 bp
C2A.tol2-mpeg....bam Coverage
C
C2A.tol2-mpeg-deltaTERT-IRES-(
-polyA-eGFP-cmcl2-tol2.bam

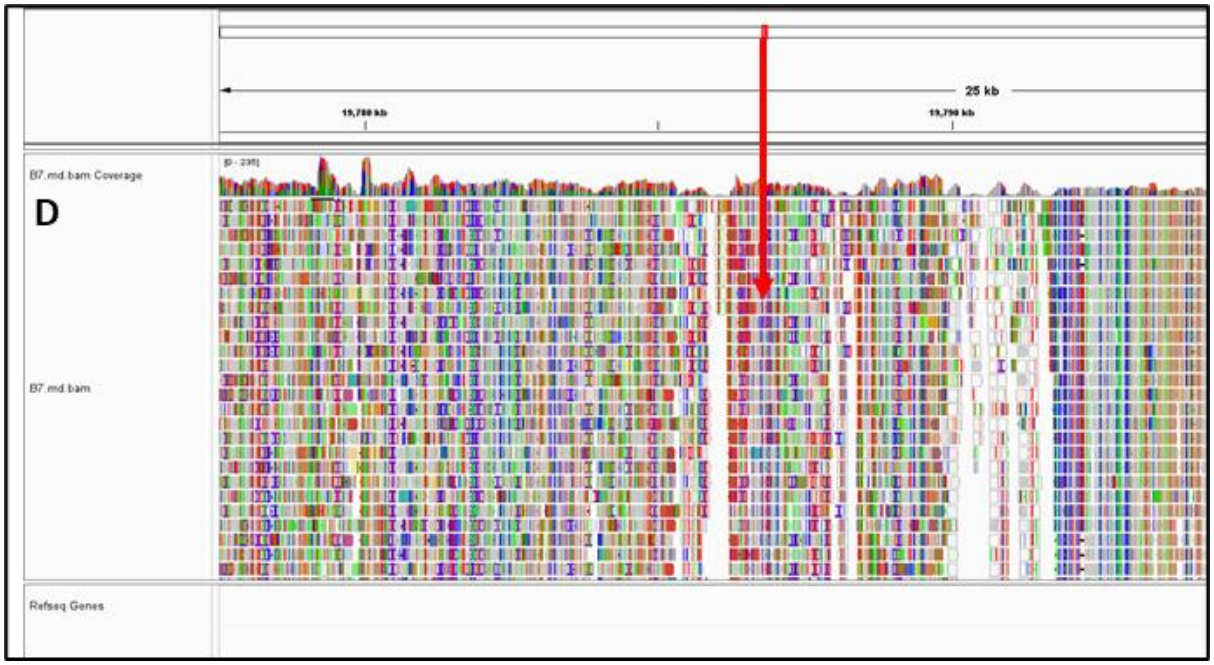

Supplementary Figure 2: A. Representative image of sequencing of the *mpeg-Δtert-IRES-GFP* inserted into the B7 potential founder line with green line indicating *tert* site. **B.** Representative image of sequencing of the *mpeg-Δtert-IRES-GFP* inserted into the C2B potential founder line with green line indicating predicted *tert* site without insertion. **C.** Representative image of sequencing of the *mpeg-Δtert-IRES-GFP* inserted into the C2A potential founder line with green line indicating predicted *tert* site without insertion. **D.** Insertion site of the transgene in the B7 *mpeg-Δtert-IRES-GFP* founder line indicated by the red arrow. Refseq genes are listed along the bottom, indicating no refseq genes at the insertion site in chromosome 16.